EMPLOYING ^{13}C TRACERS TO ELUCIDATE BACTERIAL AND MICROALGAL METABOLISM IN DYNAMIC SYSTEMS

by

Brian Oliver McConnell

A dissertation submitted to the Faculty of the University of Delaware in partial fulfillment of the requirements for the degree of Doctor of Philosophy in Chemical Engineering

Summer 2019

EMPLOYING ^{13}C TRACERS TO ELUCIDATE BACTERIAL AND MICROALGAL METABOLISM IN DYNAMIC SYSTEMS

by

Brian Oliver McConnell

Approved: _____
Eric M. Furst, Ph.D.
Chair of the Department of Chemical and Biomolecular Engineering

Approved: _____
Levi T. Thompson, Ph.D.
Dean of the College of Engineering

Approved: _____
Douglas J. Doren, Ph.D.
Interim Vice Provost for Graduate & Professional Education and Dean of the Graduate College

I certify that I have read this dissertation and that in my opinion it meets the academic and professional standard required by the University as a dissertation for the degree of Doctor of Philosophy.

Signed: _____

Maciek R. Antoniewicz, Ph.D.
Professor in charge of dissertation

I certify that I have read this dissertation and that in my opinion it meets the academic and professional standard required by the University as a dissertation for the degree of Doctor of Philosophy.

Signed: _____

Wilfred Chen, Ph.D.
Member of dissertation committee

I certify that I have read this dissertation and that in my opinion it meets the academic and professional standard required by the University as a dissertation for the degree of Doctor of Philosophy.

Signed: _____

Kelvin H. Lee, Ph.D.
Member of dissertation committee

I certify that I have read this dissertation and that in my opinion it meets the academic and professional standard required by the University as a dissertation for the degree of Doctor of Philosophy.

Signed: _____

Michael J. Betenbaugh, Ph.D.
Member of dissertation committee

ACKNOWLEDGMENTS

I am grateful for all the people who have influenced me during my academic journey. First, I would like to thank my advisor, Professor Maciek Antoniewicz. Thank you for your guidance, encouragement, and support. I have learned so much from you during the last five years. Thank you for giving me the opportunities to travel to conferences in Japan, Germany, and six US cities. These conferences were great opportunities to interact with leading researchers in metabolic engineering and improve my public speaking. I'm leaving Delaware as a much-improved researcher. I'm grateful for the opportunities that I have had within your research group, and I'm excited to transition into my next chemical engineering chapter.

I would also like to thank my committee members, Professors Wilfred Chen, Kelvin Lee, and Michael Betenbaugh, for their feedback on my research. Additionally, I would like to thank Professor Chen for accepting me into the UD Chemical Engineering Department back in 2014 when he was the Department's Director of Graduate Admissions. I would like to thank Professors Lee and Betenbaugh for their roles within the Advanced Mammalian Biomanufacturing Innovation Center (AMBIC). I did not discuss any of my AMBIC work in this dissertation, but those experiences changed my career path.

I'm grateful for all the interactions that I've had with past and present members of the Antoniewicz Lab. I've learned so much from you all during the last five years.

I will always be indebted to my undergraduate mentor from UNH, Professor Ihab Farag. His support and encouragement enabled many opportunities and changed

my future as a chemical engineer. I'm also thankful for my friends Seth, Kevin, and James. I would not have made it through undergraduate classes without you guys.

I cannot thank my family enough for all their support. My parents have made many sacrifices to give me opportunities they never had. I have tried my best not to let their sacrifices go to waste. I'm glad that my sister chose an internship in Delaware this summer. I've greatly appreciated her moral support while finishing this dissertation.

TABLE OF CONTENTS

LIST OF TABLES

LIST OF FIGURES

ABSTRACT

Climate change is one of the most threatening problems facing humanity. Instead of burning fossil fuels and increasing the atmospheric carbon dioxide (CO_2) concentration, an alternative is to recycle CO_2 by fixing it as cellular biomass and converting it to biofuels. One promising biofuel production strategy is to use *Chlorella vulgaris*, a photosynthetic microalga, to capture CO_2 from large point-source emitters and produce biodiesel from its lipids or use its carbohydrates to feed heterotrophic fermentation processes. However, due to inefficiencies in carbon metabolism, critical technical bottlenecks remain to economic production of microalgal biomass. Therefore, the first aim of this dissertation is to use ^{13}C tracers to obtain a quantitative understanding of *Chlorella vulgaris*'s metabolism in multiple trophic conditions while being subjected to cycling substrate availability and nitrogen depletion stress.

In addition to fuels, many chemicals are made from petroleum so there is a need to develop renewable chemical production systems. *Escherichia coli* has been a biotechnological workhorse since the development of recombinant DNA technology. Many strains have been engineered to produce useful metabolites and it is common that they require complex media to achieve industrially relevant rates and titers. To support further metabolic engineering of these strains, it would be advantageous to have a quantitative understanding of the flow of carbon through their metabolic pathways. However, the existing methodologies to quantify *in vivo* metabolic fluxes using ^{13}C metabolic flux analysis necessitate growth in minimal media. Therefore, the

second aim of this work is to develop a ^{13}C metabolic flux analysis methodology for elucidating fluxes of cells grown in complex media.

This dissertation begins with the development of a method to measure the carbohydrate composition and stable-isotope labeling in biomass using GC/MS. The method consists of two-stage hydrochloric acid hydrolysis, followed by chemical derivatization of the released monomer sugars, and then quantification by GC/MS.

Next, the metabolism of *C. vulgaris* is characterized in auto-, hetero-, and mixotrophic conditions. Light cycling and nitrogen depletion are major determinants of biomass composition. In the dark, the autotrophic cells cannot fix CO_2, so they must consume their starch reserves for maintenance energy. The cells change starch production/consumption mode within one hour of light condition change. Growing *C. vulgaris* cells (nitrogen replete phase) are determined to mostly be composed of protein. Upon nitrogen depletion, however, the cells change their composition and the dominant macromolecules become carbohydrates and fatty acids.

Polysaccharide secretion is a major source of starch turnover in *C. vulgaris*. Culturing heterotrophic microbes (isolated from soil) with *C. vulgaris* leads to increased biomass production. Understanding the interaction between autotrophs and heterotrophs is important because large-scale microalgal production facilities will likely be open ponds where contaminating organisms could easily enter the culture from the air.

Towards the second aim, tracer experiments with [U-^{13}C]glucose and yeast extract are used to determine the contributions of each substrate to biomass formation. The results suggest that the proteinogenic amino acids glycine, alanine, aspartate/ asparagine, and tyrosine are made from glucose even if these amino acids are present

in the medium. A novel methodology to perform ^{13}C-metabolic flux analysis of *E. coli* in the presence of glucose and yeast extract is finally presented and used to analyze wild-type *E. coli*.

Chapter 1

INTRODUCTION

1.1 Climate Change and Biofuels

Climate change, a result of increasing atmospheric greenhouse gases (GHG), is one of the most threatening problems facing humanity. Carbon dioxide emissions are of primary concern since they account for about 80% of GHG emissions. Fossil fuel combustion for electricity and transportation account for almost 60% of carbon dioxide emissions in the United States [Source: United States Environmental Protection Agency, https://www.epa.gov/ghgemissions]. Instead of burning fossil fuels and increasing the atmospheric carbon dioxide concentration, an alternative would be to capture and recycle carbon dioxide using biomass and biofuels. Additionally, many chemicals are made from petroleum so there is also a need to develop renewable chemical production processes (Miller and Nagarajan 2000).

One promising biofuel production strategy is to use photosynthetic green microalgae to capture carbon dioxide from large, point-source emitters and produce biodiesel from the microalgal lipids (J. Liu and Chen 2014). Additionally, *Escherichia coli* has been a biotechnological workhorse since the development of recombinant DNA technology. It has been engineered to be a producer of ethanol (Ingram et al. 1987), 1,3-propanediol (Nakamura and Whited 2003), amino acids (Rozzell 1999), insulin (Goeddel et al. 1979), and many other chemicals.

A recent techno-economic analysis of autotrophic microalgae for fuel production showed that the cost of microalgal biodiesel production is most sensitive to

biological parameters (the lipid content and growth rate of the microalgae) and less sensitive to process parameters (Davis, Aden, and Pienkos 2011). This will be true for many biological processes (very high value but low volume therapeutics may be an exception) where the rate, titer, and yield of the microorganism are the most important factors since they set the maximums for the entire process. Therefore, it is important to have an optimized cell/strain when beginning bioprocess development. To address these challenges, the field of metabolic engineering emerged in the mid-1990s. A key part of metabolic engineering practice is to understand the flow of carbon through metabolism by using isotopic tracer analysis and metabolic flux analysis. The work in these fields has been extensive over the past 20 years. Still, there continues to be a need for detailed metabolic studies of microalgae and development of methods to quantify *E. coli's* metabolic fluxes in complex media. The goals of this dissertation are to address those research needs and show that ^{13}C isotopic tracers are powerful tools to elucidate metabolism.

1.2 Microalgal Biodiesel

Biodiesel, alkyl monoesters of fatty acids from biomass lipids, is an attractive biofuel since it 1) can be used in petrodiesel engines with little to no modifications; 2) combusts more easily by compression (higher cetane number) than petrodiesel; 3) contains no harmful aromatics or sulfur; and 4) is biodegradable. Green microalgae (microscopic, photosynthetic, eukaryotic organisms) are an attractive biodiesel feedstock because they 1) grow in water which simplifies carbon dioxide capture from flue gases; 2) some species can be grown in saltwater or municipal wastewater; and 3) some species have a faster growth rate and oil yield than terrestrial, photosynthetic fuel-crops (Muradov and Veziroglu 2017).

The foundations of microalgal biodiesel production were laid from 1978 to 1996 during the National Renewable Energy Laboratory's (NREL) Aquatic Species Program (ASP). The ASP began because of the Carter Administration's desire to develop all parts of solar energy in response to the 1970's oil crisis. At the very beginning of the ASP, macroalgae (seaweed), microalgae, and emergents (wetland plants) were considered for their biofuel potential. It quickly became clear that microalgae were superior biodiesel feedstocks because of their composition and growth rates (Sheehan et al. 1998). Researchers within the Aquatic Species Program collected and identified 3000 algal strains; explored algal physiology, biochemistry, large-scale cultivation, and biofuel conversion; and performed techno-economic studies of biofuel production. Unfortunately, funding and petroleum prices were low in the mid-1990's so the program shut-down and the process to create microalgal biodiesel was not fully developed.

In 2005, the United States Department of Energy and Department of Agriculture estimated that roughly 50 billion gallons of gasoline equivalents (as ethanol) per year could be produced sustainably from terrestrial, non-food biomass in the US ("Billion Ton Study") (Perlack et al. 2005). This was a very significant finding because the United States consumes roughly 140 billion gallons of gasoline, 40 billion gallons of diesel, and 25 billion gallons of jet fuel annually. At the time, ethanol from terrestrial biomass was the only biofuel under consideration, and it became obvious that terrestrial, non-food biomass could not support our nation's transportation fuel requirements (Guarnieri et al. 2013).

Two years after the "Billion Ton Study", the Energy Independence and Security Act (EISA) was signed by President Bush. EISA requires, by 2022, that

biofuel production in the United States be at least 36 billion gallons per year, and 58% must be advanced biofuels. Advanced biofuels were defined as not corn ethanol, derived from renewable biomass, and having no more than 50% of the GHG emissions of the replaced fuel. Cellulosic ethanol has received a great deal of attention towards meeting EISA goals; however, ethanol does not have high enough energy density to replace diesel or jet fuel (Gopalratnam 2011).

The "Billion Ton Study" and EISA renewed interest in algal biofuels (Gopalratnam 2011) and a couple *Chlorella* spp. have received interest as potential biodiesel feedstocks because of their advantageous physiology (J. Liu and Chen 2014). *Chlorella* is a genus of unicellular, non-motile, photosynthetic, eukaryotic microalgae which can survive in fresh and salt water (J. Liu and Chen 2014). Some typical and advantageous *Chlorella* spp. traits include: rapid growth rates compared to terrestrial plants; simple life cycles; metabolic pathways similar to higher plants; high photosynthetic efficiency; ability to achieve high lipid content; and ability to grow on organic and inorganic carbon and nitrogen (J. Liu and Chen 2014; Guarnieri et al. 2013; Plaza et al. 2009; Gerken, Donohoe, and Knoshaug 2013). In regards to microalgal biodiesel production economics, non-polar lipid content is the most important factor (Davis, Aden, and Pienkos 2011) and one of the best lipid producing *Chlorella* species is *C. vulgaris*. In fact, the National Renewable Energy Laboratory, has made *Chlorella vulgaris* UTEX 395 its model green microalga because of *Chlorella vulgaris* UTEX 395's biodiesel production potential (Guarnieri et al. 2013). *Chlorella vulgaris* UTEX 395 will be the microalgae studied in this dissertation for these reasons.

1.3 Large Scale Production of Microalgae and Interactions Between Organisms

Open ponds are the most economical method of producing microalgal biomass at a large scale (Davis, Aden, and Pienkos 2011). Open ponds are usually designed as raceways which have paddle wheels to drive the flow of shallow water around closed-loop recirculation channels (Greenwell et al. 2010). They are economical production systems because of their simplicity; however, that comes with the increased risk of invasive algal species, predators, and/or pathogens entering the culture medium from the environment (Davis, Aden, and Pienkos 2011; Greenwell et al. 2010).

There are three major types of biological interactions: mutualism, commensalism, and parasitism. Mutualism is an interaction in which the partners benefit from each other. Commensalism is an interaction in which only one partner benefits (this is rare). Parasitism is an interaction in which one partner benefits at the expense of the other. The basis of many mutualistic microalgae-bacteria interactions is nutrient exchange involving carbon, nitrogen, vitamins, or hormones (Fuentes et al. 2016). Additionally, mutualistic interactions between microalgae and bacteria has been proposed as a method to increase lipid productivity and biomass yield while lowering expenses (Cooper and Smith 2015). In many parasitic microalgae-bacteria relationships, the bacteria will secrete enzymes to lyse the microalgal cells so that the bacteria can use the microalgal intracellular metabolites for growth (Fuentes et al. 2016). It is important that parasites do not enter the culture medium during large-scale microalgal cultivation otherwise the culture may crash and productivity will be compromised.

1.4 Biomass Characterization

Protein, carbohydrates, and lipids are the most abundant and commonly quantified microalgal biomass components. But, as mentioned above, microalgal biodiesel costs are most sensitive to the lipid content of the cells used in the process (Davis, Aden, and Pienkos 2011). Microalgae use non-polar lipids, mainly triacylglycerols (TAGs), as energy storage (Borowitzka and Moheimani 2013). TAGs are of great interest since their transesterification produces biodiesel. The level of TAG accumulation varies significantly between microalgal species and environmental conditions. TAG production is greatest at slow growth rates since fatty acids (FAs) are not needed to build new membranes. Nitrogen depletion is a common environmental factor that induces TAG accumulation in microalgae. *C. vulgaris* can have up to a three-fold increase in non-polar lipid content under nitrogen limitation compared to nitrogen-rich conditions (Borowitzka and Moheimani 2013). In general, microalgal TAGs contain saturated and unsaturated fatty acids that are typically 10 to 24 carbons long. *C. vulgaris*'s FAs are mainly 16 and 18 carbons long with C18:2 and C16:0 as the dominant FAs (Hu et al. 2008). The FA profile is important because saturated FAs result in biodiesel with a high cetane number whereas unsaturated FAs improve low temperature performance. *C. vulgaris*'s composition will produce biodiesel with good overall performance (J. Liu and Chen 2014).

Gravimetric solvent extraction is the classic method used to determine microalgal lipid content; however, many variations of solvent or solvent mixtures have been used (Laurens et al. 2012). A challenge with solvent extraction is that the relative amount of saturated and unsaturated lipids changes during a culture, so the extraction efficiency may not be consistent (Guarnieri et al. 2013; Laurens et al. 2012). Microalgal protein content is commonly determined by a CHNS analyzer or

colorimetric methods, and neither procedure identifies the amino acid profile (Laurens et al. 2012; Becker 1994). Microalgal carbohydrate content is commonly determined by colorimetric methods or enzymatic hydrolysis. Both methods only quantify glucose while other monosaccharides like rhamnose, arabinose, xylose, mannose, and galactose are not accounted for.

The previously described microalgal biomass characterization methods are empirical in nature, some developed decades ago, and small variations in procedures give largely differing results (Laurens et al. 2012). This makes comparison between microalgal species and laboratories difficult. Therefore, accurate analytical methods are necessary for microalgal biomass characterization. The fatty acid, amino acid, and monosaccharide profiles are important to determine since they set the microalgae's economic value and are required for metabolic analyses (Guarnieri et al. 2013). In order to understand how these biomass composition profiles were created, the organism's underlying metabolism must be quantified.

1.5 Metabolism

Metabolism is defined as the set of (bio)chemical reactions occurring inside a cell, which are typically grouped into metabolic pathways. Metabolism has many roles, some of which include: uptake of nutrients; energy generation; building block generation; and polymerization of building blocks into macromolecules. Metabolite pathways are often grouped into two large classes: catabolic or anabolic pathways. Catabolic pathways are degradative (organic nutrients converted to simple end products) and energy producing (ATP, NAD(P)H, and/or $FADH_2$) whereas anabolic pathways are synthetic (small precursors converted to larger and more complex molecules) and energy consuming (Nelson, Cox, and Lehninger 2017).

Organisms can be classed based on their source of carbon and energy. For example, photoautotrophs fix inorganic carbon (CO_2) using light as the energy source, while heterotrophs obtain their carbon and energy by catabolizing organic molecules from the environment (Nelson, Cox, and Lehninger 2017). In this work, the autotrophic green microalga *Chlorella vulgaris* is investigated. This organism can perform photosynthesis to fix carbon dioxide into complex biomolecules. *Chlorella vulgaris* is also able to consume glucose and grow in the dark (this is not true for all photosynthetic organisms). Additionally, heterotrophs like *Escherichia coli* and microbes obtained from soil are also studied in this thesis.

1.6 Isotopic Tracers to Probe Metabolism

Radioactive tracer studies have laid the foundation for our current understanding of metabolism (Jang, Chen, and Rabinowitz 2018). Some of the earliest work analyzing the path of carbon through metabolism (both autotrophic and heterotrophic) used radioactive carbon. Initial studies used ^{11}C, but it had limited utility because its half-life is only about 20 minutes. The discovery of ^{14}C in 1940, lead to many technological advances (radiocarbon dating is probably the most famous), including more extensive metabolic tracing (Gest 2004). In fact, Melvin Calvin was awarded the Nobel Prize in Chemistry in 1961 for his work utilizing ^{14}C isotope labeling to elucidate photosynthetic carbon metabolism.

Photosynthesis is a two-step process. The first step is the conversion of light energy into chemical energy. This is accomplished by using light energy to drive the splitting of water and creation biochemical energy and reducing equivalents:

$$2H_2O + 2NADP^+ + 3P_i + 3ADP \xrightarrow{light} O_2 + 2NADPH + 2H^+ + 3ATP \qquad 1.1$$

The second step of photosynthesis is the fixation of carbon dioxide. In this step, the energy and reducing equivalents generated in the first step, are used with the enzyme RuBisCO to fix carbon dioxide:

$$3CO_2 + 9ATP + 6NADPH + 6H^+ \rightarrow C_3H_6O_3\mathrm{P_i} + 9ADP + 8P_i + 6NADP^+ + 3H_2O. \quad 1.2$$

Additionally, non-carbon tracers have been used to study photosynthetic metabolism. An isotopic tracer experiment using water or carbon dioxide containing ^{18}O was used to track oxygen atoms involved in photosynthesis. It was shown that the oxygen gas produced in photosynthesis comes from water not carbon dioxide (Nelson, Cox, and Lehninger 2017).

In the almost 80 years since the discovery of ^{14}C, there have been many technological advances to further isotopic tracing of metabolism. Today, stable isotopes are preferred over radioactive isotopes, and the most common tracers possess ^{2}H, ^{13}C, and/or ^{15}N atoms. ^{13}C tracers are generally used to study carbon fluxes within metabolism whereas ^{2}H and ^{15}N tracers are used to answer specific questions related to fatty acid biosynthesis, redox metabolism, or protein synthesis (Jang, Chen, and Rabinowitz 2018).

The typical workflow for a ^{13}C tracer experiment begins with selecting the appropriate tracer to accomplish the experimental goal (answer the question of interest) (Jang, Chen, and Rabinowitz 2018; Crown, Long, and Antoniewicz 2016). Once the tracer has been selected, the cells are grown on the tracer (glucose tracers are most common). As the cells metabolize the substrate (tracer), the carbon atoms will be rearranged, and the intracellular metabolites will have labeling patterns reflecting the metabolic fluxes. Once the cells are harvested, the labeling patterns of intracellular

and extracellular metabolites are quantified using NMR or MS methods (Crown and Antoniewicz 2013). Depending on the project's goal, this may be as far as the experiment needs to go. ^{13}C metabolite labeling patterns provide information about relative pathway activities, changes in pathway contributions due to alternative routes, and nutrient contributions to the production of metabolites (Buescher et al. 2015). If quantitative analysis of the organism's metabolic fluxes is needed, then ^{13}C metabolic flux analysis is performed after obtaining the metabolite labeling profiles and external rates (growth, substrate uptake, and product secretion rates).

1.7 Overview of Metabolic Flux Analysis

An organism's metabolic state is largely defined by the metabolic fluxes through its pathways and reactions, which can be quantified *in vivo* by metabolic flux analysis (MFA). Metabolic fluxes are calculated by solving steady state mass balances around intracellular metabolites as constrained by the measured substrate uptake and product secretion rates. Metabolic networks have many connections (more reactions than intermediates), so ^{13}C labeling pattern of metabolites are used as additional measurements to create a non-linear least squares regression problem (Stephanopoulos 1999; Toya et al. 2011). The end result of ^{13}C-MFA is a map showing the connectivity of reactions with estimated fluxes and confidence intervals (Stephanopoulos 1999).

1.7.1 External Rates and Isotopic Labeling

In order to perform ^{13}C metabolic flux analysis (quantify intracellular metabolic fluxes), the external rates and isotopic labeling of intracellular metabolites or proteinogenic amino acids of growing cells (exponentially growing cells have been shown to be at metabolic steady state, i.e. the metabolic fluxes are not changing in

time) are needed. The external rates include substrate uptake rates, product secretion rates, and the growth rate. These external rates are constraints on the intracellular pathway activities. Mass spectrometry is the preferred instrument to measure the mass isotopomer distribution of intracellular metabolites or proteinogenic amino acids due to its superior sensitivity (i.e. compared to NMR based approaches) and ability to detect many metabolites. The metabolite labeling profiles are needed because they provide information about the relative contributions of pathways to the production of each metabolite. The metabolite labeling profiles should be measured at multiple timepoints to determine if the system is at isotopic steady state. Isotopic steady state is a key pre-requisite for ^{13}C-MFA. If the system is not at isotopic steady state, then additional modeling considerations are made to account for the time dependent labeling profiles (Antoniewicz 2018).

1.7.2 Metabolic Model

The metabolic model used in a ^{13}C-MFA study is a system of stoichiometric equations based on the biochemical reactions under consideration. The number of reactions which may be considered depends on the number of measurements obtained (degrees of freedom for the system of equations). Most ^{13}C-MFA metabolic models contain the reactions for the Embden-Meyerhof-Parnas pathway, Entner-Doudoroff pathway, Pentose Phosphate Pathway, Krebs cycle, pathways for significant product formation, and a lumped reaction to drain precursors to produce cellular biomass (Antoniewicz 2018).

1.7.3 Flux Calculations and Statistical Analysis

The goal of ^{13}C-MFA is to find a set of metabolic fluxes that minimizes the difference between the measured and predicted ^{13}C labeling patterns of intracellular metabolites or proteinogenic amino acids as constrained by the external rates and reaction network stoichiometry (Antoniewicz 2015a). In the past decade, several software packages have been developed and made publicly available that can perform ^{13}C-MFA. Users input their metabolic model and experimental data into the software. Then, the software calculates metabolic fluxes (with associated confidence intervals) and performs a goodness-of-fit analysis (Antoniewicz 2018).

1.7.4 Examples

In past studies, metabolic flux analysis has been used to determine the influence of light on the carbon and energy metabolism of *Chlorella pyrenoidosa* under autotrophic, mixotrophic, and cyclic light-autotrophic/dark-heterotrophic conditions. Results showed that 1) the glycolytic pathway, tricarboxylic acid cycle and mitochondrial oxidative phosphorylation maintained high flux during illumination; 2) the theoretical yields of biomass on ATP were greatest for heterotrophic growth, followed by mixotrophic and autotrophic growth; and 3) a significant amount of ATP was used for cell maintenance. At the time, these results provided valuable information about microalgal energetics and guidance to improve cell culture performance (Yang, Hua, and Shimizu 2000).

Over the years, ^{13}C-MFA methods have advanced significantly. Now, methods have been developed to describe various systems including: model organisms (Hayakawa, Matsuda, and Shimizu 2018; Kitamura, Toya, and Shimizu 2019), non-model organisms (Cordova et al. 2017), native (i.e. wild-type) microbes (C. P. Long et

al. 2017), and engineered organisms (Schwechheimer, Becker, Peyriga, Portais, and Wittmann 2018); dynamic labeling (Ma et al. 2014); mono- and co-culture (Gebreselassie and Antoniewicz 2015); and liquid and solid media (Wolfsberg, Long, and Antoniewicz 2018). However, to date, nearly all ^{13}C-MFA studies have used chemically defined media (Schwechheimer, Becker, Peyriga, Portais, and Wittmann 2018). Therefore, there is a need to develop a methodology to perform ^{13}C-MFA for cells growing in the presence of yeast extract since many industrial processes use complex media (Zamboni 2011). Since *E. coli* already has a well characterized physiology in minimal media (C. P. Long, Gonzalez, et al. 2016) and is industrially relevant, it was chosen as the test organism for method development.

1.8 Aims and Outline of this Dissertation

The overarching goal of this dissertation is to show that ^{13}C isotopic tracers can be used in a wide variety of situations and provide valuable information about metabolism and species interactions. To achieve this goal, two aims were developed. Aim #1 was to use ^{13}C tracers to obtain a quantitative understanding of *Chlorella vulgaris*'s metabolism in multiple culture conditions while being subjected to cycling substrate availability and nitrogen depletion stress. Aim #2 was to develop a ^{13}C metabolic flux analysis methodology for elucidating fluxes in complex media.

Isotopic tracers were critical to the characterization of microalgal biomass, quantification of microalgal starch turnover and carbohydrate secretion, verification of microalgal-microbe interactions in co-culture, and elucidation of *E. coli*'s metabolic fluxes during growth on glucose and yeast extract. The experimental and analytical approaches used here can be easily extended to other biological systems to assist

researchers with metabolic and physiological studies. The key findings and accomplishments of my work are described in the following chapters:

- **Chapter 2** describes the development of a method to measure carbohydrate composition and stable-isotope labeling in microalgal biomass using gas chromatography/mass spectrometry (GC/MS). The method consists of two-stage hydrochloric acid hydrolysis, followed by chemical derivatization of the released monomer sugars, and then quantification by GC/MS. Fully ^{13}C-labeled sugars are used as internal standards for composition analysis. This is a convenient, reliable, and accurate single-platform workflow which has advantages over existing methods and opens new opportunities to study carbohydrate metabolism of microalgae (and other microbes) under autotrophic, heterotrophic, and mixotrophic conditions using isotopic tracers such as $^{2}H_2O$ and ^{13}C-glucose.
- **Chapter 3** addresses the need for detailed analysis of microalgal metabolism in a variety of culturing conditions. The growth rate, glucose consumption rate, carbon dioxide and oxygen consumption/production rates, biomass yields, and biomass composition were determined for autotrophic, heterotrophic, and mixotrophic conditions. Light cycling and nitrogen depletion were shown to cause major changes in metabolism and biomass composition. The data presented in this Chapter was subsequently used to establish a genome-scale metabolic model of *Chlorella vulgaris* UTEX 395. At its time of creation, this model was the most comprehensive for any eukaryotic photosynthetic organism.

- **Chapter 4** demonstrates the usefulness of isotopic tracers for understanding an organism's metabolism in monoculture and the interactions between organisms in co-culture. $^{12}C/^{13}C$ labeling switch and pulse-chase experiments were used to study *Chlorella vulgaris* UTEX 395's highly dynamic metabolism. Polysaccharide secretion was shown as a major source of starch turnover. For a light cycled autotrophic culture, the supernatant contained 23% and 20% of total glucose equivalents during the nitrogen replete and deplete phases, respectively. We determined that *Chlorella vulgaris* does not grow on its own secreted polysaccharides; however, using soil samples and spent algal medium, a microbiome was obtained which grew on the secreted microalgal polysaccharides. During co-culture, the microalgae consumed carbon dioxide and secreted polysaccharides while the microbiome cells consumed polysaccharides and released carbon dioxide. This relationship was beneficial for the microalgae because the local carbon dioxide concentration was increased, thus promoting photosynthesis over photorespiration.
- **Chapter 5** presents a novel approach for elucidating metabolic fluxes in complex media. To date, chemically defined media (i.e. minimal media) have been used in nearly all ^{13}C-MFA studies. However, in practice, engineered strains, such as *E. coli,* are often grown in complex media that contain poorly characterized components such as yeast extract. A two-phase metabolic network model with appropriate dilution reactions (i.e. to account for yeast extract components entering metabolism) was developed to calculate metabolic fluxes in the presence of yeast extract. The flux

maps established with this model provided critical new insights that can be used for better design of media formulations, as well as better design of *E. coli* strains grown in complex media.

- **Chapter 6** reviews the main findings, conclusions, and applications of the work performed for this dissertation and addresses possible directions for future work.
- **The Appendices** provide additional figures and tables to support the main chapters. In addition, raw isotopic labeling profiles, metabolic models, and tabulated metabolic fluxes are provided.

Chapter 2

NOVEL GAS CHROMATOGRAPHY/MASS SPECTROMETRY METHOD FOR MEASURING THE COMPOSITION AND STABLE-ISOTOPE LABELING OF ALGAL BIOMASS CARBOHYDRATES

Brian McConnell and Maciek Antoniewicz

Reproduced with permission from: McConnell BO, Antoniewicz MR (2016) Measuring the Composition and Stable-Isotope Labeling of Algal Biomass Carbohydrates via Gas Chromatography/Mass Spectrometry. *Anal Chem* 88(9):4626-4628.

2.1 Introduction

Algae are a diverse group of eukaryotic organisms that can fix carbon dioxide through the process of photosynthesis. Many algae species can accumulate large amounts of carbohydrates. For example, under nitrogen starvation, the starch content of algal biomass can reach more than 50% of cell dry weight (Ho et al. 2013; Illman, Scragg, and Shales 2000; Zhang et al. 2014; Zhu et al. 2014). As a result, there is growing interest in algal biomass as a renewable carbohydrate resource for sustainable biofuel applications (Rosenberg et al. 2008; Chen et al. 2013; John et al. 2011) Accurate and precise quantification of algal biomass composition is important for screening algae species and evaluating their potential economic value in biofuel processes (Laurens et al. 2012).

The two predominant approaches for measuring algal carbohydrates are a colorimetric phenol sulfuric acid method and a two-stage sulfuric acid hydrolysis method. The colorimetric method was developed to measure the total carbohydrate

content of biomass (Dubois et al. 1956). Although this procedure is rapid and relatively straightforward, it does not distinguish between different sugars. In addition, not all sugars exhibit a similar colorimetric response, so the method can overestimate or underestimate the true carbohydrate content. An alternative sulfuric acid hydrolysis method was developed at the National Renewable Energy Laboratory (NREL) for routine carbohydrate analysis of cellular biomass (Wychen and Laurens 2015). This procedure is based on two-step acid hydrolysis, 1 h at 30 °C in 72% sulfuric acid, followed by 1 h at 121 °C in 4% sulfuric acid, to break down biomass carbohydrates into monomer sugars, which are then quantified by high-performance liquid chromatography (HPLC). Altered versions of the NREL procedure have also been proposed that reduce the degradation of sugars (Moxley and Zhang 2007).

In this contribution, we have developed an improved method for quantitative studies of carbohydrates in algal biomass. The method is based on two-stage hydrochloric acid hydrolysis, followed by chemical derivatization of the released sugars and quantification by gas chromatography/mass spectrometry (GC/MS). Carbohydrate quantification is based on isotope ratio analysis using sugar-specific standards which are isotopically unique, giving a high degree of confidence in the results. Our method is independent of growth conditions (i.e., autotrophic, mixotrophic, heterotrophic), provides precise quantification of algal biomass carbohydrates, and enables determination of stable-isotope labeling of individual monomer sugars in ^{2}H and ^{13}C tracer studies (not possible with current methods). The ability to measure stable-isotope labeling opens new opportunities for more-detailed investigations of algal metabolism using metabolic flux analysis and tracers such as $^{2}H_2O$ and ^{13}C-glucose (Antoniewicz 2015b). Overall, our approach offers a simplified

and convenient single-platform (GC/MS) workflow. We believe the presented method will have widespread applicability in biology and bioengineering systems (Antoniewicz, Stephanopoulos, and Kelleher 2006; Chang et al. 2011).

2.2 Experimental Section

2.2.1 Materials and Methods

2.2.1.1 Chemicals and Media

Chemicals were purchased from Sigma-Aldrich (St. Louis, MO). [U-^{13}C]Glucose, [U-^{13}C]xylose, [U-^{13}C]galactose, [U-^{13}C]mannose, [U-^{13}C]arabinose, and $^{2}H_2O$ were purchased from Cambridge Isotope Laboratories (Andover, MA). Growth media were purchased from PhytoTechnology Laboratories (Shawnee Mission, KS).

2.2.1.2 Strain and Culture Conditions

Chlorella vulgaris UTEX 395 was obtained from the Culture Collection of Algae at the University of Texas at Austin (Austin, TX). *C. vulgaris* was grown autotrophically at room temperature in BBM minimal medium (Phukan et al. 2011) (14/10 light-dark cycling, 80 μE/m^2/s light), or heterotrophically in BBM minimal medium supplemented with 5 g/L of glucose (in darkness). For all procedures, samples containing the equivalent of 1 mL of a culture at OD_{600} = 1 (~0.20 mg of cell dry weight) were used. All biomass samples were washed twice with glucose-free BBM medium prior to analysis.

2.2.1.3 Gas Chromatography/Mass Spectrometry (GC/MS)

GC/MS analysis was performed on an Agilent 7890B GC system equipped with a DB-5MS capillary column (30 m, 0.25 mm i.d., 0.25 μm-phase thickness; Agilent J&W Scientific), connected to an Agilent Model 5977A mass spectrometer operating under ionization by electron impact (EI) at 70 eV. An injection volume of 1 μL was used at a split ratio of 1:2 or 1:10. A split ratio of 1:2 was used to measure sugars that are less abundant in algal biomass (xylose, arabinose, and mannose), and a split ratio of 1:10 was used for glucose and galactose, which are generally more abundant. Helium flow was maintained at 1 mL/min. The source temperature was maintained at 230 °C, the MS quad temperature at 150 °C, the interface temperature at 280 °C, and the inlet temperature at 250 °C. The column started at 80 °C and held for 2 min, increased to 280 °C at a rate of 10 °C/min, and held for 12 min. The sugar derivatives separated on the GC column with the following elution times: arabinose (12.8 min), xylose (13.1 min), mannose (15.2 min), glucose (15.3 min), and galactose (15.5 min) (see the Supporting Information for a representative GC/MS chromatogram). For quantitative analysis, the m/z 284 fragments of arabinose and xylose (containing first four C atoms of the sugars (Cordova and Antoniewicz 2016)) were measured in single ion monitoring (SIM), and the m/z 370 fragments of mannose, glucose, and galactose (containing first five C atoms of the sugars (C. Long and Antoniewicz 2014)) were monitored.

2.2.1.4 Derivatization of Monomer Sugars

The aldonitrile propionate derivatization method was used to derivatize the sugars (Antoniewicz, Kelleher, and Stephanopoulos 2011). Briefly, 50 μL of 2 wt % hydroxylamine hydrochloride in pyridine was added to dried samples, which were

then incubated for 60 min at 90 °C. Next, 100 μL of propionic anhydride was added followed by incubation at 60 °C for 30 min. The samples were then immediately transferred to injection vials for GC/MS analysis.

2.2.1.5 Acid Hydrolysis of Algal Biomass

Two alternative acid hydrolysis methods were evaluated in this work: the NREL sulfuric acid method and a hydrochloric acid method. For sulfuric acid hydrolysis, the following two-step procedure was used: 1 h at 30 °C in 50 μL of 72 wt % sulfuric acid, followed by 1 h at 121 °C in 4 wt % sulfuric acid. After hydrolysis, the samples were cooled to room temperature and neutralized with 200 μL of 5 N sodium hydroxide (NaOH) solution. Salts were then precipitated via the addition of 500 μL of cold (-20 °C) ethanol. After vortexing and centrifugation, the supernatants were collected and dried under an air flow at 65 °C. For hydrochloric acid (HCl) hydrolysis, the following two-step procedure was used. First, 50 μL of 6 N HCl was added to dry samples and the samples were subjected to incubation for 1 h at 30 °C. Next, 250 μL of water was added, thus diluting the acid to 1 N, and the samples were incubated for 1 h at 110 °C. The samples were cooled to room temperature, neutralized with 50 μL of 5 N NaOH, and dried under air flow at 65 °C. For analysis of sugar composition, 20 μL of a solution containing fully ^{13}C-labeled sugars (100 mM [U-^{13}C]glucose, 12 mM [U-^{13}C]xylose, 12 mM [U-^{13}C]arabinose, 10 mM [U-^{13}C]-mannose, and 25 mM [U-^{13}C]galactose) was added after acid neutralization.

2.2.1.6 Measuring Degradation of Carbohydrates

To determine the fraction of sugars degraded by acid treatment, 20 μL of a solution containing unlabeled sugars (100 mM glucose, 12 mM xylose, 12 mM

arabinose, 10 mM mannose, and 25 mM galactose) was dried under air at 65 °C. Next, 50 µL of HCl at different concentrations (0, 0.1, 0.5, 1, 2, 4, 6 N) was added and the samples were incubated for 1 h at 110 °C. The samples were then cooled to room temperature and neutralized with NaOH. Next, 20 µL of a solution containing fully ^{13}C-labeled carbohydrates (see above) was added and the samples were dried under air at 65 °C. After derivatization, GC/MS analysis was performed. The measured mass isotopomer distributions were corrected for natural abundances using the method of Fernandez et al. (Fernandez et al. 1996). For each sugar, the fraction recovered was then determined as M_0/M_n, where M_0 is the abundance of unlabeled mass isotopomer and M_n is the abundance of fully labeled mass isotopomer.

2.2.1.7 Effect of Hydrolysis Condition on Carbohydrate Quantification

The procedure was also applied to algal biomass samples to determine the effect of hydrolysis condition on the apparent amount of sugars quantified in algal biomass. In short, 50 µL of HCl at different concentrations (0, 0.1, 0.5, 1, 2, 4, 6 N) was added to dry biomass and the samples were incubated for 1 h at 110 °C. The samples were then cooled to room temperature and neutralized with NaOH. Next, 20 µL of a solution containing fully ^{13}C-labeled sugars was added and the samples were dried under air at 65 °C. After derivatization, GC/MS analysis was performed, and the isotope ratio M_0/M_n was determined.

2.2.1.8 Carbohydrate Quantification

The amount of each sugar in algal biomass, expressed as percentage of cell dry weight, was determined as follows:

$$amount\ (\%DW) = \frac{M_0}{M_n} \times MW\ \left(\frac{g}{mol}\right) \times C_{IS}\ (mM)\ \times \frac{20\mu L/DW(mg_{DW})}{10^6} \times 100\% \quad (2.1)$$

where C_{IS} is the concentration of the ^{13}C-labeled sugar in the internal standard solution (e.g., 100 mM [U-^{13}C]glucose), MW is the molecular weight of the sugar (e.g., 180 g/mol for glucose), and DW is the amount of dry biomass used in the procedure (here, we used 0.20 mg of dry weight for each procedure).

2.2.1.9 Stable-isotope Labeling Quantification

To determine the isotopic labeling (^{13}C or ^{2}H) of algal biomass sugars in tracer experiments, performed with $^{2}H_2O$ and [U-^{13}C]glucose, algal biomass was hydrolyzed and then analyzed by GC/MS. The measured mass isotopomer distributions were corrected for natural abundances and the molar percent enrichment was determined as follows:

$$MPE = \sum \frac{i \times M_i}{n} \tag{2.2}$$

where n is the number of carbon atoms (or hydrogen atoms) in the measured fragment derived from the sugar. Specifically, for the m/z 284 fragment, n = 4 C atoms and 3 H atoms; and for the m/z 370 fragment, n = 5 C atoms and 4 H atoms.

2.3 Results and Discussion

2.3.1 Biomass Hydrolysis by Acid Treatment

The main objective of this work was to develop a GC/MS-based method for measuring both the composition of carbohydrates in algal biomass, as well as stable-isotope labeling of individual monomer sugars for metabolic flux analysis studies. For both applications, biomass carbohydrates must first be hydrolyzed into monomer sugars to be detected by GC/MS. First, we evaluated the two-step sulfuric acid hydrolysis method developed at NREL (1 h at 30 °C in 72 wt % sulfuric acid,

followed by 1 h at 121 °C in 4 wt % sulfuric acid). For GC/MS analysis, sugars were derivatized using the aldonitrile propionate method previously developed (Antoniewicz, Kelleher, and Stephanopoulos 2011).

C. vulgaris was used as a model algal system. After hydrolyzing algal biomass using the sulfuric acid method, the samples were neutralized with NaOH, evaporated, derivatized, and analyzed by GC/MS. This procedure, however, resulted in low signal intensities (total ion counts (TIC) of $< 10^3$) for the expected sugars. We hypothesized that salts formed during acid neutralization could be interfering with sugar derivatization. Thus, we included a salt-precipitation step in the protocol, by adding cold ethanol and separating out the salts by centrifugation. As expected, the signal intensities increased significantly (TIC $\approx 10^4$). However, the procedure was still cumbersome, because the evaporation step required more than 5 h to complete.

Next, we developed an alternative hydrolysis method, based on two-step hydrochloric acid hydrolysis: 1 h at 30 °C in 6 N HCl, followed by 1 h at 110 °C in 1 N HCl. After the hydrolysis step, samples were neutralized with NaOH, evaporated, derivatized and analyzed by GC/MS. With this approach, we obtained significantly higher signal intensities (TIC $> 10^5$). In addition, the evaporation step was completed within 1 h. Thus, overall the hydrochloric acid method was determined to offer several advantages over the sulfuric acid method and was selected for further optimization.

2.3.2 Measuring Degradation of Monomer Sugars

A delicate balance must be struck when optimizing the procedure for biomass hydrolysis (Moxley and Zhang 2007). On the one hand, the hydrolysis method must be harsh enough to ensure that all biomass carbohydrates are broken down into their respective monomer sugars. On the other hand, the hydrolysis procedure must not be

too harsh, or a degradation of sugars will occur. First, we validated that the first step in the hydrolysis procedure (1 h at 30 °C in 6 N HCl) did not result in sugar degradation. However, we hypothesized that the second step in the procedure at 110 °C may result in sugar degradation. Thus, we quantified the fractions of xylose, arabinose, mannose, glucose, and galactose recovered after treatment for 1 h at 110 °C in 0, 0.1, 0.5, 1, 2, 4, and 6 N HCl. Figure 2.1A shows that, for acid concentrations up to 1 N, < 8% degradation occurred for all sugars (> 92% recovered). Overall, xylose was most prone to acid degradation, resulting in 30% degradation at 2 N HCl, and > 90% degradation at 6 N HCl. Galactose was least prone to acid degradation, with 10% degradation at 2 N HCl, and 50% degradation at 6 N HCl.

2.3.3 Effect of Hydrolysis Condition on Carbohydrate Quantification

Next, we tested the effect of the hydrolysis condition on the apparent amount of sugars quantified in algal biomass. Algal biomass was hydrolyzed for 1 h at 110 °C in 0, 0.1, 0.5, 1, 2, 4, and 6 N HCl and the amount of each sugar in biomass was quantified by GC/MS using fully ^{13}C-labeled monomer sugars as internal standards. Figure 2.1B shows the amount of each sugar measured, expressed as the weight percentage of dry biomass. For all sugars, the highest apparent amount of sugar quantified was for the 1 N hydrolysis condition. For concentrations of hydrochloric acid higher than 1 N the apparent amount of biomass sugars decreased in a manner

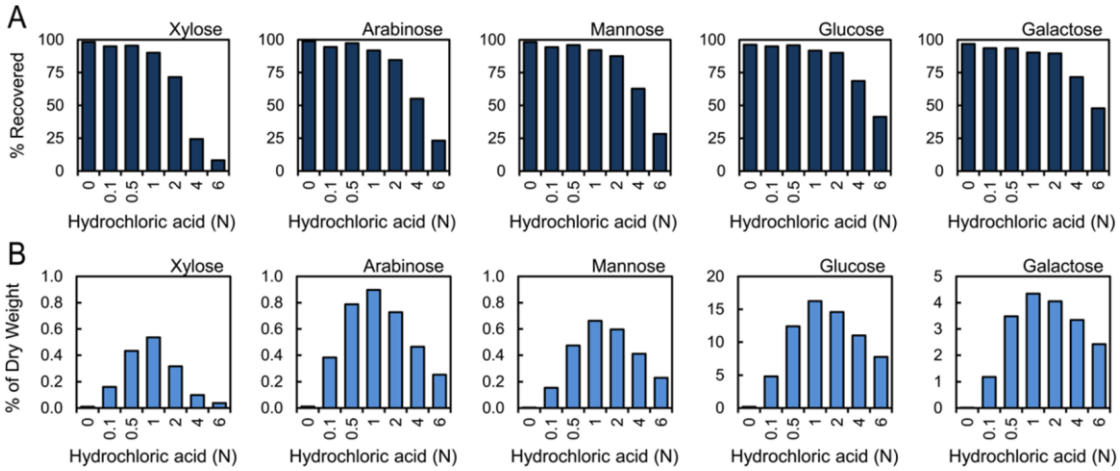

Figure 2.1 (A) Degradation of sugars treated with hydrochloric acid (HCl) at different concentrations at 110 °C for 1 h. Significant degradation occurred for acid concentrations above 1 N. (B) Effect of hydrolysis condition on the apparent amount of carbohydrates quantified in algal biomass. Incomplete hydrolysis was observed for acid concentrations below 1 N, and significant degradation of sugars occurred for acid concentrations above 1 N.

similar to that observed for Figure 2.1A, thus suggesting that degradation of the sugars was occurring. For acid concentrations of < 1 N, the apparent amount of biomass sugars quantified decreased, likely due to an incomplete breakdown of the biomass carbohydrates into monomer sugars. Thus, overall, we determined that hydrolysis for 1 h at 110 °C in 1 N hydrochloric acid was optimal.

2.3.4 Quantifying Carbohydrate Composition

We then applied the optimized two-step hydrochloric acid hydrolysis approach to quantify carbohydrate composition of *C. vulgaris* grown autotrophically. The composition was measured on day 7 (before nitrogen starvation), and on days 14 and 21 (during nitrogen starvation). (See Figure 2.2.) During nitrogen starvation, the glucose content (starch) of biomass increased significantly from 12% on day 7 to 58%

on day 21. The other significant sugar in biomass was galactose, which increased from 4% on day 7 to 7% on day 14, but then decreased to 6% on day 21. The decrease in galactose content on day 21 suggests that a net breakdown of chloroplasts was occurring (i.e., chloroplasts membranes are predominantly galactolipids and not phospholipids) (Block et al. 1983).

The amount of xylose, arabinose, and mannose increased from ~1% to 3%. These results are in good agreement with results reported previously for related algae species grown under similar conditions (Ho et al. 2013; Illman, Scragg, and Shales 2000; Zhang et al. 2014; Zhu et al. 2014).

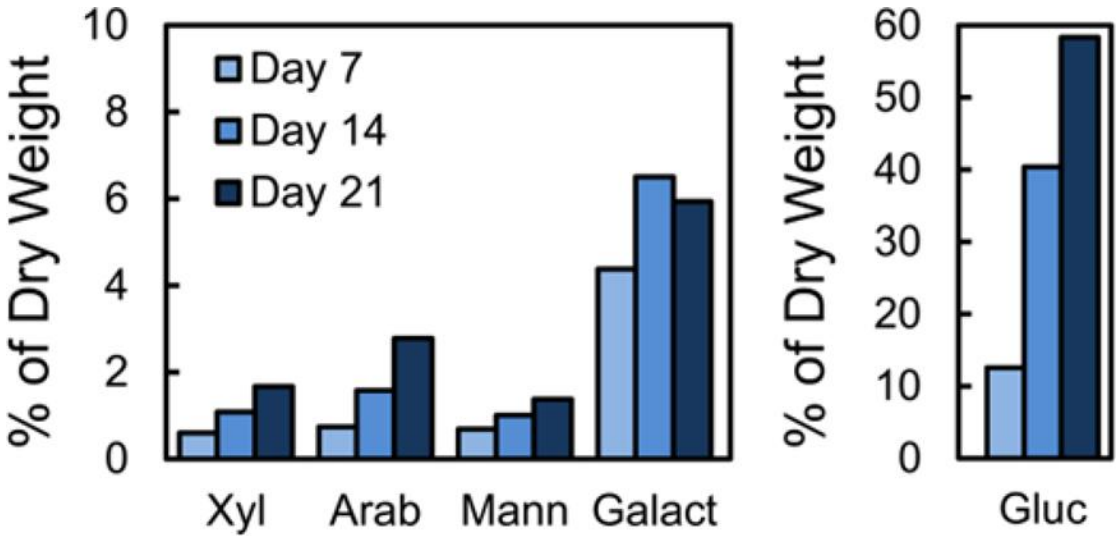

Figure 2.2 Composition of biomass carbohydrates of *C. vulgaris* grown autotrophically for 3 weeks. Day 7 represents nitrogen-replete conditions, and days 14 and 21 represent nitrogen-depleted conditions.

2.3.5 Quantifying Stable-Isotope Labeling

To demonstrate that the developed method can also be applied for stable-isotope tracing studies, e.g., for metabolic flux analysis (Antoniewicz 2015a), labeling

experiments were performed with *C. vulgaris* grown autotrophically in media containing 9% and 18% deuterated water (^2H_2O), and grown heterotrophically in medium containing 9% and 18% [U-^{13}C]glucose. Algal biomass from these tracer experiments was hydrolyzed and isotopic labeling was measured by GC/MS. As shown in Figure 2.3, for the tracer experiments with 9% and 18% ^2H_2O, the ^{2}H-labeling of biomass sugars was 9.5% ± 0.3% and 18.3% ± 0.3%, respectively. This result confirms that the developed hydrolysis procedure did not result in the breakage of C-H bonds and thus can be applied in ^{2}H-tracer studies. The fact that the measured ^{2}H-labeling matched well with expected values also suggests that kinetic isotope effects were insignificant. For the tracer experiments with 9% and 18% [U-^{13}C]glucose (98.5 at. % isotopic purity), the ^{13}C-labeling of sugars was 8.8% ± 0.3% and 17.6% ± 0.4%, respectively, thus confirming that ^{13}C labeling can be accurately measured. Taken together, these results demonstrate that the approaches developed in this work can be applied in stable-isotope labeling studies.

2.4 Conclusions

The method for carbohydrate analysis of algal biomass developed here is convenient and accurate. It is based on a single analytical platform (gas chromatography/mass spectrometry (GC/MS)) that is widely accessible; as such, the analysis should be easily accomplished in many laboratories. The ability to measure both the isotopic labeling of carbohydrates and carbohydrate composition opens new opportunities for comprehensive investigations of algal physiology and metabolism. The presented approach may also be applicable to other biological systems, for example, to investigate glycogen metabolism in microbial and mammalian systems. In

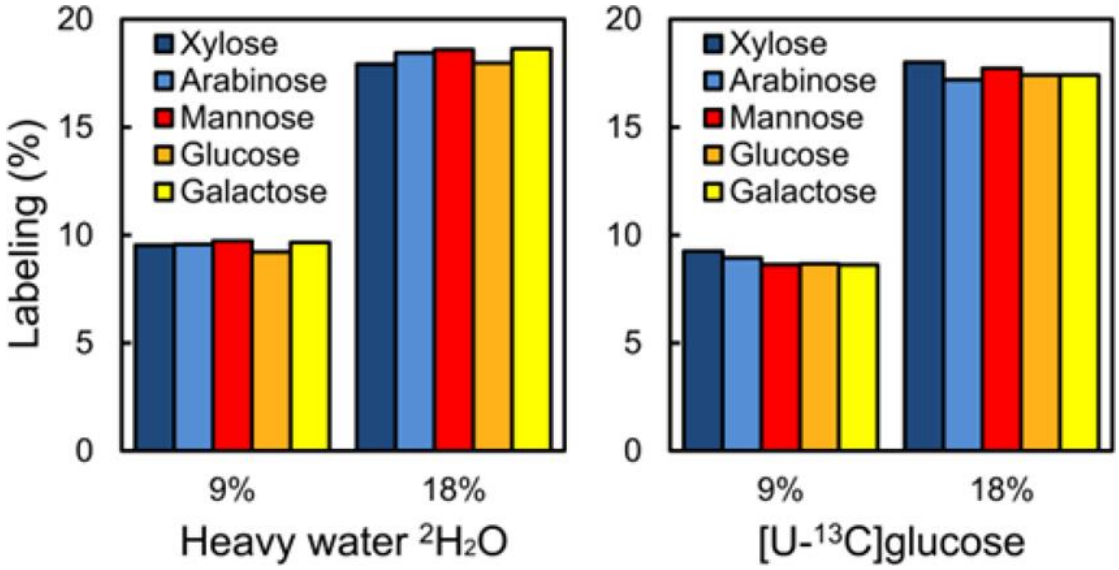

Figure 2.3 Stable-isotope labeling of *C. vulgaris* biomass carbohydrates for cells grown autotrophically in media containing 9% and 18% $^{2}H_2O$ (left), and heterotrophically in media containing 9% and 18% [U-^{13}C]glucose (right).

summary, we believe that the developed method will find widespread use in systems biology and bioengineering studies.

Chapter 3

CHARACTERIZATION OF THE GREEN MICROALGAE *CHLORELLA VULGARIS* UTEX 395 DURING AUTOTROPHIC, HETEROTROPHIC, AND MIXOTROPHIC GROWTH CONDITIONS

Data included in this chapter is reprinted with permission from: Zuñiga, Cristal, Chien-Ting Li, Tyler Huelsman, Jennifer Levering, Daniel C. Zielinski, Brian O. McConnell, Christopher P. Long, Eric P. Knoshaug, Michael T. Guarnieri, Maciek R. Antoniewicz, Michael J. Betenbaugh, and Karsten Zengler. 2016. "Genome-Scale Metabolic Model for the Green Alga *Chlorella vulgaris* UTEX 395 Accurately Predicts Phenotypes under Autotrophic, Heterotrophic, and Mixotrophic Growth Conditions." Plant Physiology 172 (1): 589–602. Journal URL: www.plantphysiol.org.

3.1 Introduction

One of the most pressing grand challenges facing humanity is to sustainably support a human population that is predicted to increase to 9 billion people by mid-century (Cohen 2003). Meeting this challenge will require the development of new and innovative renewable production systems. One approach to address the problems of dwindling reserves of non-renewable resources and rising levels of carbon dioxide (CO_2) in the atmosphere is to capture concentrated carbon dioxide emerging from waste treatment facilities, petroleum refineries, coal and other energy sources, and convert the carbon dioxide into useful products, including dietary supplements, medicinals, and biofuels (Desai and Atsumi 2013; Perez-Garcia et al. 2010; J. Liu and Chen 2014; Phukan et al. 2011). Microalgae represent a potential renewable source of such products due to their ability to use light to fix carbon dioxide into biomolecules.

Chlorella is a genus of unicellular, non-motile, photosynthetic, eukaryotic microalgae which can survive in fresh and salt water (J. Liu and Chen 2014). In regards to microalgal biodiesel production economics, non-polar lipid content is the most important factor (Davis, Aden, and Pienkos 2011) and one of the best lipid producing *Chlorella* species is *C. vulgaris* (Scott et al. 2010). *Chlorella vulgaris* UTEX 395 is a model green microalga with great biodiesel production potential and a sequenced genome (Guarnieri et al. 2013). However, due to inefficiencies in carbon metabolism, critical technical bottlenecks remain to economic production of desirable products. Therefore, it is important to obtain a quantitative understanding of *Chlorella vulgaris* UTEX 395 metabolism and physiology.

This work aims to address fundamental questions about microalgal physiology under different growth conditions. To accomplish those aims, cell growth, oxygen and carbon dioxide production and consumption, and biomass composition were analyzed for *Chlorella vulgaris* UTEX 395 in three growth conditions: autotrophic, heterotrophic, and mixotrophic. Three growth conditions were analyzed because previous work has shown that the biomass composition of algae depends strongly on the culturing condition and phase of growth (Guarnieri et al. 2013).

In general, for most microorganisms, protein, carbohydrates, and lipids are the most abundant and commonly quantified biomass components (C. P. Long and Antoniewicz 2014; McConnell and Antoniewicz 2016). Gravimetric solvent extraction is the classic method used to determine microalgal lipid content; however, many variations of solvent or solvent mixtures have been used (Laurens et al. 2012). Another problem with solvent extraction is that the relative amount of saturated and unsaturated lipids changes during a culture, so the extraction efficiency may not be

consistent (Guarnieri et al. 2013; Laurens et al. 2012). Microalgal protein content is commonly determined by an elemental (carbon, hydrogen, nitrogen, sulfur) analyzer or colorimetric methods, but neither procedure identifies the amino acid profile (Becker 1994; Laurens et al. 2012). Microalgal carbohydrate content is commonly determined by colorimetric methods or enzymatic hydrolysis. Both methods only quantify glucose while other monosaccharides like rhamnose, arabinose, xylose, mannose, and galactose are not account for. Being photosynthetic, algae contain pigments. The two most important types of pigments are chlorophylls and carotenoids. There is variation between species, but in general, chlorophylls are 0.5-1.5 % dry weight and carotenoids are 0.1-2 % dry weight (Becker 1994).

The previously described microalgal biomass characterization methods are empirical in nature, some developed decades ago, and small variations in procedures give largely differing results (Laurens et al. 2012). This makes comparison between microalgal species and laboratories difficult. Therefore, accurate analytical characterization methods are necessary for microalgal biomass characterization. The fatty acid, amino acid, and monosaccharide profiles are important to determine since they set the microalgae's economic value and are required for quantitative flux analysis modeling (Guarnieri et al. 2013).

The National Renewable Energy Laboratory (NREL) has stated that a robust system for biomass characterization is needed. The system should be accurate, precise, reproducible, organism independent, and require small sample size (Guarnieri et al. 2013). Recently, gas chromatography/mass spectrometry (GC/MS) methods have been developed to analyze amino acids, fatty acids, and carbohydrates from biological

samples (C. Long and Antoniewicz 2014; McConnell and Antoniewicz 2016). These methods have made detailed algal biomass composition analysis possible.

The physiological characterization performed in this work will support the development of genome-scale metabolic models for *Chlorella vulgaris* UTEX 395 (Zuñiga et al. 2016).

3.2 Materials and Methods

3.2.1 Materials

Growth media were purchased from PhytoTechnology Laboratories (Shawnee Mission, KS). Chemicals were purchased from Sigma-Aldrich (St. Louis, MO). ^{13}C labeled compounds were purchased from Cambridge Isotope Laboratories (Andover, MA). Media and solutions were sterile filtered with filtration units from Corning Inc (Corning, NY). Air enriched to 1% carbon dioxide was purchased from Keen Compressed Gas Company (Newark, DE).

3.2.2 Strains

Chlorella vulgaris UTEX 395 was obtained from the Culture Collection of Algae at the University of Texas at Austin (Austin, TX).

3.2.3 Culture Conditions

All cultures used Bold's Basil Medium (BBM) at 24 ± 3 °C (Bischoff and Bold 1963). BBM has a low nitrate concentration (3 mM) which allows for determination of physiological responses to nitration starvation (Andersen 2005; Phukan et al. 2011). Cells were grown in 250 mL glass bottle bioreactors (200 mL working volume) with gas sparging at 12 mL/min and continuous stirring by a stir bar. For autotrophic and

mixotrophic growth, the air was enriched with carbon dioxide such that the carbon dioxide content was 1%. The heterotrophic and mixotrophic cultures contained 10 g/L glucose as the carbon source. During autotrophic and mixotrophic growth, two 24 W fluorescent lights were used (80 $\mu E/m^2/s$) and illuminated for 14 hours per day. For heterotrophic growth, the cultures were kept in darkness.

3.2.4 Analytical Methods

Cell growth was monitored by measuring the optical density at 600 nm (OD_{600}) using a spectrophotometer (Eppendorf BioPhotometer). The OD_{600} to dry cell weight concentration was determined to be 0.159 ± 0.004, 0.19 ± 0.01, and 0.136 ± 0.005 $(g/L)/OD_{600}$ for autotrophically, heterotrophically, and mixotrophically grown algae, respectively. For heterotrophic and mixotrophic cultures, glucose concentrations were determined using a YSI 2700 biochemistry analyzer (YSI, Yellow Springs, OH). Molar percentages of carbon dioxide (CO_2, m/z 44) and oxygen (O_2, m/z 32) in the feed and off-gasses were measured by on-line mass spectrometer (Ametek Proline, Berwyn, PA) (Leighty and Antoniewicz 2012).

Analysis of biomass components was performed using GC/MS methods developed previously (C. P. Long and Antoniewicz 2014; McConnell and Antoniewicz 2016). GC/MS analysis was performed on an Agilent 7890B GC system equipped with a DB-5MS capillary column (30 m, 0.25 mm i.d., 0.25 µm-phase thickness; Agilent J & W Scientific), connected to an Agilent 5977A Mass Spectrometer. Mass isotopomer distributions were obtained by integration (Antoniewicz, Kelleher, and Stephanopoulos 2007a) and corrected for natural isotope abundances (Fernandez et al. 1996).

3.3 Results and Discussions

3.3.1 Growth Rate

Figure 3.1 shows the experimental design used in this work. For more description see the Material and Methods Section. An important consideration for the

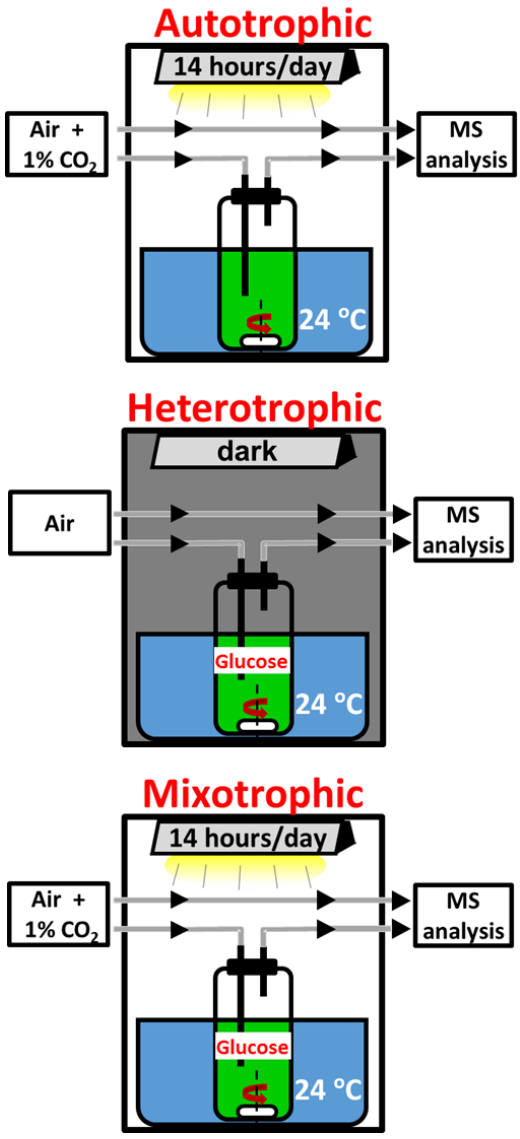

Figure 3.1 Bioreactor Design for Autotrophic (top), Heterotrophic (middle), and Mixotrophic (bottom) culturing. Continuous stirring and gas sparging (12 mL/min) into 250 mL bioreactors (200 mL working volume). Light intensity is 80 $\mu E/m^2/s$.

autotrophic and mixotrophic cultures was to perform light cycling instead of providing constant light. Previous work has shown that light cycling is important to allow the cells to oxidize the electron transporter of the photosynthetic apparatus (Sforza et al. 2012). In this work, a 14:10 light:dark cycle was found to be a good balance of light and dark time. This condition is also an industrially relevant ratio, since it is similar to summer daylight hours.

The air tubing system was designed so that a feed line went to the mass spectrometer in addition to the culture off-gas line. This allowed for accurate measurement of the change in gas composition due to microalgal metabolism.

Figure 3.2 shows the growth curves for autotrophic (1% CO_2 in air at 12 mL/min), heterotrophic (10 g/L glucose), and mixotrophic (1% CO_2 in air at 12 mL/min plus 10 g/L glucose) growth. The dashed green line represents the time at which nitrate became depleted from the medium. During the nitrogen replete phase, in all three trophic conditions, the cells grew exponentially. Table 3.1 summarizes the growth rates. The autotrophic and heterotrophic cultures had similar growth rates at 0.71 ± 0.06 and 0.63 ± 0.03 day^{-1}, respectively. In the autotrophic culture ($0.21\ g_{CO_2}/day$ feed), the cells could only fix carbon dioxide for 14 hours per day (58% of the time) whereas the heterotrophic cells could continuously consume glucose, yet they have similar growth rates in these conditions. This result suggests that the cells prefer to grow on carbon dioxide instead of glucose. The mixotrophic culture had a growth rate of 1.29 ± 0.09 day^{-1}. This corresponds approximately to the sum of the autotrophic and heterotrophic growth rates, suggesting that the cells consumed both CO_2 and glucose for growth.

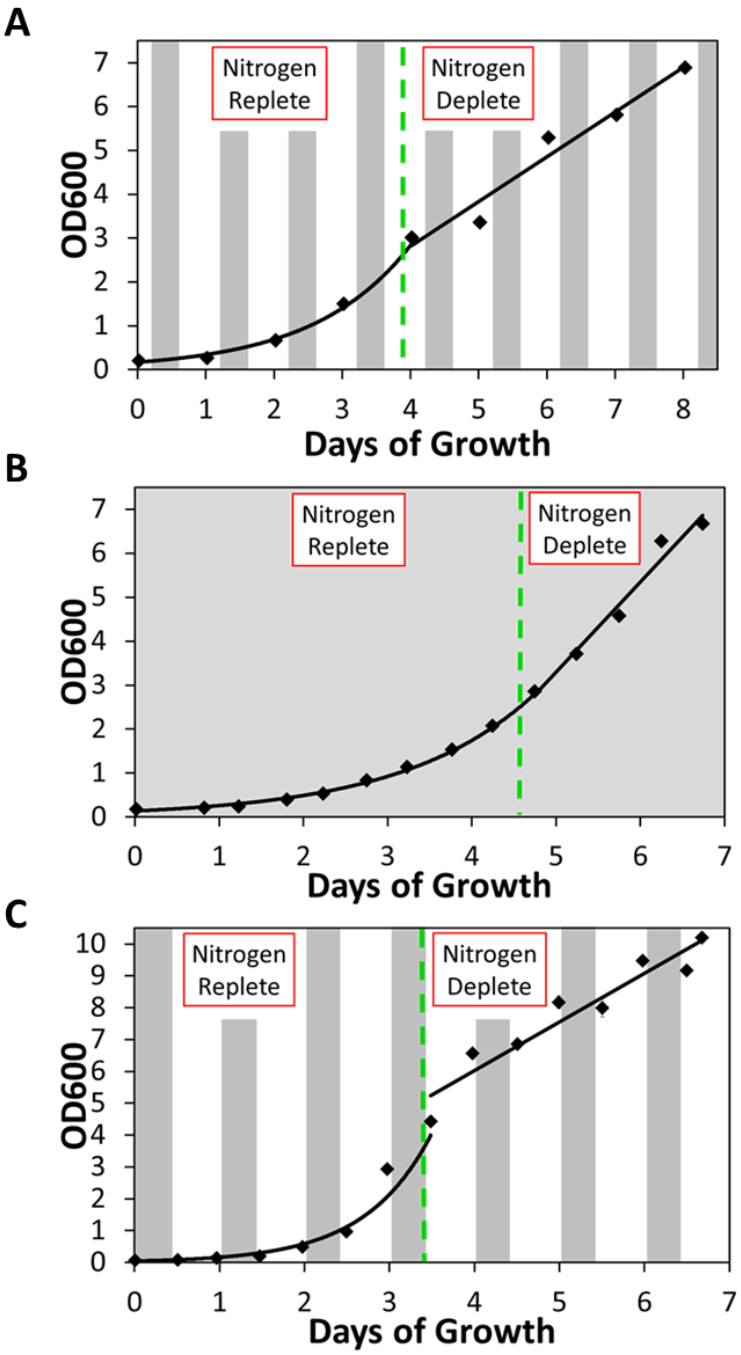

Figure 3.2 Growth Data for (A) Autotrophic, (B) Heterotrophic, and (C) Mixotrophic Conditions. The dark bars indicate time periods when the lights were turned off (the heterotrophic culture was always in darkness). The cells grow exponentially in the nitrogen replete phase. In the nitrogen deplete phase, the OD_{600} increase is approximated as linear.

Table 3.1 Summary of Growth Rates in Three Trophic Conditions during Nitrogen Replete and Depleted Phases

Condition	Nitrogen Replete (day^{-1})	Nitrogen Deplete (OD_{600}/day)
Autotrophic	0.71 ± 0.06	1.0 ± 0.1
Heterotrophic	0.63 ± 0.03	2.0 ± 0.2
Mixotrophic	1.29 ± 0.09	1.5 ± 0.2

Upon nitrate depletion (green dashed line in Figure 3.2), the OD_{600} continued to increase, although not exponentially. It has been shown before that algae can continue to incorporate carbon (and even grow) grow upon transfer into nitrogen-free medium due to their ability to breakdown chitin, which releases nitrogen for protein production (i.e. the total amount of nitrogen in the culture is not changing, the nitrogen is just being reallocated) (Guarnieri et al. 2011). Chitin is a polymer of glucosamine and structural component of the cell wall. Chlorophyll contains four nitrogen atoms and a decrease in chlorophyll content has also been observed upon nitrogen depletion for some microalgae (Merzlyak et al. 2007). (See also biomass composition analysis below for further discussion regarding the reasons for optical density change upon nitrogen depletion).

The nitrate depleted OD_{600} increase in the heterotrophic culture was linear (2.0 ± 0.2 OD_{600}/day) while in the light cycled cultures (autotrophic and mixotrophic) can be approximated as linear (1.0 ± 0.1 and 1.5 ± 0.2 OD_{600}/day, respectively). The mixotrophic culture was sampled twice a day to be able to determine the OD_{600} changes during the light and dark phases. Interestingly, even though the cells could consume glucose during the dark phase, the OD_{600} did not increase during the dark phase (in fact, it slightly decreased during the dark phase). As such, the "linear growth

rate" for the mixotrophic culture is less than in the heterotrophic culture even though they both have access to glucose.

3.3.2 Glucose Consumption in Heterotrophic and Mixotrophic Conditions

Figure 3.3 shows the glucose concentration profiles for the heterotrophic and mixotrophic cultures (Supplemental Figures B.1 and B.2 show the yield plots). For nitrogen-replete heterotrophic growth, the biomass yield on glucose was 0.34 ± 0.05 g/g. This is lower than *E. coli*'s biomass yield of 0.414 ± 0.008 g/g (C. P. Long, Gonzalez, et al. 2016). The biomass yield on glucose for nitrogen-replete mixotrophic growth was 0.52 ± 0.07 g/g. The higher biomass yield on glucose for the mixotrophic culture was expected, since cells can also fix carbon dioxide as a carbon source (which is not included in the yield calculation). The nitrogen-replete biomass specific glucose uptake rate was 1.9 ± 0.3 g/g/day and 2.5 ± 0.4 g/g/day for heterotrophic and mixotrophic growth, respectively. Thus, there was no significant difference between the glucose uptake rates for heterotrophic and mixotrophic growth. This is another example of how mixotrophic growth is the superposition of autotrophic and heterotrophic growth.

The mixotrophic dark-phase metabolism is different between the nitrogen replete and nitrogen deplete phases. During the nitrogen replete phase, glucose was consumed in the dark; however, during the nitrogen deplete phase, there was no glucose consumption in the dark. This is consistent with the fact that we did not observe an increase in OD_{600} during this time. However, the heterotrophic culture did change OD_{600} and consume glucose in darkness during the nitrogen deplete phase. These differences could be due to circadian rhythm or related to differences in protein allocation (light phase and dark phase enzymes are needed in the mixotrophic culture).

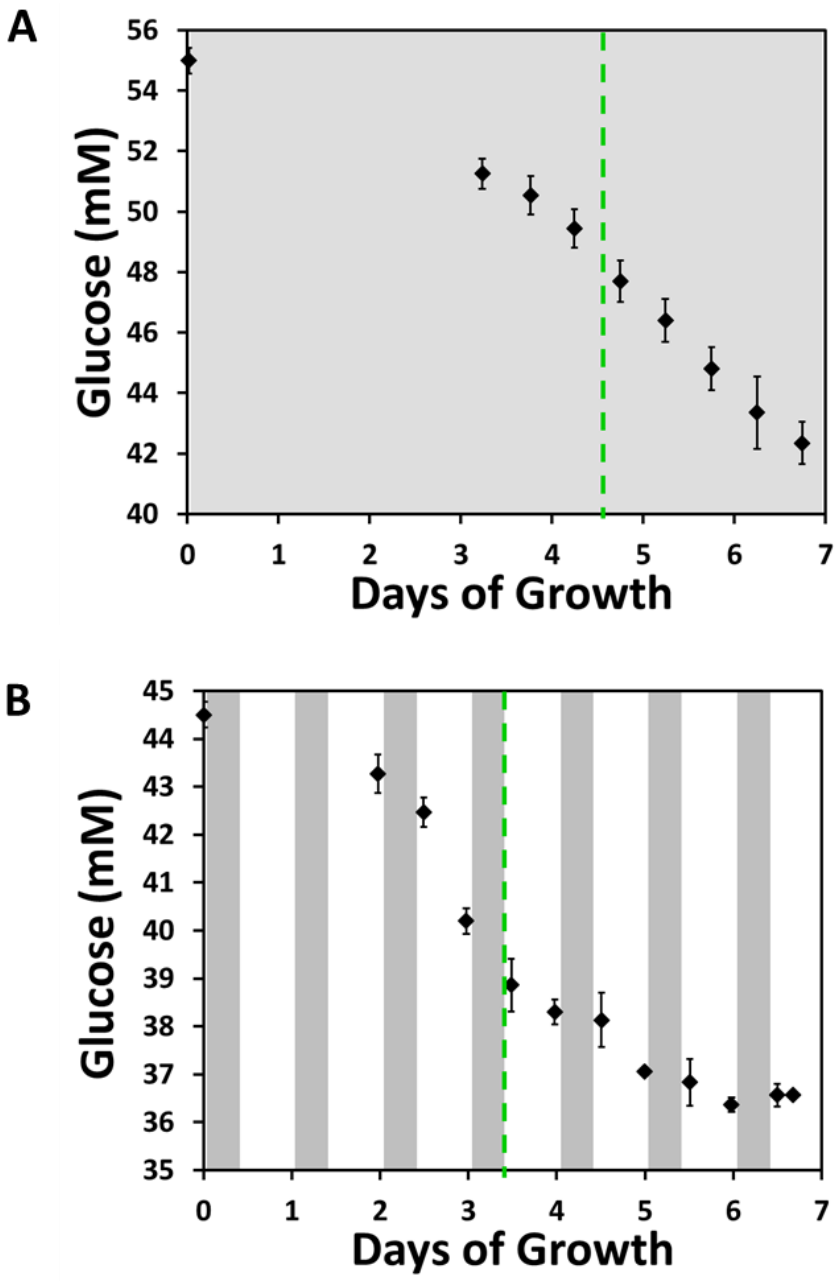

Figure 3.3 Glucose Consumption during (A) Heterotrophic and (B) Mixotrophic Growth. The dark bars indicate time periods when the lights were turned off (the heterotrophic culture was always in darkness). The vertical dashed green line indicates when nitrogen became depleted. The nitrogen-replete biomass specific glucose uptake rate is 1.9 ± 0.3 g/g/day and 2.5 ± 0.4 g/g/day for heterotrophic and mixotrophic growth, respectively.

3.3.3 Off-Gas Analysis

Figure 3.4 shows the oxygen and carbon dioxide production/consumption profiles for the three trophic conditions. As expected, we found that that the autotrophic culture consumed carbon dioxide and produced oxygen during the light phase (i.e. photosynthesis), and that the heterotrophic culture consumed oxygen and produced carbon dioxide (i.e. respiration). The autotrophic culture (Figure 3.4A) has a high carbon dioxide consumption during the first two light phases (roughly $0.019\ \mu mol_{CO_2}/g_{dw}/min$) and then the consumption decreases in subsequent days. Initially, this may be due to light attenuation and shading by other cells inside the bioreactor. Light is exponentially attenuated according to depth according to the Beer-Lambert Law:

$$I_d = I_0 e^{-kd} \tag{3.1}$$

where I_d is the photon flux density at depth d, I_0 is the incident radiation on the surface, and k is the extinction coefficient (dependent on water condition). It has been reported that because of this exponential decrease in photon flux many microalgal species have evolved in low light conditions, leading to pigments that are very effective at capturing light (Richardson, Beardall, and Raven 1983). Therefore, the cells on the perimeter of the bioreactor are expected to consume all of the available light and prevent cells in the center of the bioreactor from fixing carbon dioxide. Then, as nitrogen depletion becomes a contributing factor and the cells' growth and metabolism slows down, this results in lower carbon dioxide uptake. (Supplemental Figures B.3, B.4, and B.5 show the change in the gas carbon dioxide content.)

Another trend for the autotrophic culture was the quick transition from carbon dioxide consumption to production. Previously, in a $^{14}CO_2$ labeling study of blue-

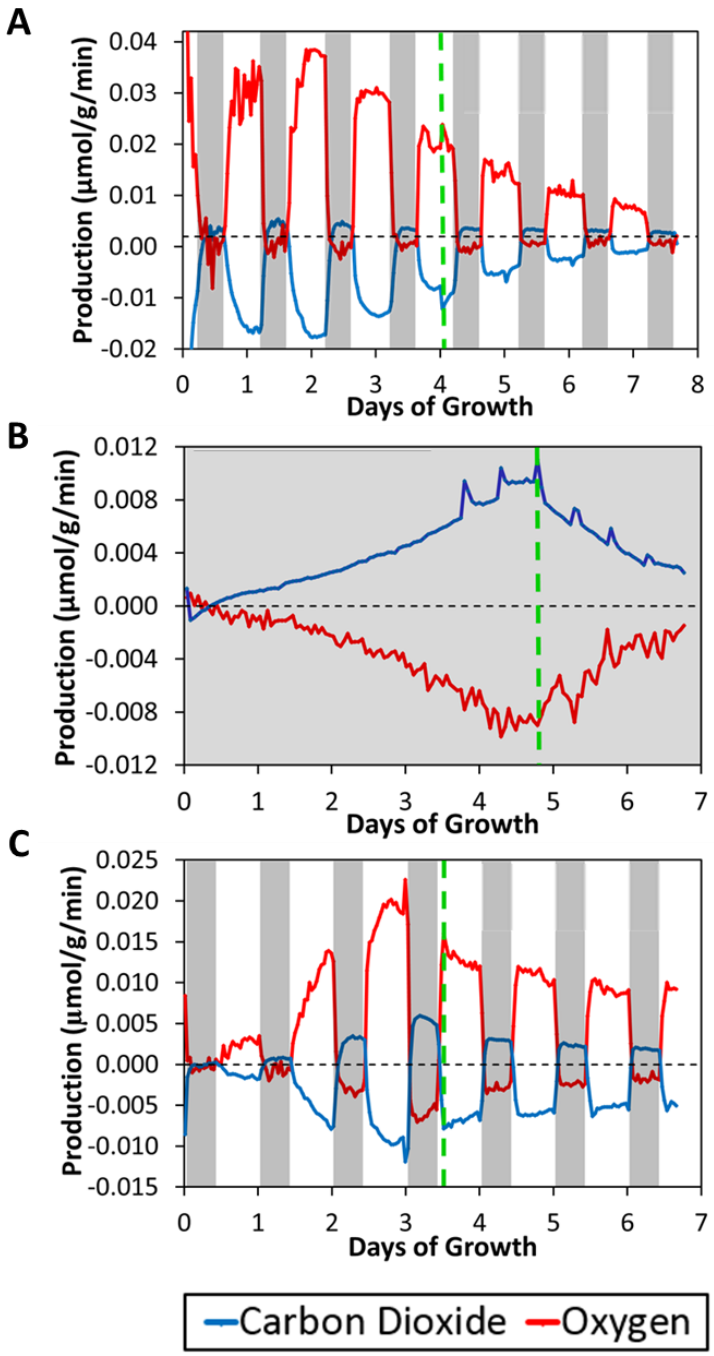

Figure 3.4 Biomass Specific Gas Production Rates for (A) Autotrophic, (B) Heterotrophic, and (C) Mixotrophic Conditions. The dark bars indicate time periods when the lights were turned off (the heterotrophic culture was always in darkness). The vertical dashed green line indicates when nitrogen became depleted.

green algae, within three minutes of introducing the labeled feed, labeling was observed in the TCA cycle (glutamate). Upon darkness, incorporation of ^{14}C into glycogen stopped almost instantaneously while incorporation of ^{14}C into aspartate lasted for less than 30 seconds. A loss of label in sugar phosphates was observed after 30 seconds (Pelroy and Bassham 1972). Green algae's response time is slower than reported in the previous study, but it confirms that photosynthetic metabolism responds very quickly to light cycling.

The respiratory quotient is defined as the ratio of carbon dioxide produced to oxygen consumed:

$$RQ = \frac{CO_{2,produced}}{O_{2,consumed}} \tag{3.2}$$

This ratio provides insight into metabolism since the oxidation of different macromolecules have different stoichiometry. The oxidation of macromolecules can be expressed as:

$$C_xH_yO_z + \left(x + \frac{y}{4} - \frac{z}{2}\right)O_2 \rightarrow xCO_2 + \left(\frac{y}{2}\right)H_2O \tag{3.3}$$

where $C_xH_yO_z$ is a macromolecule containing x carbon atoms, y hydrogen atoms, and z oxygen atoms, O_2 is oxygen, CO_2 is carbon dioxide, and H_2O is water. Using a typical composition of carbohydrates (CH_2O), the stoichiometry for the oxidation of a carbohydrate is:

$$C_1H_2O_1 + O_2 \rightarrow CO_2 + H_2O \tag{3.4}$$

thus, the respiratory quotient for carbohydrates is

$$RQ = \frac{CO_{2,produced}}{O_{2,consumed}} = \frac{1}{1} = 1. \tag{3.5}$$

Using a typical composition of lipids ($CH_2O_{0.1}$), the stoichiometry for the oxidation of lipids is:

$$C_1H_2O_{0.1} + \frac{29}{20}O_2 \rightarrow CO_2 + H_2O \quad 3.6$$

thus, the respiratory quotient for lipids is

$$RQ = \frac{CO_{2,produced}}{O_{2,consumed}} = \frac{1}{\left(\frac{29}{20}\right)} = \frac{20}{29} = 0.7. \quad 3.7$$

Protein composition and metabolism are more varied than carbohydrates and lipids, so the respiratory quotient for protein metabolism is usually approximated to be around 0.8 (McClave et al. 2003). Our measured respiratory quotient for the autotrophic culture during the nitrogen-replete light-phase was roughly -0.7 (Supplementary Figure B.6), thus indicating that a significant amount of metabolism was dedicated to lipid synthesis.

As expected for respiration, the heterotrophic culture produced carbon dioxide and consumed oxygen. The carbon dioxide production increased until nitrogen depletion and then started to decrease. Based on the measured carbon dioxide production, the growth rate was estimated to be 0.685 ± 0.005 day^{-1} which is in good agreement with the growth rate calculated based on optical density measurements (Supplemental Figure B.7). The respiratory quotient for the nitrogen replete phase was 0.79 indicating that the cells catabolized more than just glucose (Supplemental Figure B.8).

The mixotrophic culture had the same trends as the autotrophic culture during the light phase, but the magnitude of the gas rates was reduced since photosynthesis and respiration were both occurring. The magnitude of carbon dioxide production at

night was higher compared to the autotrophic culture, likely because the cells consumed glucose (nitrogen replete phase only). The respiratory quotient during the day was roughly -0.5 (Supplemental Figure B.9).

3.3.4 Biomass Yield on the Supplied Energy

Since the three cultures were using different carbon substrates, and in the case of the mixotrophic culture, multiple substrates, in order to have a fair comparison of their biomass yields, it had been suggested that it is more appropriate to calculate the yield on the basis of the amount of supplied energy instead of the mass of substrate consumed (Yang, Hua, and Shimizu 2000).

Table 3.2 summarizes the biomass yield for the three trophic conditions we performed. The increase in cell density was calculated using the increase in OD_{600} and the conversion factor to g/L described above. The energy supplied by glucose was calculated using the measured glucose consumption and multiplying by the free energy change in the reaction of glucose oxidation (2869 J/mol) (Yang, Hua, and Shimizu 2000). The energy supplied by the light source was calculated using the measured light intensity (80 μmol/m^2s), illuminated culture duration, bioreactor surface area exposed to light, and assuming that the wavelength of fluorescent light was 600 nm, so that 1 mol of photons has 200.8 kJ of energy (Yang, Hua, and Shimizu 2000). Comparing the autotrophic and mixotrophic biomass yields to the heterotrophic yields, it is clear that only a small percentage of energy was captured from the light source. This is common in plants, which typically only convert 1-2% of captured solar energy into stored chemical energy due to photosaturation (some cells receive excess light while others do not receive enough) and photorespiration (Rubisco fixing oxygen instead of carbon dioxide) (Vasudevan and Briggs 2008).

Table 3.2 Biomass Yields Based on the Supplied Energy from Light and/or Glucose.

Condition	Autotrophic	Heterotrophic	Mixotrophic
Cells Produced (g/L)	1.06	1.22	1.38
Glucose Supplied (kJ/L)	0	0.036	0.023
Light Supplied (kJ/L)	465	0	387
Biomass Yield (g/kJ)	0.0228	33.5	0.0357

3.3.5 Biomass Composition

Figure 3.5 shows the biomass quantification approach used in this work which is based on isotope ratio analysis. In short, a sample of known total biomass weight but unknown composition is combined with a known amount of ^{13}C labeled biomass with a known composition (i.e., the ^{13}C standard) and then the pooled biomass is analyzed on the GC/MS to determine the relative amount of ^{12}C and ^{13}C (C. Long and Antoniewicz 2014; McConnell and Antoniewicz 2016). From the isotope ratio and known amount of ^{13}C material, the amount of ^{12}C material is calculated.

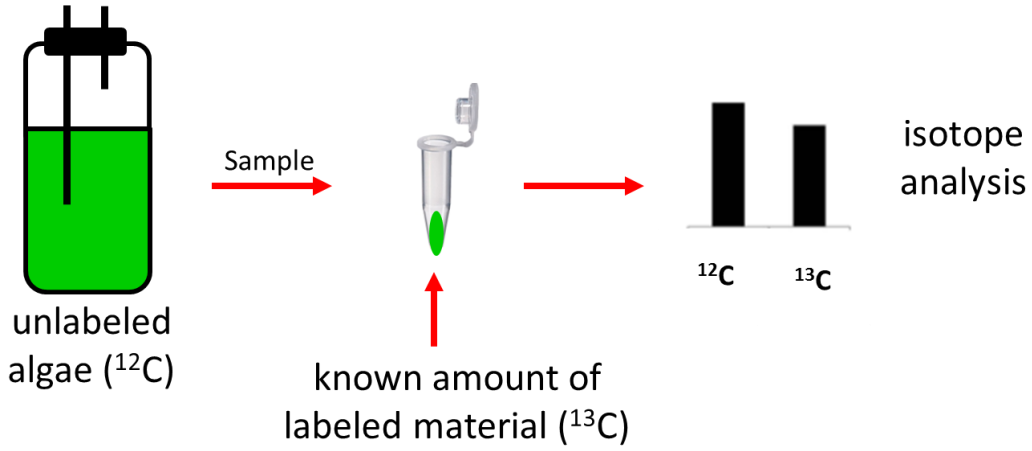

Figure 3.5 Biomass Quantification by Isotope Ratio Analysis. The sample to be quantified is combined with a fully ^{13}C-labeled biomass internal standard and the combination is analyzed on GC/MS to determine the relative amount of ^{12}C and ^{13}C.

Figure 3.6 shows the biomass composition results for (A) autotrophic, (B) heterotrophic, and (C) mixotrophic conditions. RNA (red line), never exceeded 6% of total dry weight, and was thus a minor component for all cases. This is consistent with a previous report where it was shown that cellular RNA content is correlated with growth rate and the growth rate for all of our conditions is fairly low (Kemp, Lee, and Laroche 1993). Interestingly, we found that that the RNA content during heterotrophic growth was lower compared to autotrophic and mixotrophic growth, which may be due to higher protein turnover in the light-cycled cultures. For autotrophic and mixotrophic cultures, there was a noticeable drop in RNA content upon nitrogen depletion, likely due to the fact that biomass restructuring was more significant than cellular replication in this phase.

For the nitrogen replete phase of the autotrophic culture, protein was the primary biomass component (45% of dry weight) and fatty acids were a minor component (4% of dry weight). In this condition, the cells have adequate access to nutrients and are reproducing at their maximum rate given the light and carbon dioxide supply. After nitrogen depletion in the autotrophic culture, the carbohydrate fraction increased quickly, held constant, and then decreased while the protein fraction decreased and the fatty acid fraction increased steadily (fatty acids are used by microalgae to store energy). After four days of nitrogen depletion, the fatty acid content increased to 25% of dry weight.

The heterotrophic cells did not undergo as drastic composition changes as the autotrophic culture. Carbohydrates constituted the largest fraction by dry weight for the heterotrophic cells, followed by protein and fatty acids. The heterotrophic protein content was likely lower than the autotrophic protein content due to the fact that

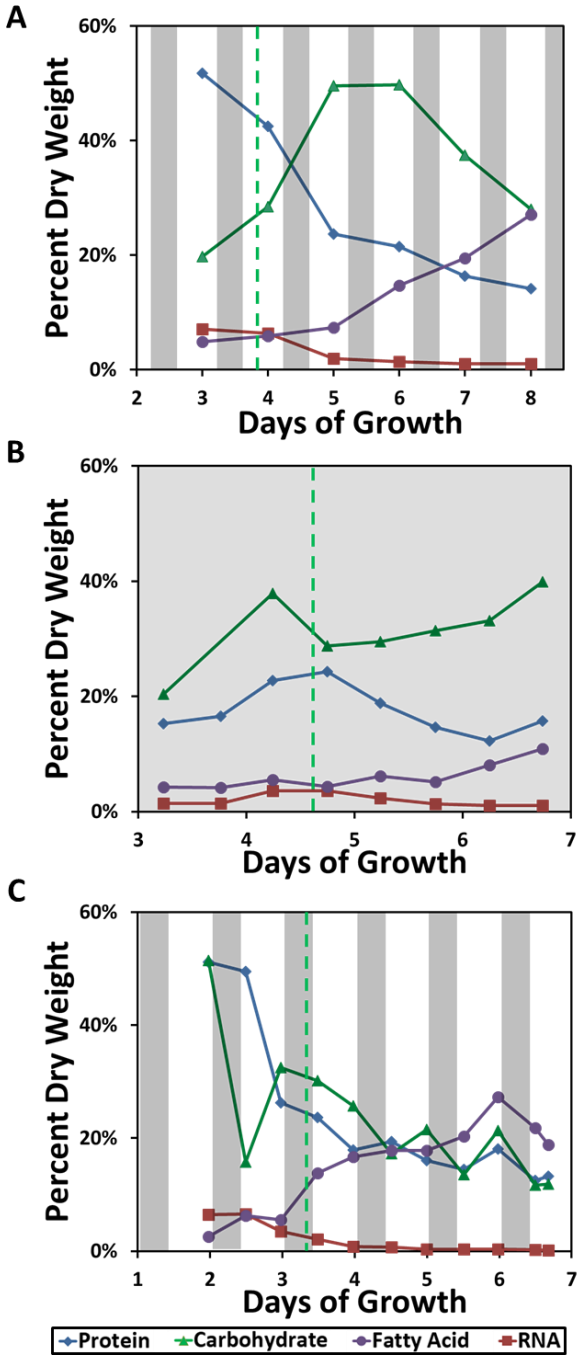

Figure 3.6 Biomass Composition by Percent Dry Weight for (A) Autotrophic, (B) Heterotrophic, and (C) Mixotrophic Conditions. The dark bars indicate time periods when the lights were turned off (the heterotrophic culture was always in darkness). The vertical dashed green line indicates when nitrogen became depleted.

autotrophic cells needed enzymes for photosynthesis during the day and enzymes for respiration at night. The protein content decreased and fatty acid content increased upon nitrogen depletion, but not to the same extent as in the autotrophic culture. This could be due to the large excess of glucose in the media. Since the cells can continuously access the substrate there was little need to store energy as lipids.

For the mixotrophic culture, in general, the carbohydrate and protein contents decreased and fatty acids increased over time. In the nitrogen depleted phase, the carbohydrate content decreased at night. During this time, the cells could consume glucose, but did not do so. This could be related to the circadian rhythm of microalgae (for the protein, fatty acid, and carbohydrate compositions, see Supplemental Table B.1 through Table B.9).

For the auto-, hetero- and mixotrophic cultures, in some cases only 70%, 50%, and 40% of the biomass by dry weight was accounted, which is lower than expected given that the classical microalgal biomass techniques usually account for roughly 85% of dry weight. However, similar analytical procedures with gas chromatography-flame ionization and high-performance liquid chromatography only accounted for 66% of dry weight of a nitrogen replete *Chlorella sp.* (Laurens et al. 2012). This suggests that biomass components which are not the specific amino acids, carbohydrates, and fatty acids that we measured comprise a signification fraction of the total biomass dry weight.

Since the biomass concentration is changing, it is useful to analyze the concentration of the components in the bioreactor (Figure 3.7). The concentration of protein in the medium is fundamentally limited by the initial nitrogen concentration in the culture medium. At the point of medium nitrogen depletion for the autotrophic

culture, the protein concentration was just under 0.2 g/L which corresponded to a proteinogenic nitrogen concentration of 2.3 mM. For this culture, the initial nitrate concentration was measured to be 2.9 mM; thus, approximately 79% of the available nitrogen was converted to proteins (nucleosides, cell wall components like chitin, and pigments such as chlorophyll may also contain nitrogen, but were not measured). The heterotrophic and mixotrophic cultures also had maximum protein concentrations close to 0.2 g/L. Upon nitrogen depletion, the protein concentration in the autotrophic culture decreased whereas it remained relatively constant in the heterotrophic and mixotrophic cultures. Nitrogen depletion resulted in more significant biomass remodeling in the autotrophic cells compared to the other trophic conditions. The autotrophic cells likely degraded protein to produce other biomass components.

The concentration of fatty acids in the bioreactors for each of the three cultures was significantly impacted by the presence of glucose as a substrate. The two glucose containing cultures never reached a fatty acid concentration of 0.3 g/L. For the autotrophic culture, on day 3 the fatty acid concentration was 0.25 g/L, and upon nitrogen depletion, the fatty acid concentration increased at a rate of 0.18 g/L/day up to a concentration of 1.0 g/L on day 8 (for comparison, the mixotrophic culture's concentration increased at a rate of 0.053 g/L/day). Due to culture volume limitations, the culture was not run beyond day 8 and thus we were not able to measure the maximum possible fatty acid concentration.

The autotrophic cells stored more carbohydrates than heterotrophic and mixotrophic cells. The cells with glucose as a substrate could always consume glucose, and thus did not need to store energy for starvation periods like the autotrophic cells had in the dark. Due to once daily sampling for the autotrophic

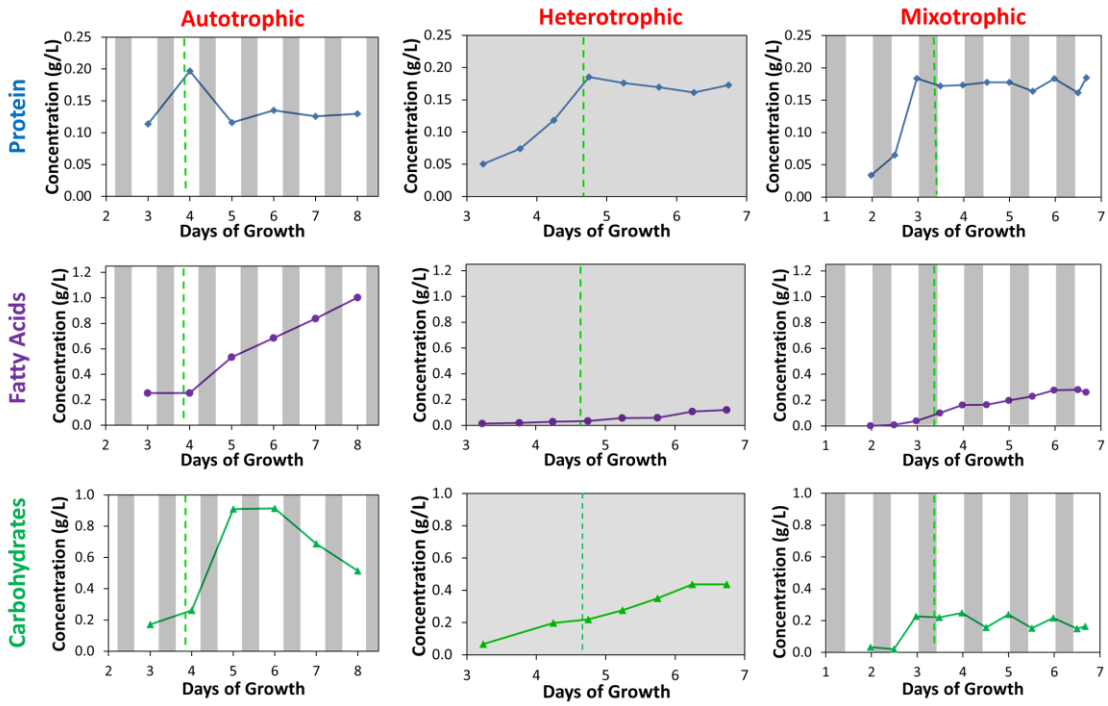

Figure 3.7 Total Concentration of Biomolecules Inside Bioreactor. Protein (top row), Fatty Acids (middle row), and Carbohydrates (bottom row) are shown for the Autotrophic (left column), Heterotrophic (center column), and Mixotrophic (right column) cultures. The dark bars indicate time periods when the lights were turned off (the heterotrophic culture was always in darkness). The vertical dashed green line indicates when nitrogen became depleted.

culture, the day/night production/consumption could not be observed. However, as is described in the next Chapter of this thesis, it was confirmed, with another culture, that autotrophic cells do consume their carbohydrates during the dark phase. Additionally, the biomass carbohydrate concentration decreased at night for the nitrogen depleted mixotrophic cells because the cells did not consume glucose substrate and they could not fix carbon dioxide.

3.3.6 Effect of Autotrophic Light Cycling on Absorbance Scan

Figure 3.8 shows the results from an additional autotrophic culture that was grown on air (i.e. 0.04% CO_2). The first observation is that growth on air (0.04% carbon dioxide) is significantly slower than growth on air enriched to 1% carbon dioxide. The culture grown on air took 24 days to reach an OD_{600} of 3.75 whereas the culture grown on 1% CO_2 enriched air reached an OD_{600} of 6.9 in just 8 days. The culture grown on air was sampled more frequently than the autotrophic culture in Figure 3.2. The frequent sampling showed that an autotrophic culture's OD_{600} does decrease during the dark period (for both nitrogen replete and deplete conditions) similar to what was observed for the nitrogen depleted mixotrophic culture in Figure 3.2.

To provide additional characterization, we used another spectrophotometer (Eppendorf BioSpectrometer with Fluorescence) to measure the culture's absorbance at multiple wavelengths. The absorbance profiles for selected days are shown in Figure 3.8B. We observed that nitrogen replete cells had a characteristic absorbance peak at 690 nm, which is known to correspond to that of Chlorophyll *a* (Nelson, Cox, and Lehninger 2017). Comparing the absorbance scans for samples collected approximately 1 hour before and after the light switch showed that the pigment content of the cells did not change (Supplemental Figure B.10). However, comparing the absorbance scans for nitrogen depleted cells to nitrogen replete cells, we found that nitrogen depletion changed the pigment content of cells (nitrogen replete cells were green, whereas nitrogen depleted cells were yellow-greenish).

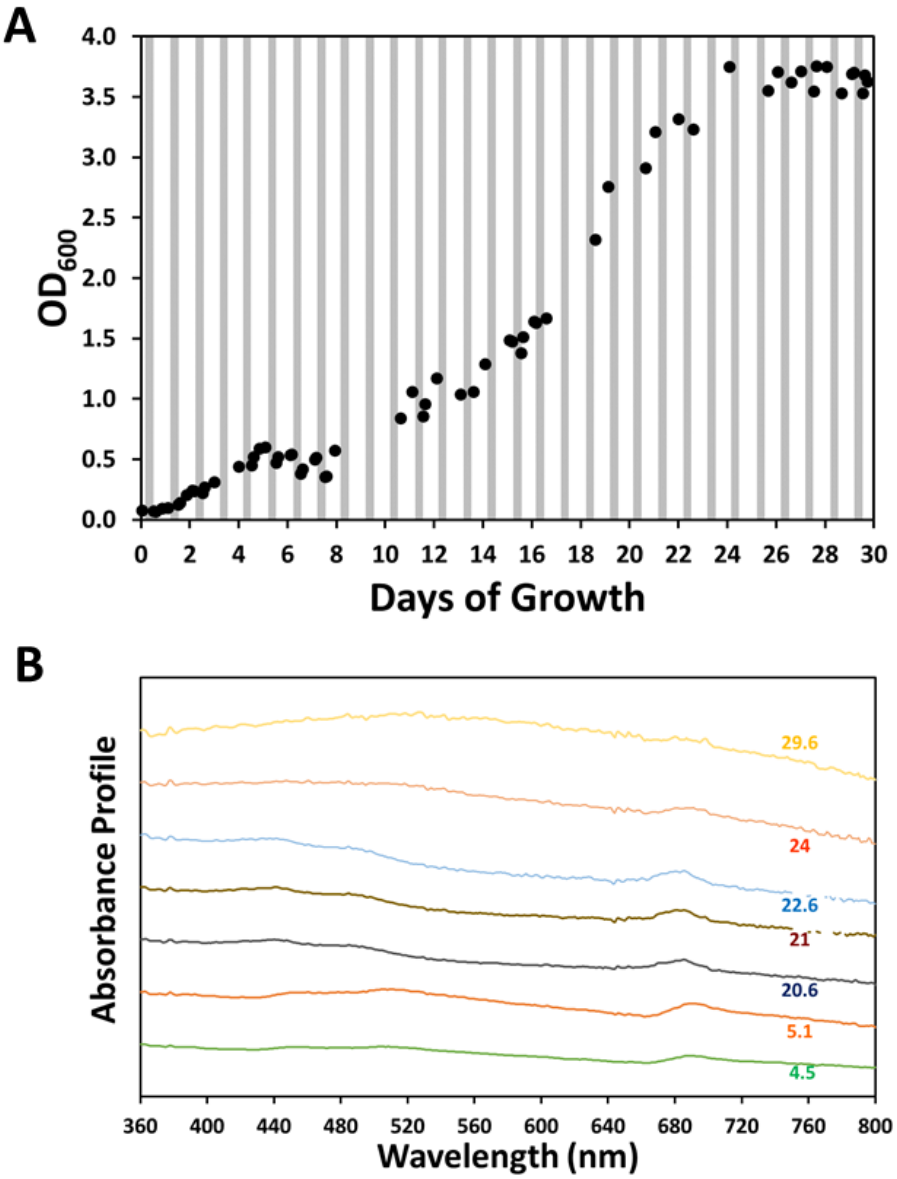

Figure 3.8 Autotrophic Light Cycling with Air Sparging. (A) The optical density decreases at night because the cells are not able to fix carbon dioxide. (B) Changes in absorbance scan profiles over time is due to changes in biomass composition.

3.4 Conclusions

The green microalga *Chlorella vulgaris* has been widely recognized as a promising candidate for biofuel production due to its natural metabolic versatility and ability to store a large amount of lipids. To maximize the production of desired products from *C. vulgaris* a quantitative understanding of its metabolism is needed. In this work, the metabolism of *C. vulgaris* UTEX 395 was characterized under autotrophic (1% CO_2 in air, 14 hours/day light), heterotrophic (10 g/L glucose), and mixotrophic (10 g/L glucose plus 1% CO_2 in air, 14 hours/day light) conditions. We demonstrated that under autotrophic and heterotrophic growth conditions the cells had the same growth rate. The results from the mixotrophic culture, suggested that mixotrophic growth is a superposition of autotrophic and heterotrophic growth. From biomass composition analysis, we determined that *C. vulgaris* is mostly composed of protein and carbohydrates during the nitrogen replete growth phase, and then upon nitrogen depletion the cells change their composition and accumulate mostly carbohydrates and fatty acids. This change in biomass composition and pigment content was also observed in the absorbance scan profiles. Light cycling in the autotrophic and mixotrophic cultures also resulted in biomass composition changes. In the dark phase, the autotrophic cells did not fix carbon dioxide; instead, the cells consumed their internal starch reserves for maintenance energy. Interestingly, in the nitrogen deplete phase, the mixotrophically grown cells did not consume glucose (and they also did not fix carbon dioxide), so they also needed to consume their internal starch reserves for maintenance.

The data obtained in this work was used to construct a genome-scale metabolic model for *C. vulgaris* UTEX 395 (Zuñiga et al. 2016) which contained 843 genes, 2294 reactions and 1770 metabolites (transcriptomic data collected by a collaborating

research group was also used for model validation). At its time of development, the model was the most comprehensive for any eukaryotic photosynthetic organism (based on the genome size and number of genes in the reconstruction). Using this genome-scale metabolic model, it was then demonstrated that flux distributions under different trophic conditions, specifically in central carbon metabolism, amino acid, nucleotide, and pigment biosynthetic pathways, were significantly affected by nitrogen starvation.

Chapter 4

METABOLITE EXCHANGE DRIVES THE SYMBIOTIC GROWTH OF *CHLORELLA VULGARIS* AND HETEROTROPHIC MICROBES

4.1 Introduction

In nature, it is common for organisms to grow in symbiosis. Symbiosis is an advantageous evolutionary tactic because the partners have access to new metabolic pathways. There are three types of symbiotic relationships: mutualism (partners benefit each other, but not necessarily to the same extent), commensalism (one partner benefits without impacting the other), or parasitism (one partner benefits at the expense of the other) (Posten and Walter 2012). Metabolite exchange, signal transduction, and gene transfer are examples of interactions between symbionts. Metabolite exchange is the most common interaction especially when the symbiosis involves an autotrophic (photosynthetic) organism and one or more heterotrophic organisms (Kouzuma and Watanabe 2015).

Microalgae are eukaryotic photosynthetic microorganisms which are present in freshwater, saltwater, and damp soil. They are the primary producers in many ecosystems and are responsible for roughly half of global oxygen production (Andersen 2005). The symbiosis between microalgae and partners such as corals (Lesser, Stat, and Gates 2013), sponges (Lee, Lee, and Lee 2001), and fungi (Hawksworth 1988) have been well documented. In fact, there are so many examples of microalgae-fungi symbioses, they have been given their own name – lichens (Kaasalainen et al. 2017). Recently, microalgae-bacteria interactions have gained

interest for fundamental understanding of their interactions and for biotechnology applications (Ramanan et al. 2016; Santos and Reis 2014; Kazamia et al. 2014; Kouzuma and Watanabe 2015). Chlorophytes of the genus *Chlorella* have been identified as common photosynthetic symbionts (Posten and Walter 2012). Some examples are that *Chlorella* spp. benefited by co-culture with *Azospirillum brasilense* and *Pseudomonas alcaligenes* but suffered with *Elizabethkingia miricola* and *Methylobacterium radiotolerans* (Guo and Tong 2014; Choix, de-Bashan, and Bashan 2012; Choix, De-Bashan, and Bashan 2012). Despite these prior studies, there is still a limited understanding of microalgae-bacteria symbiosis in nature due to species specific microenvironments and difficulty separating partners (Fuentes et al. 2016; Cooper and Smith 2015). It is important to gain more insight into the complex interactions between microalgae and bacteria for environmental protection and development of biotechnological processes (Kouzuma and Watanabe 2015).

Chlorella vulgaris is a particularly interesting species because it has the ability to remove nitrogen, phosphorus, metal ions, and organic carbon from water (relevant to waste water treatment facilities) (Wang et al. 2010) and it has the ability to accumulate large amount of carbohydrates and lipids (relevant to biofuel production) (Scott et al. 2010). Additionally, *C. vulgaris* is the National Renewable Energy Laboratory's (Golden, CO) model green microalga (Guarnieri et al. 2013). Recently, this organism's genome was sequenced and a genome-scale metabolic model was developed (Zuñiga et al. 2016).

To gain fundamental insight into symbiotic relationships, both mono- and co-cultures of the symbionts must be performed. In this study, we performed $^{12}C/^{13}C$ labeling switch and pulse-chase experiments with *C. vulgaris* and heterotrophic

microbes (obtained using soil samples and spent *C. vulgaris* medium). The foundation of the mutualistic symbiosis was identified and compared to other symbioses reported in the literature. Our results demonstrate that *C. vulgaris* uses polysaccharide secretion to increase local carbon dioxide concentrations promoting photosynthesis over photorespiration. Using adaptive laboratory evolution (ALE), a *C. vulgaris*-microbe co-culture was evolved that could reach a higher biomass concentration than *C. vulgaris* grown in monoculture. This study highlights the evolutionary advantage for microalgae to grow in symbiotic relationships and may be exploited for future biotechnology applications.

4.2 Materials and Methods

4.2.1 Materials

Growth media were purchased from PhytoTechnology Laboratories (Shawnee Mission, KS). Chemicals were purchased from Sigma-Aldrich (St. Louis, MO). ^{13}C labeled compounds were purchased from Cambridge Isotope Laboratories (Andover, MA). Media and solutions were sterile filtered with filtration units from Corning Inc (Corning, NY).

4.2.2 Strains

Chlorella vulgaris UTEX 395 was obtained from the Culture Collection of Algae at the University of Texas at Austin (Austin, TX). Microbiome cells were isolated using spent microalgal media and soil samples collected around the University of Delaware Newark campus.

4.2.3 Culture Conditions

All cultures used Bold's Basil Medium at 24 ± 3 °C (Bischoff and Bold 1963). The turnover cultures were grown in 250 mL glass bottle bioreactors (200 mL working volume) with air sparging at 12 mL/min and continuous stirring by a stir bar. All other cultures were grown in 125 mL Erlenmeyer flasks (25 mL working volume) with continuous stirring by a stir bar. During autotrophic growth, two 24 W fluorescent lights were used (80 $\mu E/m^2/s$). For light cycling, lights were on for 14 hours per day. For heterotrophic growth, the cultures were kept in darkness with an initial glucose concentration ranging from 10 to 50 mM depending on the desired final biomass concentration.

4.2.4 Analytical Methods

Cell growth was monitored by measuring the optical density at 600 nm (OD_{600}) using a spectrophotometer (Eppendorf BioPhotometer). The OD_{600} to cell dry weight concentration was determined to be 0.15 (g/L)/OD_{600}. For heterotrophic cultures, glucose concentrations were determined using a YSI 2700 biochemistry analyzer (YSI, Yellow Springs, OH). Molar percentages of carbon dioxide (CO_2, m/z 44) and ^{13}C-labeled carbon dioxide ($^{13}CO_2$, m/z 45) in the feed and off-gasses were measured by an on-line mass spectrometer (Ametek Proline, Berwyn, PA) (Leighty and Antoniewicz 2012). Quantification and labeling of biomass and secreted protein and carbohydrates were performed using GC/MS methods previously developed (C. P. Long and Antoniewicz 2014). To determine cell growth on ^{13}C labeled spent algal medium, the proteinogenic amino acids were analyzed using acid hydrolysis and tert-butyldimethylsilyl (TBDMS) derivatization as described in (Antoniewicz, Kelleher, and Stephanopoulos 2007a). For all cultures, carbohydrates were analyzed using

hydrolysis and aldonitrile propionate derivatization (McConnell and Antoniewicz 2016). For monosaccharide analysis, the hydrolysis step was omitted. GC/MS analysis was performed on an Agilent 7890B GC system equipped with a DB-5MS capillary column (30 m, 0.25 mm i.d., 0.25 µm-phase thickness; Agilent J & W Scientific), connected to an Agilent 5977A Mass Spectrometer. Mass isotopomer distributions were obtained by integration (Antoniewicz, Kelleher, and Stephanopoulos 2007a) and corrected for natural isotope abundances (Fernandez et al. 1996).

4.3 Results and Discussion

4.3.1 Light Cycling and Nitrogen Depletion Significantly Alter Autotrophic Starch Metabolism

During autotrophic light cycled cell culture (14 hours light/day, Figure 4.1a), the microalgae perform photosynthesis during the light phase to fix carbon dioxide into starch and biomass, while during the dark phase, when photosynthesis is not possible, they use stored energy for maintenance requirements. We observed that *C. vulgaris* biomass concentration significantly changed within an hour of light condition change. During the light phase, the biomass concentration increased by as much as 31%, and during the dark phase, it decreased by as much as 14%. During the nitrogen depleted phase of the cell culture, the biomass concentration decrease during the dark phase was nearly matched by the increase during the light phase, resulting in little or no net growth (Figure 4.1b).

To better understand the dramatic changes in biomass concentration (as determined from optical density measurements), the starch content was also quantified for these autotrophically grown microalgal cells (Figure 4.1c). Like the biomass concentration, significant changes in starch content were observable within an hour of

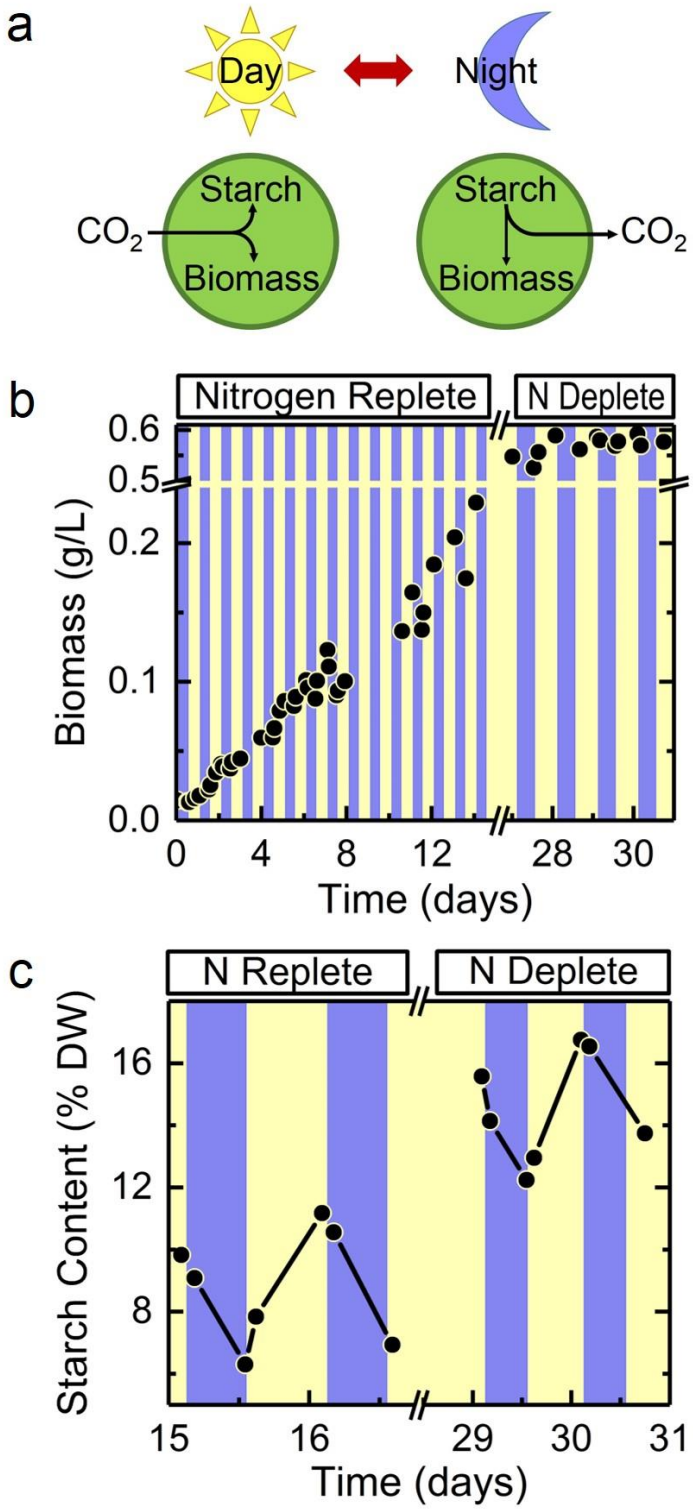
a
Day
Night
Starch
CO_2
Biomass
Starch
Biomass
CO_2
b
Nitrogen Replete
N Deplete
Biomass (g/L)
0.6
0.5
0.2
0.1
0.0
0
4
8
12
28
30
Time (days)
c
N Replete
N Deplete
Starch Content (% DW)
16
12
8
15
16
29
30
31
Time (days)

Figure 4.1 Light cycling and nitrogen depletion significantly alter autotrophic starch metabolism. (a) During illumination, the cells perform photosynthesis to convert carbon dioxide into biomass and carbon storage products like starch. In darkness, the cells need to use intracellular carbon storage as carbon and electron sources. (b) Days 0 to 14 represent nitrogen replete growth and days 27 to 31 represent the nitrogen deplete stationary phase. During the growth phase, there is an overall net increase in biomass and during the stationary phase there is an overall constant biomass concentration. Despite the overall outcome of these phases, the biomass concentration is very dynamic. The biomass concentration decreased as much as 14% in a dark phase and increased as much as 31% in a light phase. In the stationary phase, the biomass decrease during the dark phase is nearly matched by the gain during the light phase. (c) The starch content of the cells changes very quickly upon a light condition change. Also, nitrogen depletion causes the cells to store more starch since the cells cannot grow.

light change. Starch consumption in the dark was a major cause of biomass decrease, with as high as a 40% decrease in starch content during a 10-hour dark phase. This is consistent with previous reports of 35% of microalgal biomass produced during the day being consumed at night (Becker 1994). Another aspect to consider is the starch content during the growth phase (nitrogen replete phase) relative to the stationary phase (nitrogen depleted phase). During the growth phase, the starch content was roughly 9% of dry weight whereas, while in the stationary phase, the starch content was roughly 15%. Because of nitrogen depletion, the cells cannot replicate (i.e. are unable to produce new proteins), so they accumulate fixed carbon as starch. These results show that *Chlorella vulgaris's* autotrophic starch metabolism is dynamic and frequent sampling is needed to understand the performance of an autotrophically growing microalgal culture. To further understand *Chlorella vulgaris's* starch metabolism, we next quantified the rate of starch turnover.

4.3.2 Starch Turnover Occurs in Autotrophic and Heterotrophic Growth

To further understand the mechanism of starch formation and breakdown, we performed a labeling switch experiment (Figure 4.2e). First, cells were grown heterotrophically on [U-^{13}C]glucose to generate labeled biomass. Then, the cells were centrifuged (supernatant removed), washed with glucose-free Bold's Basil Medium (BBM), and grown on an unlabeled substrate as shown in Figure 4.2a. The growth profiles for the unlabeling cultures are shown in Figure 4.2b. The light cycled autotrophic culture biomass production rate was 0.59 g/L/day and the constant light autotrophic culture's was 1.12 g/L/day. These growth rates are reasonable since the light cycled culture was illuminated for 58% of the day and its biomass production was 53% of the constant light culture. Carbon dioxide gas transfer limitation could be the cause of linear growth. Glucose was provided in excess to the heterotrophic culture, so it grew exponentially at a rate of 0.56 day^{-1}.

Throughout the unlabeling period, the feed and off-gas were monitored with an on-line mass spectrometer which could distinguish between $^{12}CO_2$ (m/z 44) and $^{13}CO_2$ (m/z 45). The reasons for these measurements were (1) to confirm carbon dioxide consumption/production during the light/dark phases, respectively; and (2) to determine if there was any breakdown of labeled biomass (Figure 4.2c). The constant light autotrophic and heterotrophic cultures had no significant $^{13}CO_2$ production, indicating that labeled biomass components were not oxidized to carbon dioxide at a significant rate. These results were expected since both of those cultures had continuous access to the substrate, and thus consuming intracellular carbon storage compounds was not needed. However, the autotrophic light cycling culture did not have continuous access to a substrate, and the results were as expected very different. During the first dark phase (when starch was highly labeled), most of the produced

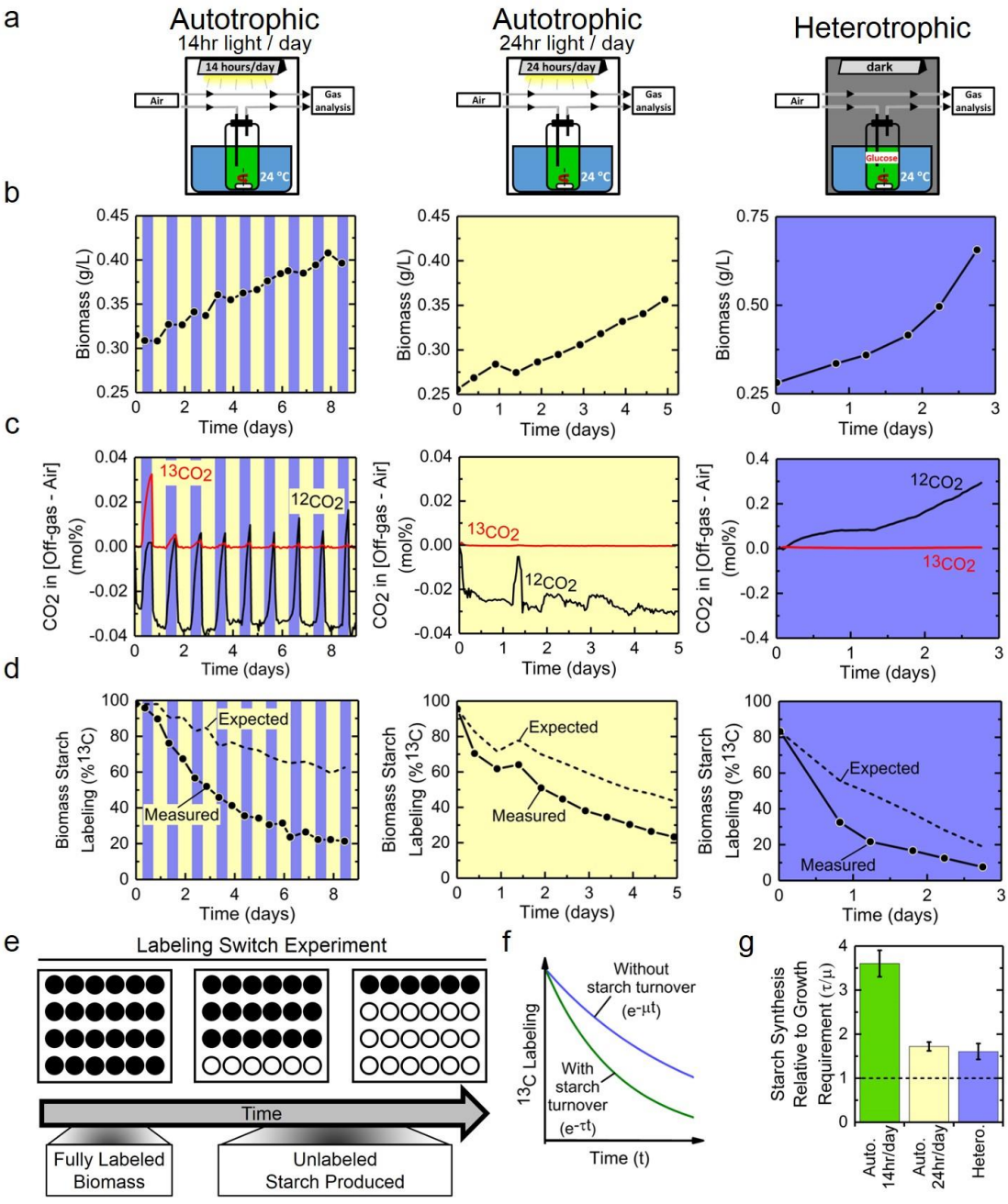
a
Autotrophic
14hr light / day
Autotrophic
24hr light / day
Heterotrophic
14 hours/day
24 hours/day
dark
Air
Gas analysis
24 °C
Glucose
b
Biomass (g/L)
Time (days)
c
CO2 in [Off-gas - Air] (mol%)
13CO2
12CO2
d
Biomass Starch Labeling (%13C)
Expected
Measured
e
Labeling Switch Experiment
Time
Fully Labeled Biomass
Unlabeled Starch Produced
f
13C Labeling
Without starch turnover (e-μt)
With starch turnover (e-τt)
Time (t)
g
Starch Synthesis Relative to Growth Requirement (τ/μ)
Auto. 14hr/day
Auto. 24hr/day
Hetero.

Figure 4.2 Labeling switch study reveals starch turnover in auto- and heterotrophic metabolism. (a) *Chlorella vulgaris* can grow autotrophically on light and carbon dioxide and/or heterotrophically on glucose. All cultures used Bold's Basil Medium with continuous gas analysis. (b) During autotrophic culture using air, the biomass concentration increases linearly due to gas transfer limitation. During heterotrophic culture, the cells grow exponentially. (c) During light cycled autotrophic growth, the cells consumed almost all of the carbon dioxide in the feed stream when illuminated but release carbon dioxide in the dark when they must catabolize intracellular carbon storage products. The constant substrate cultures either always fixed (continuous light) or released (continuous dark) carbon dioxide. (d) The cultures were inoculated with almost fully labeled cells. Since the substrates were unlabeled, as new biomass was created, the overall percentage labeling of the biomass decreased. The expected curve is the labeling percentage expected by labeling dilution without turnover. The measured biomass starch labeling are shown by the circular points. (e) This schematic shows the phases of the labeling switch experiment and how the labeling becomes diluted over time. (f) Without starch turnover, the labeling is expected to decrease because of dilution of new biomass. Therefore, the labeling will decrease as a function of the growth rate. If there is starch turnover, the labeling will decrease faster than expected and have an associated time constant. (g) All three cultures had a faster starch synthesis rate than needed for growth. The constant substrate cultures had similar τ/μ ratios indicating turnover may be an inherent part of microalgae metabolism.

carbon dioxide was ^{13}C labeled. As time progressed, the produced carbon dioxide became mostly ^{12}C, since new ^{12}C biomass was being produced during the light phase.

To determine if turnover was occurring (Figure 4.2f), we measured the average carbon labeling of biomass starch over time (Figure 4.2d). Our assumption was that if no turnover occured, then the biomass labeling would decrease due to dilution by the newly formed unlabeled biomass. However, for all three cultures, the biomass starch labeling decreased faster than expected, suggesting significant starch turnover. Using least squares regression, a turnover time constant was determined for each culture and compared to the culture's growth rate (Figure 4.2g). The ratio of the starch turnover

time constant to the growth rate for the light cycled autotrophic culture was 3.6 ± 0.3. The ratio for the constant light autotrophic and heterotrophic cultures was 1.7 ± 0.1 and 1.6 ± 0.2, respectively. Interestingly, the confidence intervals for the constant substrate cultures overlapped, but were significantly different from 1.0. Moreover, the sum of the ratios for the constant substrate cultures was within the confidence interval for the light cycled ratio. Since the starch synthesis was greater than required for growth, we concluded that there must be an accumulation of starch in the cells. However, there is a limit on the carbon:nitrogen biomass ratio. Coupling this with the gas analysis results, which showed no labeled carbon dioxide production, we decided to next check for carbohydrate secretion as a potential carbon sink (Kind et al. 2012).

4.3.3 Polysaccharides are Secreted during Growth

To test for carbohydrate secretion, the sampling procedure in Figure 4.3a was used to measure the monosaccharides (no hydrolysis of sample) and polysaccharides (after hydrolysis of sample) in the supernatant and in the cell pellet relative to the total amount present in the culture (Figures 4.3b and 4.3c). The total glucose equivalent concentration in the nitrogen replete and deplete phase was 33 and 176 mg/L, respectively. Those values were used to scale the sample concentrations. In both nitrogen phases, the total amount of free glucose made-up less than 4% of the total glucose present in the culture. The supernatant contained 23% and 20% of the total polymeric glucose in the nitrogen replete and depleted phases, respectively. Synthesis of each triose phosphate from carbon dioxide requires 6 NADPH and 9 ATP (Nelson, Cox, and Lehninger 2017). As such, it was unexpected that a large amount of polysaccharides would be secreted since they are a rich source of carbon and electrons. So, there was concern that cell breakage due to excessive culture agitation

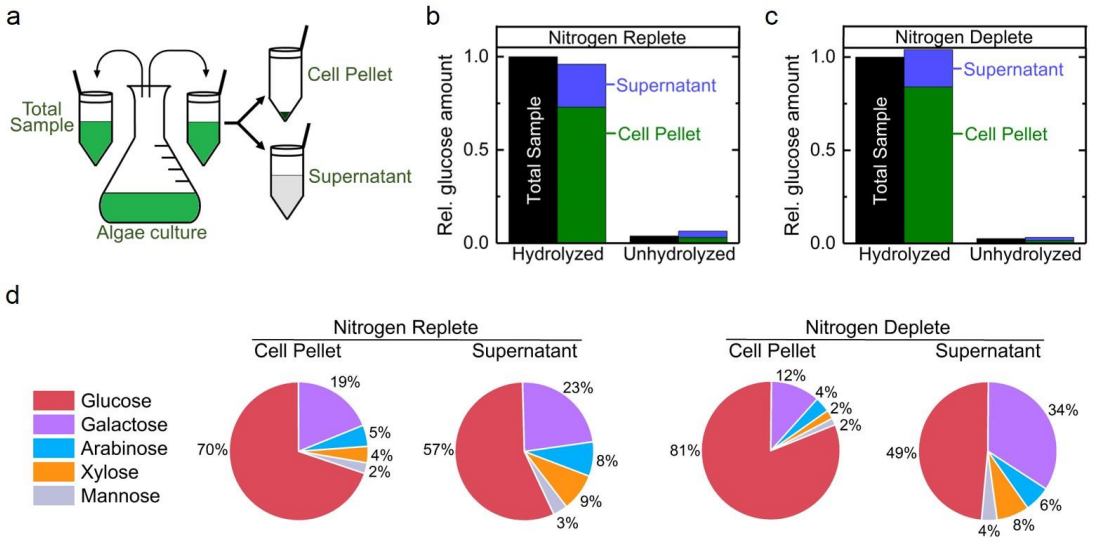

Figure 4.3 Polysaccharides, with glucose as the major monosaccharide unit, are secreted during growth. (a) Schematic of the sampling procedure for glucose quantification. After collection, samples were dried at 65 °C under air. To quantify monomer glucose, samples were derivatized for GC/MS analysis. To quantify polymer glucose, samples were hydrolyzed then derivatized for GC/MS analysis. (b) In the nitrogen replete phase, the total glucose equivalent concentration was 33 mg/L. There was a small amount of monomeric glucose relative to the amount of polymeric glucose. The supernatant contained 23% of the total amount of polymeric glucose. (c) In the nitrogen replete phase, the total glucose equivalent concentration was 176 mg/L. There was a small amount of monomeric glucose relative to the amount of polymeric glucose. The supernatant contained 20% of the total amount of polymeric glucose. (d) Glucose is the primary monosaccharide unit in the cell pellet and supernatant polysaccharides. Nitrogen depletion causes the cells to accumulate starch which leads to increased glucose content in the cell pellet. The monosaccharide profiles of the cell pellet and supernatant are different supporting the secretion and not cell breakage hypothesis.

or shearing during harvesting could be the reason polysaccharides are in the supernatant. However, the monosaccharide profiles of the cell pellet and supernatant are different and *Chlorella* sp. have two cell membranes (Posten and Walter 2012); so,

cell breakage was determined to be unlikely. Supplemental Figures C.1 and C.2 show the results of a culture with much faster stirring than in Figure 4.3 to confirm cell breakage was not the cause of carbohydrates entering the medium.

There are two possible reasons why the cells would go through the effort of fixing carbon dioxide and secreting polysaccharides. One possible reason is that the cells secret excess organic carbon created during the light phase to use as a carbon source during the dark phase. The second possible reason is that the cells secrete the organic carbon to attract a beneficial partner. To further investigate this question in more detail, we next performed follow-up [U-^{13}C]glucose tracer experiments.

4.3.4 *C. vulgaris* Cannot Grow Heterotrophically on its Secreted Polysaccharides

In the previous section, we showed that during heterotrophic growth on [U-^{13}C]glucose, polysaccharides were detected in the medium showing that the secretion is not dependent on light/photosynthesis. To determine whether or not *C. vulgaris* can grow heterotrophically on its secreted polysaccharides, the following procedure was used: (1) *C. vulgaris* was first grown on [U-^{13}C]glucose in the dark; (2) the culture was then sterile-filtered to remove cells and obtain labeled spent microalgal medium; (3) unlabeled cells were inoculated into the spent medium and allowed to grow in the dark. Interestingly, after 5 days of culture in the presence of spent microalgal medium, the microalgae biomass concentration decreased by 19% and the cells were only (20 ± 6)% labeled (Figure 4.4a). (Supplemental Figure C.3 shows the labeling patterns of amino acids.) Thus, we concluded that while the cells did consume some of the labeled material from the medium, it was not significant for net new cell growth.

4.3.5 Microbes Can Grow Heterotrophically on Secreted Microalgal Polysaccharides

Using the same labeled spent medium as in the previous section, *E. coli* (a model industrial bacterium) was grown for 6 days; the biomass concentration increased by 60% and reached (30 ± 5)% ^{13}C-labeling (Figure 4.4a). (Supplemental Figure C.4 shows the labeling patterns of amino acids.) The amount of labeling incorporation was marginally better than *C. vulgaris* (which did not increase in biomass concentration). We concluded that *E. coli* probably used both extracellular polysaccharides and intracellular carbon storage compounds to grow. Next, we wanted to find other microbes that could more effectively use *C. vulgaris* secreted polysaccharides to grow.

Soils contain a wide range of microorganisms and we hypothesized that it would likely contain one or more species capable of consuming secreted microalgal polysaccharides. Soil samples were thus collected and put into the spent algal medium without light exposure, i.e. to select microbes while avoiding selection of photosynthetic organisms. After one week (Supplemental Figure C.5 shows pictures of the cultures before and after this weeklong culture), all samples were passaged into one culture together to achieve the greatest amount of biodiversity. After 40 weeks of passaging, we obtained a microbiome culture that efficiently grew on spent algal medium (Figure 4.4b). This culture was grown on labeled spent algal medium for 7 days, increasing the biomass concentration by 630% and becoming (91 ± 6)% ^{13}C-labeled (Figure 4.4a). (Supplemental Figure C.6 shows the labeling patterns of amino acids.) Since the microbiome cells can use the secreted microalgal polysaccharides to grow, the next step was to analyze the microalgae-microbiome interaction during a co-culture.

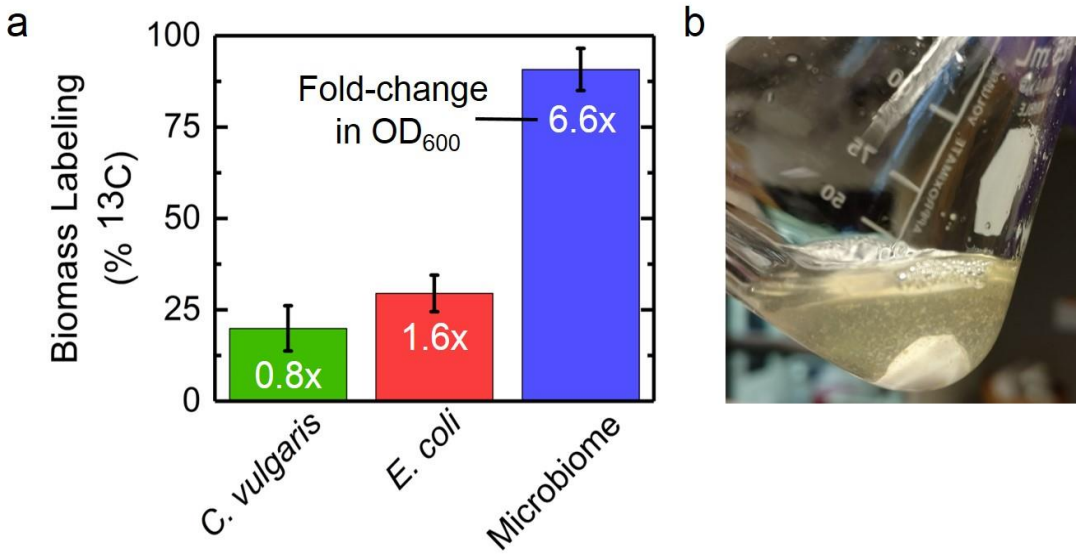

Figure 4.4 Microbiome cells can grow using secreted microalgal polysaccharides. (a) This shows the average biomass labeling (mean ± s.d. of 13 proteinogenic amino acids) of each culture after growth on labeled spent microalgal medium in the dark. *C. vulgaris* and *E. coli* had roughly the same amount of labeling; however, the microalgae did not grow. *E. coli* did not grow to a large extent, so microbiome cells were obtained from soil samples and those cells incorporate significant labeling while growing more than *E. coli*. (b) This picture of the microbiome shows that the cells clump significantly.

4.3.6 Metabolite Exchange is Basis of *C. vulgaris*-Microbiome Symbiosis

A pulse-chase experiment was performed to determine the mechanism of the interaction between *C. vulgaris* and the microbiome culture (Figure 4.5). The microalgae-microbiome co-culture had similar biomass production as the microalgae monoculture, indicating that the cells in the microbiome culture were not parasitic (Figures 4.5b and 4.5c). Due to the microalgae's photosynthetic pigments, the microalgae and microbiome cells have very different absorbance spectra (Figure 4.5d). The absorbance spectrum of the co-culture will vary depending on the relative amounts of microalgae and microbiome cells present as follows

$$\bar{A}_C = a\bar{A}_A + b\bar{A}_B \quad (4.1)$$

where $\bar{A}_C$, $\bar{A}_A$, and $\bar{A}_B$ are the absorbance spectra for the co-culture, microalgae, and microbiome, respectively, and a and b are values obtained through least squares error minimization. A calibration curve was created to convert the values of a and b into the faction of the co-culture that is microbiome cells. Using this method we determined that the co-culture contained roughly 10% microbiome cells throughout the entire co-culture.

The first information to consider for the pulse-chase experiment is the ^{13}C labeling of the glucose moiety in the supernatant. Once the ^{13}C labeled spent medium is spiked into the culture, the labeled polysaccharides will be a certain percentage of the total polysaccharides. Then, the ^{13}C polysaccharide labeling will change depending on the polysaccharide secretion. The three cases are: (1) no polysaccharide secretion, in which case the labeling will not change; (2) constant polysaccharide secretion, in which case the labeling will decrease as a function of the growth rate; (3) excess polysaccharide secretion, in which case the labeling will decrease faster than expected from monoculture results (Figure 4.5f). Figures 4.5b and 4.5c show the measured supernatant polysaccharide labeling and the expected labeling based on dilution by constant secretion. The same amount of labeled polysaccharides were spiked into each culture and both became roughly 50% labeled indicating that they had similar supernatant polysaccharide concentrations. The *C. vulgaris* monoculture measured labeling was close to the expected labeling, especially in the nitrogen deplete phase. However, the co-culture labeling decreased much faster than expected with the final measured labeling percentage being about 5%. It thus appears that the spent medium contained polysaccharides that the microbiome could not consume because the

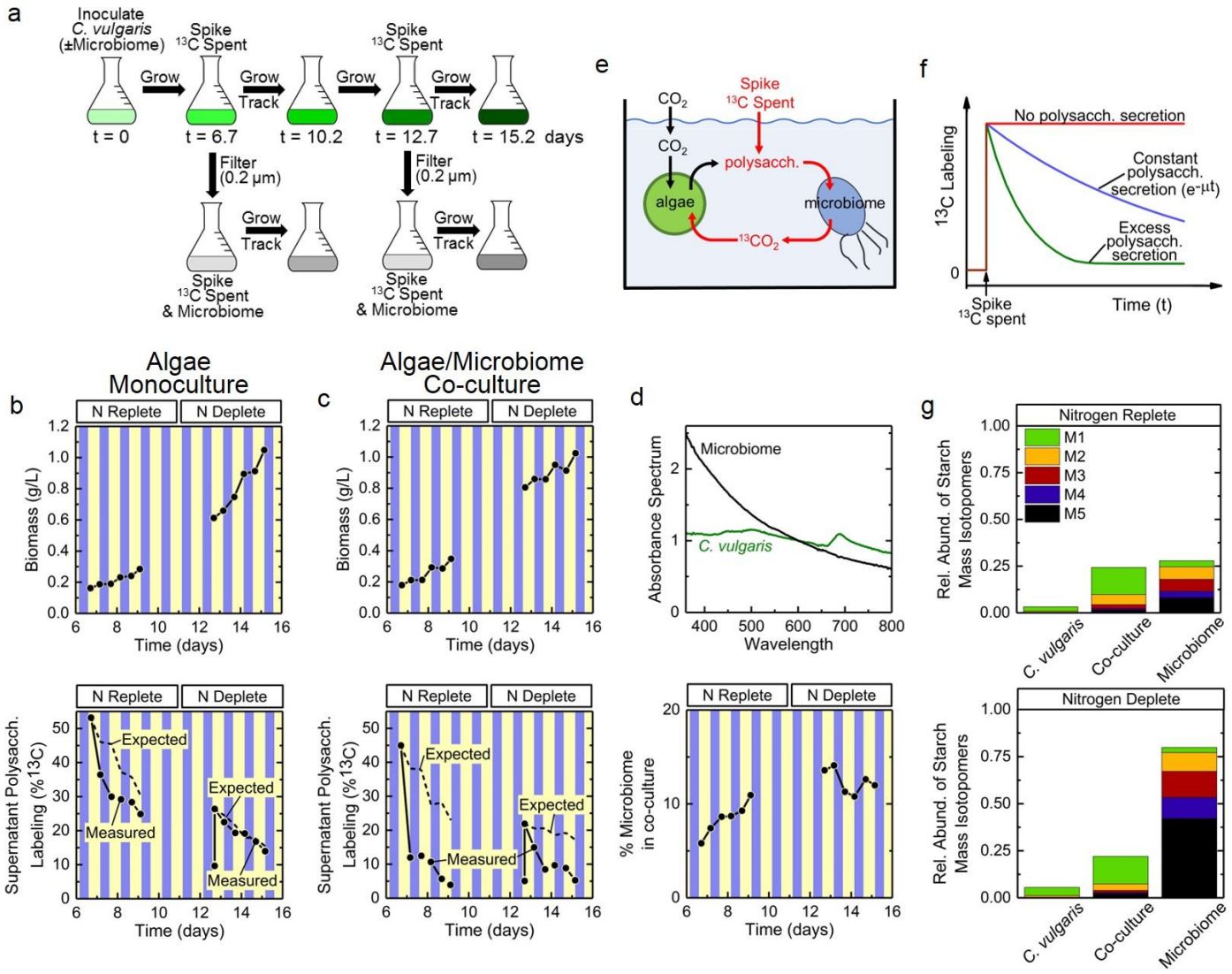
a
Inoculate
C. vulgaris
(±Microbiome)
Spike
13C Spent
Grow
Track
t = 0
t = 6.7
t = 10.2
t = 12.7
t = 15.2 days
Filter
(0.2 µm)
Spike
13C Spent
& Microbiome
e
CO2
Spike
13C Spent
polysacch.
algae
microbiome
13CO2
f
13C Labeling
No polysacch. secretion
Constant
polysacch.
secretion (e-µt)
Excess
polysacch.
secretion
0
Spike
13C spent
Time (t)
Algae
Monoculture
Algae/Microbiome
Co-culture
b
c
d
g
N Replete
N Deplete
Biomass (g/L)
Time (days)
Supernatant Polysacch.
Labeling (%13C)
Expected
Measured
Absorbance Spectrum
Microbiome
C. vulgaris
Wavelength
% Microbiome
in co-culture
Nitrogen Replete
Nitrogen Deplete
Rel. Abund. of Starch
Mass Isotopomers
M1
M2
M3
M4
M5
C. vulgaris
Co-culture
Microbiome

Figure 4.5 Polysaccharide and carbon dioxide exchange is the basis of the symbiotic relationship between *C. vulgaris* and microbiome cells. (a) Timeline and procedure for the pulse-chase experiment. (b) Algae monoculture controls for biomass production (top) and supernatant polysaccharide labeling (bottom). (c) Algae/Microbiome co-culture results for biomass production (top) and supernatant polysaccharide labeling (bottom). The co-culture growth profile is similar to the algae monoculture, so the microbiome does not appear to the parasitic. The measured co-culture supernatant polysaccharide labeling decreases much faster than the expected rate compared to the algae monoculture. (d) *C. vulgaris* and microbiome cells have very distinct absorbance spectrums. These spectrums and the spectrum of the co-culture were used to estimate than the co-culture was roughly 90% algae throughout. (e) Schematic of our proposed interaction mechanism. The algae cells fix carbon dioxide and secrete polysaccharides. The microbiome cells consume polysaccharides and release carbon dioxide. Because we pulsed in labeled polysaccharides, if this mechanism is true, singly labeled algae biomass components should be created. (f) Possible labeling patterns of polysaccharides based on secretion by algae. (g) *C. vulgaris* in the monoculture only obtains a small amount of singly labeled starch in the nitrogen replete (top) and deplete (bottom) phases. The biomass from the co-culture has more labeling especially the singly labeled starch. The microbiome cells in monoculture had the highest labeling and singly labeled starch was the least abundant. This labeling and the absorbance spectrum work indicate that the algae cells are dominant members of the co-culture. Therefore, the increased amount of singly labeled starch means that there is increased photosynthetic activity in the co-culture relative to the monoculture.

labeling stayed at roughly 5% between days 9.1 and 12.7. So, for the co-culture, the size of the unlabeled supernatant polysaccharide pool remained the same because the production and consumption rates were matched.

The next consideration was the labeling of the biomass. Figure 4.5g shows the labeling of the microalgal cells and co-culture cells 48 hours post spike and microbiome cells 40 hours post spike. For both nitrogen phases of the microalgal monoculture, singly labeled glucose was the most abundant of the labeled glucose but

less than 5% of the total glucose. The small amount of fully labeled starch indicates that the cells did not significantly uptake polysaccharides and keep the monosaccharide units intact. However, the presence of singly labeled glucose indicates that some polysaccharides were broken down and labeled carbon dioxide was produced and then re-incorporated. In the nitrogen replete phase, the co-cultured cells were 76% unlabeled and 1.5% fully labeled. In the nitrogen deplete phase, the co-cultured cells were 78% unlabeled and 2.2% fully labeled. The singly labeled fraction was 14% and 15% in the nitrogen replete and deplete, respectively. Clearly, there was an increase in the presence of singly labeled glucose in the co-culture, but it was not totally clear at first glance if that is due to increased photosynthetic activity by the microalgae or presence of microbiome cells.

The first indication of increased photosynthetic activity is that the microbiome cells were only about 10% of the co-culture (according to the absorbance scan method). The second indication is the labeling of the microbiome cells from the pulse-chase analogy experiment. In the nitrogen replete phase, the microbiome cells were 72% unlabeled and 8% fully labeled. In the nitrogen deplete phase, the cells were 20% unlabeled and 42% fully labeled. The cells were more labeled in the nitrogen deplete phase because more carbohydrates are present (more growth and labeling incorporation). It is important to note that singly labeled glucose was the least abundant labeled fraction. So, it does appear that the algae's photosynthetic activity was increased during co-culture with the microbiome cells.

4.3.7 Co-culture has Increased Photosynthetic Activity

Figure 4.5e shows the proposed mechanism of interactions between the microalgae and microbiome during the co-culture. The microalgae fix carbon dioxide

using photosynthesis and secrete polysaccharides. The microbiome consumes polysaccharides, breaks them into monomers, then produces carbon dioxide in the pentose phosphate pathway (6PG → Ru5P + CO_2) and glycolysis (Pyr → acetyl-CoA + CO_2). This process is advantageous for the microalgae because the local carbon dioxide concentration increases promoting carboxylation instead of oxidation of Rubisco (photosynthesis over photorespiration). It is important to note that there was significant clumping of cells in the co-culture which supports gas and nutrient exchange. Figure 4.6 shows flux estimates for carbon dioxide fixation and polysaccharide secretion rates using the pulse-chase experiment data and mass balances. During co-culture, the polysaccharide secretion flux increased significantly and carbon dioxide recycling was a significant portion of total carbon dioxide fixation.

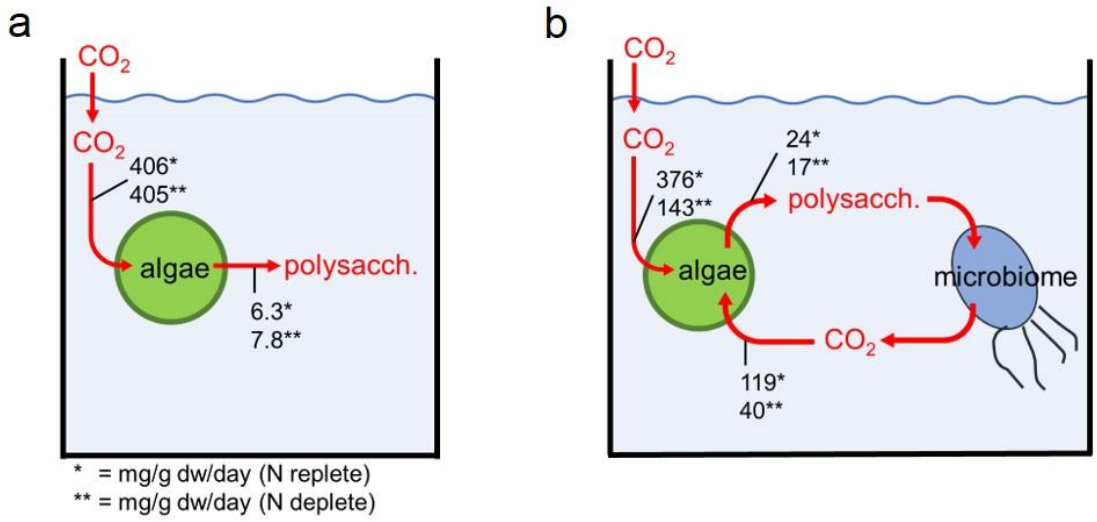

Figure 4.6 Algae respond to the presence of microbiome cells. (a) Carbon dioxide uptake and polysaccharide secretion rates for algae monoculture. (b) Carbon dioxide uptake and polysaccharide secretion rates for algae/microbiome co-culture. The polysaccharide secretion rate and nitrogen replete carbon dioxide fixation rate are increased during co-culture.

4.3.8 Adaptive Laboratory Evolution of Algae/Microbiome Co-culture

The microbiome cells used in the pulse-chase experiment (Figure 4.5) were not previously cultured with *Chlorella vulgaris*. During the analyzed time range of this initial culture, there was no growth advantage caused by the microbiome cells. However, we anticipated that by passaging the algae and microbiome cells together, they would find an optimal ratio of each cell type, leading to superior biomass production compared to a microalgal monoculture.

To test this hypothesis, four autotrophic, light-cycled adaptive laboratory evolution cultures were performed:

- *C. vulgaris* monoculture
- *C. vulgaris* with Microbiome v2.2 cells (two passages on spent algal medium, frozen, two pre-cultures on spent algal medium)
- *C. vulgaris* with Microbiome v9.2 cells (nine passages on spent algal medium, frozen, two pre-cultures on spent algal medium)
- *C. vulgaris* with Microbiome v26 cells (twenty-six passages on spent algal medium)

and their growth curves are shown in Figure 4.7(A-D) and a summary of peak OD_{600}'s is given in Figure 4.7E. The peak OD_{600} for the initial *C. vulgaris* culture was 4.2 while the co-cultures with Microbiome v2.2, v9.2, and v26 were 7.5, 5.9, and 7.3, respectively. After six passages, the peak OD_{600} for the monoculture increased by 1.2-fold compared to its initial culture while the Microbiome v2.2, v9.2, and v26 co-cultures had 1.2-, 1.1-, and 1.2-fold increases, respectively. Comparing the sixth passage cultures, having the microbiome cells present lead to a 1.6-fold increase in peak OD_{600} compared to the monoculture (OD_{600} of 5.1 vs 8.2).

The ALE experiment was carried out over 32 months with the cultures being passaged over 40 times. Even over this long time-span, the co-cultures reached higher peak OD_{600}'s than the monoculture. Using the absorbance scan quantification method for Day 15, the Microbiome cells were 8%, 5% and 10% for the Microbiome 2.2, 9.2,

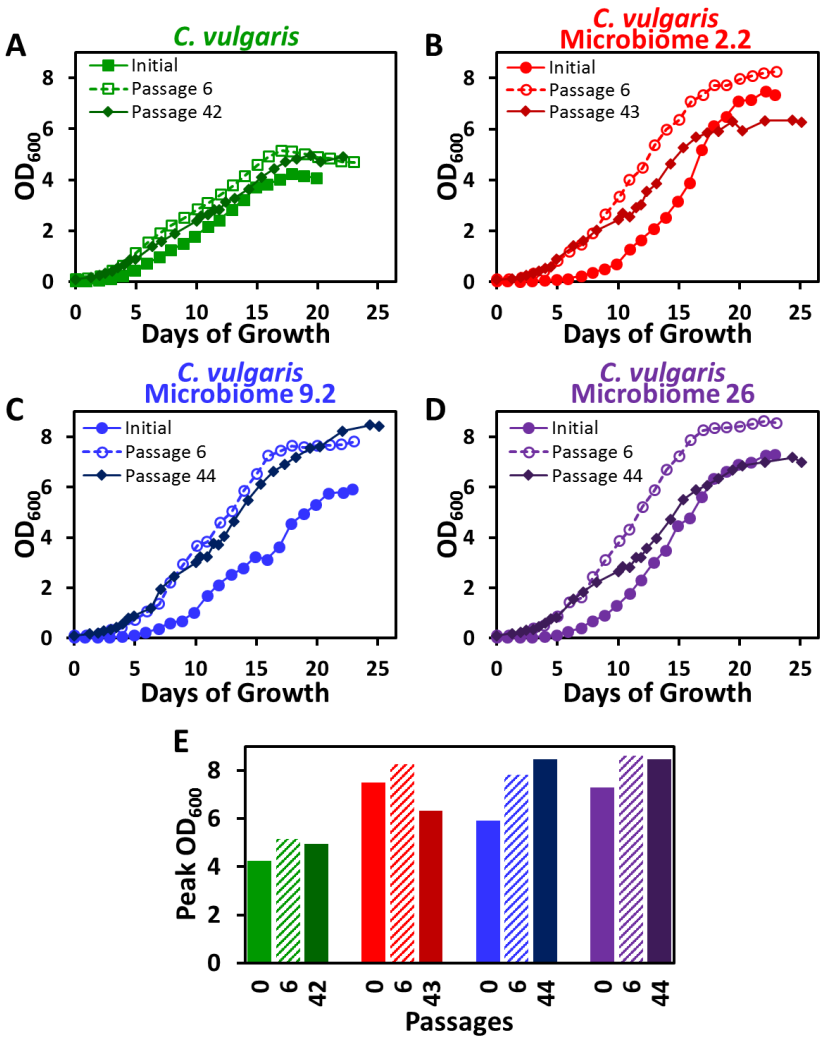

Figure 4.7 Adaptive Laboratory Evolution (A) ALE of *Chlorella vulgaris* monoculture. The 42 passages were performed over the course of 32 months. (B) ALE of *C. vulgaris* and Microbiome 2.2. Microbiome 2.2 cells had the following history before their initial culture with algae: two passages on spent algal medium, frozen, two pre-cultures on spent algal medium, inoculum. (C) ALE of *C. vulgaris* and Microbiome 9.2. Microbiome 9.2 cells had the following history before their initial culture with algae: nine passages on spent algal medium, frozen, two pre-cultures on spent algal medium, inoculum. (D) ALE of *C. vulgaris* and Microbiome 26. Microbiome 26 cells were passaged twenty-six times in spent algal medium before their initial culture with algae. (E) Peak OD_{600}. The peak OD_{600} for each of the cultures is summarized here using the same colors as in the other subplots. All cultures were inoculated at OD_{600} = 0.1.

and 26 co-cultures, respectively. This indicates that the relationship between *C. vulgaris* and the Microbiome cells is stable and not parasitic.

4.4 Conclusions

The results of this work show that *Chlorella vulgaris*'s metabolism is highly dynamic and photosynthetic activity is increased by metabolite exchange with microbiome cells during co-culture. Because of inconsistent sunlight in nature (clouds, shading, nighttime) photosynthetic organisms have adapted to use starch and other internal carbon storage during periods of darkness. In this study, we showed that during light cycled autotrophic culture, *C. vulgaris* produced and consumed starch during light and dark phases, respectively. The cells change production/consumption mode within one hour of light condition change. This raised questions about the presence/extent of starch turnover. Starch turnover was present and at the same rate relative to the growth rate during constant autotrophic and heterotrophic growth. A significant cause of starch turnover was polysaccharide secretion. We showed that secreting polysaccharides was beneficial to the microalgae because during co-culture with microbiome cells their photosynthetic activity was increased.

This work has broader impacts in microalgal ecology and for biotechnology applications. Our observation of polysaccharide secretion and selection of cells from soil samples confirms that microalgae are primary producers for many ecosystems. Due to their desirable physiology, microalgae have been studied for biotechnological applications related to food, health supplements, and biofuel production (Sheehan et al. 1998; Dismukes et al. 2008; Rosenberg et al. 2008; Jones and Mayfield 2012; B. Liu and Benning 2013; Desai and Atsumi 2013; Wijffels, Kruse, and Hellingwerf 2013; Levering, Broddrick, and Zengler 2015; Heimann 2016; Scott et al. 2010). Two

important considerations for large-scale, outdoor microalgal biomass production are that sunlight is not constant and that contaminating organisms could enter the culture from the air (Santos and Reis 2014). This work has provided insight into light-cycled autotrophic growth and the need to limit biomass loss during dark phases. Additionally, adding the microbiome cells to a microalgal culture could increase the biodiversity of the culture and reduce unwanted contamination by other organisms.

Chapter 5

ELUCIDATING FLUXES IN COMPLEX MEDIA: ^{13}C METABOLIC FLUX ANALYSIS OF *ESCHERICHIA COLI* GROWN IN THE PRESENCE OF YEAST EXTRACT

5.1 Introduction

For the past two decades, understanding and quantifying metabolic fluxes has played an important role in the field of metabolic engineering (Zupke and Stephanopoulos 1994; Stephanopoulos 1999). Initially, metabolic flux analysis (MFA) was based on balancing fluxes within a metabolic model (reaction network stoichiometry) constrained by external rates (i.e. substrate uptake and product secretion rates) (Papoutsakis and Meyer 1985a, 1985b). Over the years, MFA methods have advanced to use isotopic labeling data (i.e. ^{13}Carbon tracers) (Wiechert 2001; Crown, Long, and Antoniewicz 2016) and sophisticated computer programs (Yoo et al. 2008; Young 2014) to describe various systems including: model microbes (Hayakawa, Matsuda, and Shimizu 2018; Kitamura, Toya, and Shimizu 2019), non-model microbes (Cordova et al. 2017), wild-type strains (C. P. Long et al. 2017), and engineered organisms (Schwechheimer, Becker, Peyriga, Portais, and Wittmann 2018); dynamic labeling (Ma et al. 2014); mono- and co-culture (Gebreselassie and Antoniewicz 2015); and liquid and solid media (Wolfsberg, Long, and Antoniewicz 2018).

The typical workflow for ^{13}C metabolic flux analysis begins with a tracer experiment. Here, the organism of interest is grown on a labeled substrate. For

example, [1,2-^{13}C]glucose has been shown to be an effective tracer for quantifying metabolic fluxes (Crown, Long, and Antoniewicz 2016). During steady-state growth, relevant external rates are measured (e.g. substrate uptake, product secretion, and growth rates) and isotopic labeling of proteinogenic amino acids is measured. Next, a computer program, such as Metran or INCA, enables the estimation of the metabolic fluxes by using experimental data, least squares regression, and a metabolic model (Yoo et al. 2008; Young 2014).

As discussed above, ^{13}C-MFA has been applied to many diverse organisms and experimental conditions. However, to date, nearly all ^{13}C-MFA studies have used chemically defined media (Schwechheimer, Becker, Peyriga, Portais, and Wittmann 2018). This is a problem since in practice many engineered strains and non-model organisms are grown in media containing yeast extract (or at least supplemented with additional carbon substrates beyond a single sugar). Yeast extract contains the water-soluble components of autolyzed yeast (usually *Saccharomyces cerevisiae*) and is an excellent source of vitamins, amino acids, peptides, and carbohydrates. Adding yeast extract to culture medium creates a rich environment for the cells to grow. The problem with using yeast extract for quantitative cell culture analysis is that yeast extract's composition is largely undefined and variable (each manufacturer has a slightly different production process which they claim yields a superior yeast extract product). Because of this, a methodology to determine metabolic fluxes during growth on yeast extract has not been fully developed.

In 2018, ^{13}C isotope tracer experiments with labeled yeast extract were performed on *Ashyba gossypii B2*, a filamentous hemiascomycete and industrial riboflavin overproducer strain. This was the first example of calculating carbon fluxes

for a system containing yeast extract. The approach followed in this study was to measure proteinogenic amino acids, glycogen, and riboflavin labeling patterns and combine that with additional labeling data from a prior study (Schwechheimer, Becker, Peyriga, Portais, Sauer, et al. 2018) to facilitate quantitative calculation of carbon fluxes during the growth and production phases. The approach for estimating metabolic fluxes during growth was as follows:

- Obtain the biomass composition of *A. gossypii* from a previously published genome-scale metabolic model (Ledesma-Amaro et al. 2014) with an adjustment of the lipid content
- Obtain riboflavin's precursor demand from the literature
- Calculate uptake rates of amino acids
- Calculate carbon fluxes using stoichiometric balances, ^{13}C labeling information, and the measured external rates.

The key findings from this study were:

- yeast extract is the major carbon source during growth;
- the TCA cycle was highly active while the pentose phosphate pathway and gluconeogenesis both had low flux
- guanine and GTP from yeast extract were incorporated in riboflavin (Schwechheimer, Becker, Peyriga, Portais, and Wittmann 2018).

In this Chapter, a novel methodology to quantify metabolic fluxes in the presence of yeast extract is presented. It is an improvement to the previous work (Schwechheimer, Becker, Peyriga, Portais, and Wittmann 2018) because the network model used for flux calculations is larger (103 vs 65 fluxes), it does not require measuring amino acid uptake rates, and uses a widely available software (Metran, (Yoo et al. 2008)). With the development of this methodology, future metabolic engineering projects involving complex media will be able to utilize ^{13}C-MFA to guide engineering efforts.

5.2 Materials and Methods

5.2.1 Materials

M9 minimal medium salts powder was purchased from Difco. Yeast Extract powder and glucose were purchased from Fisher Scientific. [U-^{13}C]glucose (98.9% ^{13}C) and [1,2-^{13}C]glucose (99.9% ^{13}C) were purchased from Cambridge Isotope Laboratories (Andover, MA). Glucose and yeast extract stock solutions were filter sterilized using Corning 0.22 μm filters. Derivatization chemicals were purchased from Sigma Aldrich. The centrifuge was a Beckman Coulter Microfuge 18. 1.5 mL Flex Tubes from Eppendorf were used for sample collection and storage.

5.2.2 Strain and Culture Conditions

E. coli K-12 MG1655 (ATCC Cat. No. 700926, Manassas, VA) was used for all experiments. First, a pre-culture was grown overnight in M9 minimal medium with 2 g/L unlabeled glucose starting from a 10% glycerol frozen stock. For the tracer experiments, the initial glucose concentration for all cultures was 1.7 g/L and the yeast extract concentration was either 0, 0.5, 1, or 2 g/L. The initial optical density (OD_{600}) of the inoculated cultures was approximately 0.01. Cells were grown aerobically in 125 mL baffled Pyrex shake flasks (25 mL initial volume) in a shaker (Barnstead Lab-Line Max^{Q} 4000) at 37 °C with 225 rpm shaking.

5.2.3 Analytical Methods

Cell growth was tracked by measuring the optical density at 600 nm (OD_{600}) using an Eppendorf Bio-Photometer with BRAND GMBH cuvettes. Biomass concentration was determined by converting the optical density with a conversion factor of 0.33 $g_{dw}/L/OD_{600}$ (C. P. Long, Gonzalez, et al. 2016). Medium glucose

concentration was measured using a YSI 2700 biochemistry analyzer (YSI, Yellow Springs, OH). Medium acetate concentration was measured by GC/MS (as described below) and HPLC (Agilent 1200 series). Medium and biomass samples were collected at OD_{600} of approximately 0.5, 1, 2, and 3 or until *E. coli* stopped growing. At each timepoint, samples were collected for protein, carbohydrate, and fatty acids analysis. The sample volume at each timepoint was such that enough biomass was collected for analysis of protein labeling (0.2 mg); carbohydrate labeling (0.2 mg); and fatty acid labeling (0.4 mg). Samples were centrifuged at 18,000 g for 5 minutes, and the supernatant and cell pellet were stored separately at -80 °C.

5.2.4 Gas Chromatography/Mass Spectrometry

Quantification of concentration and isotopic labeling analysis of *E. coli* biomass and yeast extract components were performed using previously published GC/MS methods (C. Long and Antoniewicz 2014; McConnell and Antoniewicz 2016). For analysis of protein, samples were hydrolyzed and amino acids were derivatized by tert-butyldimethylsilyl (TBDMS) for GC/MS analysis (Antoniewicz, Kelleher, and Stephanopoulos 2007a). For carbohydrate analysis, samples were hydrolyzed and then aldonitrile propionate derivatization was performed (McConnell and Antoniewicz 2016). GC/MS analysis was performed using an Agilent 7890B GC system equipped with a DB-5MS capillary column (30 m, 0.25 mm i.d., 0.25 µm-phase thickness; Agilent J & W Scientific), connected to an Agilent 5977A Mass Spectrometer operating under ionization by electron impact at 70 eV. Helium flow was at 1 mL/min. The source temperature was 230 °C, the MS quad temperature at 150 °C, the interface temperature at 280 °C, and the inlet temperature at 250 °C. Mass isotopomer distributions were obtained by integration (Antoniewicz, Kelleher, and

Stephanopoulos 2007a) and corrected for natural isotope abundances (Fernandez et al. 1996).

5.2.5 Metabolic Network Model

A detailed network model of *E. coli* metabolism was constructed based on previously published models (Antoniewicz et al. 2007; Leighty and Antoniewicz 2012; C. P. Long et al. 2018). The network model contained reactions for glycolysis, pentose phosphate pathway, ED pathway, TCA cycle, anaplerotic reactions, one-carbon metabolism, and amino acid biosynthesis (Table D.1). Dilution fluxes were added to describe unlabeled carbon from yeast extract contributing to the labeling patterns of proteinogenic amino acids. The Two Metabolic State Dilution Model is based on a co-culture modeling approach (Gebreselassie and Antoniewicz 2015).

5.2.6 Metabolic Flux Analysis

^{13}C-MFA was performed using the Metran software (Yoo et al. 2008), which is based on the elementary metabolite units framework (Antoniewicz, Kelleher, and Stephanopoulos 2007b). Fluxes were estimated by minimizing the variance-weighted sum of squared residuals (SSR) between the experimentally measured and model predicted extracellular rates and mass isotopomer distributions of proteinogenic amino acids using non-linear least-squares regression. Confidence intervals for all fluxes were calculated by evaluating the sensitivity of the minimized SSR to flux variations (Antoniewicz, Kelleher, and Stephanopoulos 2006).

5.2.7 Goodness-of-Fit Analysis

If the experimental data do not have large errors and the model is correct, then the minimized variance-weighted SSR is a stochastic variable with χ^2-distribution.

Within Metran, the flux results were subjected to a χ^2-statistical test to assess the goodness-of-fit and determine if the metabolic network model was appropriate to describe the data. The degree of freedom is the number of fitted measurements (n) minus the number of estimated independent parameters (p). Then, the acceptable SSR range is between $\chi^2_{\frac{\alpha}{2}}(n-p)$ and $\chi^2_{1-\frac{\alpha}{2}}(n-p)$ where α is the significance level (Antoniewicz, Kelleher, and Stephanopoulos 2006). The model was deemed inappropriate if the SSR value was above the upper threshold of the χ^2-statistical test (Wolfsberg, Long, and Antoniewicz 2018).

5.3 Results and Discussion

5.3.1 Amino Acid Content of *E. coli* and *S. cerevisiae*

Yeast extract contains the water-soluble components of autolyzed yeast (usually *Saccharomyces cerevisiae*) which is an excellent source of vitamins, amino acids, peptides, and carbohydrates. The exact content of yeast extract is unknown, and the composition of yeast extract will vary by vendor (Kasprow, Lange, and Kirwan 1998). However, the amino acid content of yeast extract typically reflects the protein content of the yeast cells. Figure 5.1 shows the proteinogenic amino acid content of *S. cerevisiae* as reported in the literature (Forster et al. 2003) compared to *E. coli* amino acid composition (C. P. Long, Gonzalez, et al. 2016). Alanine (Ala), glutamate/ glutamine (Glx), and aspartate/asparagine (Asx) are the three most abundant proteinogenic amino acids at roughly 40-45 mmol/100 g cells. Tyrosine (Tyr), histidine (His), and methionine (Met) are the three least abundant proteinogenic amino acids at roughly 5-10 mmol/100 g cells.

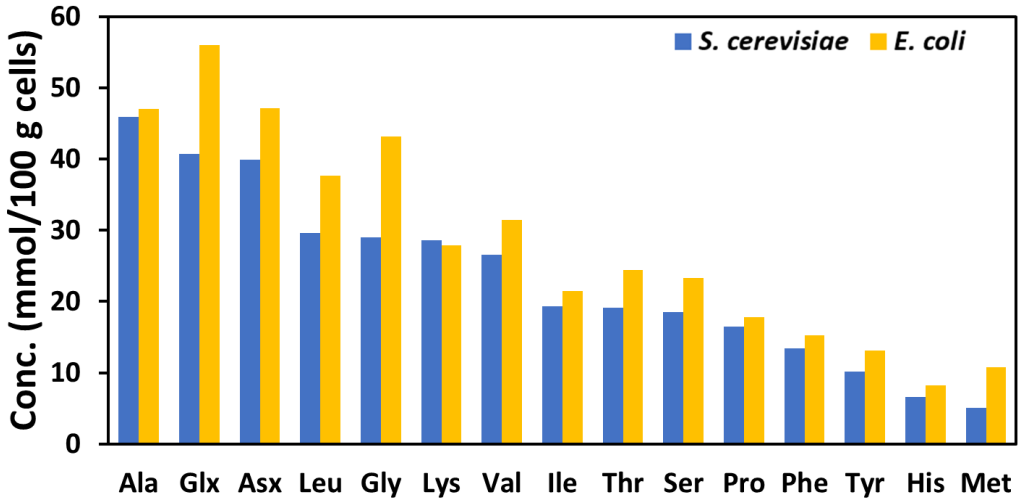

Figure 5.1 Amino acid content of *Saccromyces cerevisiae* and *E. coli*. The amino acid profiles are similar, but *E. coli* has an overall higher amino acid content. Based on discrepancies in the amino acid contents, methionine, glycine, glutamate/glutamine, aspartate/asparagine, and leucine will likely become depleted quickly

It is important to compare the amino acid profiles of the two organisms to gain initial insights into which amino acids may possibly become depleted from the medium early in the cell culture, assuming amino acid uptake is directly proportional to the biomass composition. Based on the reported biomass composition data, glutamate/glutamine, glycine, aspartate/asparagine, leucine, and methionine are the amino acids with the largest discrepancies in proteinogenic amino acid content between *E. coli* and *S. cerevisiae*. Based on this analysis and assuming consumed amino acids go straight to biomass proteins, these amino acids may be expected to become depleted first from the medium.

5.3.2 Contribution of Glucose and Yeast Extract to Biomass Formation

Before performing metabolic flux analysis, we first quantified the contribution of glucose and yeast extract to biomass formation. This was accomplished by performing a set of tracer experiments using 1.7 g/L [U-^{13}C]glucose with either 0, 0.5, 1, or 2 g/L of yeast extract (Figure 5.2A). Since the glucose was fully ^{13}C labeled and the yeast extract was fully unlabeled, we could use mass spectrometry to distinguish between these isotopes and determine which substrate contributed carbon to the various biomass components. Additionally, GC/MS allowed us to determine if amino acids remained intact, or were broken down and converted into other metabolites based on the labeling profiles, i.e. partially labeled metabolites would have been created from carbon originally contained in both glucose and yeast extract.

5.3.2.1 Yeast Extract Supplementation Increases Biomass Titer

Figure 5.2B shows the growth curves of the cultures described in Figure 5.2A. All cultures were inoculated at an OD_{600} of approximately 0.01. At the very early stages of growth, all three yeast extract cultures grew at a similar rate. This would suggest that none of the major components from the yeast extract had been depleted yet. However, starting around hour 2, the 0.5 g/L yeast extract culture's growth rate slowed down; and starting around hour 3.5, the 1 g/L yeast extract started to slow down as well (relative to the 2 g/L yeast extract). Figure 5.2C summarizes the growth rates for each of the four cultures up to an OD_{600} of about 1.0. The no yeast extract culture's growth rate was $0.65 \pm 0.01\ h^{-1}$. Addition of 0.5 g/L yeast extract resulted in a significant increase in the growth rate at $1.03 \pm 0.08\ h^{-1}$. The 1 g/L and 2 g/L yeast extract cultures had similar growth rates up to an OD_{600} of 1 at $1.31 \pm 0.07\ h^{-1}$ and $1.37 \pm 0.05\ h^{-1}$, respectively, which is roughly a 2-fold increase over the no

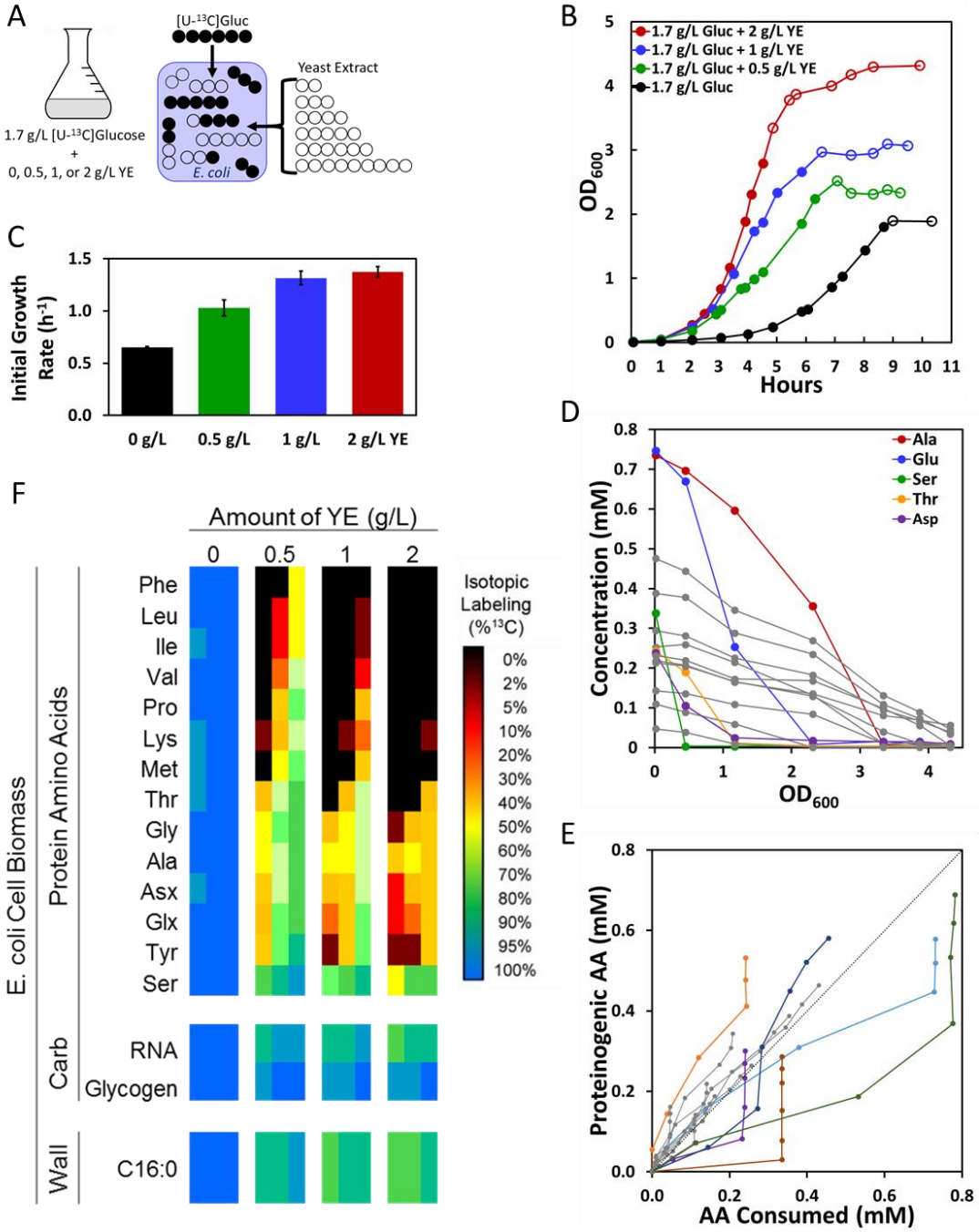
A
[U-13C]Gluc
Yeast Extract
1.7 g/L [U-13C]Glucose
+
0, 0.5, 1, or 2 g/L YE
E. coli
B
1.7 g/L Gluc + 2 g/L YE
1.7 g/L Gluc + 1 g/L YE
1.7 g/L Gluc + 0.5 g/L YE
1.7 g/L Gluc
OD600
Hours
C
Initial Growth Rate (h-1)
0 g/L
0.5 g/L
1 g/L
2 g/L YE
D
Ala
Glu
Ser
Thr
Asp
Concentration (mM)
OD600
E
Proteinogenic AA (mM)
AA Consumed (mM)
F
Amount of YE (g/L)
0
0.5
1
2
E. coli Cell Biomass
Protein Amino Acids
Carb
Wall
Phe
Leu
Ile
Val
Pro
Lys
Met
Thr
Gly
Ala
Asx
Glx
Tyr
Ser
RNA
Glycogen
C16:0
Isotopic Labeling (%13C)
0%
2%
5%
10%
20%
30%
40%
50%
60%
70%
80%
90%
95%
100%

Figure 5.2 Relative Contributions of Glucose and Yeast Extract to Biomass. (A) Experimental Design. Four parallel cultures were performed with [U-^{13}C]glucose and varying concentrations of yeast extract. (B) Growth curves. Open circles denote that the glucose concentration is 0 mM. Only the 2 g/L yeast extract culture contains enough carbon for the cells to continue growing after glucose depletion. (C) Initial Growth Rate. The growth rate was calculated up to OD_{600} = 1 for each culture. (D) Amino acid consumption for 1.7 g/L glucose + 2 g/L yeast extract. Alanine, Glutamate, Serine, Threonine, and Aspartate are the amino acids with the highest consumption rates. (E) Actual vs Predicted Amino Acid Consumption. The AA Consumed was obtained by direct measurement. The Proteinogenic AA was obtained by measuring the culture's optical density, converting that g_{dw}/L, and using previously reported biomass composition data. (F) Labeling Profiles. The average carbon labeling is shown for each of the four cultures. Each column is time-course moving from left to right.

yeast extract culture. For analysis of biomass yields and glucose uptake rates, see Figure 5.6 and Table 5.1.

An additional benefit for this experiment was to be able to observe the change in OD_{600} upon glucose depletion (in Figure 5.2B open circles denote glucose = 0 g/L). For three cultures (excluding the 2 g/L yeast extract culture), upon glucose depletion the OD_{600} remained relatively constant. This suggests that for these cultures the late stage of growth was on glucose, whereas the late stage of growth for the 2 g/L yeast extract culture was on yeast extract as carbon sources. In other words, the major carbon sources from yeast extract in the 0.5 g/L and 1 g/L cultures become depleted before glucose whereas the opposite was true for 2 g/L yeast extract. More detailed analysis of yeast extract depletion was obtained by measuring the amino acid concentration in the medium during the culture (Figure 5.2D).

5.3.2.2 Amino Acid Consumption from Yeast Extract Medium

Alanine and glutamate are the two most abundant amino acids in the Fisher Scientific yeast extract (2 g/L yeast extract contains about 0.75 mM of each of those amino acids). Tyrosine, methionine, and proline are the three least abundant amino acids (ranging from roughly 0.05 to 0.15 mM for 2 g/L yeast extract). These results agree with *S. cerevisiae* proteinogenic amino acid content shown in Figure 5.1. Supplemental Figure D.1 compares the amino acid profile of *S. cerevisiae* and Fisher Scientific yeast extract.

We determined that five amino acids experienced a non-constant uptake rate indicating that they were not only consumed for protein production but also used as intracellular carbon sources. Serine, aspartate, and threonine were consumed quickly and depleted by an OD_{600} of 1. Glutamate was depleted before an OD_{600} of 1.5 and alanine was depleted around an OD_{600} of 3. The carbon from these amino acids was likely entering central carbon metabolism; thus, these amino acids were considered as potential sources of labeling dilution and incorporated into our initial metabolic model.

Figure 5.2E shows the actual versus predicted amino acid consumption. "Amino acid consumed" (mM, x-axis) is the concentration of an amino acid consumed from the medium and was calculated from the data shown in Figure 5.2D. "Proteinogenic amino acid" (mM, y-axis) is the concentration of proteinogenic amino acid within the culture. This was calculated using measured OD_{600} values and previously published physiological and biomass composition data (C. P. Long, Gonzalez, et al. 2016). In this Figure, if the data fall on the dashed line, then the consumption rate matches the biomass composition requirement. If the data is above the dashed line, then the consumption is lower than the biomass composition

requirement, which suggests that the particular amino acid is being made from other amino acids or glucose. If the data fall below the dashed line, then the consumption rate is higher than the biomass composition requirement, which suggests that the particular amino acid is either being converted into another amino acid or degraded to generate energy.

The highly consumed amino acids seen in Figure 5.2D (alanine, glutamate, serine, and threonine) are the amino acids with the largest deviations below the dashed line. This result strongly suggests that these amino acids were used for more than just protein synthesis. The "Asx" data is the combined results for aspartate and asparagine because while hydrolyzing the protein to amino acids, asparagine degrades to aspartate so we cannot measure asparagine in the biomass directly. When looking at the "Asx" line, initially it is below the dashed line and then it jumps above the dashed line. The initial segment represents aspartate consumption and the final segment is for asparagine consumption. So, this result indicates that aspartate is used for more than just biomass protein synthesis.

Glycine was the amino acid with the largest deviation above the dashed line. This suggests that the consumption was lower than the biomass composition requirement and that glycine was being produced from other amino acids or from glucose. It is well known that serine and glycine can be interconverted through one-carbon metabolism (Amelio et al. 2014). Since serine had a very high uptake rate, glycine was likely being made from serine.

An additional trend observed in our data is that upon depletion from the medium, an amino acid is no longer consumed, but it is made from other carbon sources. This leads to the vertical line segments in Figure 5.2E. The amino acids

which deviated the most from the dashed line in Figure 5.2E were the first targets to include in the metabolic modeling.

5.3.2.3 Other Components of Yeast Extract

Additional analysis was performed on the culture medium to determine the presence or absence of peptides, monosaccharides, or polysaccharides. Supplemental Figure D.2 shows the concentration of protein in the medium for the three yeast extract containing cultures. The medium protein concentration was relatively constant throughout the cultures. The 0.5 g/L, 1 g/L, and 2 g/L yeast extract supplementation had medium protein concentrations of 0.044 g/L, 0.087 g/L, and 0.17 g/L, respectively. This result suggests that *E. coli* does not consume protein from the medium and that the protein content of yeast extract is relatively low (less than 10% by weight).

To quantify the glucose content in yeast extract, the glucose concentration was measured by a YSI Analyzer and then the labeling of glucose was measured by GC/MS. Unlabeled glucose was less than 0.5% of the total glucose, indicating that yeast extract contributed very little glucose to the medium. Free ribose was not detected.

To test for the presence of polysaccharides, medium samples were hydrolyzed and then analyzed on the GC/MS. For the 2 g/L yeast extract culture, the glucose content of polysaccharides was only about 0.1 g/L which is small (6%) compared to the free glucose concentration of 1.7 g/L. Yeast extract's contribution of ribose to the medium was not quantified, but ribose was detected by GC/MS indicating that yeast extract does contain some ribose within polysaccharides.

5.3.2.4 Time-Course Biomass Labeling

Figure 5.2F shows a heat map of the time-course isotopic labeling percentage of various *E. coli* biomass components for the four tracer cultures. All of the biomass components within the no yeast extract control culture were above 93% which confirms that there were very small amounts of other carbon substrates present in the culture. Within the proteinogenic amino acid section, the amino acids listed at the top are only produced from glucose when they are depleted from the medium. For the amino acids listed at the bottom of the section, those amino acids are produced from glucose even if the amino acid is present in the medium. The varied degree of labeling shows that the consumption and synthesis phases vary for each of the amino acids. Serine was previously shown to be quickly consumed from the medium (Figure 5.2D). Since serine was depleted from the medium, it had to be produced from the glucose; therefore, it was the amino acid with the highest average carbon labeling. Inspection of the ribose labeling suggests that there was a contribution of ribose from the yeast extract to *E. coli*'s RNA.

5.3.3 Amino Acid Synthesis and Degradation Pathways

Figure 5.3 shows the network model for *E. coli* central carbon metabolism (black arrows) along with amino acid synthesis nodes (blue arrows) and amino acid degradation nodes (red arrows). This central carbon metabolism model with amino acid synthesis reactions has been shown to be effective for describing *E. coli* metabolism in previous studies (Leighty and Antoniewicz 2012). The amino acid degradation pathways were obtained from the literature (Link et al. 2015). The nodes identified from literature were used for the initial model testing.

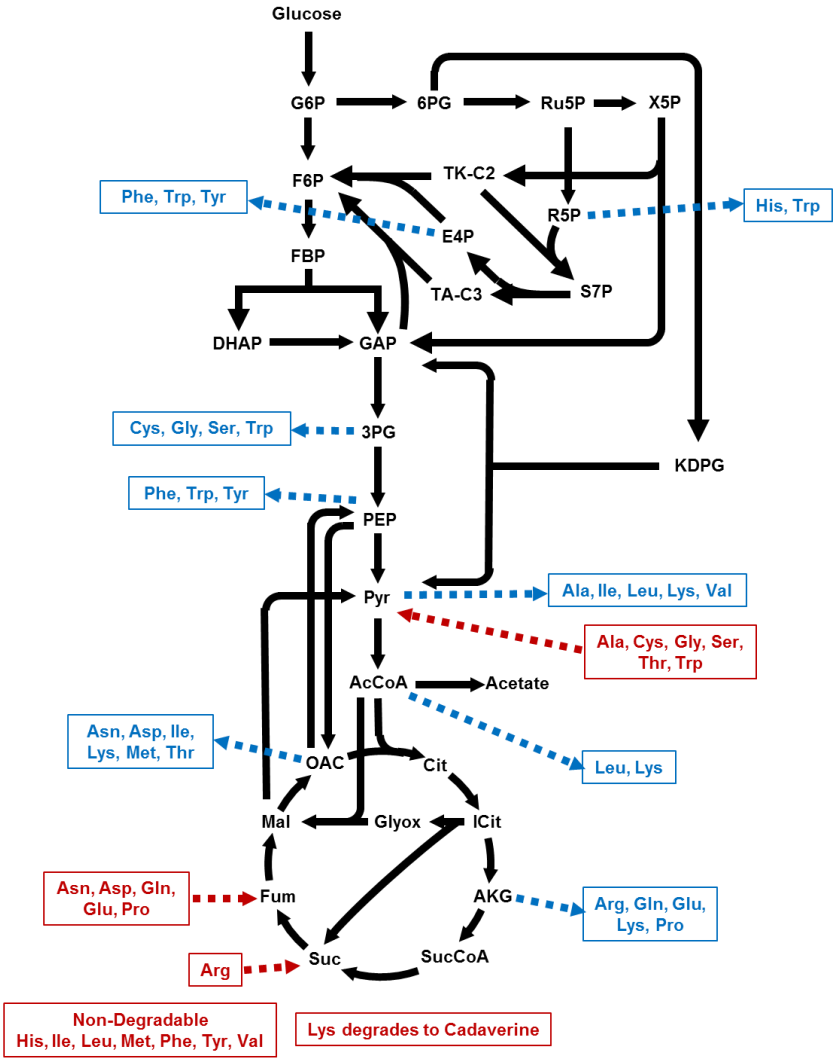

Figure 5.3 Amino acid synthesis and degradation pathways in *E. coli*. The black arrows represent reactions within central carbon metabolism. The blue arrows represent synthesis of amino acids from central carbon metabolism. The red arrows represent degradation of amino acids to central carbon metabolism. Consuming amino acids from the medium dramatically increases *E. coli*'s growth rate due to decreased carbon and energetic costs required to synthesize amino acids from glucose and ammonium. Consuming amino acids rather than synthesizing amino acids saves 0.134 mol ATP and 0.122 mol NADPH per Cmol Biomass.

Additionally, coupling the biomass synthesis reaction stoichiometry (amino acid → biomass) with the energetic cost (ATP and NADPH) to make amino acids from central carbon metabolite precursors, it is possible to calculate the ATP and NADPH saved by not having to synthesize amino acids. Per C-mol of biomass formed, 0.134 mol ATP and 0.122 mol NADPH are saved by consuming amino acids from the medium. There is also the kinetic benefit of not having to synthesize the amino acids.

5.3.4 Single Source of Dilution Model

It has been shown previously that CO_2 dilution is needed for flux analysis in minimal media (Leighty and Antoniewicz 2012). So, the base model used in this work already contained carbon dioxide dilution. As an initial test, models with one additional source of dilution were tested to investigate if that was sufficient to describe the labeling profiles obtained in the [U-^{13}C]glucose and unlabeled yeast extract cultures. Figure 5.4A shows the network model with the tested dilution reactions in red. These dilution sources were chosen based on the amino acid consumption profiles shown above and the metabolic nodes associated with those amino acids.

Figure 5.4B shows the sum of square residuals for the various models tested. The control model only contained carbon dioxide dilution and it resulted in SSR's over 2000 for three different timepoints of the 2 g/L yeast extract culture (upper limit of the acceptable range was 165). Eight different single dilution models were tested and including pyruvate dilution was the most beneficial. Adding pyruvate dilution reduced the SSR from over 2000 to about 500-600. It makes sense that adding pyruvate dilution resulted in a significant SSR reduction since six amino acids degrade into pyruvate and pyruvate is a key node in central carbon metabolism

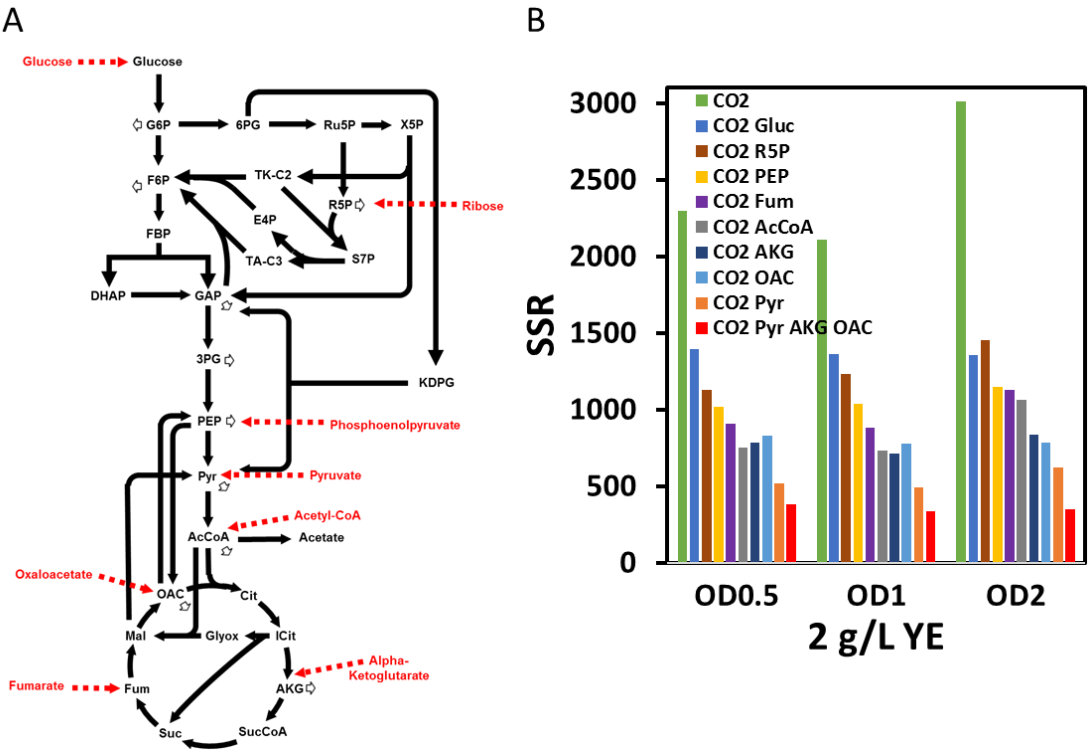

Figure 5.4 Single Dilution Source Model Testing. (A) Network map. The filled black arrows represent reactions typically contained within a network model of *E. coli* central carbon metabolism. The open black arrows represent reactions for metabolites going towards biomass synthesis. The red dashed arrows represent reactions for labeling dilution due to carbon from yeast extract entering central carbon metabolism. For the testing in this section, only one red arrow was active during model testing. (B) Summary of Model SSR. The base model contains CO_2 dilution so all models contained that dilution. Since including one additional dilution flux did not yield acceptable fits, a triple dilution model was tested using the three best single dilutions. However, that did not provide an acceptable fit either.

(Link et al. 2015). However, these SSR's were still above the upper limit of the acceptable range of approximately 165. Alpha-ketoglutarate and oxaloacetate dilutions were helpful since they are precursors for eleven amino acids. As an extension, the three most beneficial dilutions (pyruvate, alpha-ketoglutarate, and oxaloacetate) were

combined for a triple-dilution model. This had a slight improvement in SSR, but it was still not within the acceptable range, so another model expansion was necessary.

5.3.5 Parallel Dilution Model

Since a more sophisticated metabolic model was needed than the triple-dilutions model, a parallel dilution model was created as shown in Figure 5.5A. This model still has a single central carbon metabolism network. However, there are two different dilution states, although the core metabolic fluxes are the same in each state. There are two dilution states because some components of the yeast extract become depleted, so it is impossible for them to contribute unlabeled carbon to metabolism. The dilution sources in State #1 are ribose, pyruvate, serine, oxaloacetate, and alpha-ketoglutarate. Serine and oxaloacetate are the two dilution sources that are present in State #1 but not State #2.

Figure 5.5B shows that this model was able to obtain a statistically acceptable fit up to an OD_{600} of 2 for each of the yeast extract cultures except for an OD_{600} of 2 in the 0.5 g/L yeast extract culture which was just slightly above the acceptable range. For this analysis, an acceptable fit means that the model was able to reproduce the labeling of proteinogenic amino acids. Since this tracer experiment was performed with [U-^{13}C]glucose and unlabeled yeast extract, an acceptable model can properly distinguish between amino acid carbons that were derived from glucose or yeast extract. This model was deemed acceptable to be used in a proper tracer experiment with [1,2-^{13}C]glucose, instead of [U-^{13}C]glucose, for 13C metabolic flux analysis; i.e. while [U-^{13}C]glucose was a good tracer to determine the relative contributions of glucose and yeast extract to biomass, it does not provide informative labeling patterns that can be used to calculate metabolic fluxes (Crown, Long, and Antoniewicz 2016).

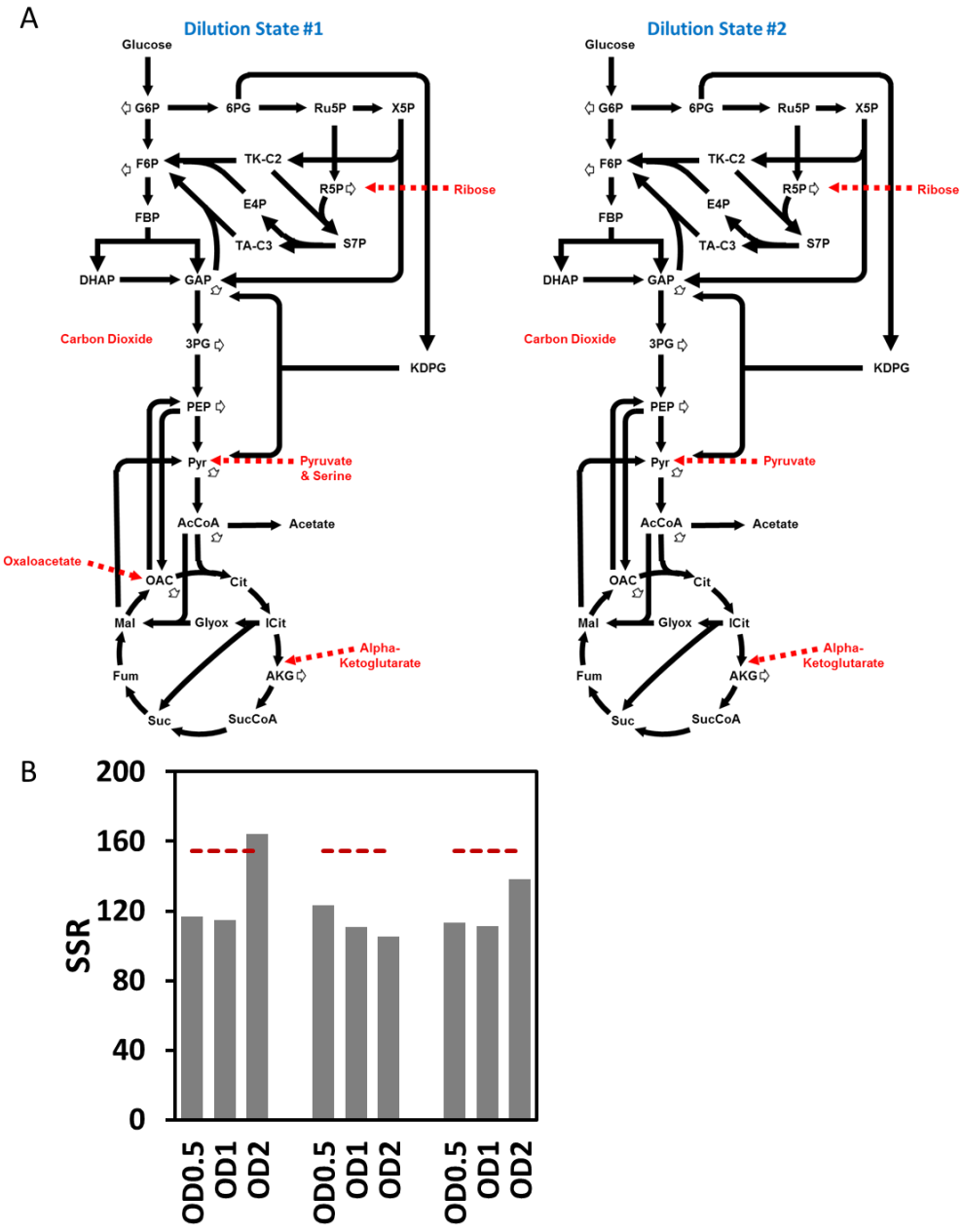

Figure 5.5 Parallel Dilution Model Testing. (A) Network model. This model contains two different dilution states, but the metabolic fluxes shown in black are the same for each state. Dilution State #2 does not contain serine or oxaloacetate dilution because the components of yeast extract related to these metabolites become depleted early in the culture. (B) SSR Summary. All the timepoints were acceptable except for OD = 2 for the 0.5 g/L yeast extract culture.

5.3.6 Two Metabolic States Dilution Model

Figure 5.6A shows the experimental design for the tracer experiments that were performed with [1,2-^{13}C]glucose. First, the Parallel Dilution Model was used to calculate metabolic fluxes for these cultures; however, the fits were not statistically acceptable. So, further analysis was needed to develop another representative metabolic model.

5.3.6.1 Glucose Uptake Rate

The first step was to analyze the glucose uptake for each of the four cultures. Figure 5.6B show the biomass yield on glucose, $Y_{X/S}$, for the four cultures:

$$Y_{X/S} = \frac{\Delta C_{biomass}}{\Delta C_{glucose}}$$

where $\Delta C_{biomass}$ is the change in biomass concentration and $\Delta C_{glucose}$ is the change in glucose concentration for a given amount of time. The no yeast extract culture had the lowest biomass yield on glucose at $0.331 \pm 0.004\ g_{dw}/g_{gluc}$ (which is similar to previously reported biomass yield of 0.414 ± 0.008 g/g in (C. P. Long, Gonzalez, et al. 2016)). The yeast extract containing cultures had a higher yield on glucose since they also obtained carbon and electrons from the yeast extract. The biomass yield for the 0.5 g/L, 1 g/L, and 2 g/L yeast extract cultures were 0.49 ± 0.01, 0.57 ± 0.01, and $0.64 \pm 0.01\ g_{dw}/g_{gluc}$, respectively. Thus, the biomass yield on glucose increased with increasing yeast extract concentration, as could be expected.

The biomass specific glucose uptake rate was calculated as follows:

$$-q_s = \frac{\mu}{Y_{X/S}}$$

where μ is the growth rate and $Y_{X/S}$ is the biomass yield on glucose. Table 5.1 lists the specific growth rate, biomass yield, and glucose uptake rate for the four cultures. The

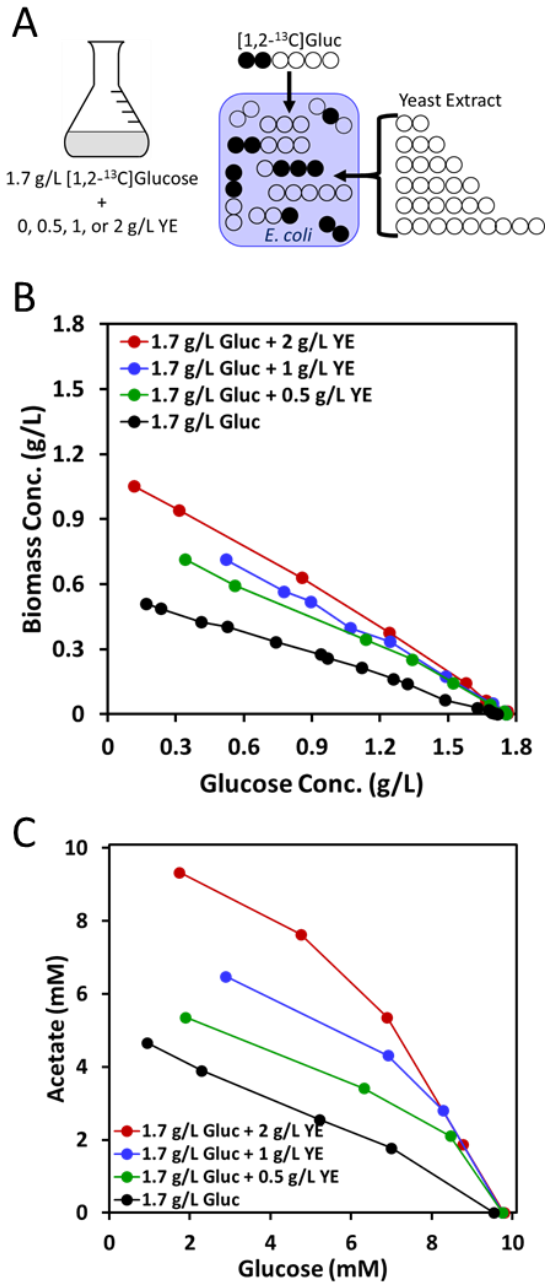

Figure 5.6 Tracer experiment with [1,2-^{13}C]glucose and unlabeled yeast extract. (A) Experimental Design. As the various substrates are metabolized, there will be carbon rearrangements and changes in labeling patterns. (B) Biomass Yield on Glucose. Yeast extract supplementation increases the biomass yield on glucose. (C) Acetate Yield. For yeast extract cultures, initially the acetate yield is high and then it lowers as metabolites are consumed from the medium.

no yeast extract culture had the lowest glucose uptake rate at 1.72 ± 0.01 g/g/h (similar to previously reported glucose uptake rate of 1.53 ± 0.04 g/g/h in (C. P. Long, Gonzalez, et al. 2016)). The glucose uptake rate for the 0.5 and 1 g/L yeast extract cultures were similar. Increasing the yeast extract concentration to 2 g/L slightly reduced the glucose uptake rate, possibly because there was even more opportunity to consume the amino acids.

Table 5.1 *E. coli*'s Physiological Response to Yeast Extract Supplementation in Cultures with M9 Minimal Salts and Glucose

YE Concentration (g/L)	Growth Rate (1/h)	Biomass Yield (g_{dw}/g_{gluc})	Glucose Uptake Rate ($g_{gluc}/g_{dw}/h$)
0 g/L YE	0.57 ± 0.02	0.331 ± 0.004	1.72 ± 0.01
0.5 g/L YE	1.11 ± 0.10	0.49 ± 0.01	2.25 ± 0.05
1 g/L YE	1.29 ± 0.09	0.57 ± 0.01	2.26 ± 0.05
2 g/L YE	1.34 ± 0.04	0.64 ± 0.01	2.09 ± 0.03

5.3.6.2 Acetate Yield

The next step was to analyze the acetate yield. The acetate yield is defined as

$$Y_{A/S} = \frac{\Delta C_{acetate}}{\Delta C_{glucose}}$$

where $\Delta C_{acetate}$ is the change in concentration of acetate and $\Delta C_{glucose}$ is the change in concentration of glucose over a given time range. The plot of acetate concentration vs glucose concentration is shown in Figure 5.6C. The acetate yield is the slope of the data in this plot. The no yeast extract culture had a relatively constant yield of 0.58 ± 0.04 mol/mol (which is slightly lower than the previously reported acetate yield of 0.714 ± 0.003 mol/mol in (C. P. Long, Gonzalez, et al. 2016)). For the yeast extract

containing cultures, there appeared to be two different slopes, an early and a late phase yield. Table 5.2 shows the acetate yield in the two phases of each culture. Initially, the cultures had a rather high acetate yield of 1.83, 2.01, and 2.04 ± 0.03 mol/mol for the 0.5 g/L, 1 g/L, and 2 g/L yeast extract cultures, respectively. Then, as the components of the yeast extract become depleted, the acetate yield decreased to 0.51 ± 0.05, 0.56, and 0.58 mol/mol for the 0.5 g/L, 1 g/L, and 2 g/L yeast extract cultures, respectively, which is surprisingly similar to the acetate yield for the no yeast extract culture.

Since there were two phases of acetate yield, the central carbon metabolism fluxes will be different in each phase. Therefore, the Parallel Dilution Model was expanded so that the metabolic fluxes in each state can be unique and State #1 has a high acetate yield while State #2 has a low acetate yield. The dilution fluxes are the same as a Parallel Dilution Model. Figure 5.7 shows the network model for this Two Metabolic States Dilution Model.

Table 5.2 Acetate Yield on Glucose with Varying Yeast Extract Supplementation

YE Concentration (g/L)	Early Yield (mol/mol)*	Late Yield (mol/mol)*
0 g/L YE	0.58 ± 0.04	N/A
0.5 g/L YE	1.83	0.51 ± 0.05
1 g/L YE	2.01	0.56
2 g/L YE	2.04 ± 0.03	0.58

* Yield without an error were calculated using only two measurements

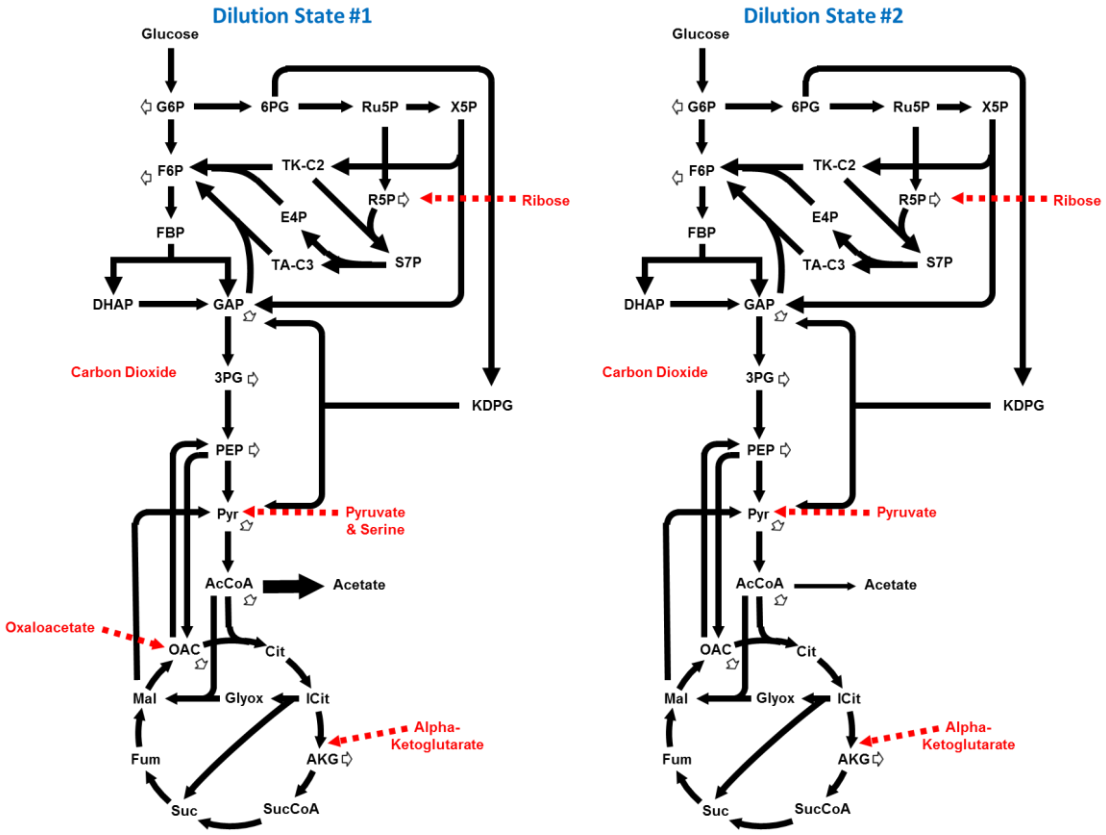

Figure 5.7 Two Metabolic States Dilution Model. Due to the variable acetate yield, a new model was developed with two dilution states that have unique metabolic fluxes. Also, Dilution State #1 has a large acetate yield and Dilution State #2 has a low acetate yield. The dilution fluxes are the same as in the Parallel Dilution Model.

5.3.7 ^{13}C Metabolic Flux Analysis

5.3.7.1 1.7 g/L [1,2-^{13}C]glucose without Yeast Extract

The first task was to calculate the metabolic fluxes for the 1.7 g/L [1,2-^{13}C]glucose culture using previously established methods to confirm that the control case worked and gain confidence in the cell culture execution and GC/MS data collection processes. Figure 5.8 shows the flux results obtained in this study using

[1,2-^{13}C]glucose as the only carbon source (Table D.2 contains the measured mass isotopomer distributions used to calculate fluxes. Table D.3 shows the flux result details.) In this study, the normalized fluxes (i.e. relative to glucose uptake rate) of glycolysis and oxidative pentose phosphate pathway were 68 ± 1 and 30 ± 1, respectively. This is in good agreement with the previously reported 77 ± 0.3 and 22 ± 0.3 (Wolfsberg, Long, and Antoniewicz 2018). In this study, the flux into AcCoA from pyruvate was 110 ± 6 and the fluxes out of AcCoA were 66 ± 10 to acetate and 17 ± 2 to citrate (balance was drained for biomass formation). This is in good agreement with the previously reported 107 ± 4, 64 ± 6, and 19 ± 1, respectively (Wolfsberg, Long, and Antoniewicz 2018). Overall, there was good agreement with previously published flux maps which gives confidence in the experimental data collected in this study.

The main sources of disagreement for the above results is the tracer selection. In this study, a single tracer was used, whereas in (Wolfsberg, Long, and Antoniewicz 2018), three different tracers were used in parallel. Additionally, this study used shake flasks whereas the other study used small-scale bubble-column bioreactors (C. P. Long et al. 2017).

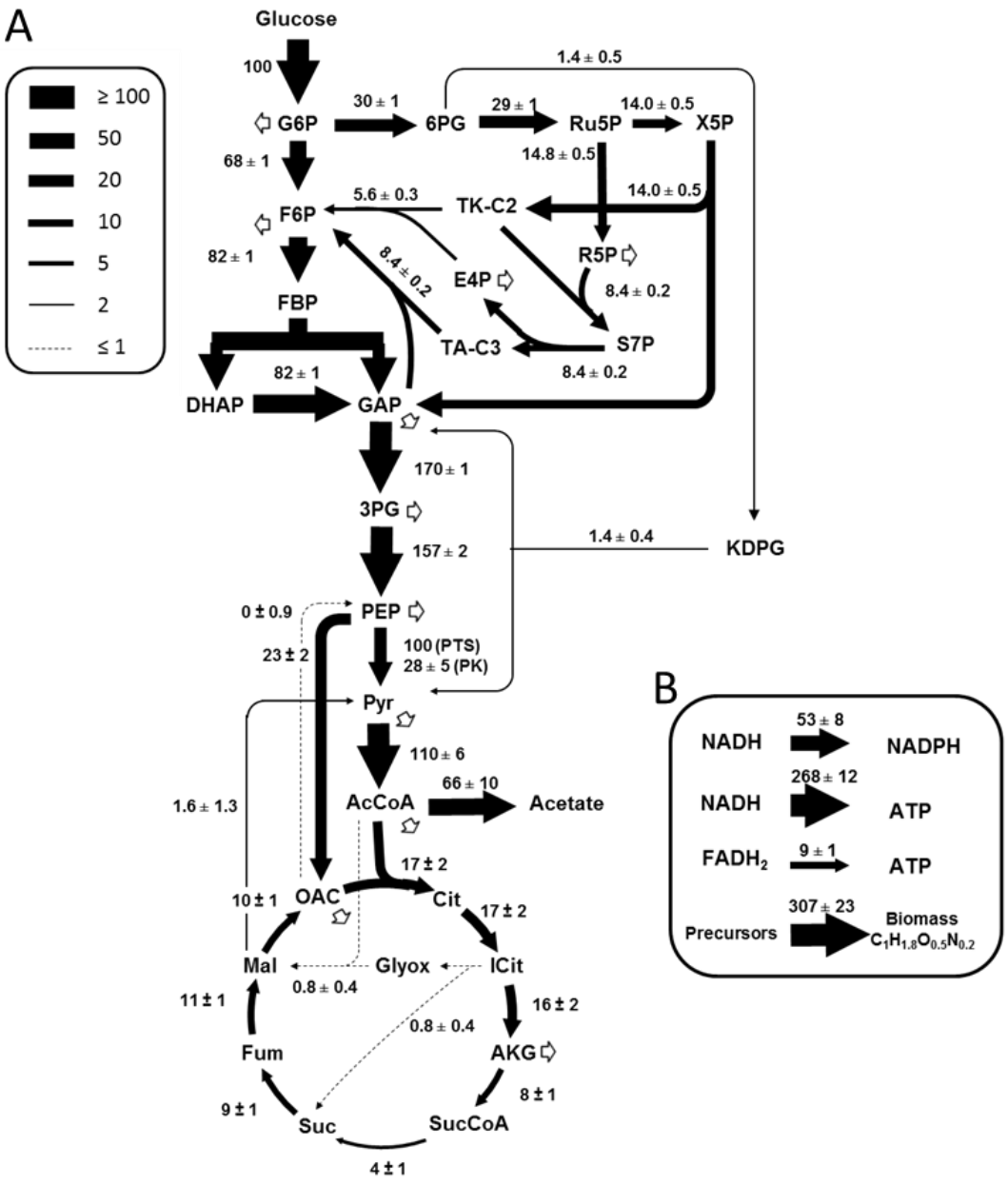

Figure 5.8 1.7 g/L [1,2-^{13}C]Glucose Flux Map. (A) This flux map compares closely to previously published flux maps done with parallel fitting. (B) The energy balances and precursor drain to biomass also compare well to previously published work.

5.3.7.2 1.7 g/L [1,2-^{13}C]glucose + 0.5 g/L Yeast Extract

The Two Metabolic States Dilution Model was able to obtain a statistically acceptable fit for the 1.7 g/L [1,2-^{13}C]glucose + 0.5 g/L yeast extract cultures at OD_{600} of 0.4, 1.0, and 2.2. The flux results are shown in Figure 5.9. (Table D.2 contains the measured mass isotopomer distributions used to calculate fluxes. Table D.4 shows the flux result details.) Comparing the two metabolic states, the following observations can be made:

- State #1 has a lower flux through the oxidative pentose phosphate pathway
- State #1 has a higher flux through glycolysis
- State #1 has a higher flux to acetate
- State #1 has very low TCA cycle fluxes
- State #2 has more central carbon metabolite precursors drained to biomass
- State #2 has low dilution fluxes.

Additionally, comparing State #1 and State #2 to the flux map obtained for the no yeast extract culture, it is seen that State #2 is very similar to the fluxes for growth solely on glucose. This confirms that State #1 represents the fluxes for growth on glucose and yeast extract simultaneously while State #2 represents the fluxes for growth on glucose alone. Knowing this, the trends observed in State #1 can be explained. The flux through the oxidative pentose phosphate pathway is reduced during growth on yeast extract and glucose since the demand for NADPH is reduced because the cells can obtain amino acids from the medium. The oxidative pentose phosphate pathway is not eliminated though because some NADPH is still needed for other anabolic processes such as fatty acid biosynthesis. Additionally, the TCA cycle fluxes and the precursor drain to biomass are very low because the cells can consume amino acids from the medium and do not need to synthesize them. State #2 has low

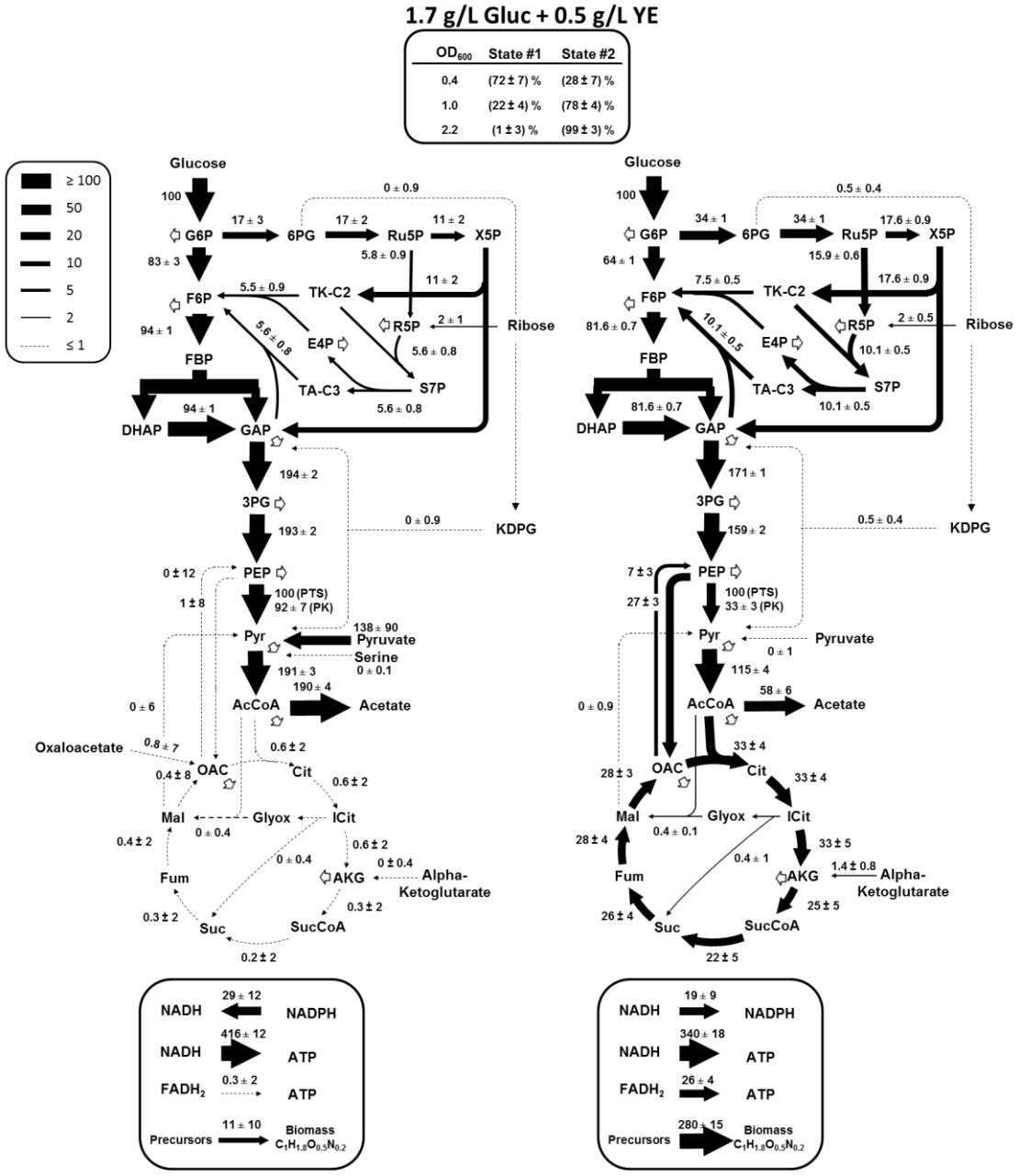

Figure 5.9 ^{13}C Metabolic Flux Analysis of *E. coli* growth on 1.7 g/L [1,2-^{13}C]glucose + 0.5 g/L yeast extract. The estimated flux map was determined using proteinogenic amino acid, glycogen, and RNA labeling data. White arrows represent outflux to biomass.

dilution fluxes because it approximates later stages of the culture when the major components of yeast extract have been depleted. Additionally, State #2's TCA cycle fluxes are higher than the 0 g/L, but the AKG drain to biomass is similar for both.

Figure 5.9 also shows the energy balance fluxes. The transhydrogenase flux for $NADH \rightarrow NADPH$ is in opposite directions for State #1 and State #2. State #1 occurs during simultaneous growth on glucose and yeast extract which is a rich environment so the cells have low NADPH needs. This flux is higher for the no yeast extract culture than State #2 for the 0.5 g/L yeast extract culture reflecting the higher NADPH demand without obtaining amino acids from yeast extract. Another difference is with the oxidative phosphorylation flux, i.e. $NADH \rightarrow ATP$. NADH is produced by catabolic reactions which have higher fluxes for growth on yeast extract.

5.3.7.3 1.7 g/L [1,2-^{13}C]glucose + 1 g/L Yeast Extract

The Two Metabolic States Dilution Model was able to obtain a statistically acceptable fit for the 1.7 g/L [1,2-^{13}C]glucose + 1 g/L yeast extract cultures at OD_{600} of 0.6, 1.0, and 2.2. The flux results are shown in Figure 5.10. (Table D.2 contains the measured mass isotopomer distributions used to calculate fluxes. Table D.5 shows the flux result details.) Comparing the two metabolic states, the following observations can be made:

- State #1 has a lower flux through the oxidative pentose phosphate pathway
- State #1 has a higher flux through glycolysis
- State #1 has a higher flux to acetate
- State #1 has very low TCA cycle fluxes
- State #2 has more central carbon metabolite precursors drained to biomass.

Additionally, comparing State #1 and State #2 to the flux map obtained for the no yeast extract culture, it is seen that State #2 is very similar to the fluxes for growth

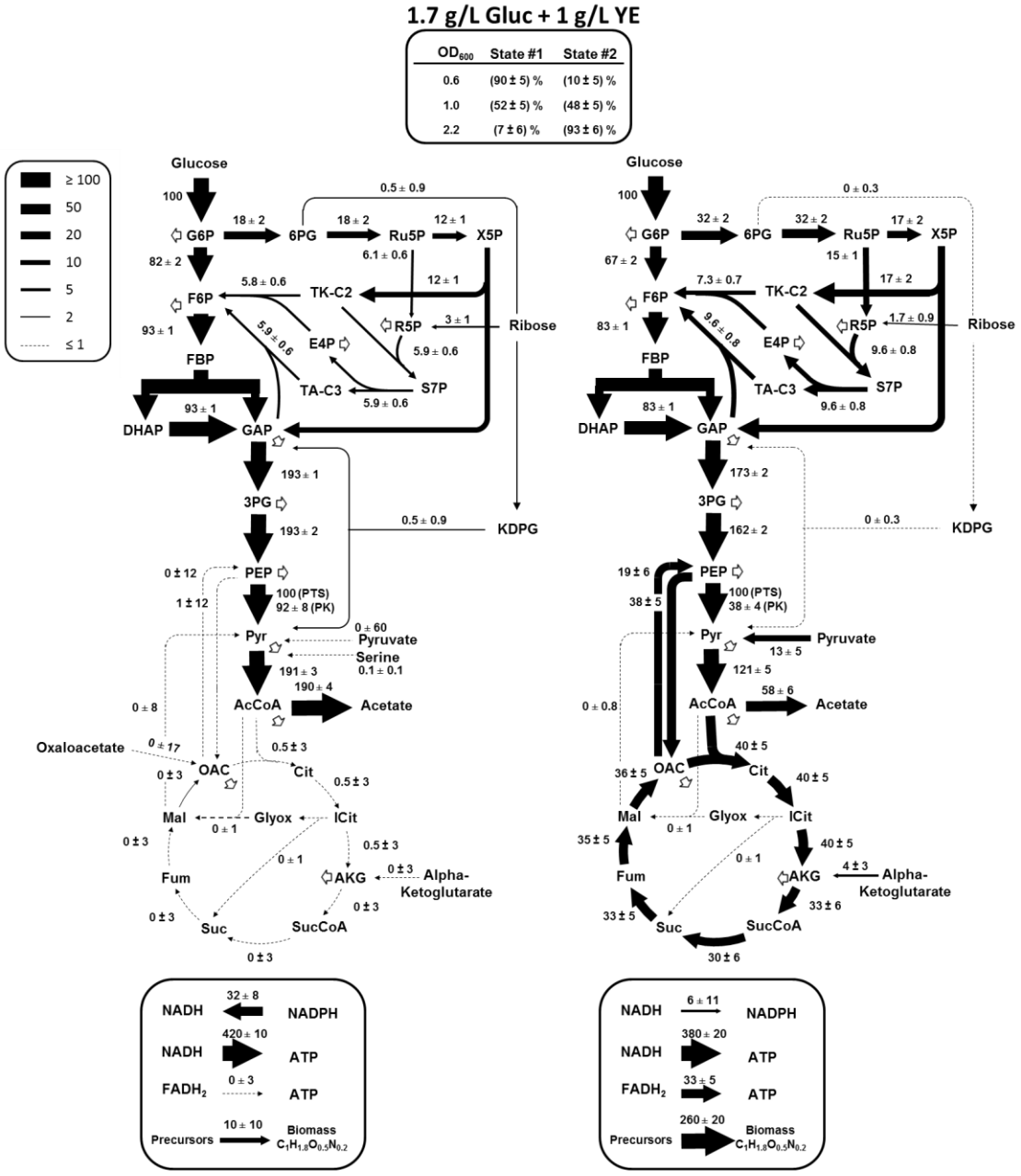

Figure 5.10 ^{13}C Metabolic Flux Analysis of *E. coli* growth on 1.7 g/L [1,2-^{13}C]glucose + 1 g/L yeast extract. The estimated flux map was determined using proteinogenic amino acid, glycogen, and RNA labeling data. White arrows represent outflux to biomass.

solely on glucose with the exception that its TCA cycle fluxes are about half that of the no yeast extract control. This confirms that State #1 represents the fluxes for growth on glucose and yeast extract simultaneously while State #2 represents the fluxes for growth on glucose. Thus, the trends seen in State #1 are similar to those for 0.5 g/L yeast extract.

The TCA cycle fluxes are higher in State #2 than in the no yeast extract control culture because its growth rate is higher, so a higher TCA cycle activity is needed to create biomass precursors and energy for anabolism. Figure 5.10 also shows the energy balance fluxes. The trends here as the same as for 0.5 g/L yeast extract.

5.3.7.4 1.7 g/L [1,2-^{13}C]glucose + 2 g/L Yeast Extract

The Two Metabolic States Dilution Model was able to obtain a statistically acceptable fit for the 1.7 g/L [1,2-^{13}C]glucose + 2 g/L yeast extract cultures at OD_{600} of 0.4, 1.1, and 1.9. The flux results are shown in Figure 5.11. (Table D.2 contains the measured mass isotopomer distributions used to calculate fluxes. Table D.6 shows the flux result details.) Comparing the 2 g/L yeast extract fluxes to the 0.5 g/L and 1 g/L yeast extract fluxes, they are all similar with most flux confidence intervals overlapping. The main exception is with the alpha-ketoglutarate dilution flux for State #2 in the 2 g/L yeast extract culture. This is likely due to the culture still having significant amounts of yeast extract remaining in the medium at an OD_{600} of 1.9 considering that the culture's final OD_{600} was over 4. Figure 5.11 also shows the energy balance fluxes. The trends here as the same as for 0.5 g/L yeast extract.

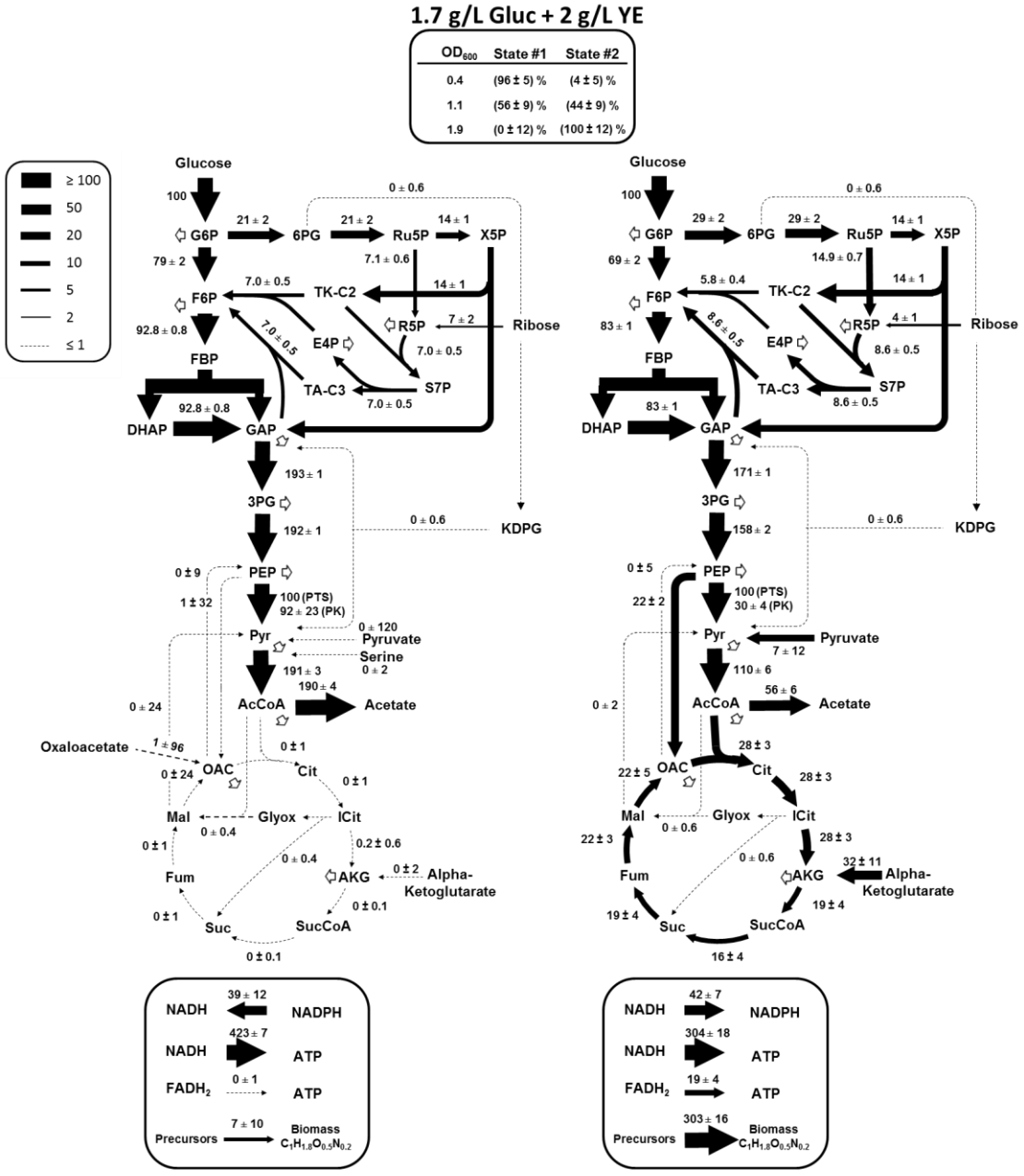

Figure 5.11 ^{13}C Metabolic Flux Analysis of *E. coli* growth on 1.7 g/L [1,2-^{13}C]glucose + 2 g/L yeast extract. The estimated flux map was determined using proteinogenic amino acid, glycogen, and RNA labeling data. White arrows represent outflux to biomass.

5.3.7.5 Transition from State #1 to State #2 Metabolism

To capture the transition from State #1 and State #2, for a given timepoint, the model can calculate the relative contributions of each metabolism to the creation of protein up to that timepoint. Using the 0.5 g/L yeast extract culture as an example, the first timepoint for which labeling data was collected and entered into Metran was OD_{600} = 0.4. Metran then calculated that State #1 was 72% and State #2 was 28%. This means that 72% of the protein present at OD_{600} = 0.4 was created by the fluxes shown in State #1 metabolism and 28% of the protein present at OD_{600} of 0.4 was created by the fluxes shown in State #2 metabolism. To get the relative State contributions at a given timepoint, labeling of intracellular metabolites instead of protein needs to be used. Intracellular metabolites have high turnover rates, therefore the labeling will represent the current metabolic state of the cells. This is different than protein which is a running history of the metabolic state.

At the top of Figures 5.9, 5.10, and 5.11 are the relative amounts of State #1 and State #2 at three timepoints for the 0.5 g/L, 1 g/L, and 2 g/L yeast extract cultures, respectively. For the 2 g/L yeast extract culture, at an OD_{600} of 0.4, 96% of the protein was created by State #1 fluxes. Then, by an OD_{600} of 1.1, 56% of the protein has been made by State #1. Assuming the protein of *E. coli* does not change, a mass balance on protein can be performed:

$$\left(OD_{t_i}\right)\left(F_{t_i}^{j}\right) + \left(OD_{t_{i+1}}\right)\left(F_{t_{i+1}}^{j}\right) = \left(OD_{t_{i+2}}\right)\left(F_{t_{i+2}}^{j}\right) \qquad 5.1$$

where OD_{t_i} is the optical density at the end of time segment i and $F_{t_i}^{j}$ is the fraction of State j protein at the end of time segment i. Performing a mass balance of State #1 protein from OD_{600} of 0.4 to 1.1:

$$\left(OD_{t_1}\right)\left(F_{t_1}^1\right) + \left(OD_{t_2}\right)\left(F_{t_2}^1\right) = \left(OD_{t_3}\right)\left(F_{t_3}^1\right) \quad 5.2$$

then rearranging,

$$F_{t_2}^1 = \frac{\left(OD_{t_3}\right)\left(F_{t_3}^1\right) - \left(OD_{t_1}\right)\left(F_{t_1}^1\right)}{OD_{t_2}} \quad 5.3$$

gives,

$$F_{t_2}^1 = \frac{(1.1)(0.56) - (0.4)(0.96)}{(1.1-0.4)} = 0.33 \quad 5.4$$

Propagation of errors for $F_{t_2}^1$ assuming that the error associated with OD_{600} measurements is much smaller than the error associated with the fraction estimations gives,

$$\left(\Delta F_{t_2}^1\right)^2 = \left(\frac{\delta F_2}{\delta F_3}\right)^2 (\Delta F_3)^2 + \left(\frac{\delta F_2}{\delta F_1}\right)^2 (\Delta F_1)^2 = \left(\frac{OD_3}{OD_2}\right)^2 (\Delta F_3)^2 + \left(\frac{OD_1}{OD_2}\right)^2 (\Delta F_1)^2 \quad 5.5$$

so

$$\begin{aligned} \Delta F_{t_2}^1 &= \sqrt{\left(\frac{OD_3}{OD_2}\right)^2 (\Delta F_3)^2 + \left(\frac{OD_1}{OD_2}\right)^2 (\Delta F_1)^2} \\ &= \sqrt{\left(\frac{1.1}{1.1-0.4}\right)^2 (0.09)^2 + \left(\frac{0.4}{1.1-0.4}\right)^2 (0.05)^2} = 0.14 \end{aligned} \quad 5.6$$

This means that as the cells grew from an OD_{600} of 0.4 to an OD_{600} of 1.1, the labeling of 33 ± 14 % of the newly produced protein is described from State #1's metabolic fluxes.

Repeating this analysis for the 1 g/L yeast extract culture from an OD_{600} of 0.6 to 1,

$$F_{t_2}^1 = \frac{\left(OD_{t_3}\right)\left(F_{t_3}^1\right) - \left(OD_{t_1}\right)\left(F_{t_1}^1\right)}{OD_{t_2}} = \frac{(1)(0.52) - (0.6)(0.9)}{(1-0.6)} = -0.05 \quad 5.7$$

$$\Delta F_{t_2}^1 = \sqrt{\left(\frac{OD_3}{OD_2}\right)^2 (\Delta F_3)^2 + \left(\frac{OD_1}{OD_2}\right)^2 (\Delta F_1)^2}$$

$$= \sqrt{\left(\frac{1.0}{1.0-0.6}\right)^2 (0.05)^2 + \left(\frac{0.6}{1.0-0.6}\right)^2 (0.05)^2} = 0.15 \qquad 5.8$$

gives that, as the cells grew from an OD_{600} of 0.6 to an OD_{600} of 1, the labeling of -5 ± 15 % of the newly produced protein is described from State #1's metabolic fluxes. Since the confidence interval contains negative numbers, it is possible that protein turnover is occurring or that assuming a constant biomass composition is not accurate.

Repeating this analysis for the 0.5 g/L yeast extract culture,

$$F_{t_2}^1 = \frac{(OD_{t_3})\left(F_{t_3}^1\right) - (OD_{t_1})(F_{t_1}^1)}{OD_{t_2}} = \frac{(1)(0.22) - (0.4)(0.77)}{(1-0.4)} = -0.15 \qquad 5.9$$

$$\Delta F_{t_2}^1 = \sqrt{\left(\frac{OD_3}{OD_2}\right)^2 (\Delta F_3)^2 + \left(\frac{OD_1}{OD_2}\right)^2 (\Delta F_1)^2}$$
$$= \sqrt{\left(\frac{1.0}{1.0-0.4}\right)^2 (0.04)^2 + \left(\frac{0.4}{1.0-0.4}\right)^2 (0.07)^2} = 0.08 \qquad 5.10$$

gives that, as the cells grew from an OD_{600} of 0.4 to an OD_{600} of 1, the labeling of -15 ± 8 % of the newly produced protein is described from State #1's metabolic fluxes. This means that there is protein turnover or that assuming a constant biomass composition is not accurate. Performing this mass balance analysis for the second time span (i.e. OD_{600} 1 to 2), all the fractional contributions from State #1 are negative which means that there is protein turnover or changes in the protein content of the cells over time.

5.3.8 Analysis of Protein Turnover

One of the first checks for protein turnover is to look for partially labeled amino acids. If the glucose carbons stay together, [U-^{13}C]glucose would only produce [U-^{13}C]amino acids. If the carbons from yeast extract amino acids stay together, yeast

extract would only produce naturally labeled amino acids. However, if yeast extract amino acids are degraded to central carbon metabolites and those carbons are then used to create other amino acids, there will be partially labeled amino acids. Valine and leucine are two good amino acids to analyze because they are made by the condensation of two central carbon metabolism precursors:

$$Pyr(abc) + Pyr(def) + Glu\ (ghijk) + \ NADPH \rightarrow Val(abcef) + CO_2(d) + AKG(ghijk)$$

where Pyr is pyruvate, Glu is glutamate, $NADPH$ is nicotinamide adenine dinucleotide phosphate, Val is valine, CO_2 is carbon dioxide, AKG is alpha-ketoglutarate, and lower-case letters are used to track carbon transitions and

$$AcCoA(ab) + Pyr(cde) + Pyr(fgh) + Glu(ijklm) + NADPH \rightarrow Leu(abdghe) + CO_2(c) + CO_2(f) + AKG(ijklm) + NADH$$

where $AcCoA$ is acetyl coenzyme A, Pyr is pyruvate, Glu is glutamate, $NADPH$ is nicotinamide adenine dinucleotide phosphate, Leu is leucine, CO_2 is carbon dioxide, AKG is alpha-ketoglutarate, $NADH$ is nicotinamide adenine dinucleotide, and lower-case letters are used to track carbon transitions. The only way that a partially labeled valine could be present is if an unlabeled pyruvate combines with a labeled pyruvate. Unlabeled pyruvate can only be present if it comes from degraded yeast extract amino acids or pyruvate itself is within the yeast extract. But, the pyruvate content of yeast extract is low (measured to be 0.003 mM for 2 g/L yeast extract) so that contribution would be low. The only way that a partially labeled leucine could be present is if there is either an unlabeled AcCoA or pyruvate. Unlabeled AcCoA or pyruvate can only be present if they come from degraded yeast extract amino acids or are contained within

the yeast extract. But, the AcCoA and pyruvate content of yeast extract are low, so those contributions would be low.

Figure 5.12A shows the time-course labeling of valine (288 m/z fragment) and Figure 5.12B shows the time-course labeling of leucine (274 m/z fragment) for the four different cultures with [U-^{13}C]glucose (experimental design in Figure 5.2). The fractionally labeled isotopomers (i.e. not M_0 or M_n) sum to less than 10%. M_{n-1} is generally the largest fractionally labeled isotopomer and is likely the result of incomplete labeling of the [U-^{13}C]glucose tracer. From this analysis, we can conclude that it is unlikely that amino acids are being degraded, entering central carbon metabolism, and then being converted back into amino acids.

If there is protein turnover, the labeling of amino acids will change faster than is expected based on dilution of newly formed biomass. For example, this type of analysis was performed in Section 4.3.2 "Starch turnover occurs in autotrophic and heterotrophic growth". By an OD_{600} of 1 in the 0.5 g/L yeast extract culture, the valine in the medium was depleted. So, after that timepoint, new valine would either be produced from glucose carbons or carbons from turned-over protein. The measured time constant is 0.33 h^{-1} (slope from the slope of $ln(1-M_n)$ vs time) and the dilution constant is 0.40 h^{-1}. Unfortunately, given that the time constants were calculated by using two points, there could potentially be significant errors in these values. Based on this analysis and the flux results, it does appear that protein turnover occurs in cultures containing yeast extract. Further experimentation should be performed to better quantify protein turnover.

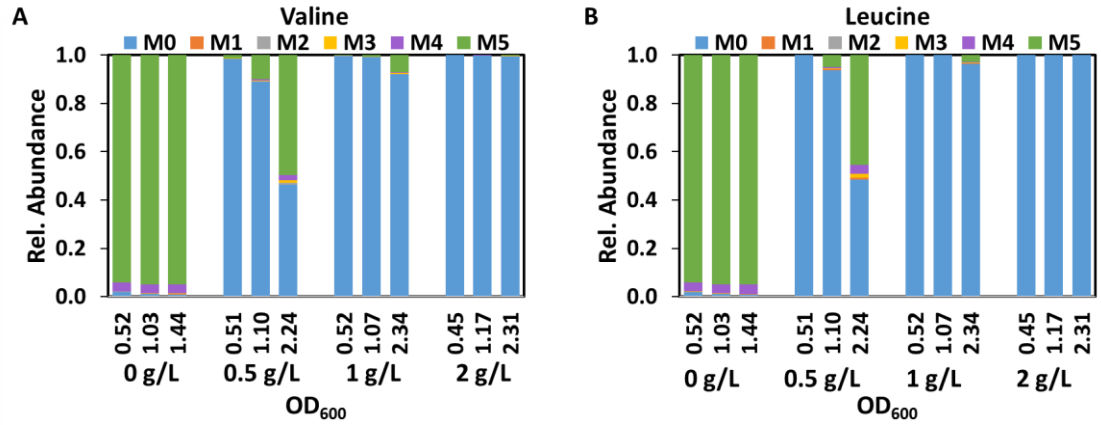

Figure 5.12 Mass Isotopomer Distributions. (A) MID for the 288 m/z fragment of Valine for multiple timepoints for each of the four cultures containing [U-^{13}C]glucose. (B) MID for the 274 m/z fragment of Leucine for multiple timepoints for each of the four cultures containing [U-^{13}C]glucose.

5.4 Conclusions

In this work, a novel methodology was developed to perform ^{13}C-metabolic flux analysis of *E. coli* in the presence of glucose and yeast extract. First, the relative contributions of glucose and yeast extract to biomass were determined. We identified that proteinogenic glycine, alanine, aspartate/asparagine, and tyrosine were made from glucose even when the amino acids were present in the medium. Serine was consumed very quickly from the medium, and as a result significant amounts of proteinogenic serine was made from glucose. Through a series of model iterations, a final model was established that describes the protein labeling at multiple cell densities for multiple yeast extract concentrations. The overall modeling framework is broadly based on the recently developed co-culture ^{13}C-MFA framework (Gebreselassie and Antoniewicz 2015; Wolfsberg, Long, and Antoniewicz 2018).

The main impact of this work is to extend the ^{13}C-MFA toolbox to include organisms which are grown in complex media. Yeast extract is a commonly used medium supplement (Kasprow, Lange, and Kirwan 1998) and applying the methods developed in this work is expected to help researchers further their understanding of relevant biological systems. In the long run, this could enable further metabolic engineering efforts to obtain superior biological production systems.

In future work, it will be important to validate if protein turnover is occurring. Additionally, applying these methods to other organisms to test for model robustness will be important. Finally, it would be beneficial to use intracellular metabolite labeling instead of protein labeling so that the fluxes at a timepoint could be calculated instead of determining the history of fluxes up to the timepoint (like in this study). Expanding the model framework to include more than two metabolic states would also give better resolution/insight into the transition from growth of glucose and yeast extract to growth on glucose alone.

Chapter 6

CONCLUSIONS AND FUTURE WORK

6.1 Carbohydrate Analysis by Gas Chromatography/Mass Spectrometry

Chapter 2 described the development of a two-stage hydrochloric acid hydrolysis process which struck a balance between being harsh enough to degrade polysaccharides into monosaccharides without being too harsh and causing significant monosaccharide degradation. In the high temperature (second) step, it was shown that for hydrochloric acid concentrations up to 1 N, less than 8% degradation occurred for all sugars (greater than 92% recovered). Overall, xylose was most prone to acid degradation, resulting in 30% degradation at 2 N hydrochloric acid, and greater than 90% degradation at 6 N hydrochloric acid. Galactose was least prone to acid degradation, with 10% degradation at 2 N hydrochloric acid, and 50% degradation at 6 N hydrochloric acid. Coupling this hydrolysis process with a previously established chemical derivatization protocol (Antoniewicz, Kelleher, and Stephanopoulos 2011) enabled the quantification of isotopic labeling of xylose, arabinose, mannose, glucose, and galactose released from biomass by gas chromatography/mass spectrometry. Additionally, this protocol and isotopic ratio analysis enables the quantification of biomass carbohydrates.

One of main advantages of this protocol is that it relies on gas chromatography/mass spectrometry which is a widely accessible analytical platform. This method was used in a study which showed that ^{13}C metabolic flux analysis of microbial and mammalian systems is enhanced with GC/MS measurements of

glycogen and RNA labeling (C. P. Long, Au, et al. 2016). Specifically, these researchers showed that including the isotopic labeling of the glucose moiety of glycogen and the ribose moiety of RNA enabled precise quantification of net and exchange fluxes in the pentose phosphate pathway. With this discovery, more metabolic engineering projects should utilize carbohydrate labeling, and this method will be a useful resource.

Additionally, this carbohydrate protocol was used in a study which showed that aldolase B mediated fructose metabolism drives the metabolic reprogramming of colon cancer metastasis (Bu et al. 2018). Specifically, this carbohydrate protocol was used to show that [U-^{13}C]fructose labels upper glycolytic intermediates and nucleotide precursors in colon cancer cells.

One extension for this carbohydrate characterization protocol is to the analysis of the macromolecule deoxyribonucleic acid (DNA). DNA is a polynucleotide with monomeric units containing a nucleobase base (adenine, cytosine, guanine, and thymine), deoxyribose (a sugar), and a phosphate group. It is possible that the hydrolysis step developed here could be used to release deoxyribose from DNA (it has been shown to release ribose from RNA). This would be valuable because DNA represents roughly 3% of biomass by dry weight (C. P. Long and Antoniewicz 2014; Antoniewicz 2018), and as the carrier of genetic information, is an important macromolecule. One critical obstacle would be the abundance of DNA in biomass samples. Since DNA is less abundant than the other macromolecules, larger cell pellets will probably be required for this analysis.

6.2 Physiological Characterization of *Chlorella vulgaris*

To maximize the production of desired products from *C. vulgaris* a quantitative understanding of metabolism is needed. In **Chapter 3**, the metabolism of *C. vulgaris* UTEX 395 was characterized in autotrophic (1% CO_2 in air, 14 hours/day light), heterotrophic (10 g/L glucose), and mixotrophic (10 g/L glucose plus 1% CO_2 in air, 14 hours/day light) conditions. The autotrophic and heterotrophic cells had the same growth rate (roughly 0.66 day^{-1}). The physiological characterization of the mixotrophic culture showed that mixotrophic growth is the superposition of autotrophic and heterotrophic growth.

Light cycling and nitrogen depletion were shown to be two major drivers of biomass composition changes. In the dark, the autotrophic cells cannot fix carbon dioxide, so they must consume their starch reserves for maintenance energy. Mixotrophic conditions are advantageous over autotrophic conditions because the sugar substrate can be metabolized in the dark so that cells do not need to consume their internal starch reserves. This was confirmed for mixotrophic cells growing in the nitrogen replete phase. However, during the nitrogen deplete phase, the mixotrophic cells preferred to consume starch reserves over extracellular glucose. This may be due to circadian rhythm programming. In general, growing *C. vulgaris* cells (i.e. in nitrogen replete phase) are mostly composed of proteins and carbohydrates. Upon nitrogen depletion, the cells change their composition and become mostly carbohydrates and fatty acids. Considering techno-economic studies which showed that lipid content and growth rate are the two most significant factors influencing microalgal biodiesel cost (Davis, Aden, and Pienkos 2011), it seems likely that a microalgal biodiesel production process would have two culturing phases: first is a rapid growth phase where as many cells as possible are created; and then a second

phase where no new cells are made but lipid accumulation is induced by nitrogen starvation.

In **Chapter 4**, further exploration of *Chlorella vulgaris*'s highly dynamic metabolism and photosynthetic activity was performed. It was shown that during light cycled autotrophic culture, *C. vulgaris* produced and consumed starch during light and dark phases, respectively. The cells changed the production/consumption mode within one hour of light condition change. A labeling switch experiment showed that the starch synthesis relative to the growth requirement for light-cycled autotrophic, constant-light autotrophic, and heterotrophic growth was 3.6 ± 0.3, 1.7 ± 0.1, and 1.6 ± 0.2, respectively. Carbon dioxide production was shown to be a minor contributor to starch turnover whereas polysaccharide secretion was shown to be significant (20-25% of the total glucose equivalents present in the culture was located extracellularly).

The physiological characterization data obtained in this work was used to establish a genome-scale metabolic model for *C. vulgaris* UTEX 395 (Zuñiga et al. 2016). Flux distributions under the different trophic conditions showed that central carbon metabolism, and amino acid, nucleotide, and pigment biosynthetic pathways were affected by nitrogen starvation.

Now that the genome-scale model of *Chlorella vulgaris* has been developed, the next step would be to calculate metabolic fluxes during each of the trophic conditions. For heterotrophic and mixotrophic growth, labeled glucose tracers could be used with traditional ^{13}C-MFA methods. However, for autotrophic growth, the more complicated isotopically nonstationary metabolic flux analysis method must be performed (INST-MFA). Specifically, INST-MFA must be performed to calculate

autotrophic metabolic fluxes because isotopic steady state with a single carbon containing tracer (carbon dioxide) is the fully labeled condition which provides no information about fluxes. To perform INST-MFA, a culture would need to be performed with unlabeled carbon dioxide, then a rapid change to ^{13}C labeled carbon dioxide would need to be made, and time-course measurements of intracellular metabolite labeling collected (Young et al. 2011). This is a difficult experiment to perform because rapid sampling (multiple samples must be collected during the transient labeling process which could take as little as 5 minutes) and rapid quenching of metabolism (so that measured labeling patterns match the actual labeling when the cells were in the bioreactor) are required.

6.3 Autotroph-Heterotroph Interactions

The work described in **Chapter 4** on autotroph-heterotroph interactions has broader implications for microalgal ecology and biotechnological applications. In terms of ecological impact, the observations in this work confirm that microalgae are the primary producers for many ecosystems through product secretion in addition to the entire cells being eaten. In terms of biotechnological impact, two important considerations for large-scale outdoor microalgal biomass production are that sunlight is not constant and that contaminating organisms could enter the culture from the air (Santos and Reis 2014). This work has provided insights into light cycled autotrophic growth and the need to limit biomass loss during dark phases. Additionally, adding the Microbiome cells to a microalgal culture increased the biodiversity of the culture and could reduce unwanted contamination by other organisms. It was shown that secreting polysaccharides is beneficial to the microalgae because during co-culture with microbiome cells their photosynthetic activity was increased.

Work is in progress to identify the members of the Microbiome described in **Chapter 4**. This will be accomplished by performing 16S ribosomal RNA (rRNA) gene sequencing (Woese and Fox 1977; Woese, Kandlert, and Wheelis 1990) at the University of Delaware DNA Sequencing and Genotyping Center (Delaware Biotechnology Institute, Newark, DE, USA). Using 16S rRNA gene sequences to identify bacteria has become common practice because this gene is present in almost all bacteria, its function has not changed over time, and it is 1500 base-pairs long (Janda and Abbott 2007). Once the Microbiome members have been identified, more work can be done to understand their metabolism in isolation and within the community. It will be interesting to determine if specific members of the community have specific "jobs" and if they can consume microalgal polysaccharides independently. Additionally, it will be interesting to determine if diazotrophic (nitrogen fixing) organisms belong to the community because that would allow the community to obtain both its carbon and nitrogen from gaseous sources (Villa, Ray, and Barney 2014).

Many microalgae species are auxotrophic for B Vitamins and must obtain them from microbial partners (Croft, Warren, and Smith 2006). *Chlorella vulgaris* is not auxotrophic for B Vitamins (Croft, Warren, and Smith 2006), but it is possible that the Microbiome cells isolated in this study could be providing complex organic carbon molecules to the microalgae cells. *Chlorella vulgaris*'s growth was tested on 50% BBM (minimal medium used in all *C. vulgaris* cultures in this dissertation) and 50% spent medium from cultures containing *C. vulgaris*, Microbiome cells grown on glucose, Microbiome cells grown on *C. vulgaris* secreted polysaccharides, or co-culture of *C. vulgaris* and Microbiome cells, but no significant growth improvements

were observed compared to 50% BBM with 50% water. However, metabolomic analysis of medium samples could give insight into additional exchanged metabolites.

6.4 ^{13}C-MFA in Complex Media

Finally, in **Chapter 5**, a novel methodology to perform ^{13}C-metabolic flux analysis of *E. coli* in the presence of glucose and yeast extract was presented. Tracer experiments with [U-^{13}C]glucose and varying levels of yeast extract showed that proteinogenic glycine, alanine, aspartate/asparagine, and tyrosine are largely made from glucose even if the amino acids are present in the medium. These experiments also showed that, for Fisher Scientific yeast extract, serine was consumed very quickly from the medium, and thus significant amounts of proteinogenic serine had to be made from glucose.

A metabolic model which can describe the protein labeling at multiple cell densities for multiple yeast extract concentrations was developed. It is based on a recently developed co-culture ^{13}C-MFA framework (Gebreselassie and Antoniewicz 2015; Wolfsberg, Long, and Antoniewicz 2018). The main impact of this work is to extend the ^{13}C-MFA toolbox to include organisms which are grown using complex media. From the analysis of wild-type *E. coli* in this Chapter, it appears that at high cell densities, protein turnover occurs. Most ^{13}C-MFA studies have been performed on cells at low cell densities (below an optical density of 1) so the extent of protein turnover has not been reported in those studies.

In future work, it will be important to validate more rigorously if protein turnover is occurring. Applying the developed modeling methodology to other organisms to test for robustness will also be important. Moreover, it would be beneficial to use intracellular metabolite labeling instead of protein labeling so that the

fluxes at a particular timepoint could be calculated instead of determining the history of fluxes up to the timepoint (like in this study). Performing parallel labeling experiments (Antoniewicz 2015b) will result in more isotopic labeling measurements which should help with calculating dilution fluxes more precisely. Expanding the model framework to include more than two metabolic states would also give better resolution/insight into the transition from growth on glucose and yeast extract to growth on glucose alone.

REFERENCES

Amelio, Ivano, Francesca Cutruzzola, Alexey Antonov, Massimiliano Agostini, and Gerry Melino. 2014. "Serine and Glycine Metabolism in Cancer." *Trends in Biochemical Sciences* 39 (4): 191–98. https://doi.org/10.1016/j.tibs.2014.02.004.

Andersen, Robert. 2005. *Algal Culturing Techniques*.

Antoniewicz, Maciek R., Joanne K. Kelleher, and Gregory Stephanopoulos. 2007a. "Accurate Assessment of Amino Acid Mass Isotopomer Distributions for Metabolic Flux Analysis." *Analytical Chemistry* 79 (19): 7554–59. https://doi.org/10.1021/ac0708893.

———. 2007b. "Elementary Metabolite Units (EMU): A Novel Framework for Modeling Isotopic Distributions." *Metabolic Engineering* 9 (1): 68–86.

Antoniewicz, Maciek R. 2015a. "Methods and Advances in Metabolic Flux Analysis: A Mini-review." *Journal of Industrial Microbiology and Biotechnology* 42: 317–25. https://doi.org/10.1007/s10295-015-1585-x.

———. 2015b. "Parallel Labeling Experiments for Pathway Elucidation and 13 C Metabolic Flux Analysis." *Current Opinion in Biotechnology* 36: 91–97. https://doi.org/10.1016/j.copbio.2015.08.014.

———. 2018. "A Guide to 13C Metabolic Flux Analysis for the Cancer Biologist." *Experimental & Molecular Medicine* 50 (19): 1–13. https://doi.org/10.1038/s12276-018-0060-y.

Antoniewicz, Maciek R, Joanne K Kelleher, and Gregory Stephanopoulos. 2006. "Determination of Confidence Intervals of Metabolic Fluxes Estimated from Stable Isotope Measurements." *Metabolic Engineering* 8: 324–37. https://doi.org/10.1016/j.ymben.2006.01.004.

———. 2011. "Measuring Deuterium Enrichment of Glucose Hydrogen Atoms by Gas Chromatography/Mass Spectrometry." *Analytical Chemistry* 83: 3211–16. https://doi.org/10.1021/ac200012p.

Antoniewicz, Maciek R, David F Kraynie, Lisa A Laffend, Joanna Gonzalez-Lergier, Joanne K Kelleher, and Gregory Stephanopoulos. 2007. "Metabolic Flux Analysis in a Nonstationary System: Fed-Batch Fermentation of a High Yielding Strain of E . Coli Producing 1,3-Propanediol." *Metabolic Engineering* 9: 277–92. https://doi.org/10.1016/j.ymben.2007.01.003.

Antoniewicz, Maciek R, Gregory Stephanopoulos, and Joanne K Kelleher. 2006. "Evaluation of Regression Models in Metabolic Physiology: Predicting Fluxes from Isotopic Data without Knowledge of the Pathway." *Metabolomics* 2 (1): 41–52. https://doi.org/10.1007/s11306-006-0018-2.

Becker, E.W. 1994. *Microalgae: Biotechnology and Microbiology*.

Bischoff, Harry W., and Harold C. Bold. 1963. "Some Soil Algae from Enchanted Rock and Related Algal Species." In *Phycological Studies*, 1–95.

Block, Maryse Anne, Albert-jean Dorne, Jacques Joyard, and Roland Douce. 1983. "Preparation and Characterization of Membrane Fractions Enriched in Outer and Inner Envelope Membranes from Spinach Chloroplasts." *The Journal of Biological Chemistry* 258 (83): 13281–86.

Borowitzka, Michael A, and Navid R Moheimani. 2013. *Algae for Biofuels and Energy*. First. New York: Springer.

Bu, Pengcheng, Kai-yuan Chen, Kun Xiang, Christelle Johnson, Scott B Crown, Nikolai Rakhilin, Yiwei Ai, et al. 2018. "Aldolase B-Mediated Fructose Metabolism Drives Metabolic Reprogramming of Colon Cancer Liver Metastasis." *Cell Metabolism* 27 (6): 1249–62. https://doi.org/10.1016/j.cmet.2018.04.003.

Buescher, Joerg M, Maciek R Antoniewicz, Laszlo G Boros, Shawn C Burgess, Henri Brunengraber, Clary B Clish, Ralph J Deberardinis, et al. 2015. "A Roadmap for Interpreting 13C Metabolite Labeling Patterns from Cells." *Current Opinion in Biotechnology* 34: 189–201. https://doi.org/10.1016/j.copbio.2015.02.003.

Chang, Roger L, Lila Ghamsari, Ani Manichaikul, Erik F Y Hom, Santhanam Balaji, Weiqi Fu, Yun Shen, et al. 2011. "Metabolic Network Reconstruction of Chlamydomonas Offers Insight into Light-Driven Algal Metabolism." *Molecular Systems Biology* 7 (518). https://doi.org/10.1038/msb.2011.52.

Chen, Chun-yen, Xin-qing Zhao, Hong-wei Yen, Shih-hsin Ho, Chieh-lun Cheng, Duu-Jong Lee, Feng-Wu Bai, and Jo-Shu Chang. 2013. "Microalgae-Based Carbohydrates for Biofuel Production." *Biochemical Engineering Journal* 78: 1–10. https://doi.org/10.1016/j.bej.2013.03.006.

Choix, Francisco J., Luz E. de-Bashan, and Yoav Bashan. 2012. “Enhanced Accumulation of Starch and Total Carbohydrates in Alginate-Immobilized Chlorella Spp. Induced by Azospirillum Brasilense: II. Heterotrophic Conditions.” *Enzyme and Microbial Technology* 51 (5): 300–309. https://doi.org/10.1016/j.enzmictec.2012.07.012.

Choix, Francisco J, Luz E De-Bashan, and Yoav Bashan. 2012. “Enhanced Accumulation of Starch and Total Carbohydrates in Alginate-Immobilized Chlorella Spp . Induced by Azospirillum Brasilense : I . Autotrophic Conditions.” *Enzyme and Microbial Technology* 51 (5): 294–99. https://doi.org/10.1016/j.enzmictec.2012.07.013.

Cohen, Joel E. 2003. “Human Population: The Next Half Century.” *Science* 302 (5648): 1172–76.

Cooper, Matthew B, and Alison G Smith. 2015. “Exploring Mutualistic Interactions between Microalgae and Bacteria in the Omics Age.” *Current Opinion in Plant Biology* 26: 147–53. https://doi.org/10.1016/j.pbi.2015.07.003.

Cordova, Lauren T, and Maciek R Antoniewicz. 2016. “13C Metabolic Flux Analysis of the Extremely Thermophilic, Fast Growing, Xylose-Utilizing Geobacillus Strain LC300.” *Metabolic Engineering* 33: 148–57. https://doi.org/10.1016/j.ymben.2015.06.004.

Cordova, Lauren T, Robert M Cipolla, Adti Swarup, Christopher P Long, and Maciek R Antoniewicz. 2017. “13C Metabolic Flux Analysis of Three Divergent Extremely Thermophilic Bacteria: Geobacillus Sp . LC300 , Thermus Thermophilus HB8 , and Rhodothermus Marinus DSM 4252.” *Metabolic Engineering* 44: 182–90. https://doi.org/10.1016/j.ymben.2017.10.007.

Croft, Martin T, Martin J Warren, and Alison G Smith. 2006. “Algae Need Their Vitamins.” *Eukaryotic Cell* 5 (8): 1175–83. https://doi.org/10.1128/EC.00097-06.

Crown, Scott B, and Maciek R Antoniewicz. 2013. “Publishing 13C Metabolic Flux Analysis Studies: A Review and Future Perspectives.” *Metabolic Engineering* 20: 42–48. https://doi.org/10.1016/j.ymben.2013.08.005.

Crown, Scott B, Christopher P Long, and Maciek R Antoniewicz. 2016. “Optimal Tracers for Parallel Labeling Experiments and 13C Metabolic Flux Analysis: A New Precision and Synergy Scoring System.” *Metabolic Engineering* 38: 10–18. https://doi.org/10.1016/j.ymben.2016.06.001.

Davis, Ryan, Andy Aden, and Philip T Pienkos. 2011. “Techno-Economic Analysis of Autotrophic Microalgae for Fuel Production.” *Applied Energy* 88 (10): 3524–31.

https://doi.org/10.1016/j.apenergy.2011.04.018.

Desai, Shuchi H., and Shota Atsumi. 2013. “Photosynthetic Approaches to Chemical Biotechnology.” *Current Opinion in Biotechnology* 24 (6): 1031–36. https://doi.org/10.1016/j.copbio.2013.03.015.

Dismukes, G. Charles, Damian Carrieri, Nicholas Bennette, Gennady M. Ananyev, and Matthew C. Posewitz. 2008. “Aquatic Phototrophs: Efficient Alternatives to Land-Based Crops for Biofuels.” *Current Opinion in Biotechnology* 19 (3): 235–40. https://doi.org/10.1016/j.copbio.2008.05.007.

Dubois, Michel, K A Gilles, J K Hamilton, P A Rebers, and Fred Smith. 1956. “Colorimetric Method for Determination of Sugars and Related Substances.” *Analytical Chemistry* 28: 350–56. https://doi.org/10.1021/ac60111a017.

Fernandez, Charles A, Christine Des Rosiers, Stephen F Previs, France David, and Henri Brunengrabert. 1996. “Correction of 13C Mass Isotopomer Distributions for Natural Stable Isotope Abundance.” *Journal of Mass Spectrometry* 31 (January 1995): 255–62.

Forster, Jochen, Iman Famili, Patrick Fu, Bernhard Ø Palsson, and Jens Nielsen. 2003. “Genome-Scale Reconstruction of the Saccharomyces Cerevisiae Metabolic Network.” *Genome Research* 13: 244–53. https://doi.org/10.1101/gr.234503.complex.

Fuentes, Juan Luis, Ines Garbayo, Maria Cuaresma, Zaida Montero, Manuel Gonzalez-Del-Valle, and Carlos Vilchez. 2016. “Impact of Microalgae-Bacteria Interactions on the Production of Algal Biomass and Associated Compounds.” *Marine Drugs* 14 (100): 1–16. https://doi.org/10.3390/md14050100.

Gebreselassie, Nikodimos A, and Maciek R Antoniewicz. 2015. “13C-Metabolic Flux Analysis of Co-Cultures: A Novel Approach.” *Metabolic Engineering* 31: 132–39. https://doi.org/10.1016/j.ymben.2015.07.005.

Gerken, Henri G, Bryon Donohoe, and Eric P Knoshaug. 2013. “Enzymatic Cell Wall Degradation of Chlorella Vulgaris and Other Microalgae for Biofuels Production.” *Planta* 237: 239–53. https://doi.org/10.1007/s00425-012-1765-0.

Gest, Howard. 2004. “Samuel Ruben’ s Contributions to Research on Photosynthesis and Bacterial Metabolism with Radioactive Carbon.” *Photosynthesis Research* 80: 77–83.

Goeddel, David V., Dennis G. Kleid, Francisco Bolivar, Herbert L Heyneker, Daniel G Yansura, Roberto Crea, Tadaaki Hirosef, Adam Kraszewskit, Keiichi Itakuraf,

and Arthur D Riggstt. 1979. “Expression in Escherichia Coli of Chemically Synthesized Genes for Human Insulin.” *Proceedings of the National Academy of Science* 76 (1): 106–10.

Gopalratnam, Arjun. 2011. “Algal Biofuels: The Backstory.” *Chemical Engineering Progress Magazine*, 2011.

Greenwell, H.C., L.M.L. Laurens, R.J. Shields, R.W. Lovitt, and K.J. Flynn. 2010. “Placing Microalgae on the Biofuels Priority List: A Review of the Technological Challenges.” *Journal of the Royal Society Interface* 7: 703–26.

Guarnieri, Michael T., Lieve ML. Laurens, Eric P. Knoshaug, Yat-Chen Chou, Bryon S. Donohoe, and Phillip T. Pienkos. 2013. “Complex System Engineering: A Case Study for an Unsequenced Microalga.” In *Engineering Complex Phenotypes in Industrial Strains*, 201–31.

Guarnieri, Michael T, Ambarish Nag, Sharon L Smolinski, Al Darzins, Michael Seibert, and Philip T Pienkos. 2011. “Examination of Triacylglycerol Biosynthetic Pathways via De Novo Transcriptomic and Proteomic Analyses in an Unsequenced Microalga.” *PLoS ONE* 6 (10): e25851. https://doi.org/10.1371/journal.pone.0025851.

Guo, Zhi, and Yen Wah Tong. 2014. “The Interactions between Chlorella Vulgaris and Algal Symbiotic Bacteria under Photoautotrophic and Photoheterotrophic Conditions.” *Journal of Applied Phycology* 26 (3): 1483–92. https://doi.org/10.1007/s10811-013-0186-1.

Hawksworth, D. L. 1988. “The Variety of Fungal-algal Symbioses, Their Evolutionary Significance, and the Nature of Lichens.” *Botanical Journal of the Linnean Society* 96 (1): 3–20. https://doi.org/10.1111/j.1095-8339.1988.tb00623.x.

Hayakawa, Kenshi, Fumio Matsuda, and Hiroshi Shimizu. 2018. “13C-metabolic Flux Analysis of Ethanol-assimilating Saccharomyces Cerevisiae for S-adenosyl-L-methionine Production.” *Microbial Cell Factories* 17 (82): 1–13. https://doi.org/10.1186/s12934-018-0935-6.

Heimann, Kirsten. 2016. “Novel Approaches to Microalgal and Cyanobacterial Cultivation for Bioenergy and Biofuel Production.” *Current Opinion in Biotechnology* 38: 183–89. https://doi.org/10.1016/j.copbio.2016.02.024.

Ho, Shih-hsin, Shu-wen Huang, Chun-yen Chen, Tomohisa Hasunuma, Akihiko Kondo, and Jo-Shu Chang. 2013. “Characterization and Optimization of Carbohydrate Production from an Indigenous Microalga Chlorella Vulgaris FSP-E.” *Bioresource Technology* 135: 157–65.

https://doi.org/10.1016/j.biortech.2012.10.100.

Hu, Qiang, Milton Sommerfeld, Eric Jarvis, Maria Ghirardi, Matthew Posewitz, Michael Seibert, and Al Darzins. 2008. "Microalgal Triacylglycerols as Feedstocks for Biofuel Production: Perspectives and Advances." *The Plant Journal* 54: 621–39. https://doi.org/10.1111/j.1365-313X.2008.03492.x.

Illman, A M, A H Scragg, and S W Shales. 2000. "Increase in Chlorella Strains Calorific Values When Grown in Low Nitrogen Medium." *Enzyme and Microbial Technology* 27: 631–35.

Ingram, L.O., T Conway, D.P. Clark, G.W. Sewell, and J.F. Preston. 1987. "Genetic Engineering of Ethanol Production in Escherichia Coli." *Applied and Environmental Biology* 53 (10): 2420–25.

Janda, J Michael, and Sharon L Abbott. 2007. "16S RRNA Gene Sequencing for Bacterial Identification in the Diagnostic Laboratory: Pluses, Perils, and Pitfalls." *Journal of Clinical Microbiology* 45 (9): 2761–64. https://doi.org/10.1128/JCM.01228-07.

Jang, Cholsoon, Li Chen, and Joshua D Rabinowitz. 2018. "Metabolomics and Isotope Tracing." *Cell* 173 (4): 822–37. https://doi.org/10.1016/j.cell.2018.03.055.

John, Rojan P, G S Anisha, K Madhavan Nampoothiri, and Ashok Pandey. 2011. "Micro and Macroalgal Biomass: A Renewable Source for Bioethanol." *Bioresource Technology* 102 (1): 186–93. https://doi.org/10.1016/j.biortech.2010.06.139.

Jones, Carla S., and Stephen P. Mayfield. 2012. "Algae Biofuels: Versatility for the Future of Bioenergy." *Current Opinion in Biotechnology* 23 (3): 346–51. https://doi.org/10.1016/j.copbio.2011.10.013.

Kaasalainen, Ulla, Alexander R. Schmidt, Jouko Rikkinen, R. N. S. Sodhi, and K. Muehlenbachs. 2017. "Diversity and Ecological Adaptations in Palaeogene Lichens." *Nature Plants* 3 (5): 17049. https://doi.org/10.1038/nplants.2017.49.

Kasprow, Robert P, Andrew J Lange, and Donald J Kirwan. 1998. "Correlation of Fermentation Yield with Yeast Extract Composition as Characterized by Near-Infrared Spectroscopy." *Biotechnology Progress* 14: 318–25.

Kazamia, Elena, Anthony S Riseley, Christopher J Howe, and Alison G Smith. 2014. "An Engineered Community Approach for Industrial Cultivation of Microalgae." *Industrial Biotechnology* 10 (3): 184–90. https://doi.org/10.1089/ind.2013.0041.An.

Kemp, P F, S Lee, and J Laroche. 1993. “Estimating the Growth Rate of Slowly Growing Marine Bacteria from RNA Content.” *Applied and Environmental Biology* 59 (8): 2594–2601.

Kind, Tobias, John K. Meissen, Dawei Yang, Fernando Nocito, Arpana Vaniya, Yu Shen Cheng, Jean S. VanderGheynst, and Oliver Fiehn. 2012. “Qualitative Analysis of Algal Secretions with Multiple Mass Spectrometric Platforms.” *Journal of Chromatography A* 1244: 139–47. https://doi.org/10.1016/j.chroma.2012.04.074.Qualitative.

Kitamura, Sayaka, Yoshihiro Toya, and Hiroshi Shimizu. 2019. “13C-Metabolic Flux Analysis Reveals Effect of Phenol on Central Carbon Metabolism in Escherichia Coli.” *Frontiers in Microbiology* 10 (1010): 1–8. https://doi.org/10.3389/fmicb.2019.01010.

Kouzuma, Atsushi, and Kazuya Watanabe. 2015. “Exploring the Potential of Algae/Bacteria Interactions.” *Current Opinion in Biotechnology* 33: 125–29. https://doi.org/10.1016/j.copbio.2015.02.007.

Laurens, Lieve M L, Thomas A Dempster, Howland D T Jones, Edward J Wolfrum, Stefanie Van Wychen, Jordan S P Mcallister, Michelle Rencenberger, Kylea J Parchert, and Lindsey M Gloe. 2012. “Algal Biomass Constituent Analysis: Method Uncertainties and Investigation of the Underlying Measuring Chemistries.” *Analytical Chemistry* 84: 1879–87. https://doi.org/10.1021/ac202668c.

Ledesma-Amaro, Rodrigo, Eduard J Kerkhoven, Jose Luis Revuelta, and Jens Nielsen. 2014. “Genome Scale Metabolic Modeling of the Riboflavin Overproducer Ashbya Gossypii.” *Biotechnology and Bioengineering* 111 (6): 1191–99. https://doi.org/10.1002/bit.25167.

Lee, Yoo Kyung, Jung-hyun Lee, and Hong Kum Lee. 2001. “Microbial Symbiosis in Marine Sponges.” *The Journal of Microbiology* 39 (4): 254–64.

Leighty, Robert W., and Maciek R. Antoniewicz. 2012. “Parallel Labeling Experiments with [U-13C]Glucose Validate E. Coli Metabolic Network Model for 13C Metabolic Flux Analysis.” *Metabolic Engineering* 14 (5): 533–41. https://doi.org/10.1016/j.ymben.2012.06.003.

Lesser, M. P., M. Stat, and R. D. Gates. 2013. “The Endosymbiotic Dinoflagellates (Symbiodinium Sp.) of Corals Are Parasites and Mutualists.” *Coral Reefs* 32 (3): 603–11. https://doi.org/10.1007/s00338-013-1051-z.

Levering, Jennifer, Jared Broddrick, and Karsten Zengler. 2015. “Engineering of

Oleaginous Organisms for Lipid Production." *Current Opinion in Biotechnology* 36: 32–39. https://doi.org/10.1016/j.copbio.2015.08.001.

Link, Hannes, Tobias Fuhrer, Luca Gerosa, Nicola Zamboni, and Uwe Sauer. 2015. "Real-Time Metabolome Profiling of the Metabolic Switch between Starvation and Growth." *Nature Methods* 12 (11): 1091–97. https://doi.org/10.1038/nmeth.3584.

Liu, Bensheng, and Christoph Benning. 2013. "Lipid Metabolism in Microalgae Distinguishes Itself." *Current Opinion in Biotechnology* 24 (2): 300–309. https://doi.org/10.1016/j.copbio.2012.08.008.

Liu, Jin, and Feng Chen. 2014. "Biology and Industrial Applications of Chlorella: Advances and Prospects." In *Microalgae Biotechnology - Advances in Biochemical Engineering/Biotechnology*, 1–36. https://doi.org/10.1007/10.

Long, Christopher, and Maciek Antoniewicz. 2014. "Quantifying Biomass Composition by Gas Chromatography/Mass Spectrometry." *Analytical Chemistry* 86 (19): 9423–27. https://doi.org/10.1021/ac502734e.Quantifying.

Long, Christopher P, and Maciek R Antoniewicz. 2014. "Quantifying Biomass Composition by Gas Chromatography/Mass Spectrometry." *Analytical Chemistry* 86: 9423–27. https://doi.org/10.1021/ac502734e.

Long, Christopher P, Jennifer Au, Jacqueline E Gonzalez, and Maciek R Antoniewicz. 2016. "13C Metabolic Flux Analysis of Microbial and Mammalian Systems Is Enhanced with GC-MS Measurements of Glycogen and RNA Labeling." *Metabolic Engineering* 38: 65–72. https://doi.org/10.1016/j.ymben.2016.06.007.

Long, Christopher P, Jacqueline E Gonzalez, Robert M Cipolla, and Maciek R Antoniewicz. 2017. "Metabolism of the Fast-Growing Bacterium Vibrio Natriegens Elucidated by 13C Metabolic Flux Analysis." *Metabolic Engineering* 44: 191–97. https://doi.org/10.1016/j.ymben.2017.10.008.

Long, Christopher P, Jacqueline E Gonzalez, Adam M Feist, Bernhard O Palsson, and Maciek R Antoniewicz. 2018. "Dissecting the Genetic and Metabolic Mechanisms of Adaptation to the Knockout of a Major Metabolic Enzyme in Escherichia Coli." *Proceedings of the National Academy of Science* 115 (1): 222–27. https://doi.org/10.1073/pnas.1716056115.

Long, Christopher P, Jacqueline E Gonzalez, Nicholas R Sandoval, and Maciek R Antoniewicz. 2016. "Characterization of Physiological Responses to 22 Gene Knockouts in Escherichia Coli Central Carbon Metabolism." *Metabolic Engineering* 37: 102–13. https://doi.org/10.1016/j.ymben.2016.05.006.

Ma, Fangfang, Lara J Jazmin, Jamey D Young, and Doug K Allen. 2014. "Isotopically Nonstationary 13C Flux Analysis of Changes in Arabidopsis Thaliana Leaf Metabolism Due to High Light Acclimation." *Proceedings of the National Academy of Science* 111 (47): 16967–72. https://doi.org/10.1073/pnas.1319485111.

McClave, Stephen A, Cynthia C Lowen, Melissa J Kleber, J Wesley McConnell, Laura Y Jung, and Linda J Goldsmith. 2003. "Clinical Use of the Respiratory Quotient Obtained From Indirect Calorimetry." *Journal of Parenteral and Enteral Nutrition* 27 (1): 21–26. https://doi.org/10.1177/014860710302700121.

McConnell, Brian O., and Maciek R. Antoniewicz. 2016. "Measuring the Composition and Stable-Isotope Labeling of Algal Biomass Carbohydrates via Gas Chromatography/Mass Spectrometry." *Analytical Chemistry* 88 (9): 4624–28. https://doi.org/10.1021/acs.analchem.6b00779.

Merzlyak, Mark N, Olga B Chivkunova, Olga A Gorelova, Irina V Reshetnikova, Alexei E Solovchenko, Inna Khozin-goldberg, and Zvi Cohen. 2007. "EFFECT OF NITROGEN STARVATION ON OPTICAL PROPERTIES , PIGMENTS , AND ARACHIDONIC ACID CONTENT OF THE UNICELLULAR GREEN ALGA PARIETOCHLORIS INCISA (TREBOUXIOPHYCEAE, CHLOROPHYTA)." *Journal of Phycology* 43: 833–43. https://doi.org/10.1111/j.1529-8817.2007.00375.x.

Miller, Joseph Ar, and Vasantha Nagarajan. 2000. "The Impact of Biotechnology on the Chemical Industry in the 21st Century." *Trends in Biotechnology* 18 (5): 190–91.

Moxley, Geoffery, and Y-H Percival Zhang. 2007. "More Accurate Determination of Acid-Labile Carbohydrates in Lignocellulose by Modified Quantitative Saccharification." *Energy and Fuels* 21 (9): 3684–88.

Muradov, Nazim Z., and Nejat Veziroglu. 2017. *Carbon-Neutral Fuels and Energy Carriers*. CRC Press.

Nakamura, Charles E., and Gregory M. Whited. 2003. "Metabolic Engineering for the Microbial Production of 1,3-Propanediol." *Current Opinion in Biotechnology* 14: 454–59. https://doi.org/10.1016/j.copbio.2003.08.005.

Nelson, David L., Michael M Cox, and Albert L. Lehninger. 2017. *Lehninger Principles of Biochemistry*.

Papoutsakis, Eleftherios Terry, and Charles L Meyer. 1985a. "Equations and Calculations of Product Yields and Preferred Pathways for Butanediol and

Mixed-Acid Fermentations." *Biotechnology and Bioengineering* 27: 50–66.

———. 1985b. "Fermentation Equations for Propionic- Acid Bacteria and Production of Assorted Oxychemicals from Various Sugars." *Biotechnology and Bioengineering* 27: 67–80.

Pelroy, R.A., and J.A. Bassham. 1972. "Photosynthetic and Dark Carbon Metabolism in Unicellular Blue-Green Algae." *Archives of Microbiology* 86: 25–38.

Perez-Garcia, Octavio, Froylan ME Escalante, Luz E De-Bashan, and Yoav Bashan. 2010. "Heterotrophic Cultures of Microalgae: Metabolism and Potential Products." *Water Research* 45 (1): 11–36. https://doi.org/10.1016/j.watres.2010.08.037.

Perlack, Robert D., Lynn L. Wright, Anthony F. Turhollow, Robin L. Graham, Bryce J. Stokes, and Donald C. Erbach. 2005. "Biomass as Feedstock for a Bioenergy and Bioproducts Industry: The Technical Feasibility of a Billion-Ton Annual Supply."

Phukan, Mayur M, Rahul S Chutia, B K Konwar, and R Kataki. 2011. "Microalgae Chlorella as a Potential Bio-Energy Feedstock." *Applied Energy* 88 (10): 3307–12. https://doi.org/10.1016/j.apenergy.2010.11.026.

Plaza, Merichel, Miguel Herrero, Alejandro Cifuentes, and Elena Ibanez. 2009. "Innovative Natural Functional Ingredients from Microalgae." *Journal of Agriculture and Food Chemistry* 57: 7159–70. https://doi.org/10.1021/jf901070g.

Posten, Clemens, and Christian Walter. 2012. *Microalgal Biotechnology: Potential and Production*. *De Gruyter*.

Ramanan, Rishiram, Byung Hyuk Kim, Dae Hyun Cho, Hee Mock Oh, and Hee Sik Kim. 2016. "Algae-Bacteria Interactions: Evolution, Ecology and Emerging Applications." *Biotechnology Advances* 34 (1): 14–29. https://doi.org/10.1016/j.biotechadv.2015.12.003.

Richardson, B Y K, J Beardall, and J A Raven. 1983. "ADAPTATION OF UNICELLULAR ALGAE TO IRRADIANCE: AN ANALYSIS OF STRATEGIES." *The New Phytologist* 93: 157–91.

Rosenberg, Julian N, George A Oyler, Loy Wilkinson, and Michael J Betenbaugh. 2008. "A Green Light for Engineered Algae: Redirecting Metabolism to Fuel a Biotechnology Revolution." *Current Opinion in Biotechnology* 19: 430–36. https://doi.org/10.1016/j.copbio.2008.07.008.

Rozzell, J David. 1999. “Commercial Scale Biocatalysis: Myths and Realities.” *Bioorganic Medicinal Chemistry* 7: 2253–61.

Santos, Carla A., and Alberto Reis. 2014. “Microalgal Symbiosis in Biotechnology.” *Applied Microbiology and Biotechnology* 98 (13): 5839–46. https://doi.org/10.1007/s00253-014-5764-x.

Schwechheimer, Susanne Katharina, Judith Becker, Lindsay Peyriga, Jean-charles Portais, Daniel Sauer, Rolf Müller, Birgit Hoff, et al. 2018. “Improved Riboflavin Production with Ashbya Gossypii from Vegetable Oil Based on 13C Metabolic Network Analysis with Combined Labeling Analysis by GC/MS, LC/MS, 1D, and 2D NMR.” *Metabolic Engineering* 47: 357–73. https://doi.org/10.1016/j.ymben.2018.04.005.

Schwechheimer, Susanne Katharina, Judith Becker, Lindsay Peyriga, Jean Charles Portais, and Christoph Wittmann. 2018. “Metabolic Flux Analysis in Ashbya Gossypii Using 13C-labeled Yeast Extract: Industrial Riboflavin Production under Complex Nutrient Conditions.” *Microbial Cell Factories* 17 (162): 1–22. https://doi.org/10.1186/s12934-018-1003-y.

Scott, Stuart A., Matthew P. Davey, John S. Dennis, Irmtraud Horst, Christopher J. Howe, David J. Lea-Smith, and Alison G. Smith. 2010. “Biodiesel from Algae: Challenges and Prospects.” *Current Opinion in Biotechnology* 21 (3): 277–86. https://doi.org/10.1016/j.copbio.2010.03.005.

Sforza, Eleonora, Diana Simionato, Giorgio Mario Giacometti, Alberto Bertucco, and Tomas Morosinotto. 2012. “Adjusted Light and Dark Cycles Can Optimize Photosynthetic Efficiency in Algae Growing in Photobioreactors.” *PLoS ONE* 7 (6): e38975. https://doi.org/10.1371/journal.pone.0038975.

Sheehan, John, Terri Dunahay, John Benemann, and Paul Roessler. 1998. “A Look Back at the U.S. Department of Energy’ s Aquatic Species Program: Biodiesel from Algae.” *National Renewable Energy Laboratory*, 1–294. https://doi.org/10.2172/15003040.

Stephanopoulos, Gregory. 1999. “Metabolic Fluxes and Metabolic Engineering.” *Metabolic Engineering* 1: 1–11.

Toya, Yoshihiro, Nobuaki Kono, Kazuharu Arakawa, and Masaru Tomita. 2011. “Metabolic Flux Analysis and Visualization.” *Journal of Proteome Research* 10: 3313–23. https://doi.org/10.1021/pr2002885.

Vasudevan, Palligarnai T, and Michael Briggs. 2008. “Biodiesel Production - Current State of the Art and Challenges.” *Journal of Industrial Microbiology and*

Biotechnology 35: 421–30. https://doi.org/10.1007/s10295-008-0312-2.

Villa, Juan A, Erin E Ray, and Brett M Barney. 2014. "Azotobacter Vinelandii Siderophore Can Provide Nitrogen to Support the Culture of the Green Algae Neochloris Oleoabundans and Scenedesmus Sp. BA032." *FEMS Microbiology Letters* 351: 70–77. https://doi.org/10.1111/1574-6968.12347.

Wang, Liang, Min Min, Yecong Li, Paul Chen, Yifeng Chen, Yuhuan Liu, Yingkuan Wang, and Roger Ruan. 2010. "Cultivation of Green Algae Chlorella Sp. in Different Wastewaters from Municipal Wastewater Treatment Plant." *Applied Biochemistry and Biotechnology* 162 (4): 1174–86. https://doi.org/10.1007/s12010-009-8866-7.

Wiechert, Wolfgang. 2001. "13C Metabolic Flux Analysis." *Metabolic Engineeri* 3: 195–206.

Wijffels, René H., Olaf Kruse, and Klaas J. Hellingwerf. 2013. "Potential of Industrial Biotechnology with Cyanobacteria and Eukaryotic Microalgae." *Current Opinion in Biotechnology* 24 (3): 405–13. https://doi.org/10.1016/j.copbio.2013.04.004.

Woese, Carl R, and George E Fox. 1977. "Phylogenetic Structure of the Prokaryotic Domain: The Primary Kingdoms." *Proceedings of the National Academy of Science* 74 (11): 5088–90.

Woese, Carl R, Otto Kandlert, and Mark L Wheelis. 1990. "Towards a Natural System of Organisms: Proposal for the Domains Archaea, Bacteria, and Eucarya." *Proceedings of the National Academy of Science* 87: 4576–79.

Wolfsberg, Eric, Christopher P Long, and Maciek R Antoniewicz. 2018. "Metabolism in Dense Microbial Colonies: 13C Metabolic Flux Analysis of E . Coli Grown on Agar Identifies Two Distinct Cell Populations with Acetate Cross-Feeding." *Metabolic Engineering* 49: 242–47. https://doi.org/10.1016/j.ymben.2018.08.013.

Wychen, Stefanie Van, and Lieve M L Laurens. 2015. "Determination of Total Carbohydrates in Algal Biomass." *National Renewable Energy Laboratory Technical Report*, no. December.

Yang, Chen, Qiang Hua, and Kazuyuki Shimizu. 2000. "Energetics and Carbon Metabolism during Growth of Microalgal Cells under Photoautotrophic, Mixotrophic and Cyclic Light-Autotrophic/Dark-Heterotrophic Conditions." *Biochemical Engineering Journal* 6: 87–102.

Yoo, Hyuntae, Maciek R Antoniewicz, Gregory Stephanopoulos, and Joanne K Kelleher. 2008. "Quantifying Reductive Carboxylation Flux of Glutamine to

Lipid in a Brown Adipocyte Cell Line." *The Journal of Biological Chemistry* 283 (30): 20621–27. https://doi.org/10.1074/jbc.M706494200.

Young, Jamey D. 2014. "INCA: A Computational Platform for Isotopically Non-Stationary Metabolic Flux Analysis." *Bioinformatics* 30 (9): 1333–35. https://doi.org/10.1093/bioinformatics/btu015.

Young, Jamey D, Avantika A Shastri, Gregory Stephanopoulos, and John A Morgan. 2011. "Mapping Photoautotrophic Metabolism with Isotopically Nonstationary 13C Flux Analysis." *Metabolic Engineering* 13: 656–65. https://doi.org/10.1016/j.ymben.2011.08.002.

Zamboni, Nicola. 2011. "13C Metabolic Flux Analysis in Complex Systems." *Current Opinion in Biotechnology* 22 (1): 103–8. https://doi.org/10.1016/j.copbio.2010.08.009.

Zhang, Weiguo, Peiliang Zhang, Hao Sun, Maozhen Chen, Shan Lu, and Pengfu Li. 2014. "Effects of Various Organic Carbon Sources on the Growth and Biochemical Composition of Chlorella Pyrenoidosa." *Bioresource Technology* 173: 52–58. https://doi.org/10.1016/j.biortech.2014.09.084.

Zhu, Shunni, Yajie Wang, Wei Huang, Jin Xu, Zhongming Wang, Jingliang Xu, and Zhenhong Yuan. 2014. "Enhanced Accumulation of Carbohydrate and Starch in Chlorella Zofingiensis Induced by Nitrogen Starvation." *Applied Biochemistry and Biotechnology* 174: 2435–45. https://doi.org/10.1007/s12010-014-1183-9.

Zuñiga, Cristal, Chien-Ting Li, Tyler Huelsman, Jennifer Levering, Daniel C. Zielinski, Brian O. McConnell, Christopher P. Long, et al. 2016. "Genome-Scale Metabolic Model for the Green Alga *Chlorella Vulgaris* UTEX 395 Accurately Predicts Phenotypes under Autotrophic, Heterotrophic, and Mixotrophic Growth Conditions." *Plant Physiology* 172 (1): 589–602. https://doi.org/10.1104/pp.16.00593.

Zupke, C, and G Stephanopoulos. 1994. "Modeling of Isotope Distributions and Intracellular Fluxes in Metabolic Networks Using Atom Mapping Matrices." *Biotechnology Progress* 10: 489–98. https://doi.org/10.1021/bp00029a006.

Appendix A

SUPPLEMENTARY MATERIAL FOR CHAPTER 2

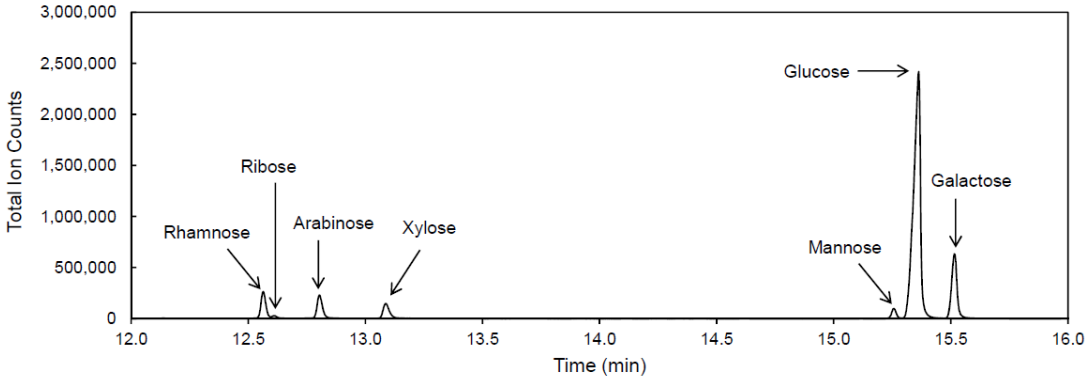

Figure A.1 Representative GC/MS chromatogram of hydrolyzed algae. The identities of all peaks were verified with ^{13}C-labeled standards.

Table A.1 Mass Isotopomer Distributions of Biomass Carbohydrates for *C. vulgaris* UTEX 395 Grown in Batch Cultures

MEASURED MASS ISOTOPOMER DISTRIBUTIONS					CORRECTED MASS ISOTOPOMER DISTRIBUTIONS				
	Autotrophic 9% D_2O	Autotrophic 18% D_2O	Heterotrophic 9% [U-^{13}C]glucose	Heterotrophic 18% [U-^{13}C]glucose		Autotrophic 9% D_2O	Autotrophic 18% D_2O	Heterotrophic 9% [U-^{13}C]glucose	Heterotrophic 18% [U-^{13}C]glucose
Xyl284 (M0)	63.6	47.4	71.8	59.1	Xyl284 (M0)	74.8	55.8	84.3	69.4
Xyl284 (M1)	28.4	37.4	15.8	18.4	Xyl284 (M1)	21.9	35.1	5.7	11.1
Xyl284 (M2)	6.4	12.2	4.1	7.9	Xyl284 (M2)	2.7	8.0	2.1	6.0
Xyl284 (M3)	1.2	2.4	2.9	4.4	Xyl284 (M3)	0.4	0.9	2.7	3.9
Xyl284 (M4)	0.2	0.4	4.6	8.9	Xyl284 (M4)	0.1	0.2	4.8	9.4
Xyl284 (M5)	0.1	0.1	0.9	1.3	Xyl284 (M5)	0.1	0.1	0.4	0.4
Arab284 (M0)	63.9	46.7	71.5	60.2	Arab284 (M0)	75.2	54.9	84.1	70.6
Arab284 (M1)	28.1	37.2	16.6	18.5	Arab284 (M1)	21.4	35.1	6.7	10.9
Arab284 (M2)	5.9	12.8	5.0	8.1	Arab284 (M2)	2.2	8.7	2.9	6.2
Arab284 (M3)	1.6	2.6	1.9	3.5	Arab284 (M3)	1.0	1.0	1.4	2.8
Arab284 (M4)	0.2	0.5	4.4	8.7	Arab284 (M4)	0.1	0.1	4.8	9.3
Arab284 (M5)	0.2	0.2	0.6	1.1	Arab284 (M5)	0.2	0.2	0.2	0.2
Mann370 (M0)	55.0	36.2	67.4	55.1	Mann370 (M0)	67.9	44.7	83.2	67.9
Mann370 (M1)	32.2	39.4	17.8	18.1	Mann370 (M1)	26.2	39.5	5.6	8.9
Mann370 (M2)	9.9	17.6	7.1	10.5	Mann370 (M2)	4.9	12.5	4.8	8.8
Mann370 (M3)	2.3	5.2	2.7	5.3	Mann370 (M3)	0.8	2.7	1.9	4.3
Mann370 (M4)	0.4	1.2	0.8	1.9	Mann370 (M4)	0.1	0.5	0.4	1.3
Mann370 (M5)	0.1	0.3	3.7	7.9	Mann370 (M5)	0.0	0.1	4.1	8.9
Mann370 (M6)	0.0	0.1	0.6	1.2	Mann370 (M6)	0.0	0.0	0.0	0.0

Gluc370 (M0)	55.3	37.0	67.9	56.2	Gluc370 (M0)	68.3	45.7	83.7	69.3
Gluc370 (M1)	32.7	39.3	17.5	17.7	Gluc370 (M1)	26.7	39.1	5.2	8.2
Gluc370 (M2)	9.5	17.9	6.8	10.0	Gluc370 (M2)	4.3	12.9	4.5	8.2
Gluc370 (M3)	1.9	4.8	2.6	5.1	Gluc370 (M3)	0.4	2.1	1.8	4.1
Gluc370 (M4)	0.3	0.9	0.7	1.8	Gluc370 (M4)	0.0	0.2	0.4	1.1
Gluc370 (M5)	0.2	0.2	4.0	8.1	Gluc370 (M5)	0.2	0.0	4.5	9.1
Gluc370 (M6)	0.0	0.0	0.6	1.1	Gluc370 (M6)	0.0	0.0	0.0	0.0
Galact370 (M0)	54.3	35.9	68.5	57.4	Galact370 (M0)	67.0	44.3	84.5	70.7
Galact370 (M1)	33.3	39.3	17.4	17.5	Galact370 (M1)	27.7	39.4	4.8	7.6
Galact370 (M2)	9.9	18.5	6.3	8.9	Galact370 (M2)	4.6	13.6	3.9	7.0
Galact370 (M3)	2.0	5.1	2.3	4.5	Galact370 (M3)	0.5	2.3	1.5	3.6
Galact370 (M4)	0.3	1.0	0.7	1.7	Galact370 (M4)	0.1	0.2	0.4	1.1
Galact370 (M5)	0.1	0.3	4.3	8.9	Galact370 (M5)	0.0	0.1	4.9	10.1
Galact370 (M6)	0.0	0.0	0.6	1.3	Galact370 (M6)	0.0	0.0	0.0	0.0

Table A.2 Isotopic Labeling Summary for *C. vulgaris* UTEX 395 Grown in Batch Cultures.

ISOTOPIC LABELING				
	Autotrophic 9% D_2O	Autotrophic 18% D_2O	Heterotrophic 9% [U-^{13}C]glucose	Heterotrophic 18% [U-^{13}C]glucose
	[%^{2}H]	[%^{2}H]	[%^{13}C]	[%^{13}C]
Xylose	9.5	17.9	9.3	18.0
Arabinose	9.6	18.4	8.9	17.2
Mannose	9.7	18.6	8.6	17.7
Glucose	9.2	18.0	8.7	17.4
Galactose	9.7	18.6	8.6	17.4
AVG	9.5	18.3	8.8	17.6
SD	0.2	0.3	0.3	0.3

Appendix B

SUPPLEMENTARY MATERIAL FOR CHAPTER 3

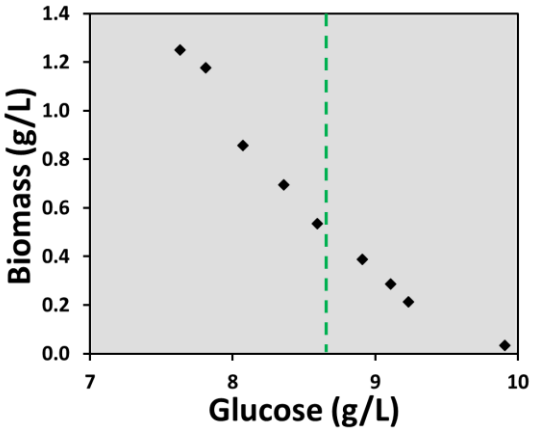

Figure B.1 Biomass Yield for Heterotrophic Growth. This culture was always in darkness. The vertical dashed green line indicates when nitrogen became depleted.

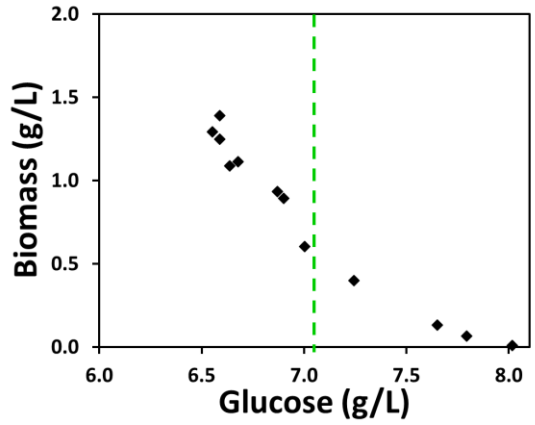

Figure B.2 Biomass Yield on Glucose for Mixotrophic Growth. The vertical dashed green line indicates when nitrogen became depleted.

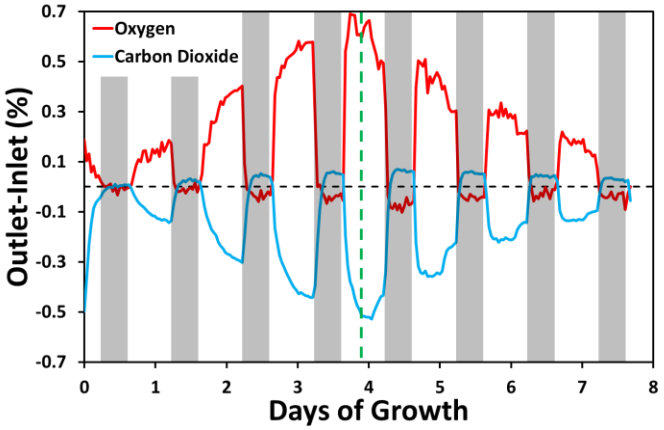

Figure B.3 Off-Gas Analysis for Autotrophic Growth. The dark bars indicate time periods when the lights were turned off. The vertical dashed green line indicates when nitrogen became depleted.

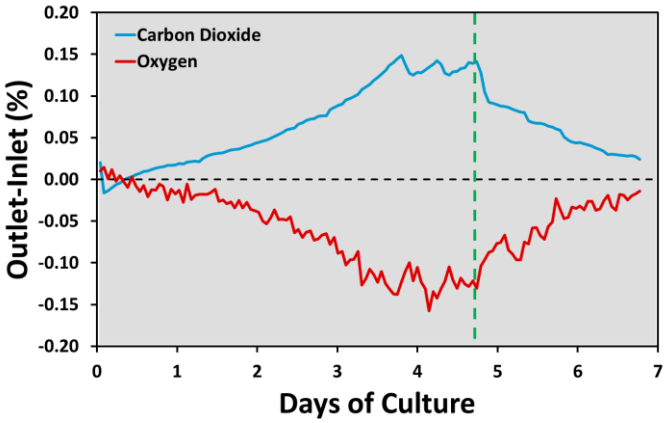

Figure B.4 Off-Gas Analysis for Heterotrophic Growth. The lights were always turned off. The vertical dashed green line indicates when nitrogen became depleted.

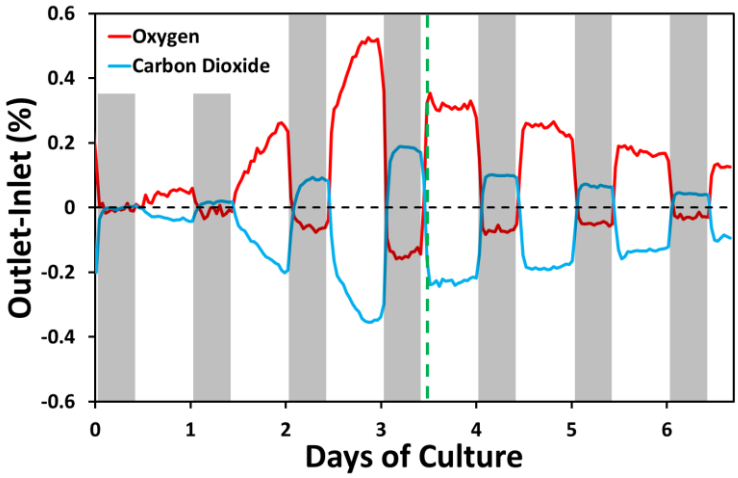

Figure B.5 Off-Gas Analysis for Mixotrophic Growth. The dark bars indicate time periods when the lights were turned off. The vertical dashed green line indicates when nitrogen became depleted.

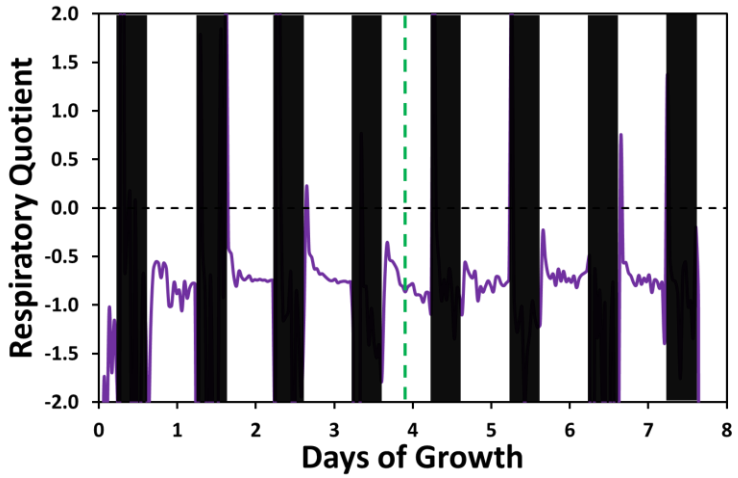

Figure B.6 Respiratory Quotient for Autotrophic Growth. Due to small changes in oxygen content (relative to the feed's oxygen content), the nighttime oxygen measurement had large variability. This led to large variability in the nighttime RQ. For ease of visualization, the nighttime bars were made black instead of gray.

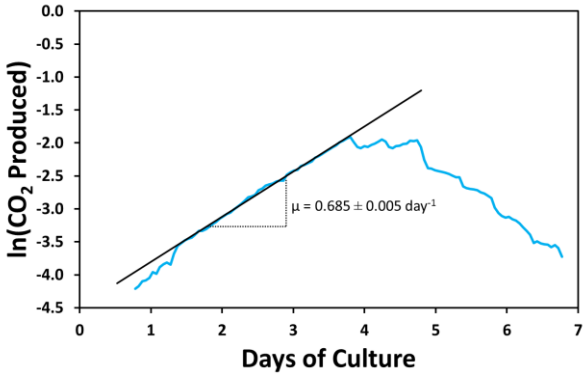

Figure B.7 Natural Logarithm of Net CO_2 Production. CO_2 production rate increased exponentially during exponential growth. From this data, the specific growth rate can be calculated.

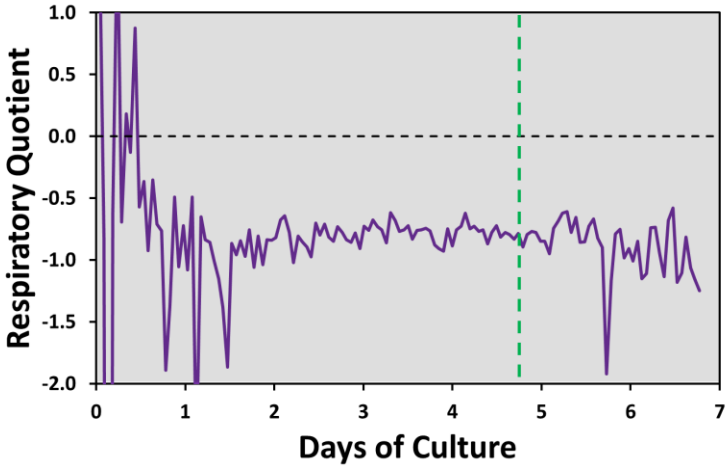

Figure B.8 Respiratory Quotient for Heterotrophic Growth. Due to small changes in oxygen content (relative to the feed's oxygen content) while the cell density was low, the RQ for the first 1.5 days was very noisy.

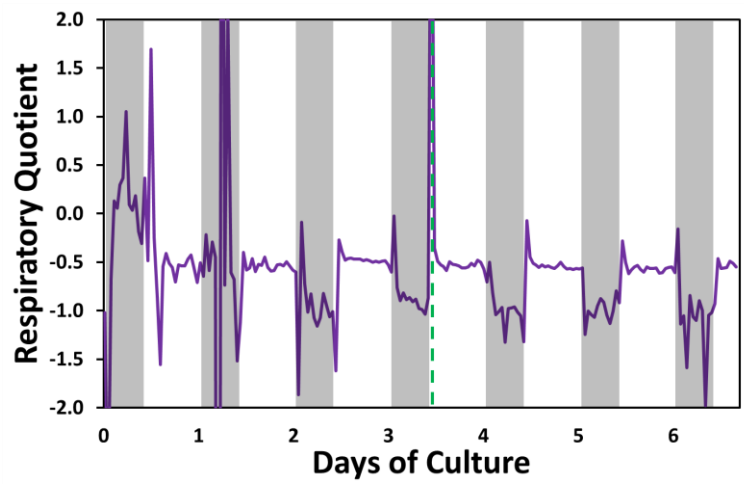

Figure B.9 Respiratory Quotient for Mixotrophic Growth. Due to small changes in oxygen content (relative to the feed's oxygen content) while the cell density was low, the RQ for the first 1.5 days was very noisy.

Table B.1 Fatty Acid Composition Profile (wt% of total fatty acids) of *C. vulgaris* Grown Autotrophically.

Days of Growth	**3.02**	**4.02**	**5.02**	**6.02**	**7.02**	**8.02**
C14	1.08	0.35	0.50	0.32	0.29	0.21
C16:1	1.19	0.05	0.03	0.01	0.00	0.00
C16:2	15.3	15.9	11.8	6.65	9.78	6.48
C16:0	37.6	31.2	35.3	32.8	33.6	28.3
C17:0 a	2.07	1.97	2.93	0.96	0.99	0.90
C17:0 b	0.47	0.42	1.42	0.59	0.62	0.54
C18:1	2.73	2.30	6.78	20.5	15.3	4.52
C18:2	18.4	25.0	24.7	16.7	13.4	20.5
C18:3	18.8	17.1	7.44	8.77	11.7	27.1
C18:0	2.42	5.62	9.06	12.7	14.4	11.4
C17:0	2.54	2.39	4.35	1.55	1.61	1.44

Table B.2 Fatty Acid Composition Profile (wt% of total fatty acids) of *C. vulgaris* Grown Heterotrophically.

Days of Growth	**3.23**	**3.76**	**4.24**	**4.75**	**5.24**	**5.75**	**6.25**	**6.74**
C14	1.60	0.56	0.54	0.54	0.39	0.36	0.26	0.29
C16:1	2.04	0.14	0.07	0.06	0.02	0.01	0.00	0.00
C16:2	6.01	5.06	5.77	6.00	6.65	13.03	9.77	10.63
C16:0	31.6	33.5	31.4	37.0	36.2	44.2	33.6	36.0
C17:0 a	3.01	3.40	2.52	2.73	3.36	3.62	2.60	2.34
C17:0 b	1.15	0.97	0.57	0.56	1.06	1.36	0.91	0.95
C18:1	9.07	8.74	8.19	10.24	7.66	4.77	7.01	6.52
C18:2	20.4	22.4	25.9	21.4	22.6	2.14	16.8	15.8
C18:3	11.5	14.9	17.9	15.5	14.2	19.5	19.2	16.0
C18:0	13.6	10.4	7.06	6.02	7.80	11.0	9.92	11.5
C17:0	4.16	4.37	3.09	3.29	4.42	4.98	3.51	3.29

Table B.3 Fatty Acid Composition Profile (wt% of total fatty acids) of *C. vulgaris* Grown Mixotrophically.

Days of Growth	**1.98**	**2.49**	**2.98**	**3.49**	**3.98**	**4.51**	**4.99**	**5.51**	**5.98**	**6.50**	**6.68**
C14	3.26	1.42	1.17	0.37	0.27	0.38	0.33	0.34	0.32	0.36	0.41
C16:1	6.81	5.43	1.36	0.48	0.70	1.79	0.91	1.03	1.23	1.25	1.48
C16:2	10.4	7.82	4.50	6.93	7.18	2.78	7.37	8.96	7.48	6.93	7.57
C16:3	0.00	9.78	8.60	13.04	27.38	2.99	27.2	29.3	28.6	23.5	22.1
C16:0	42.8	36.3	30.1	27.7	30.1	41.2	36.6	36.1	37.9	36.6	39.0
C17:0 a	0.86	0.81	0.35	0.41	0.39	0.04	1.12	1.13	0.91	1.19	2.07
C17:0 b	0.68	0.33	0.20	0.66	0.59	0.80	0.97	0.97	1.11	1.45	1.73
C18:1	9.69	6.14	6.61	0.95	5.19	4.96	8.81	6.39	8.04	10.6	7.28
C18:2	12.1	13.9	19.6	24.3	9.80	22.4	1.67	1.14	0.85	1.49	1.86
C18:3	13.6	17.5	27.4	21.7	13.9	16.4	8.97	8.30	7.59	9.88	9.60
C18:0	0.00	0.65	0.13	3.53	4.52	6.19	6.06	6.34	5.93	6.75	6.92

Table B.4 Amino Acid Composition (μmol/$g_{Protein}$) of *C. vulgaris* Grown Autotrophically.

Days of Growth	3.02	4.02	5.02	6.02	7.02	8.03
Ala	1023	1007	1021	1032	1033	1046
Gly	907	921	916	913	913	912
Val	594	605	601	599	600	600
Leu	775	800	813	814	812	807
Ile	336	343	341	338	338	335
Pro	465	473	482	482	485	484
Met	186	190	187	184	184	183
Ser	537	542	548	556	561	562
Thr	449	462	469	472	472	474
Phe	354	371	373	367	363	355
Asx	775	783	760	754	747	746
Glx	1014	971	930	925	936	943
Lys	499	475	476	478	476	472
His	150	149	146	145	143	140
Tyr	256	256	274	273	272	269

Table B.5 Amino Acid Composition (μmol/$g_{Protein}$) of *C. vulgaris* Grown Heterotrophically.

Days of Growth	3.23	3.76	4.24	4.75	5.24	5.75	6.25	6.74
Ala	1119	1109	1095	1058	1030	1035	1029	1125
Gly	821	854	859	880	889	896	890	890
Val	564	569	574	586	592	591	591	580
Leu	735	738	749	771	795	801	809	796
Ile	303	305	310	319	327	329	330	324
Pro	523	539	523	526	492	486	487	474
Met	181	196	205	190	200	200	199	193
Ser	498	511	517	524	539	548	549	539
Thr	422	424	428	441	454	458	462	460
Phe	319	320	325	336	347	350	352	346
Asx	772	762	762	771	763	758	754	743
Glx	1107	1078	1057	1025	995	963	964	891
Lys	464	466	470	478	481	483	480	474

His	151	136	139	142	150	153	152	150
Tyr	232	235	240	247	259	264	267	266

Table B.6 Amino Acid Composition (μmol/$g_{Protein}$) of *C. vulgaris* Grown Mixotrophically.

Days of Growth	**1.98**	**2.49**	**2.98**	**3.49**	**3.98**	**4.51**	**4.99**	**5.51**	**5.98**	**6.50**	**6.68**
Ala	1014	1041	1057	1029	1040	1052	1057	1059	1062	1065	1070
Gly	856	894	893	904	902	903	900	898	901	899	902
Val	536	585	587	606	601	601	600	600	600	600	599
Leu	687	740	754	793	797	804	801	798	795	797	797
Ile	297	327	329	341	338	337	337	336	335	334	334
Pro	435	458	457	478	481	479	481	480	481	480	481
Met	271	190	184	191	188	186	182	180	183	180	181
Ser	495	538	525	557	562	539	549	567	569	567	559
Thr	430	459	446	468	469	468	469	475	475	473	474
Phe	299	322	335	349	347	341	344	341	340	336	338
Asx	771	780	750	757	749	746	744	739	737	738	731
Glx	1093	1056	1043	906	915	942	942	936	924	945	944
Lys	691	518	522	528	512	497	492	492	493	485	480
His	149	159	149	156	154	159	149	148	149	147	147
Tyr	232	239	251	266	267	259	263	264	269	264	267

Table B.7 Carbohydrate Composition Profile (wt% of total carbohydrates) of *C. vulgaris* Grown Autotrophically.

Days of Growth	**3.02**	**5.02**	**6.02**	**7.02**	**8.03**
Glucose	77.8	80.5	77.4	76.5	73.7
Galactose	15.6	11.7	12.3	11.7	11.6
Mannose	2.26	2.57	4.09	5.58	7.94
Xylose	2.44	2.48	2.92	3.07	3.32
Arabinose	1.93	2.79	3.22	3.22	3.45

Table B.8 Carbohydrate Composition Profile (wt% of total carbohydrates) of *C. vulgaris* Grown Heterotrophically.

Days of Growth	3.23	4.24	4.75	5.24	5.75	6.25	6.74
Glucose	82.8	56.1	82.1	84.6	86.3	86.9	85.9
Galactose	8.94	38.7	9.00	9.78	8.46	7.67	8.04
Mannose	0.98	0.84	1.14	1.36	1.52	1.60	1.82
Xylose	2.00	1.53	1.87	2.05	1.82	1.76	1.97
Arabinose	5.27	2.88	5.87	2.23	1.87	2.07	2.23

Table B.9 Carbohydrate Composition Profile (wt% of total carbohydrates) of *C. vulgaris* Grown Mixotrophically.

Days of Growth	1.98	2.49	2.98	3.49	3.98	4.51	4.99	5.51	5.98	6.50	6.68
Glucose	90.1	70.9	92.4	85.6	81.8	66.9	75.5	58.6	68.0	53.5	58.0
Galactose	5.33	16.6	4.38	7.40	8.73	15.3	10.6	16.9	12.8	17.7	15.7
Mannose	1.11	4.47	0.988	2.44	4.20	8.66	6.81	12.9	10.1	15.7	14.3
Xylose	1.61	4.81	0.911	2.32	2.71	5.16	3.73	6.45	4.93	7.24	6.62
Arabinose	1.84	3.25	1.28	2.24	2.53	4.04	3.42	5.11	4.21	5.82	5.38

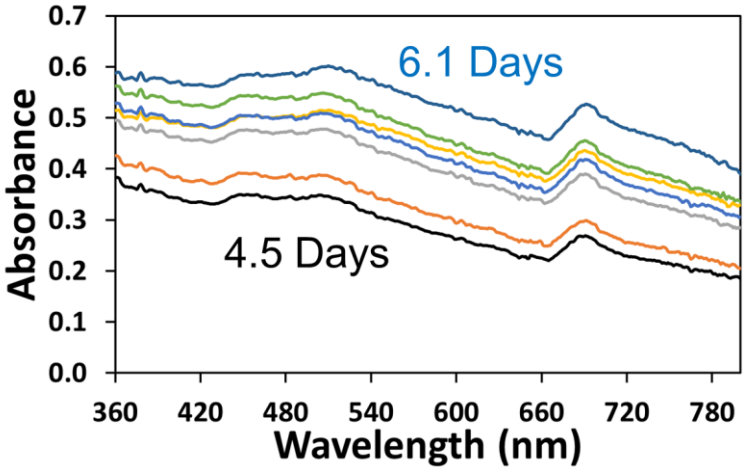

Figure B.10 Absorbance Scan Profiles for Samples Taken Between Day 4.5 and Day 6.1. Even with light cycling, the absorbance profiles do not change.

Appendix C

SUPPLEMENTARY MATERIAL FOR CHAPTER 4

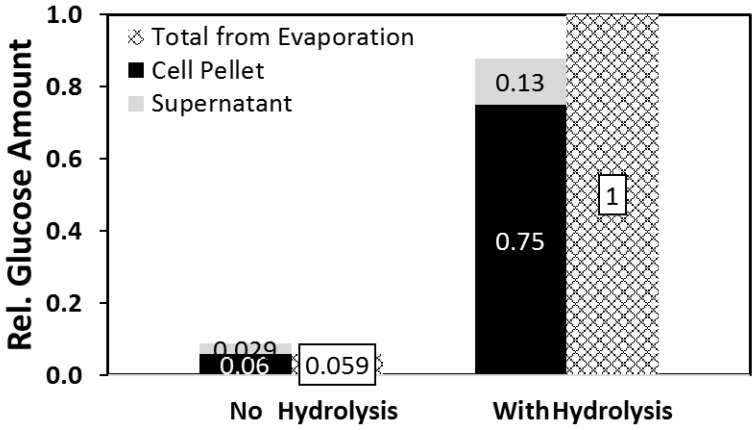

Figure C.1 Relative Amounts of Glucose in Cell Pellets and Supernatants from a Fast Stirring Autotrophic Culture during the Nitrogen Replete Phase.

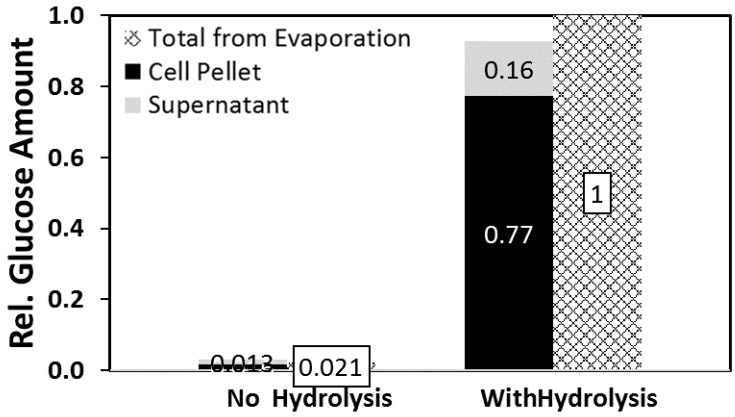

Figure C.2 Relative Amounts of Glucose in Cell Pellets and Supernatants from a Fast Stirring Autotrophic Culture during the Nitrogen Deplete Phase.

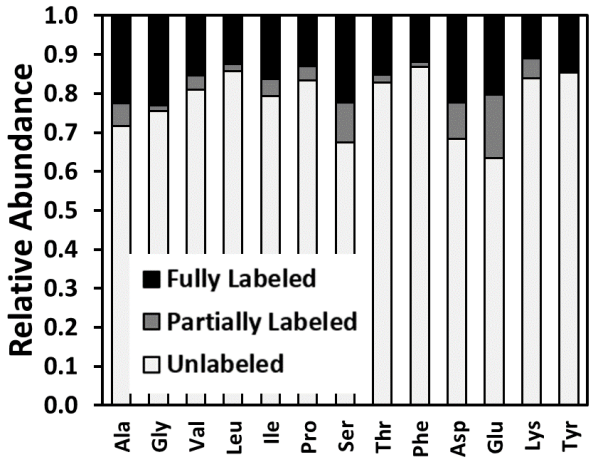

Figure C.3 Proteinogenic Amino Acid Labeling Patterns of *C. vulgaris* Grown Heterotrophically on Labeled Spent Medium.

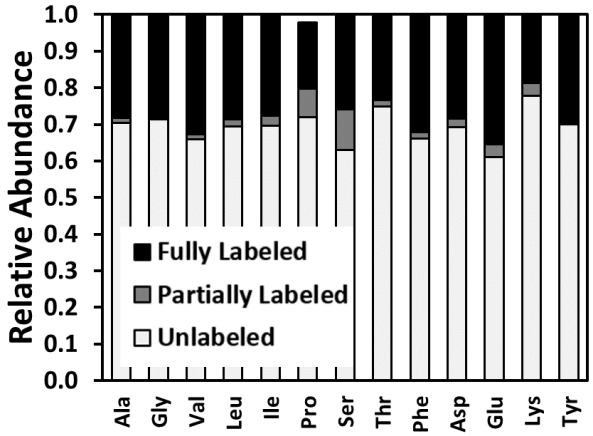

Figure C.4 Proteinogenic Amino Acid Labeling Patterns of *E. coli* Grown Heterotrophically on Labeled Spent Medium.

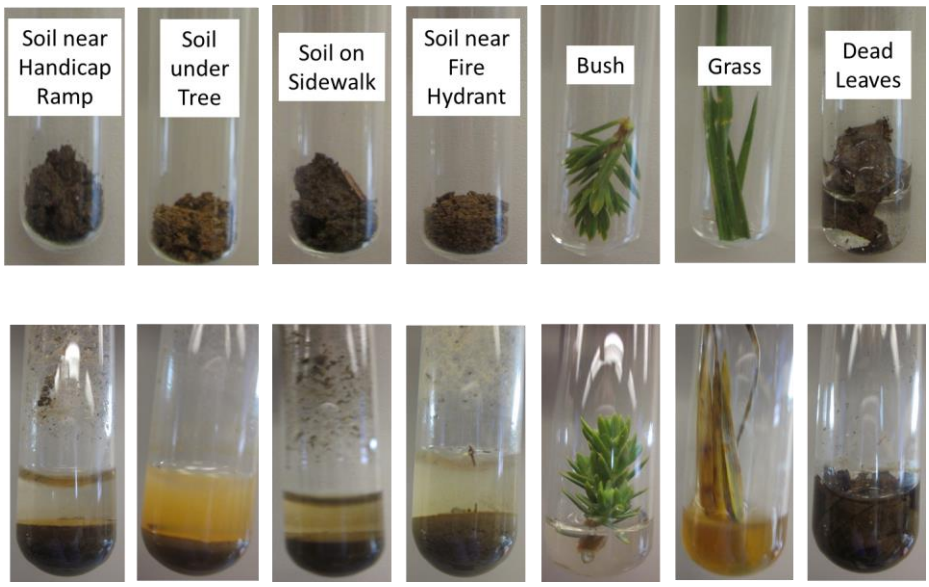

Figure C.5 Beginning of Microbiome Selection Process. The top row shows the samples that were collected. The bottom row shows the samples with 1 mL of spent algal medium after one week in darkness.

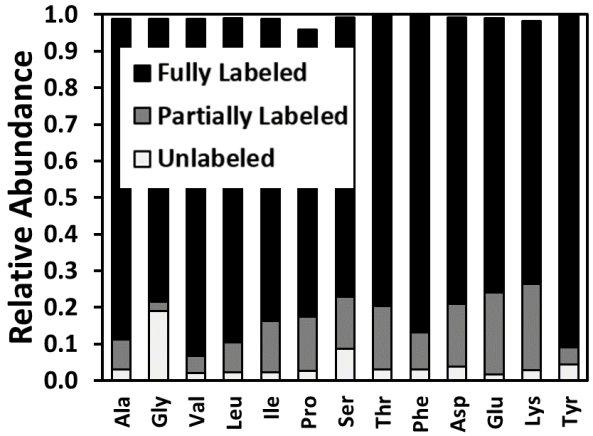

Figure C.6 Proteinogenic Amino Acid Labeling Patterns of Microbiome Cells Grown Heterotrophically on Labeled Spent Medium.

Appendix D

SUPPLEMENTARY MATERIAL FOR CHAPTER 5

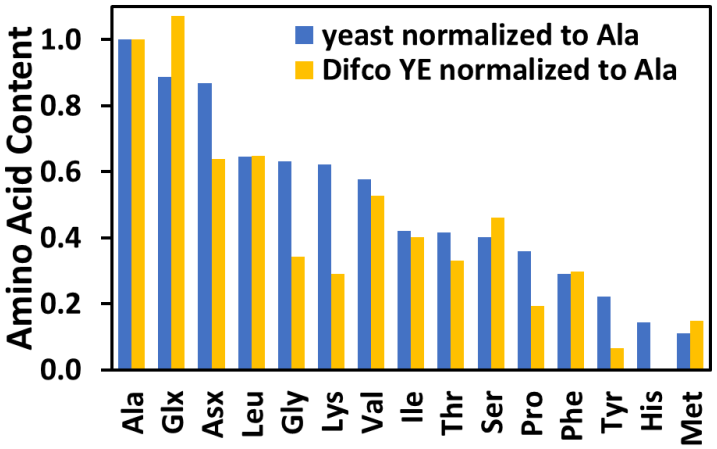

Figure D.1 Amino Acid Profiles of *S. cerevisiae*'s Protein and Fisher Scientific Yeast Extract.

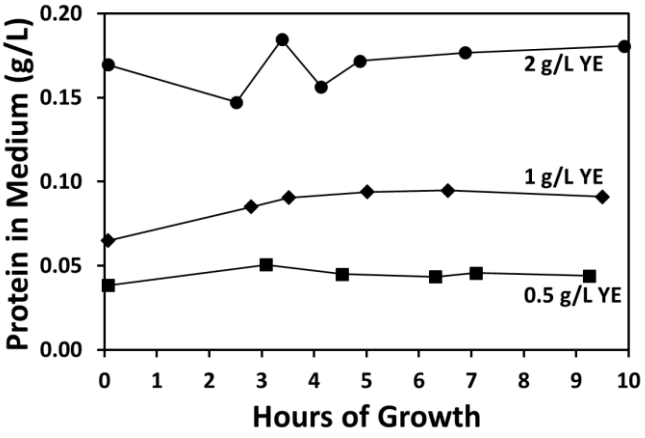

Figure D.2 Protein Concentration in the Medium due to Yeast Extract Supplementation

Table D.1 Metabolic network model of *E. coli*

Glycolysis

v1 Gluc.ext (abcdef) + PEP (ghi) → G6P (abcdef) Pyr (ghi)
v2 G6P (abcdef) ↔ F6P (abcdef)
v3 F6P (abcdef) + ATP ↔ FBP (abcdef)
v4 FBP (abcdef) ↔ DHAP (cba) + GAP (def)
v5 DHAP (abc) ↔ GAP (abc)
v6 GAP (abc) ↔ 3PG (abc) + ATP + NADH
v7 3PG (abc) ↔ PEP (abc)
v8 PEP (abc) ↔ Pyr (abc) + ATP

Pentose phosphatepathway

v9 G6P (abcdef) → 6PG (abcdef) + NADPH
v10 6PG (abcdef) → Ru5P (bcdef) + CO_2 (a) + NADPH
v11 Ru5P (abcde) ↔ X5P (abcde)
v12 Ru5P (abcde) ↔ R5P (abcde)
v13 X5P (abcde) ↔ TK-C2 (ab) + GAP (cde)
v14 F6P (abcdef) ↔ TK-C2 (ab) + E4P (cdef)
v15 S7P (abcdefg) ↔ TK-C2 (ab) + R5P (cdefg)
v16 F6P (abcdef) ↔ TA-C3 (abc) + GAP (def)
v17 S7P (abcdefg) ↔ TA-C3 (abc) + E4P (defg)

Entner–Doudoroff pathway

v18 6PG (abcdef) → KDPG (abcdef)
v19 KDPG (abcdef) → Pyr (abc) + GAP (def)

TCA Cycle

v20 Pyr (abc) → AcCoA (bc) + CO_2 (a) + NADH
v21 OAC (abcd) + AcCoA (ef) → Cit (dcbfea)
v22 Cit (abcdef) ↔ ICit (abcdef)
v23 ICit (abcdef) ↔ AKG (abcde) + CO2 (f) + NADPH
v24 AKG (abcde) → SucCoA (bcde) + CO_2 (a) + NADH
v25 SucCoA (bcde) + CO2.int (a) + NADH → AKG (abcde)
v26 SucCoA (abcd) ↔ Suc (1/2 abcd + 1/2 dcba) + ATP
v27 Suc (1/2 abcd + 1/2 dcba) ↔ Fum (1/2 abcd + 1/2 dcba) + $FADH_2$
v28 Fum (1/2 abcd + 1/2 dcba) ↔ Mal (abcd)
v29 Mal (abcd) ↔ OAC (abcd) + NADH

Glyoxylate Shunt

v30 ICit (abcdef) ↔ Glyox (ab) + Suc (1/2 edcf + 1/2 fcde)

v31 Glyox (ab) + AcCoA (cd) → Mal (abdc)

Amphibolic reactions

v32 Mal (abcd) → Pyr (abc) + CO_2 (d) + NADPH

v33 Mal (abcd) → Pyr (abc) + CO_2 (d) + NADH

v34 PEP (abc) + CO_2 (d) → OAC (abcd)

v35 OAC (abcd) + ATP → PEP (abc) + CO_2 (d)

Acetic acid formation

v36 AcCoA (ab) ↔ Ac (ab) + ATP

Amino acid biosynthesis

v37 AKG (abcde) + NADPH + NH_3 → Glu (abcde)

v38 Glu (abcde) + ATP + NH_3 → Gln (abcde)

v39 Glu (abcde) + ATP + 2NADPH → Pro (abcde)

v40 Glu (abcde) + CO_2 (f) + Gln (ghijk) + Asp (lmno) + AcCoA (pq) + 5ATP + NADPH → Arg (abcdef) + AKG (ghijk) + Fum (lmno) + Ac (pq)

v41 OAC (abcd) + Glu (efghi) → Asp (abcd) + AKG (efghi)

v42 Asp (abcd) +2ATP + NH_3 → Asn (abcd)

v43 Pyr (abc) + Glu (defgh) → Ala (abc) + AKG (defgh)

v44 3PG (abc) + Glu (defgh) → Ser (abc) + AKG (defgh) + NADH

v45 Ser (abc) ↔ Gly (ab) + MEETHF (c)

v46 Gly (ab) → CO2 (a) + MEETHF (b) + NADH + NH_3

v47 CO_2.int (a) + MEETHF (b) NADH + NH_3 → Gly (ab)

v48 Thr (abcd) → Gly (ab) + AcCoA (cd) + NADH

v49 Ser (abc) + AcCoA (de) + 3ATP + 4NADPH + SO_4 → Cys (abc) + Ac (de)

v50 Asp (abcd) + Pyr (efg) + Glu (hijkl) + SucCoA (mnop) + ATP + 2NADPH → LL-DAP (abcdgfe) + AKG (hijkl) + Suc (1/2 mnop + 1/2 ponm)

v51 LL-DAP (abcdefg) → Lys (abcdef) + CO_2 (g)

v52 Asp (abcd) + 2ATP + 2NADPH → Thr (abcd)

v53 Asp (abcd) + METHF (e) + Cys (fgh) + SucCoA (ijkl) + ATP + 2NADPH → Met (abcde) + Pyr (fgh) + Suc (1/2 ijkl + 1/2 lkji) + NH_3

v54 Pyr (abc) + Pyr (def) + Glu (ghijk) + NADPH → Val (abcef) + CO_2 (d) + AKG (ghijk)

v55 AcCoA (ab) + Pyr (cde) + Pyr (fgh) + Glu (ijklm) + NADPH → Leu (abdghe) + CO_2 (c) + CO_2 (f) + AKG (ijklm) + NADH

v56 Thr (abcd) + Pyr (efg) + Glu (hijkl) + NADPH → Ile (abfcdg) + CO_2 (e) + AKG (hijkl) + NH_3

v57 PEP (abc) + PEP (def) + E4P (ghij) + Glu (klmno) + ATP + NADPH → Phe (abcefghij) + CO_2 (d) + AKG (klmno)

v58 PEP (abc) + PEP (def) + E4P (ghij) + Glu (klmno) + ATP + NADPH → Tyr

(abcefghij) + CO_2 (d) + AKG (klmno) + NADH

v59 Ser (abc) + R5P (defgh) + PEP (ijk) + E4P (lmno) + PEP (pqr) + Gln (stuvw) + 3ATP + NADPH → Trp (abcedklmnoj) + CO_2 (i) + GAP (fgh) + Pyr (pqr) + Glu (stuvw)

v60 R5P (abcde) + FTHF (f) + Gln (ghijk) + Asp (lmno) + 5ATP → His (edcbaf) + AKG (ghijk) + Fum (lmno) +2NADH

v61 Ser (abc) → Pyr (abc) +NH_3

One-carbon metabolism

v62 MEETHF (a) + NADH → METHF (a)

v63 MEETHF (a) → FTHF (a) + NADPH

Oxidative phosphorylation

v64 NADH + 1/2 O_2 → 2ATP

v65 FADH2 + 1/2 O_2 → 1ATP

Transhydrogenation

v66 NADH ↔ NADPH

ATP hydrolysis

v67 ATP → ATP:ext

Transport

v68 Ac (ab) → Ac.ext (ab)

v69 CO_2 (a) → CO_2.ext (a)

v70 O_2.ext → O_2

v71 NH_3.ext → NH_3

v72 SO_4.ext → SO_4

Biomass formation

v73 0.488Ala + 0.281Arg + 0.229Asn + 0.229Asp + 0.087Cys + 0.250Glu + 0.250Gln + 0.582Gly + 0.090His + 0.276Ile + 0.428Leu + 0.326Lys + 0.146Met + 0.176Phe + 0.210Pro + 0.205Ser + 0.241Thr + 0.054Trp + 0.131Tyr + 0.402Val + 0.205G6P + 0.071F6P + 0.754R5P + 0.129GAP + 0.619 3PG + 0.051PEP + 0.083Pyr + 2.510AcCoA + 0.087AKG + 0.340OAC + 0.443MEETHF + 33.247ATP + 5.363NADPH → 39.68Biomass + 1.455NADH

Labeling Dilutions (when applicable)

v74 CO_2.M0 + CO_2 → CO_2 + CO_2.snk

v75 Pyr.M0 + Pyr → Pyr + Pyr.snk

v76 OAC.M0 + OAC → OAC + OAC.snk

v77 AKG.M0 + AKG → AKG + AKG.snk

v78 Ser.M0 + Ser → Ser + Ser.snk
v79 R5P.M0 + R5P→ R5P + R5P.snk

Co-culture Reactions (First duplicate the above reactions and designate one set with".1" and the second set as ".2", below reactions are for 3 timepoints)

v80 Ala.a1 + Gly.a1 + Val.a1 + Leu.a1 + Ile.a1 + Pro.a1 + Met.a1 + Ser.a1 + Thr.a1 + Phe.a1 + Asp.a1 + Glu.a1 + Lys.a1 + His.a1 + Tyr.a1 + G6P.a1 + R5P.a1 → X-a1

v81 Ala.a2 + Gly.a2 + Val.a2 + Leu.a2 + Ile.a2 + Pro.a2 + Met.a2 + Ser.a2 + Thr.a2 + Phe.a2 + Asp.a2 + Glu.a2 + Lys.a2 + His.a2 + Tyr.a2 + G6P.a2 + R5P.a2 → X-a2

v82 Ala.a3 + Gly.a3 + Val.a3 + Leu.a3 + Ile.a3 + Pro.a3 + Met.a3 + Ser.a3 + Thr.a3 + Phe.a3 + Asp.a3 + Glu.a3 + Lys.a3 + His.a3 + Tyr.a3 + G6P.a3 + R5P.a3 → X-a3

v83 Ala.1 + Gly.1 + Val.1 + Leu.1 + Ile.1 + Pro.1 + Met.1 + Ser.1 + Thr.1 + Phe.1 + Asp.1 + Glu.1 + Lys.1 + His.1 + Tyr.1 + G6P.1 + R5P.1 → Ala.a1 + Gly.a1 + Val.a1 + Leu.a1 + Ile.a1 + Pro.a1 + Met.a1 + Ser.a1 + Thr.a1 + Phe.a1 + Asp.a1 + Glu.a1 + Lys.a1 + His.a1 + Tyr.a1 + G6P.a1 + R5P.a1 + Ala.1 + Gly.1 + Val.1 + Leu.1 + Ile.1 + Pro.1 + Met.1 + Ser.1 + Thr.1 + Phe.1 + Asp.1 + Glu.1 + Lys.1 + His.1 + Tyr.1 + G6P.1 + R5P.1

v84 Ala.1 + Gly.1 + Val.1 + Leu.1 + Ile.1 + Pro.1 + Met.1 + Ser.1 + Thr.1 + Phe.1 + Asp.1 + Glu.1 + Lys.1 + His.1 + Tyr.1 + G6P.1 + R5P.1 → Ala.a2 + Gly.a2 + Val.a2 + Leu.a2 + Ile.a2 + Pro.a2 + Met.a2 + Ser.a2 + Thr.a2 + Phe.a2 + Asp.a2 + Glu.a2 + Lys.a2 + His.a2 + Tyr.a2 + G6P.a2 + R5P.a2 + Ala.1 + Gly.1 + Val.1 + Leu.1 + Ile.1 + Pro.1 + Met.1 + Ser.1 + Thr.1 + Phe.1 + Asp.1 + Glu.1 + Lys.1 + His.1 + Tyr.1 + G6P.1 + R5P.1

v85 Ala.1 + Gly.1 + Val.1 + Leu.1 + Ile.1 + Pro.1 + Met.1 + Ser.1 + Thr.1 + Phe.1 + Asp.1 + Glu.1 + Lys.1 + His.1 + Tyr.1 + G6P.1 + R5P.1 → Ala.a3 + Gly.a3 + Val.a3 + Leu.a3 + Ile.a3 + Pro.a3 + Met.a3 + Ser.a3 + Thr.a3 + Phe.a3 + Asp.a3 + Glu.a3 + Lys.a3 + His.a3 + Tyr.a3 + G6P.a3 + R5P.a3 + Ala.1 + Gly.1 + Val.1 + Leu.1 + Ile.1 + Pro.1 + Met.1 + Ser.1 + Thr.1 + Phe.1 + Asp.1 + Glu.1 + Lys.1 + His.1 + Tyr.1 + G6P.1 + R5P.1

v86 Ala.2 + Gly.2 + Val.2 + Leu.2 + Ile.2 + Pro.2 + Met.2 + Ser.2 + Thr.2 + Phe.2 + Asp.2 + Glu.2 + Lys.2 + His.2 + Tyr.2 + G6P.2 + R5P.2 → Ala.a1 + Gly.a1 + Val.a1 + Leu.a1 + Ile.a1 + Pro.a1 + Met.a1 + Ser.a1 + Thr.a1 + Phe.a1 + Asp.a1 + Glu.a1 + Lys.a1 + His.a1 + Tyr.a1 + G6P.a1 + R5P.a1 + Ala.2 + Gly.2 + Val.2 + Leu.2 + Ile.2 + Pro.2 + Met.2 + Ser.2 + Thr.2 + Phe.2 + Asp.2 + Glu.2 + Lys.2 + His.2 + Tyr.2 + G6P.2 + R5P.2

v87 Ala.2 + Gly.2 + Val.2 + Leu.2 + Ile.2 + Pro.2 + Met.2 + Ser.2 + Thr.2 + Phe.2 + Asp.2 + Glu.2 + Lys.2 + His.2 + Tyr.2 + G6P.2 + R5P.2 → Ala.a2 + Gly.a2 + Val.a2 + Leu.a2 + Ile.a2 + Pro.a2 + Met.a2 + Ser.a2 + Thr.a2 + Phe.a2 + Asp.a2 + Glu.a2 + Lys.a2 + His.a2 + Tyr.a2 + G6P.a2 + R5P.a2 + Ala.2 + Gly.2 + Val.2 + Leu.2 + Ile.2 + Pro.2 + Met.2 + Ser.2 + Thr.2 + Phe.2 + Asp.2

+ Glu.2 + Lys.2 + His.2 + Tyr.2 + G6P.2 + R5P.2

v88 Ala.2 + Gly.2 + Val.2 + Leu.2 + Ile.2 + Pro.2 + Met.2 + Ser.2 + Thr.2 + Phe.2 + Asp.2 + Glu.2 + Lys.2 + His.2 + Tyr.2 + G6P.2 + R5P.2 → Ala.a3 + Gly.a3 + Val.a3 + Leu.a3 + Ile.a3 + Pro.a3 + Met.a3 + Ser.a3 + Thr.a3 + Phe.a3 + Asp.a3 + Glu.a3 + Lys.a3 + His.a3 + Tyr.a3 + G6P.a3 + R5P.a3 + Ala.2 + Gly.2 + Val.2 + Leu.2 + Ile.2 + Pro.2 + Met.2 + Ser.2 + Thr.2 + Phe.2 + Asp.2 + Glu.2 + Lys.2 + His.2 + Tyr.2 + G6P.2 + R5P.2

Table D.2 Mass Isotopomer Distributions from *E. coli* experiments with [1,2-^{13}C]Glucose and Varying Concentrations of Yeast Extract

g/L YE	**0**				**0.5**			**1**			**2**			
OD600	**0.5**	**0.8**	**1.3**	**1.6**	**0.4**	**1.0**	**2.2**	**0.5**	**1.0**	**2.2**	**0.4**	**1.1**	**1.9**	**2.9**
Ala232(M0)	40.5	40.5	40.7	40.6	59.5	55.3	48.6	58.0	60.7	55.1	63.1	60.6	62.3	60.7
Ala232(M1)	15.1	15.0	15.1	15.1	15.2	15.8	15.6	14.9	15.5	15.7	15.2	15.3	15.6	15.9
Ala232(M2)	34.8	34.9	34.8	34.8	20.2	22.9	28.3	21.6	19.1	23.2	17.4	19.3	17.7	18.8
Ala232(M3)	6.8	6.9	6.8	6.8	3.7	4.4	5.5	4.0	3.5	4.4	3.2	3.6	3.2	3.5
Ala232(M4)	2.7	2.7	2.7	2.7	1.4	1.6	2.1	1.5	1.3	1.6	1.1	1.3	1.1	1.2
Ala260(M0)	40.2	40.1	40.1	40.2	58.6	54.5	47.8	57.1	59.7	54.1	62.2	59.7	61.4	59.7
Ala260(M1)	12.6	12.7	12.7	12.9	14.8	14.9	14.1	14.5	15.1	14.8	15.2	14.9	15.3	15.4
Ala260(M2)	35.8	35.7	35.7	35.6	20.5	23.2	28.7	21.9	19.5	23.7	17.7	19.7	18.1	19.2
Ala260(M3)	7.9	8.0	7.9	7.9	4.3	5.2	6.6	4.6	4.1	5.3	3.5	4.1	3.7	4.1
Ala260(M4)	3.0	3.1	3.0	3.0	1.5	1.9	2.4	1.6	1.4	1.9	1.2	1.4	1.3	1.4
Ala260(M5)	0.5	0.5	0.4	0.5	0.2	0.3	0.4	0.2	0.2	0.3	0.2	0.2	0.2	0.2
Gly218(M0)	46.8	46.6	46.7	46.8	63.7	58.4	53.3	67.7	64.1	58.6	75.0	67.8	64.8	62.5
Gly218(M1)	40.1	40.3	40.2	40.2	26.4	30.7	34.9	23.1	26.0	30.6	17.1	23.0	25.5	27.4
Gly218(M2)	9.9	10.0	9.9	9.9	8.0	8.7	9.2	7.6	8.0	8.6	6.8	7.6	7.9	8.2
Gly218(M3)	3.1	3.1	3.1	3.1	1.9	2.3	2.6	1.6	1.8	2.2	1.0	1.5	1.8	1.9
Gly246(M0)	43.9	43.6	43.6	43.6	62.1	56.1	50.7	66.3	62.3	56.3	73.8	66.4	63.1	60.5
Gly246(M1)	40.7	40.7	40.6	40.5	26.7	30.5	34.4	23.5	26.4	30.3	17.7	23.4	25.9	27.6
Gly246(M2)	11.4	11.5	11.6	11.7	8.8	10.3	11.3	8.2	8.9	10.3	7.2	8.2	8.7	9.3
Gly246(M3)	3.5	3.6	3.6	3.6	2.1	2.6	3.1	1.7	2.1	2.6	1.1	1.7	2.0	2.2
Gly246(M4)	0.6	0.6	0.6	0.6	0.3	0.5	0.6	0.3	0.3	0.5	0.2	0.3	0.3	0.4
Val260(M0)	21.9	21.8	21.7	21.8	73.0	68.9	47.7	73.3	73.0	70.5	73.3	73.3	73.2	72.9
Val260(M1)	11.7	11.5	11.6	11.6	18.1	17.6	15.1	18.1	18.1	17.8	18.1	18.2	18.1	18.1
Val260(M2)	34.7	35.0	35.0	34.9	7.3	9.5	20.9	7.2	7.3	8.6	7.1	7.1	7.2	7.3
Val260(M3)	12.3	12.2	12.3	12.2	1.2	2.1	6.8	1.2	1.2	1.8	1.2	1.2	1.2	1.2
Val260(M4)	15.3	15.4	15.3	15.3	0.3	1.5	7.5	0.2	0.3	1.0	0.2	0.2	0.3	0.3
Val260(M5)	3.1	3.0	3.0	3.0	0.0	0.3	1.5	0.0	0.0	0.2	0.0	0.0	0.0	0.1
Val260(M6)	1.1	1.1	1.1	1.1	0.0	0.1	0.5	0.0	0.0	0.1	0.0	0.0	0.0	0.0
Val288(M0)	21.7	21.6	21.6	21.6	72.7	68.7	47.5	73.1	72.7	70.3	73.1	73.1	73.0	72.7
Val288(M1)	10.2	10.2	10.2	10.3	18.1	17.6	14.6	18.1	18.1	17.7	18.2	18.2	18.1	18.1
Val288(M2)	35.1	35.1	35.2	35.2	7.5	9.6	20.9	7.3	7.5	8.8	7.3	7.3	7.3	7.5
Val288(M3)	11.9	12.0	12.0	12.0	1.3	2.2	6.7	1.2	1.3	1.8	1.2	1.2	1.2	1.3

Val288(M4)	16.1	16.1	16.1	15.9	0.4	1.5	7.7	0.3	0.3	1.1	0.2	0.2	0.3	0.4
Val288(M5)	3.5	3.6	3.6	3.5	0.1	0.3	1.8	0.0	0.1	0.2	0.0	0.0	0.0	0.1
Val288(M6)	1.3	1.2	1.3	1.2	0.0	0.1	0.6	0.0	0.0	0.1	0.0	0.0	0.0	0.0
Val288(M7)	0.2	0.2	0.2	0.2	0.0	0.0	0.1	0.0	0.0	0.0	0.0	0.0	0.0	0.0
Leu274(M0)	12.6	12.4	12.3	12.4	73.2	70.9	44.3	73.2	73.2	72.6	73.2	73.2	73.3	73.2
Leu274(M1)	15.9	15.9	16.0	16.1	18.4	18.5	17.5	18.3	18.4	18.4	18.3	18.4	18.3	18.3
Leu274(M2)	24.1	24.3	24.3	24.4	7.0	7.7	15.5	7.1	7.1	7.2	7.1	7.1	7.0	7.1
Leu274(M3)	22.4	22.4	22.4	22.4	1.1	1.9	11.0	1.1	1.1	1.3	1.1	1.1	1.1	1.1
Leu274(M4)	13.9	13.9	13.9	13.8	0.2	0.6	6.6	0.2	0.2	0.3	0.2	0.2	0.2	0.2
Leu274(M5)	8.6	8.6	8.5	8.5	0.0	0.3	3.8	0.0	0.0	0.1	0.0	0.0	0.0	0.0
Leu274(M6)	2.0	2.0	2.0	1.9	0.0	0.1	0.9	0.0	0.0	0.0	0.0	0.0	0.0	0.0
Leu274(M7)	0.6	0.6	0.6	0.6	0.0	0.0	0.2	0.0	0.0	0.0	0.0	0.0	0.0	0.0
Ile200(M0)	19.5	18.9	18.8	18.9	80.9	78.7	50.9	81.0	80.9	80.0	81.0	80.9	81.0	80.8
Ile200(M1)	13.3	13.5	13.8	13.8	14.2	14.3	15.0	14.2	14.2	14.2	14.2	14.3	14.2	14.2
Ile200(M2)	31.6	31.4	31.3	31.3	4.3	5.2	16.1	4.2	4.2	4.6	4.2	4.2	4.2	4.2
Ile200(M3)	15.8	16.2	16.4	16.4	0.6	1.1	8.9	0.5	0.5	0.8	0.5	0.5	0.5	0.6
Ile200(M4)	14.2	14.2	13.9	13.8	0.1	0.5	6.2	0.1	0.1	0.2	0.1	0.1	0.1	0.1
Ile200(M5)	4.6	4.8	4.7	4.7	0.0	0.2	2.4	0.0	0.0	0.1	0.0	0.0	0.0	0.0
Ile200(M6)	0.9	0.9	0.9	0.9	0.0	0.0	0.4	0.0	0.0	0.0	0.0	0.0	0.0	0.0
Ile200(M7)	0.2	0.2	0.2	0.2	0.0	0.0	0.1	0.0	0.0	0.0	0.0	0.0	0.0	0.0
Ile274(M0)	17.5	17.0	17.0	16.9	72.9	71.0	45.9	72.9	72.9	72.1	73.0	72.9	72.9	72.8
Ile274(M1)	13.4	13.4	13.6	13.7	18.6	18.5	17.1	18.6	18.6	18.5	18.5	18.6	18.6	18.5
Ile274(M2)	30.0	29.9	29.7	29.8	7.1	7.9	17.0	7.1	7.1	7.4	7.1	7.1	7.1	7.1
Ile274(M3)	16.8	17.1	17.3	17.3	1.2	1.8	9.6	1.2	1.2	1.4	1.2	1.2	1.2	1.2
Ile274(M4)	14.9	14.9	14.7	14.7	0.2	0.7	6.7	0.2	0.2	0.4	0.2	0.2	0.2	0.2
Ile274(M5)	5.6	5.7	5.8	5.8	0.0	0.2	2.9	0.0	0.0	0.1	0.0	0.0	0.0	0.0
Ile274(M6)	1.5	1.5	1.5	1.5	0.0	0.1	0.7	0.0	0.0	0.0	0.0	0.0	0.0	0.0
Ile274(M7)	0.3	0.3	0.4	0.4	0.0	0.0	0.2	0.0	0.0	0.0	0.0	0.0	0.0	0.0
Met218(M0)	20.3	19.7	19.8	19.9	77.8	51.3	35.9	78.1	75.1	52.3	78.2	78.1	77.2	62.8
Met218(M1)	25.3	25.4	25.5	25.6	13.7	20.1	23.1	13.5	14.6	20.0	13.5	13.6	13.8	17.8
Met218(M2)	25.7	25.8	25.8	25.8	7.2	15.8	20.7	7.1	8.1	15.4	7.1	7.1	7.4	12.0
Met218(M3)	20.0	20.2	20.0	19.9	1.0	8.9	13.9	1.0	1.7	8.6	1.0	1.0	1.2	5.2
Met218(M4)	6.8	7.0	7.0	6.9	0.2	3.1	5.1	0.2	0.5	3.0	0.2	0.2	0.3	1.7
Met218(M5)	1.9	1.9	1.9	1.9	0.0	0.8	1.3	0.0	0.1	0.8	0.1	0.0	0.1	0.4
Met320(M0)	16.4	15.9	16.0	16.1	69.3	44.8	30.4	69.6	66.7	45.6	69.6	69.5	68.8	55.5
Met320(M1)	21.3	21.1	21.4	21.5	18.0	20.1	20.5	17.9	18.4	20.0	17.8	17.9	18.0	19.6
Met320(M2)	24.5	24.6	24.7	24.7	10.0	16.8	20.4	10.0	10.8	16.4	10.0	10.0	10.1	13.9
Met320(M3)	21.4	21.6	21.5	21.4	2.0	10.3	15.5	1.9	2.8	10.0	1.9	1.9	2.2	6.5
Met320(M4)	10.3	10.6	10.3	10.3	0.5	5.1	8.3	0.5	0.9	5.1	0.5	0.5	0.6	3.0
Met320(M5)	4.5	4.6	4.5	4.4	0.1	2.1	3.6	0.1	0.3	2.1	0.1	0.1	0.1	1.1
Met320(M6)	1.2	1.3	1.3	1.2	0.0	0.6	1.1	0.0	0.1	0.6	0.0	0.0	0.0	0.4
Met320(M7)	0.4	0.4	0.4	0.3	0.0	0.2	0.3	0.0	0.0	0.2	0.0	0.0	0.0	0.1
Ser362(M0)	33.7	33.0	32.4	32.0	41.9	38.7	36.0	44.0	41.4	38.9	51.2	43.7	41.7	40.6
Ser362(M1)	24.0	25.7	27.7	28.3	20.9	23.0	24.4	19.4	21.8	22.8	19.6	20.0	21.9	22.5
Ser362(M2)	32.1	31.4	30.2	30.1	28.7	29.3	30.2	28.3	28.2	29.3	22.8	28.0	28.0	28.3
Ser362(M3)	10.1	10.0	9.7	9.7	8.6	9.0	9.4	8.4	8.6	9.0	6.5	8.3	8.4	8.6
Ser390(M0)	30.9	29.7	28.5	28.1	39.1	35.8	33.1	41.4	38.8	35.9	48.8	41.1	39.0	37.7

Ser390(M1)	21.4	23.0	25.1	25.6	19.4	20.8	21.9	18.2	20.3	20.7	18.9	18.8	20.3	20.7
Ser390(M2)	31.8	31.4	30.6	30.5	27.9	28.9	29.7	27.3	27.5	28.8	22.3	27.1	27.4	27.9
Ser390(M3)	10.7	10.7	10.7	10.7	9.0	9.8	10.3	8.7	9.0	9.8	6.8	8.7	9.0	9.2
Ser390(M4)	4.3	4.2	4.1	4.1	3.6	3.9	4.0	3.6	3.6	3.9	2.7	3.5	3.6	3.7
Ser390(M5)	1.0	1.0	0.9	0.9	0.8	0.9	0.9	0.8	0.8	0.9	0.6	0.8	0.8	0.8
Thr376(M0)	28.1	27.7	27.9	28.1	57.3	42.5	34.2	64.4	53.4	42.1	64.7	63.8	54.6	46.9
Thr376(M1)	20.4	20.9	21.0	21.0	22.0	22.8	23.1	22.1	22.2	23.0	22.1	22.1	22.2	22.7
Thr376(M2)	29.8	29.6	29.5	29.4	14.2	20.9	24.4	10.4	16.0	20.9	10.2	10.7	15.4	18.9
Thr376(M3)	14.7	14.8	14.7	14.6	4.7	9.6	12.6	2.4	5.9	9.7	2.3	2.6	5.5	8.0
Thr376(M4)	5.4	5.4	5.4	5.4	1.5	3.3	4.4	0.6	1.9	3.3	0.6	0.7	1.8	2.7
Thr376(M5)	1.6	1.6	1.6	1.6	0.4	0.9	1.3	0.1	0.5	1.0	0.1	0.1	0.5	0.8
Thr404(M0)	25.7	25.3	25.8	25.9	56.3	40.6	31.8	63.5	52.3	40.1	63.8	63.0	53.4	45.1
Thr404(M1)	17.5	17.7	18.0	18.1	21.5	20.4	19.9	22.6	21.2	20.5	22.5	22.5	21.3	20.9
Thr404(M2)	30.0	30.0	29.8	29.9	14.6	21.4	24.6	10.7	16.4	21.4	10.5	10.9	16.0	19.3
Thr404(M3)	15.4	15.5	15.5	15.4	4.9	10.2	13.4	2.5	6.3	10.4	2.5	2.7	5.8	8.7
Thr404(M4)	8.2	8.2	7.9	7.7	2.0	5.3	7.4	0.6	2.8	5.4	0.6	0.7	2.5	4.3
Thr404(M5)	2.5	2.5	2.4	2.3	0.5	1.6	2.3	0.1	0.8	1.6	0.1	0.2	0.7	1.2
Thr404(M6)	0.7	0.7	0.7	0.6	0.1	0.5	0.7	0.0	0.2	0.5	0.0	0.0	0.2	0.4
Phe302(M0)	42.7	42.5	42.5	42.6	72.5	72.3	60.8	72.5	72.4	72.4	72.5	72.4	72.5	72.5
Phe302(M1)	41.0	41.1	41.1	41.1	18.9	19.1	27.4	19.0	18.9	19.0	18.9	19.0	18.9	18.9
Phe302(M2)	12.5	12.5	12.5	12.5	7.3	7.4	9.5	7.3	7.4	7.3	7.3	7.3	7.3	7.4
Phe302(M3)	3.8	3.9	3.9	3.8	1.2	1.3	2.3	1.3	1.3	1.3	1.3	1.3	1.3	1.3
Phe308(M0)	15.0	14.6	14.5	14.5	70.4	70.0	48.1	70.5	70.5	70.3	70.5	70.4	70.4	70.4
Phe308(M1)	9.6	9.5	9.7	9.6	20.2	20.2	16.1	20.2	20.1	20.2	20.1	20.3	20.2	20.1
Phe308(M2)	28.1	27.9	28.0	28.0	7.5	7.7	15.4	7.5	7.6	7.5	7.5	7.5	7.5	7.5
Phe308(M3)	14.5	14.7	14.7	14.9	1.4	1.5	6.9	1.4	1.4	1.5	1.4	1.4	1.4	1.4
Phe308(M4)	18.4	18.5	18.4	18.4	0.3	0.4	7.3	0.3	0.3	0.3	0.3	0.3	0.3	0.3
Phe308(M5)	7.8	7.9	8.0	7.9	0.1	0.1	3.4	0.1	0.1	0.1	0.1	0.1	0.1	0.1
Phe308(M6)	4.6	4.7	4.6	4.6	0.0	0.1	1.9	0.0	0.0	0.0	0.0	0.0	0.0	0.0
Phe308(M7)	1.7	1.7	1.7	1.7	0.0	0.0	0.7	0.0	0.0	0.0	0.0	0.0	0.0	0.0
Phe308(M8)	0.4	0.5	0.5	0.5	0.0	0.0	0.2	0.0	0.0	0.0	0.0	0.0	0.0	0.0
Phe336(M0)	14.9	14.5	14.3	14.4	70.0	69.6	47.7	70.0	69.9	69.8	69.9	69.9	69.9	69.9
Phe336(M1)	8.8	8.8	8.8	8.9	20.4	20.3	15.9	20.4	20.4	20.3	20.4	20.4	20.3	20.4
Phe336(M2)	27.9	27.8	27.8	27.8	7.7	7.9	15.5	7.7	7.8	7.8	7.7	7.7	7.7	7.7
Phe336(M3)	14.2	14.3	14.6	14.7	1.4	1.6	6.9	1.5	1.5	1.5	1.5	1.5	1.5	1.5
Phe336(M4)	18.8	18.7	18.7	18.6	0.3	0.4	7.4	0.3	0.3	0.4	0.3	0.3	0.3	0.3
Phe336(M5)	8.1	8.3	8.3	8.3	0.1	0.1	3.5	0.1	0.1	0.1	0.1	0.2	0.2	0.1
Phe336(M6)	4.8	4.9	4.9	4.8	0.0	0.1	2.0	0.0	0.0	0.0	0.0	0.1	0.1	0.0
Phe336(M7)	1.8	1.9	1.9	1.9	0.0	0.0	0.8	0.0	0.0	0.0	0.0	0.0	0.0	0.0
Phe336(M8)	0.5	0.5	0.5	0.5	0.0	0.0	0.2	0.0	0.0	0.0	0.0	0.0	0.0	0.0
Phe336(M9)	0.1	0.1	0.1	0.1	0.0	0.0	0.1	0.0	0.0	0.0	0.0	0.0	0.0	0.0
Asp302(M0)	39.1	39.0	39.4	39.5	61.1	52.9	46.8	64.7	59.2	52.9	69.1	64.0	59.7	55.6
Asp302(M1)	36.1	35.7	36.4	36.6	25.0	27.7	29.5	23.6	25.6	27.4	21.1	24.0	25.5	26.7
Asp302(M2)	19.4	19.8	18.9	18.6	11.3	15.5	18.8	9.6	12.2	15.7	8.2	9.8	11.9	14.2
Asp302(M3)	5.4	5.5	5.3	5.2	2.6	3.9	4.9	2.1	2.9	4.0	1.6	2.2	2.9	3.5
Asp390(M0)	28.2	27.6	27.7	27.9	52.1	42.1	34.6	56.2	49.7	41.9	61.1	55.4	50.3	45.2
Asp390(M1)	20.2	20.5	20.6	20.5	21.4	22.3	22.8	21.4	21.8	22.5	21.7	21.4	21.7	22.3

Asp390(M2)	29.8	29.7	29.6	29.7	17.6	21.6	24.4	15.5	18.5	21.5	12.6	15.9	18.2	20.1
Asp390(M3)	14.7	15.0	14.9	14.8	6.2	9.6	12.4	4.9	7.0	9.7	3.4	5.1	6.8	8.5
Asp390(M4)	5.5	5.5	5.5	5.5	2.2	3.4	4.4	1.6	2.4	3.4	1.0	1.7	2.4	3.0
Asp390(M5)	1.6	1.6	1.6	1.6	0.5	1.0	1.3	0.4	0.6	1.0	0.2	0.4	0.6	0.8
Asp418(M0)	25.8	25.2	25.6	25.8	50.8	40.2	32.2	55.2	48.1	39.9	60.1	54.2	48.8	43.3
Asp418(M1)	17.6	17.7	17.9	17.9	20.5	20.2	19.8	21.1	20.5	20.3	22.0	21.1	20.6	20.6
Asp418(M2)	29.9	29.8	29.7	29.8	18.2	22.0	24.7	15.9	19.1	21.8	12.9	16.4	18.8	20.7
Asp418(M3)	15.4	15.6	15.5	15.4	6.6	10.4	13.2	5.2	7.6	10.5	3.6	5.5	7.3	9.2
Asp418(M4)	8.2	8.4	8.1	7.9	2.9	5.3	7.2	2.0	3.4	5.4	1.1	2.1	3.3	4.5
Asp418(M5)	2.5	2.6	2.5	2.4	0.8	1.6	2.2	0.5	1.0	1.6	0.2	0.5	0.9	1.3
Asp418(M6)	0.7	0.8	0.7	0.7	0.2	0.5	0.7	0.1	0.3	0.5	0.1	0.1	0.2	0.4
Glu330(M0)	19.1	18.6	18.9	18.9	54.6	35.6	27.4	63.1	49.2	35.7	65.5	63.1	50.9	41.4
Glu330(M1)	15.3	15.5	15.2	15.0	18.6	18.9	18.9	19.0	18.8	19.1	19.2	19.0	18.8	19.2
Glu330(M2)	31.5	31.4	31.8	31.9	16.6	23.7	26.3	12.6	18.7	23.5	11.4	12.6	18.0	21.5
Glu330(M3)	15.5	15.8	15.5	15.4	5.6	11.4	14.2	3.2	7.2	11.5	2.6	3.2	6.7	9.6
Glu330(M4)	14.1	14.0	14.1	14.2	3.6	7.8	9.9	1.6	4.7	7.7	1.0	1.6	4.3	6.3
Glu330(M5)	3.4	3.5	3.4	3.4	0.8	2.0	2.5	0.3	1.1	1.9	0.2	0.3	1.0	1.5
Glu330(M6)	1.1	1.1	1.1	1.1	0.2	0.6	0.7	0.1	0.3	0.6	0.1	0.1	0.3	0.5
Glu432(M0)	15.2	14.6	14.6	14.6	48.1	30.3	22.7	56.0	43.1	30.4	58.2	55.8	44.6	35.8
Glu432(M1)	13.3	13.3	13.3	13.3	20.1	17.6	16.4	21.5	19.5	17.7	22.0	21.6	19.8	18.7
Glu432(M2)	27.7	27.6	27.7	27.8	17.8	22.7	24.3	14.8	19.4	22.5	13.9	14.8	18.8	21.2
Glu432(M3)	18.0	18.4	18.4	18.4	7.2	13.5	16.4	4.6	8.9	13.5	3.9	4.7	8.4	11.6
Glu432(M4)	15.6	15.7	15.7	15.6	4.5	9.7	12.1	2.2	5.9	9.6	1.5	2.2	5.5	7.9
Glu432(M5)	7.0	7.2	7.2	7.1	1.6	4.3	5.7	0.6	2.3	4.3	0.4	0.7	2.1	3.4
Glu432(M6)	2.5	2.5	2.5	2.5	0.5	1.5	1.9	0.2	0.8	1.5	0.1	0.2	0.7	1.1
Glu432(M7)	0.7	0.7	0.7	0.7	0.1	0.4	0.6	0.0	0.2	0.4	0.0	0.0	0.2	0.3
Lys329(M0)	17.4	16.8	16.9	17.0	68.1	58.5	39.6	68.6	67.0	60.0	68.8	68.7	67.8	66.0
Lys329(M1)	14.1	14.1	14.2	14.2	20.8	20.0	18.2	20.8	20.7	20.1	20.8	20.7	20.7	20.6
Lys329(M2)	29.2	29.1	29.1	29.2	8.5	12.0	18.7	8.2	8.9	11.5	8.1	8.2	8.6	9.3
Lys329(M3)	17.2	17.5	17.6	17.5	1.9	5.0	11.3	1.8	2.3	4.6	1.7	1.8	2.0	2.7
Lys329(M4)	14.7	14.7	14.6	14.5	0.5	2.9	7.8	0.4	0.8	2.5	0.4	0.4	0.6	1.0
Lys329(M5)	5.9	6.0	5.9	5.9	0.1	1.2	3.5	0.1	0.2	1.0	0.1	0.1	0.2	0.4
Lys329(M6)	1.7	1.7	1.7	1.7	0.1	0.3	1.0	0.1	0.1	0.3	0.1	0.1	0.1	0.1
Lys431(M0)	14.8	14.4	14.3	14.5	61.1	52.3	34.8	61.6	60.1	53.7	62.0	61.8	61.2	59.1
Lys431(M1)	12.4	12.4	12.6	12.7	23.4	21.7	18.1	23.7	23.4	22.0	23.6	23.5	23.2	23.0
Lys431(M2)	27.2	27.0	27.0	27.2	11.3	13.9	18.9	11.0	11.6	13.5	10.9	10.9	11.2	11.9
Lys431(M3)	17.5	17.8	17.9	17.8	3.0	5.9	11.8	2.8	3.3	5.5	2.7	2.8	3.0	3.7
Lys431(M4)	16.3	16.4	16.3	16.1	0.9	3.6	9.2	0.7	1.2	3.2	0.7	0.7	1.0	1.5
Lys431(M5)	7.6	7.7	7.6	7.5	0.2	1.6	4.6	0.2	0.3	1.4	0.1	0.2	0.3	0.5
Lys431(M6)	3.1	3.2	3.1	3.0	0.1	0.6	1.9	0.0	0.1	0.6	0.0	0.0	0.1	0.2
Lys431(M7)	0.9	0.9	0.9	0.9	0.0	0.2	0.6	0.0	0.0	0.2	0.0	0.0	0.0	0.1
Lys431(M8)	0.2	0.2	0.2	0.2	0.0	0.1	0.2	0.0	0.0	0.0	0.0	0.0	0.0	0.0
His338(M0)	3.0	2.7	2.6	2.6	68.1	45.5	26.8	68.6	67.8	46.7	68.6	68.7	68.5	59.2
His338(M1)	25.3	24.7	25.3	25.5	20.8	22.7	23.7	20.7	20.7	22.2	20.6	20.6	20.7	21.8
His338(M2)	37.2	37.1	37.1	37.2	8.0	17.5	25.5	7.8	8.2	16.9	7.8	7.7	7.8	11.8
His338(M3)	22.0	22.5	22.1	22.1	2.4	9.2	15.2	2.2	2.5	9.1	2.2	2.2	2.2	4.9
His338(M4)	8.8	9.2	9.0	8.9	0.6	3.6	6.2	0.5	0.6	3.6	0.5	0.5	0.5	1.6

His338(M5)	2.7	2.8	2.8	2.7	0.2	1.1	1.9	0.1	0.2	1.1	0.2	0.1	0.2	0.5
His338(M6)	0.8	0.8	0.8	0.8	0.1	0.3	0.5	0.0	0.1	0.3	0.1	0.0	0.0	0.1
His338(M7)	0.2	0.2	0.2	0.2	0.0	0.1	0.1	0.0	0.0	0.1	0.0	0.0	0.0	0.0
His440(M0)	2.4	2.0	2.0	1.9	61.4	41.0	24.0	62.0	61.0	42.0	61.9	61.9	61.8	53.3
His440(M1)	21.6	21.2	21.6	21.8	23.7	23.1	22.1	23.7	23.7	22.8	23.8	23.8	23.8	23.7
His440(M2)	28.2	28.1	28.3	28.6	10.9	16.3	21.0	10.7	11.0	15.9	10.7	10.7	10.7	13.1
His440(M3)	21.3	21.5	21.4	21.3	2.9	9.5	14.9	2.8	3.0	9.2	2.8	2.8	2.8	5.5
His440(M4)	16.0	16.3	16.0	15.8	0.8	6.1	10.6	0.7	0.9	6.0	0.7	0.7	0.7	2.8
His440(M5)	7.2	7.5	7.3	7.2	0.2	2.8	5.0	0.1	0.3	2.8	0.1	0.1	0.1	1.1
His440(M6)	2.5	2.6	2.5	2.5	0.1	1.0	1.7	0.0	0.1	1.0	0.0	0.0	0.0	0.4
His440(M7)	0.7	0.8	0.7	0.7	0.0	0.3	0.5	0.0	0.0	0.3	0.0	0.0	0.0	0.1
His440(M8)	0.2	0.2	0.2	0.2	0.0	0.1	0.1	0.0	0.0	0.1	0.0	0.0	0.0	0.0
Tyr302(M0)	42.2	42.2	42.2	42.2	63.1	52.9	48.2	71.5	60.6	53.0	71.8	71.3	61.6	56.3
Tyr302(M1)	41.3	41.3	41.3	41.3	25.8	33.0	36.4	19.7	27.5	32.9	19.4	19.8	26.8	30.6
Tyr302(M2)	12.6	12.6	12.6	12.6	9.0	11.1	11.9	7.5	9.6	11.1	7.5	7.6	9.4	10.4
Tyr302(M3)	3.9	3.9	3.9	3.9	2.1	3.0	3.4	1.3	2.3	3.0	1.3	1.4	2.2	2.7
Tyr302(M4)	0.0	0.0	0.0	0.0	0.0	0.0	0.0	0.0	0.0	0.0	0.0	0.0	0.0	0.0
Rib173(M0)	63.4	62.1	58.4	58.4	63.4	63.4	60.6	65.0	63.7	60.9	68.7	65.8	64.2	65.0
Rib173(M1)	9.9	10.1	14.0	14.0	9.8	9.6	11.6	9.2	9.7	11.8	9.3	8.8	9.9	9.1
Rib173(M2)	25.0	26.0	25.7	25.7	25.1	25.2	25.9	24.2	24.8	25.5	20.6	23.7	24.2	24.2
Rib173(M3)	1.7	1.8	1.8	1.8	1.7	1.7	1.8	1.7	1.7	1.8	1.5	1.6	1.7	1.7
Rib284(M0)	3.8	3.5	3.8	3.7	10.7	8.8	7.6	14.0	10.8	9.3	22.5	14.3	11.6	10.7
Rib284(M1)	54.6	52.4	52.4	52.0	46.3	48.3	47.5	44.7	46.9	46.9	43.3	44.7	46.7	48.2
Rib284(M2)	31.0	32.4	31.6	32.2	29.7	30.3	31.1	28.2	29.5	30.4	23.7	28.2	29.0	29.1
Rib284(M3)	8.9	9.8	10.0	10.1	11.3	10.8	11.6	11.2	10.8	11.3	9.0	10.9	10.7	10.2
Rib284(M4)	1.3	1.5	1.7	1.6	1.7	1.6	1.8	1.6	1.6	1.7	1.2	1.5	1.7	1.5
Rib284(M5)	0.3	0.4	0.4	0.4	0.4	0.4	0.4	0.3	0.3	0.4	0.3	0.3	0.3	0.3
Gluc173(M0)	82.4	80.9	79.8	79.5	83.1	78.1	75.9	82.3	80.4	76.3	81.0	82.4	79.1	80.2
Gluc173(M1)	8.7	8.7	9.0	9.0	8.9	9.2	9.4	9.0	9.2	9.4	10.2	8.8	9.7	9.1
Gluc173(M2)	8.2	9.6	10.4	10.7	7.3	11.9	13.7	7.7	9.3	13.1	7.1	8.0	9.5	10.0
Gluc173(M3)	0.6	0.7	0.8	0.8	0.7	0.9	1.1	1.1	1.1	1.2	1.8	0.8	1.7	0.7
Gluc370(M0)	6.6	2.0	1.2	1.4	10.4	5.5	2.8	10.9	6.2	3.1	15.0	7.4	5.8	5.2
Gluc370(M1)	4.2	3.7	4.0	4.2	5.1	6.0	5.7	5.3	5.5	5.8	5.7	5.0	5.3	5.9
Gluc370(M2)	67.8	70.7	70.5	69.8	64.9	64.4	65.1	64.4	66.6	65.5	61.8	66.9	67.4	66.5
Gluc370(M3)	17.2	19.0	19.5	19.7	15.8	19.1	20.7	15.8	17.4	20.1	14.2	16.6	17.3	17.9
Gluc370(M4)	3.5	4.0	4.1	4.1	3.3	4.3	4.8	3.2	3.7	4.6	2.8	3.5	3.6	3.8
Gluc370(M5)	0.5	0.6	0.6	0.6	0.5	0.6	0.8	0.5	0.6	0.7	0.4	0.5	0.5	0.6
Gluc370(M6)	0.1	0.1	0.1	0.1	0.1	0.1	0.1	0.1	0.1	0.1	0.1	0.1	0.1	0.1

Table D.3 Results of ^{13}C-MFA for *E. coli* grown on 1.7 g/L [1,2-^{13}C]glucose. The fluxes are normalized to a substrate uptake rate of 100. 95% confidence intervals of fluxes were determined by evaluating the sensitivity of the minimized SSR to flux variations.

Number of fitted data sets :			1
Number of fitted measurements :			164
SSR :			49.2
Flux	best fit	LB95	UB95
G6P.1 <=> F6P.1 (net)	68.2	67.0	69.4
G6P.1 <=> F6P.1 (exch)	136.1	99.5	200.4
F6P.1 + ATP.1 -> FBP.1 + ADP.1	81.7	80.4	82.9
FBP.1 <=> DHAP.1 + GAP.1 (net)	81.7	80.4	82.9
FBP.1 <=> DHAP.1 + GAP.1 (exch)	591.6	0.0	100592.0
DHAP.1 <=> GAP.1 (net)	81.7	80.4	82.9
DHAP.1 <=> GAP.1 (exch)	64.6	0.0	100065.0
GAP.1 + NAD.1 + ADP.1 + Pi.1 <=> 3PG.1 + ATP.1 + NADH.1 (net)	169.7	166.8	172.7
GAP.1 + NAD.1 + ADP.1 + Pi.1 <=> 3PG.1 + ATP.1 + NADH.1 (exch)	39.4	0.0	13837.5
3PG.1 <=> PEP.1 (net)	156.6	151.8	161.4
3PG.1 <=> PEP.1 (exch)	3956.0	0.0	103956.0
PEP.1 + ADP.1 -> Pyr.1 + ATP.1	27.5	17.6	37.6
G6P.1 + NADP.1 -> 6PG.1 + NADPH.1	30.2	29.1	31.3
6PG.1 + NADP.1 -> Ru5P.1 + CO2.1 + NADPH.1	28.8	27.3	30.2
Ru5P.1 <=> X5P.1 (net)	14.0	13.0	14.9
Ru5P.1 <=> X5P.1 (exch)	130.6	37.1	10362.1
Ru5P.1 <=> R5P.1 (net)	14.8	13.7	15.9
Ru5P.1 <=> R5P.1 (exch)	0.0	0.0	11144.8
X5P.1 <=> GAP.1 + E-C2.1 (net)	14.0	13.0	14.9
X5P.1 <=> GAP.1 + E-C2.1 (exch)	62.2	37.1	10255.6
F6P.1 <=> E4P.1 + E-C2.1 (net)	-5.6	-6.2	-5.0
F6P.1 <=> E4P.1 + E-C2.1 (exch)	6.5	5.5	7.3
S7P.1 <=> R5P.1 + E-C2.1 (net)	-8.4	-8.8	-8.0
S7P.1 <=> R5P.1 + E-C2.1 (exch)	247.9	0.0	14508.4
F6P.1 <=> GAP.1 + E-C3.1 (net)	-8.4	-8.8	-8.0
F6P.1 <=> GAP.1 + E-C3.1 (exch)	38.3	28.2	51.6
S7P.1 <=> E4P.1 + E-C3.1 (net)	8.4	8.0	8.8

S7P.1 <=> E4P.1 + E-C3.1 (exch)	0.1	0.0	10922.4
6PG.1 -> KDPG.1	1.4	0.5	2.3
KDPG.1 -> GAP.1 + Pyr.1	1.4	0.5	2.3
Pyr.1 + NAD.1 -> AcCoA.1 + CO2.1 + NADH.1	110.1	97.9	122.3
AcCoA.1 + OAC.1 -> Cit.1	17.1	13.9	20.4
Cit.1 <=> ICit.1 (net)	17.1	13.9	20.4
Cit.1 <=> ICit.1 (exch)	604.0	0.0	100604.0
ICit.1 + NADP.1 <=> AKG.1 + CO2.1 + NADPH.1 (net)	16.3	13.2	19.8
ICit.1 + NADP.1 <=> AKG.1 + CO2.1 + NADPH.1 (exch)	2.9	0.0	10647.4
AKG.1 + NAD.1 -> SucCoA.1 + CO2.1 + NADH.1	7.9	5.9	10.6
SucCoA.1 + ADP.1 + Pi.1 <=> Suc.1 + ATP.1 (net)	4.3	2.5	6.7
SucCoA.1 + ADP.1 + Pi.1 <=> Suc.1 + ATP.1 (exch)	205.2	0.0	100205.0
Suc.1 + FAD.1 <=> Fum.1 + FADH2.1 (net)	8.7	6.7	11.1
Suc.1 + FAD.1 <=> Fum.1 + FADH2.1 (exch)	0.0	0.0	100000.0
Fum.1 <=> Mal.1 (net)	11.1	8.7	13.7
Fum.1 <=> Mal.1 (exch)	9654.1	50.2	21131.1
Mal.1 + NAD.1 <=> OAC.1 + NADH.1 (net)	10.3	7.9	13.0
Mal.1 + NAD.1 <=> OAC.1 + NADH.1 (exch)	77.4	45.1	136.6
ICit.1 <=> Glyox.1 + Suc.1 (net)	0.8	0.0	1.7
ICit.1 <=> Glyox.1 + Suc.1 (exch)	0.0	0.0	0.7
AcCoA.1 + Glyox.1 -> Mal.1	0.8	0.0	1.7
Mal.1 + NADP.1 -> Pyr.1 + CO2.1 + NADPH.1	1.6	0.0	5.2
PEP.1 + CO2.1 -> OAC.1 + Pi.1	23.0	18.3	28.2
OAC.1 + ATP.1 -> PEP.1 + CO2.1 + ADP.1	0.0	0.0	3.5
AcCoA.1 + ADP.1 + Pi.1 <=> Ac.1 + ATP.1 (net)	65.6	46.6	84.6
AcCoA.1 + ADP.1 + Pi.1 <=> Ac.1 + ATP.1 (exch)	593.2	0.0	100593.0
AKG.1 + NADPH.1 + NH3.1 -> Glu.1 + NADP.1	49.3	41.9	56.6
Glu.1 + ATP.1 + NH3.1 -> Gln.1 + ADP.1 + Pi.1	4.7	4.0	5.4
Glu.1 + 2 NADPH.1 + ATP.1 -> Pro.1 + 2 NADP.1 + ADP.1 + Pi.1	1.6	1.4	1.9
Glu.1 + CO2.1 + Gln.1 + NADPH.1 + Asp.1 + AcCoA.1 + 5 ATP.1 -> Arg.1 + AKG.1 + Fum.1+ Ac.1	2.2	1.9	2.5
OAC.1 + Glu.1 -> Asp.1 + AKG.1	13.6	11.5	15.8
Asp.1 + NH3.1 + 2 ATP.1 -> Asn.1 + 2 ADP.1 + 2 Pi.1	1.8	1.5	2.0

Pyr.1 + Glu.1 -> Ala.1 + AKG.1	3.8	3.2	4.3
3PG.1 + Glu.1 + NAD.1 -> Ser.1 + NADH.1 + AKG.1 + Pi.1	8.4	7.1	9.6
Ser.1 + THF.1 <=> Gly.1 + MEETHF.1 (net)	4.6	3.9	5.3
Ser.1 + THF.1 <=> Gly.1 + MEETHF.1 (exch)	3.2	2.7	3.8
Gly.1 + THF.1 + NAD.1 <=> CO2.1 + MEETHF.1 + NH3.1 + NADH.1 (net)	0.1	0.1	0.4
Gly.1 + THF.1 + NAD.1 <=> CO2.1 + MEETHF.1 + NH3.1 + NADH.1 (exch)	0.2	0.0	0.9
Thr.1 + NAD.1 -> Gly.1 + AcCoA.1 + NADH.1	0.1	0.0	0.5
Ser.1 + AcCoA.1 + SO4.1 + 3 ATP.1 + 4 NADPH.1 -> Cys.1 + Ac.1 + 4 NADP.1 + 3ADP.1	1.8	1.5	2.1
Asp.1 + Pyr.1 + Glu.1 + 2 NADPH.1 + ATP.1 + SucCoA.1 -> LL-DAP.1 + AKG.1 + Suc.1	2.5	2.1	2.9
LL-DAP.1 -> Lys.1 + CO2.1	2.5	2.1	2.9
Asp.1 + 2 NADPH.1 + 2 ATP.1 -> Thr.1 + 2 NADP.1 + 2 ADP.1 + 2 Pi.1	4.1	3.4	4.9
Asp.1 + METHF.1 + Cys.1 + 2 NADPH.1 + ATP.1 + SucCoA.1 -> Met.1 + Pyr.1 + 2NADP.1 + ADP.1 + Suc.1 + NH3	1.1	1.0	1.3
2 Pyr.1 + NADPH.1 + Glu.1 -> Val.1 + CO2.1 + NADP.1 + AKG.1	3.1	2.7	3.6
2 Pyr.1 + AcCoA.1 + Glu.1 + NADPH.1 + NAD.1 -> Leu.1 + 2 CO2.1 + AKG.1 + NADP.1	3.3	2.8	3.8
Thr.1 + Pyr.1 + Glu.1 + NADPH.1 -> Ile.1 + CO2.1 + AKG.1 + NADP.1 + NH3.1	2.1	1.8	2.5
E4P.1 + 2 PEP.1 + Glu.1 + NADPH.1 + ATP.1 -> Phe.1 + CO2.1 + AKG.1 + NADP.1	1.4	1.2	1.6
E4P.1 + 2 PEP.1 + Glu.1 + NADPH.1 + NAD.1 + ATP.1 -> Tyr.1 + CO2.1 + AKG.1	1.0	0.9	1.2
E4P.1 + 2 PEP.1 + R5P.1 + Ser.1 + Gln.1 + NADPH.1 + 3 ATP.1 -> Trp.1 + CO2.1 + AKG.1 + NADH.1	0.4	0.4	0.5
R5P.1 + FTHF.1 + Gln.1 + Asp.1 + 5 ATP.1 + 2 NAD.1 -> His.1 + 2 NADH.1 + AKG.1 + Fum	0.2	0.1	0.2
MEETHF.1 + NADH.1 -> METHF.1 + NAD.1	1.1	1.0	1.3
MEETHF.1 + NADP.1 -> FTHF.1 + NADPH.1	0.2	0.1	0.2
NADH.1 + NADP.1 <=> NADPH.1 + NAD.1 (net)	53.3	37.1	69.4
NADH.1 + NADP.1 <=> NADPH.1 + NAD.1 (exch)	166.0	0.0	11767.5
0.488Ala+0.281Arg+0.229Asn+0.229Asp+0.087Cys +0.250Glu+0.250Gln+0.582Gly+0.090His+0.276Ile	7.7	6.6	8.9

+0.428Leu+0.326Lys+0.146Met+0.176Phe+0.210Pro +0.205Ser+0.241Thr+0.054Trp+0.131Tyr+0.402Val +0.205G6P+0.071F6P+0.754R5P+0.129GAP+0.619 3PG+0.051PEP+0.083Pyr+2.510AcCoA+0.087AKG +0.340OAC+0.443MEETHF+33.247ATP+5.363 NADPH → 39.68Biomass + 1.455NADH			
ATP.1 -> ATP.Ext	430.5	310.0	551.9
Ac.1 -> Ac.Ext + X-ac1	69.6	51.1	88.1
CO2.1 -> CO2.Ext	156.8	147.6	166.2
O2.Ext -> O2.1	138.4	126.7	150.3
NH3.Ext -> NH3.1	52.3	44.5	60.0
SO4.Ext -> SO4.1	1.8	1.5	2.1
Gluc.Ext + PEP.1 -> G6P.1 + Pyr.1 + X-glc1	100.0	100.0	100.0
NADH.1 + 0.5 O2.1 + 2 ADP.1 + 2 Pi.1 -> NAD.1 + 2 ATP.1	268.1	243.6	292.9
FADH2.1 + 0.5 O2.1 + ADP.1 + Pi.1 -> FAD.1 + ATP.1	8.7	6.7	11.1
CO2.M0 + CO2.1 -> CO2.1 + CO2.snk	66.2	45.0	92.5
Uptake rate of CO2.M0	66.2	45.0	92.5
Uptake rate of Gluc.Ext	100.0	100.0	100.0
Uptake rate of O2.Ext	138.4	126.7	150.3
Uptake rate of NH3.Ext	52.3	44.5	60.0
Uptake rate of SO4.Ext	1.8	1.5	2.1
Output rate of Ac.Ext	69.6	51.1	88.1
Output rate of CO2.Ext	156.8	147.6	166.2
Output rate of CO2.snk	66.2	45.0	92.5
Output rate of ATP.Ext	430.5	310.0	551.9
Output rate of Biomass.1	307.3	261.7	352.8
Output rate of X-glc1	100.0	100.0	100.0
Output rate of X-ac1	69.6	51.1	88.1
Output rate of X-a1	100.0	100.0	100.0
Output rate of X-a2	100.0	100.0	100.0
Output rate of X-a3	100.0	100.0	100.0
Net production rate of ADP.1	-430.5	-551.9	-310.0
Net production rate of Pi.1	-444.6	-563.8	-326.2
Fractional labeling of Ala.a1	1.0	1.0	1.0
Fractional labeling of Gly.a1	1.0	1.0	1.0
Fractional labeling of Val.a1	1.0	1.0	1.0

Fractional labeling of Leu.a1	1.0	1.0	1.0
Fractional labeling of Ile.a1	1.0	1.0	1.0
Fractional labeling of Met.a1	1.0	1.0	1.0
Fractional labeling of Ser.a1	1.0	1.0	1.0
Fractional labeling of Thr.a1	1.0	1.0	1.0
Fractional labeling of Phe.a1	1.0	1.0	1.0
Fractional labeling of Asp.a1	1.0	1.0	1.0
Fractional labeling of Glu.a1	1.0	1.0	1.0
Fractional labeling of Lys.a1	1.0	1.0	1.0
Fractional labeling of His.a1	1.0	1.0	1.0
Fractional labeling of Tyr.a1	1.0	1.0	1.0
Fractional labeling of R5P.a1	1.0	1.0	1.0
Fractional labeling of G6P.a1	0.9	0.9	0.9

Table D.4 Results of ^{13}C-MFA for *E. coli* grown on 1.7 g/L [1,2-^{13}C]glucose + 0.5 g/L yeast extract. The fluxes are normalized to a substrate uptake rate of 100. 95% confidence intervals of fluxes were determined by evaluating the sensitivity of the minimized SSR to flux variations.

Fit for *E. coli* 2 g/L [12]Gluc + 0.5 g/L YE			
Number of fitted data sets :			3
Number of fitted measurements :			498
SSR :			191.7
Flux	best fit	LB95	UB95
G6P.1 <=> F6P.1 (net)	83.0	78.2	88.5
G6P.1 <=> F6P.1 (exch)	113.8	51.6	1187.6
G6P.2 <=> F6P.2 (net)	64.5	62.2	67.3
G6P.2 <=> F6P.2 (exch)	422.9	263.6	1428.3
F6P.1 + ATP.1 -> FBP.1 + ADP.1	94.1	90.6	96.0
F6P.2 + ATP.2 -> FBP.2 + ADP.2	81.6	80.2	83.1
FBP.1 <=> DHAP.1 + GAP.1 (net)	94.1	90.6	96.0
FBP.1 <=> DHAP.1 + GAP.1 (exch)	412.6	0.0	100413.0
FBP.2 <=> DHAP.2 + GAP.2 (net)	81.6	80.2	83.1
FBP.2 <=> DHAP.2 + GAP.2 (exch)	146.7	0.0	100147.0
DHAP.1 <=> GAP.1 (net)	94.1	90.6	96.0
DHAP.1 <=> GAP.1 (exch)	251.5	0.0	100252.0

DHAP.2 <=> GAP.2 (net)	81.6	80.2	83.1
DHAP.2 <=> GAP.2 (exch)	0.2	0.0	100000.0
GAP.1 + NAD.1 + ADP.1 + Pi.1 <=> 3PG.1 + ATP.1 + NADH.1 (net)	193.7	189.8	195.9
GAP.1 + NAD.1 + ADP.1 + Pi.1 <=> 3PG.1 + ATP.1 + NADH.1 (exch)	591.0	0.0	100591.0
GAP.2 + NAD.2 + ADP.2 + Pi.2 <=> 3PG.2 + ATP.2 + NADH.2 (net)	170.7	168.4	173.2
GAP.2 + NAD.2 + ADP.2 + Pi.2 <=> 3PG.2 + ATP.2 + NADH.2 (exch)	12421.9	372.8	22888.1
3PG.1 <=> PEP.1 (net)	193.3	188.9	195.9
3PG.1 <=> PEP.1 (exch)	569.5	0.0	100570.0
3PG.2 <=> PEP.2 (net)	158.9	155.3	162.6
3PG.2 <=> PEP.2 (exch)	13474.1	314.6	23946.2
PEP.1 + ADP.1 -> Pyr.1 + ATP.1	92.1	67.6	95.2
PEP.2 + ADP.2 -> Pyr.2 + ATP.2	33.2	27.1	40.0
G6P.1 + NADP.1 -> 6PG.1 + NADPH.1	17.0	11.5	21.7
G6P.2 + NADP.2 -> 6PG.2 + NADPH.2	34.1	31.3	36.3
6PG.1 + NADP.1 -> Ru5P.1 + CO2.1 + NADPH.1	17.0	11.4	21.4
6PG.2 + NADP.2 -> Ru5P.2 + CO2.2 + NADPH.2	33.5	30.5	36.1
Ru5P.1 <=> X5P.1 (net)	11.1	7.4	14.1
Ru5P.1 <=> X5P.1 (exch)	63.8	20.2	10252.8
Ru5P.2 <=> X5P.2 (net)	17.6	15.7	19.3
Ru5P.2 <=> X5P.2 (exch)	49.0	42.2	55.1
Ru5P.1 <=> R5P.1 (net)	5.8	3.9	7.4
Ru5P.1 <=> R5P.1 (exch)	533.9	0.0	10991.1
Ru5P.2 <=> R5P.2 (net)	15.9	14.6	17.0
Ru5P.2 <=> R5P.2 (exch)	1943.9	11.8	11945.5
X5P.1 <=> GAP.1 + E-C2.1 (net)	11.1	7.4	14.1
X5P.1 <=> GAP.1 + E-C2.1 (exch)	60.5	20.1	10281.6
X5P.2 <=> GAP.2 + E-C2.2 (net)	17.6	15.7	19.3
X5P.2 <=> GAP.2 + E-C2.2 (exch)	18358.5	45.9	28440.5
F6P.1 <=> E4P.1 + E-C2.1 (net)	-5.5	-7.0	-3.6
F6P.1 <=> E4P.1 + E-C2.1 (exch)	8.3	4.0	12.9
F6P.2 <=> E4P.2 + E-C2.2 (net)	-7.5	-8.4	-6.6
F6P.2 <=> E4P.2 + E-C2.2 (exch)	13.8	11.5	16.0
S7P.1 <=> R5P.1 + E-C2.1 (net)	-5.6	-7.1	-3.8

S7P.1 <=> R5P.1 + E-C2.1 (exch)	92.4	0.0	10325.9
S7P.2 <=> R5P.2 + E-C2.2 (net)	-10.1	-10.9	-9.1
S7P.2 <=> R5P.2 + E-C2.2 (exch)	0.0	0.0	1.6
F6P.1 <=> GAP.1 + E-C3.1 (net)	-5.6	-7.1	-3.8
F6P.1 <=> GAP.1 + E-C3.1 (exch)	18.7	0.3	44.1
F6P.2 <=> GAP.2 + E-C3.2 (net)	-10.1	-10.9	-9.1
F6P.2 <=> GAP.2 + E-C3.2 (exch)	65.3	50.4	84.2
S7P.1 <=> E4P.1 + E-C3.1 (net)	5.6	3.8	7.1
S7P.1 <=> E4P.1 + E-C3.1 (exch)	0.7	0.0	10968.7
S7P.2 <=> E4P.2 + E-C3.2 (net)	10.1	9.1	10.9
S7P.2 <=> E4P.2 + E-C3.2 (exch)	488.5	0.0	100488.0
6PG.1 -> KDPG.1	0.0	0.0	3.7
6PG.2 -> KDPG.2	0.5	0.0	1.7
KDPG.1 -> GAP.1 + Pyr.1	0.0	0.0	3.7
KDPG.2 -> GAP.2 + Pyr.2	0.5	0.0	1.7
Pyr.1 + NAD.1 -> AcCoA.1 + CO2.1 + NADH.1	191.3	183.3	195.3
Pyr.2 + NAD.2 -> AcCoA.2 + CO2.2 + NADH.2	115.2	107.3	123.8
AcCoA.1 + OAC.1 -> Cit.1	0.6	0.0	9.1
AcCoA.2 + OAC.2 -> Cit.2	33.4	26.0	40.9
Cit.1 <=> ICit.1 (net)	0.6	0.0	9.1
Cit.1 <=> ICit.1 (exch)	264.6	0.0	100265.0
Cit.2 <=> ICit.2 (net)	33.4	26.0	40.9
Cit.2 <=> ICit.2 (exch)	203.7	0.0	100204.0
ICit.1 + NADP.1 <=> AKG.1 + CO2.1 + NADPH.1 (net)	0.6	0.0	9.2
ICit.1 + NADP.1 <=> AKG.1 + CO2.1 + NADPH.1 (exch)	321.2	0.0	65688.7
ICit.2 + NADP.2 <=> AKG.2 + CO2.2 + NADPH.2 (net)	33.0	22.7	40.9
ICit.2 + NADP.2 <=> AKG.2 + CO2.2 + NADPH.2 (exch)	125.4	0.0	11907.2
AKG.1 + NAD.1 -> SucCoA.1 + CO2.1 + NADH.1	0.3	0.0	9.1
AKG.2 + NAD.2 -> SucCoA.2 + CO2.2 + NADH.2	25.4	14.8	33.6
SucCoA.1 + ADP.1 + Pi.1 <=> Suc.1 + ATP.1 (net)	0.2	0.0	9.1
SucCoA.1 + ADP.1 + Pi.1 <=> Suc.1 + ATP.1 (exch)	251.8	0.0	100252.0
SucCoA.2 + ADP.2 + Pi.2 <=> Suc.2 + ATP.2 (net)	22.1	11.3	30.5
SucCoA.2 + ADP.2 + Pi.2 <=> Suc.2 + ATP.2	236.3	0.0	100236.0

(exch)			
Suc.1 + FAD.1 <=> Fum.1 + FADH2.1 (net)	0.3	0.0	9.0
Suc.1 + FAD.1 <=> Fum.1 + FADH2.1 (exch)	325.8	0.0	100326.0
Suc.2 + FAD.2 <=> Fum.2 + FADH2.2 (net)	25.8	18.2	33.6
Suc.2 + FAD.2 <=> Fum.2 + FADH2.2 (exch)	164.1	0.0	10250.0
Fum.1 <=> Mal.1 (net)	0.4	0.0	9.0
Fum.1 <=> Mal.1 (exch)	731.1	0.0	11429.2
Fum.2 <=> Mal.2 (net)	27.9	20.4	35.7
Fum.2 <=> Mal.2 (exch)	79.2	44.1	165.3
Mal.1 + NAD.1 <=> OAC.1 + NADH.1 (net)	0.4	-20.7	9.9
Mal.1 + NAD.1 <=> OAC.1 + NADH.1 (exch)	57.0	0.0	14057.7
Mal.2 + NAD.2 <=> OAC.2 + NADH.2 (net)	28.2	22.6	35.6
Mal.2 + NAD.2 <=> OAC.2 + NADH.2 (exch)	1959.1	53.0	12471.0
ICit.1 <=> Glyox.1 + Suc.1 (net)	0.0	0.0	1.6
ICit.1 <=> Glyox.1 + Suc.1 (exch)	0.0	0.0	0.4
ICit.2 <=> Glyox.2 + Suc.2 (net)	0.4	0.0	5.4
ICit.2 <=> Glyox.2 + Suc.2 (exch)	1.1	0.0	3.5
AcCoA.1 + Glyox.1 -> Mal.1	0.0	0.0	1.6
AcCoA.2 + Glyox.2 -> Mal.2	0.4	0.0	5.4
Mal.1 + NADP.1 -> Pyr.1 + CO2.1 + NADPH.1	0.0	0.0	25.9
Mal.2 + NADP.2 -> Pyr.2 + CO2.2 + NADPH.2	0.0	0.0	3.5
PEP.1 + CO2.1 -> OAC.1 + Pi.1	1.0	0.0	32.7
PEP.2 + CO2.2 -> OAC.2 + Pi.2	27.4	21.8	33.9
OAC.1 + ATP.1 -> PEP.1 + CO2.1 + ADP.1	0.0	0.0	49.1
OAC.2 + ATP.2 -> PEP.2 + CO2.2 + ADP.2	7.2	1.6	14.3
AcCoA.1 + ADP.1 + Pi.1 <=> Ac.1 + ATP.1 (net)	190.0	179.4	194.8
AcCoA.1 + ADP.1 + Pi.1 <=> Ac.1 + ATP.1 (exch)	228.6	0.0	100229.0
AcCoA.2 + ADP.2 + Pi.2 <=> Ac.2 + ATP.2 (net)	57.5	45.8	68.9
AcCoA.2 + ADP.2 + Pi.2 <=> Ac.2 + ATP.2 (exch)	335.0	0.0	100335.0
AKG.1 + NADPH.1 + NH3.1 -> Glu.1 + NADP.1	1.9	0.0	6.8
AKG.2 + NADPH.2 + NH3.2 -> Glu.2 + NADP.2	45.0	39.9	50.0
Glu.1 + ATP.1 + NH3.1 -> Gln.1 + ADP.1 + Pi.1	0.2	0.0	0.6
Glu.2 + ATP.2 + NH3.2 -> Gln.2 + ADP.2 + Pi.2	4.3	3.8	4.7
Glu.1 + 2 NADPH.1 + ATP.1 -> Pro.1 + 2 NADP.1 + ADP.1 + Pi.1	0.1	0.0	0.2
Glu.2 + 2 NADPH.2 + ATP.2 -> Pro.2 + 2 NADP.2 + Pi.2 + ADP.2	1.5	1.3	1.6

Glu.1 + CO2.1 + Gln.1 + NADPH.1 + Asp.1 + AcCoA.1 + 5 ATP.1 -> Arg.1 + AKG.1 + Fum.1 + Ac.1	0.1	0.0	0.3
Glu.2 + CO2.2 + Gln.2 + NADPH.2 + Asp.2 + AcCoA.2 + 5 ATP.2 -> Arg.2 + AKG.2 + Fum.2 + Ac.2	2.0	1.8	2.2
OAC.1 + Glu.1 -> Asp.1 + AKG.1	0.7	0.0	2.6
OAC.2 + Glu.2 -> Asp.2 + AKG.2	12.7	11.2	14.2
Asp.1 + NH3.1 + 2 ATP.1 -> Asn.1 + 2 ADP.1 + 2 Pi.1	0.1	0.0	0.2
Asp.2 + NH3.2 + 2 ATP.2 -> Asn.2 + 2 ADP.2 + 2 Pi.2	1.6	1.4	1.8
Pyr.1 + Glu.1 -> Ala.1 + AKG.1	0.1	0.0	0.5
Pyr.2 + Glu.2 -> Ala.2 + AKG.2	3.4	3.1	3.8
3PG.1 + Glu.1 + NAD.1 -> Ser.1 + NADH.1 + AKG.1 + Pi.1	0.2	0.0	0.8
3PG.2 + Glu.2 + NAD.2 -> Ser.2 + NADH.2 + AKG.2 + Pi.2	7.5	6.6	8.3
Ser.1 + THF.1 <=> Gly.1 + MEETHF.1 (net)	0.1	0.0	0.4
Ser.1 + THF.1 <=> Gly.1 + MEETHF.1 (exch)	0.0	0.0	0.1
Ser.2 + THF.2 <=> Gly.2 + MEETHF.2 (net)	4.0	3.6	4.5
Ser.2 + THF.2 <=> Gly.2 + MEETHF.2 (exch)	2.7	2.4	3.2
Gly.1 + THF.1 + NAD.1 <=> CO2.1 + MEETHF.1 + NH3.1 + NADH.1 (net)	0.1	0.0	0.5
Gly.1 + THF.1 + NAD.1 <=> CO2.1 + MEETHF.1 + NH3.1 + NADH.1 (exch)	555.7	555.7	15837.7
Gly.2 + THF.2 + NAD.2 <=> CO2.2 + MEETHF.2 + NH3.2 + NADH.2 (net)	0.3	0.1	0.4
Gly.2 + THF.2 + NAD.2 <=> CO2.2 + MEETHF.2 + NH3.2 + NADH.2 (exch)	0.0	0.0	0.8
Thr.1 + NAD.1 -> Gly.1 + AcCoA.1 + NADH.1	0.2	0.0	0.9
Thr.2 + NAD.2 -> Gly.2 + AcCoA.2 + NADH.2	0.4	0.0	0.7
Ser.1 + AcCoA.1 + SO4.1 + 3 ATP.1 + 4 NADPH.1 -> Cys.1 + Ac.1 + 4 NADP.1 + 3ADP.1	0.1	0.0	0.2
Ser.2 + AcCoA.2 + SO4.2 + 3 ATP.2 + 4 NADPH.2 -> Cys.2 + Ac.2 + 4 NADP.2 + 3ADP.2	1.6	1.5	1.8
Asp.1 + Pyr.1 + Glu.1 + 2 NADPH.1 + ATP.1 + SucCoA.1 -> LL-DAP.1 + AKG.1 + Suc.1 + 2NADP.1 + ADP.1	0.1	0.0	0.3
Asp.2 + Pyr.2 + Glu.2 + 2 NADPH.2 + ATP.2 + SucCoA.2 -> LL-DAP.2 + AKG.2 + Suc.2 +	2.3	2.0	2.6

2NADP.2 + ADP.2			
LL-DAP.1 -> Lys.1 + CO2.1	0.1	0.0	0.3
LL-DAP.2 -> Lys.2 + CO2.2	2.3	2.0	2.6
Asp.1 + 2 NADPH.1 + 2 ATP.1 -> Thr.1 + 2 NADP.1 + 2 ADP.1 + 2 Pi.1	0.4	0.0	1.4
Asp.2 + 2 NADPH.2 + 2 ATP.2 -> Thr.2 + 2 NADP.2 + 2 ADP.2 + 2 Pi.2	4.0	3.4	4.6
Asp.1 + METHF.1 + Cys.1 + 2 NADPH.1 + ATP.1 + SucCoA.1 -> Met.1 + Pyr.1 + Suc.1 + NH3.1 + 2NADP.1 + ADP.1	0.0	0.0	0.1
Asp.2 + METHF.2 + Cys.2 + 2 NADPH.2 + ATP.2 + SucCoA.2 -> Met.2 + Pyr.2 + Suc.2 + NH3.2 + 2NADP.2 + ADP.2	1.0	0.9	1.1
2 Pyr.1 + NADPH.1 + Glu.1 -> Val.1 + CO2.1 + NADP.1 + AKG.1	0.1	0.0	0.4
2 Pyr.2 + NADPH.2 + Glu.2 -> Val.2 + CO2.2 + NADP.2 + AKG.2	2.8	2.5	3.1
2 Pyr.1 + AcCoA.1 + Glu.1 + NADPH.1 + NAD.1 -> Leu.1 + 2 CO2.1 + AKG.1 + NA	0.1	0.0	0.4
2 Pyr.2 + AcCoA.2 + Glu.2 + NADPH.2 + NAD.2 -> Leu.2 + 2 CO2.2 + AKG.2 + NA	3.0	2.7	3.4
Thr.1 + Pyr.1 + Glu.1 + NADPH.1 -> Ile.1 + CO2.1 + AKG.1 + NADP.1 + NH3.1	0.1	0.0	0.3
Thr.2 + Pyr.2 + Glu.2 + NADPH.2 -> Ile.2 + CO2.2 + AKG.2 + NADP.2 + NH3.2	1.9	1.7	2.2
E4P.1 + 2 PEP.1 + Glu.1 + NADPH.1 + ATP.1 -> Phe.1 + CO2.1 + AKG.1 + NADP.1	0.0	0.0	0.2
E4P.2 + 2 PEP.2 + Glu.2 + NADPH.2 + ATP.2 -> Phe.2 + CO2.2 + AKG.2 + NADP.2	1.2	1.1	1.4
E4P.1 + 2 PEP.1 + Glu.1 + NADPH.1 + NAD.1 + ATP.1 -> Tyr.1 + CO2.1 + AKG.1 + NADH.1	0.0	0.0	0.1
E4P.2 + 2 PEP.2 + Glu.2 + NADPH.2 + NAD.2 + ATP.2 -> Tyr.2 + CO2.2 + AKG.2 + NADH.2	0.9	0.8	1.0
E4P.1 + 2 PEP.1 + R5P.1 + Ser.1 + Gln.1 + NADPH.1 + 3 ATP.1 -> Trp.1 + CO2.1 + GAP.1 + Pyr.1 + Glu.1	0.0	0.0	0.1
E4P.2 + 2 PEP.2 + R5P.2 + Ser.2 + Gln.2 + NADPH.2 + 3 ATP.2 -> Trp.2 + CO2.2 + GAP.2 + Pyr.2 + Glu.2	0.4	0.3	0.4
R5P.1 + FTHF.1 + Gln.1 + Asp.1 + 5 ATP.1 + 2 NAD.1 -> His.1 + 2 NADH.1 + AKG.1 + Fum.1 + 2NADH.1	0.0	0.0	0.0

R5P.2 + FTHF.2 + Gln.2 + Asp.2 + 5 ATP.2 + 2 NAD.2 -> His.2 + 2 NADH.2 + AKG.2 + Fum.2 + 2NADH.2	0.1	0.1	0.2
MEETHF.1 + NADH.1 -> METHF.1 + NAD.1	0.0	0.0	0.1
MEETHF.2 + NADH.2 -> METHF.2 + NAD.2	1.0	0.9	1.1
MEETHF.1 + NADP.1 -> FTHF.1 + NADPH.1	0.0	0.0	0.0
MEETHF.2 + NADP.2 -> FTHF.2 + NADPH.2	0.1	0.1	0.2
NADH.1 + NADP.1 <=> NADPH.1 + NAD.1 (net)	-29.3	-62.1	-12.5
NADH.1 + NADP.1 <=> NADPH.1 + NAD.1 (exch)	17.6	0.0	327.0
NADH.2 + NADP.2 <=> NADPH.2 + NAD.2 (net)	18.7	2.4	39.0
NADH.2 + NADP.2 <=> NADPH.2 + NAD.2 (exch)	36.6	0.0	100037.0
0.488Ala.1+0.281Arg.1+0.229Asn.1+0.229Asp.1+ 0.087Cys.1+0.250Glu.1+0.250Gln.1+0.582Gly.1+ 0.09His.1+0.276Ile.1+0.428Leu.1+0.326Lys.1+0.146 Met.1 + 0.176Phe.1+0.210Pro.1 + 0.205Ser.1 + 0.241 Thr.1 + 0.054 Trp.1 +0.131Tyr.1+0.402Val.1 + 0.205 G6P.1 +0.071F6P.1+0.754R5P.1 + 0.129 GAP.1 + 0.619 3PG.1 +0.051PEP.1 + 0.083 Pyr.1 +2.510AcCoA.1+ 0.087AKG.1 + 0.340 OAC.1 + 0.443MEETHF.1+33.247ATP.1+5.363NADPH.1 → 39.68Biomass.1 + 1.455NADH.1	0.3	0.0	1.0
0.488Ala.2+0.281Arg.2+0.229Asn.2+0.229Asp.2+ 0.087Cys.2+0.250Glu.2+0.250Gln.2+0.582Gly.2+ 0.09His.2+0.276Ile.2+0.428Leu.2+0.326Lys.2+0.146 Met.2 + 0.176Phe.2+0.210Pro.2 + 0.205Ser.2 + 0.241 Thr.2 + 0.054 Trp.2 +0.131Tyr.2+0.402Val.2 + 0.205 G6P.2 +0.071F6P.2+0.754R5P.2 + 0.129 GAP.2 + 0.619 3PG.2 +0.051PEP.2 + 0.083 Pyr.2 +2.510AcCoA.2+ 0.087AKG.2 + 0.340 OAC.2 + 0.443MEETHF.2+33.247ATP.2+5.363NADPH.2 → 39.68Biomass.2 + 1.455NADH.2	7.1	6.3	7.8
ATP.1 -> ATP.Ext	1203.1	1118.7	1246.6
ATP.2 -> ATP.Ext	631.7	506.5	747.5
Ac.1 -> Ac.Ext + X-ac1	190.1	180.0	194.8
Ac.2 -> Ac.Ext + X-ac2	61.1	49.8	72.2
CO2.1 -> CO2.Ext	208.9	200.6	227.3
CO2.2 -> CO2.Ext	200.8	181.4	220.5
O2.Ext -> O2.1	208.2	198.5	226.7
O2.Ext -> O2.2	184.1	163.1	205.1
NH3.Ext -> NH3.1	1.9	0.0	6.9

NH3.Ext -> NH3.2	47.6	42.3	52.9
SO4.Ext -> SO4.1	0.1	0.0	0.2
SO4.Ext -> SO4.2	1.6	1.5	1.8
NADH.1 + 0.5 O2.1 + 2 ADP.1 + 2 Pi.1 -> NAD.1 + 2 ATP.1	416.1	396.5	442.9
NADH.2 + 0.5 O2.2 + 2 ADP.2 + 2 Pi.2 -> NAD.2 + 2 ATP.2	342.4	306.7	377.4
FADH2.1 + 0.5 O2.1 + ADP.1 + Pi.1 -> FAD.1 + ATP.1	0.3	0.0	9.0
FADH2.2 + 0.5 O2.2 + ADP.2 + Pi.2 -> FAD.2 + ATP.2	25.8	18.2	33.6
Ala.a1 + Gly.a1 + Val.a1 + Leu.a1 + Ile.a1 + Pro.a1 + Met.a1 + Ser.a1 + Thr.a1 + Phe.a1 + Asp.a1 + Glu.a1 + Lys.a1 + His.a1 + Tyr.a1 + G6P.a1 + R5P.a1 → X-a1	100.0	100.0	100.0
Ala.a2 + Gly.a2 + Val.a2 + Leu.a2 + Ile.a2 + Pro.a2 + Met.a2 + Ser.a2 + Thr.a2 + Phe.a2 + Asp.a2 + Glu.a2 + Lys.a2 + His.a2 + Tyr.a2 + G6P.a2 + R5P.a2 → X-a2	100.0	100.0	100.0
Ala.a3 + Gly.a3 + Val.a3 + Leu.a3 + Ile.a3 + Pro.a3 + Met.a3 + Ser.a3 + Thr.a3 + Phe.a3 + Asp.a3 + Glu.a3 + Lys.a3 + His.a3 + Tyr.a3 + G6P.a3 + R5P.a3 → X-a3	100.0	100.0	100.0
Ala.1 + Gly.1 + Val.1 + Leu.1 + Ile.1 + Pro.1 + Met.1 + Ser.1 + Thr.1 + Phe.1 + Asp.1 + Glu.1 + Lys.1 + His.1 + Tyr.1 + G6P.1 + R5P.1 → Ala.a1 + Gly.a1 + Val.a1 + Leu.a1 + Ile.a1 + Pro.a1 + Met.a1 + Ser.a1 + Thr.a1 + Phe.a1 + Asp.a1 + Glu.a1 + Lys.a1 + His.a1 + Tyr.a1 + G6P.a1 + R5P.a1 + Ala.1 + Gly.1 + Val.1 + Leu.1 + Ile.1 + Pro.1 + Met.1 + Ser.1 + Thr.1 + Phe.1 + Asp.1 + Glu.1 + Lys.1 + His.1 + Tyr.1 + G6P.1 + R5P.1	72.2	60.3	88.1
Ala.1 + Gly.1 + Val.1 + Leu.1 + Ile.1 + Pro.1 + Met.1 + Ser.1 + Thr.1 + Phe.1 + Asp.1 + Glu.1 + Lys.1 + His.1 + Tyr.1 + G6P.1 + R5P.1 → Ala.a2 + Gly.a2 + Val.a2 + Leu.a2 + Ile.a2 + Pro.a2 + Met.a2 + Ser.a2 + Thr.a2 + Phe.a2 + Asp.a2 + Glu.a2 + Lys.a2 + His.a2 + Tyr.a2 + G6P.a2 + R5P.a2 + Ala.1 + Gly.1 + Val.1 + Leu.1 + Ile.1 + Pro.1 + Met.1 + Ser.1 + Thr.1 + Phe.1 + Asp.1 + Glu.1 + Lys.1 + His.1 + Tyr.1 + G6P.1 + R5P.1	22.4	17.2	32.2
Ala.1 + Gly.1 + Val.1 + Leu.1 + Ile.1 + Pro.1 +Met.1	1.4	0.0	11.2

+ Ser.1 + Thr.1 + Phe.1 + Asp.1 + Glu.1 + Lys.1 + His.1 + Tyr.1 + G6P.1 + R5P.1 → Ala.a3 + Gly.a3 + Val.a3 + Leu.a3 + Ile.a3 + Pro.a3 + Met.a3 + Ser.a3 + Thr.a3 + Phe.a3 + Asp.a3 + Glu.a3 + Lys.a3 + His.a3 + Tyr.a3 + G6P.a3 + R5P.a3 + Ala.1 + Gly.1 + Val.1 + Leu.1 + Ile.1 + Pro.1 + Met.1 + Ser.1 + Thr.1 + Phe.1 + Asp.1 + Glu.1 + Lys.1 + His.1 + Tyr.1 + G6P.1 + R5P.1			
Ala.2 + Gly.2 + Val.2 + Leu.2 + Ile.2 + Pro.2 + Met.2 + Ser.2 + Thr.2 + Phe.2 + Asp.2 + Glu.2 + Lys.2 + His.2 + Tyr.2 + G6P.2 + R5P.2 → Ala.a1 + Gly.a1 + Val.a1 + Leu.a1 + Ile.a1 + Pro.a1 + Met.a1 + Ser.a1 + Thr.a1 + Phe.a1 + Asp.a1 + Glu.a1 + Lys.a1 + His.a1 + Tyr.a1 + G6P.a1 + R5P.a1 + Ala.2 + Gly.2 + Val.2 + Leu.2 + Ile.2 + Pro.2 + Met.2 + Ser.2 + Thr.2 + Phe.2 + Asp.2 + Glu.2 + Lys.2 + His.2 + Tyr.2 + G6P.2 + R5P.2	27.8	11.9	39.7
Ala.2 + Gly.2 + Val.2 + Leu.2 + Ile.2 + Pro.2 + Met.2 + Ser.2 + Thr.2 + Phe.2 + Asp.2 + Glu.2 + Lys.2 + His.2 + Tyr.2 + G6P.2 + R5P.2 → Ala.a2 + Gly.a2 + Val.a2 + Leu.a2 + Ile.a2 + Pro.a2 + Met.a2 + Ser.a2 + Thr.a2 + Phe.a2 + Asp.a2 + Glu.a2 + Lys.a2 + His.a2 + Tyr.a2 + G6P.a2 + R5P.a2 + Ala.2 + Gly.2 + Val.2 + Leu.2 + Ile.2 + Pro.2 + Met.2 + Ser.2 + Thr.2 + Phe.2 + Asp.2 + Glu.2 + Lys.2 + His.2 + Tyr.2 + G6P.2 + R5P.2	77.6	67.8	82.8
Ala.2 + Gly.2 + Val.2 + Leu.2 + Ile.2 + Pro.2 + Met.2 + Ser.2 + Thr.2 + Phe.2 + Asp.2 + Glu.2 + Lys.2 + His.2 + Tyr.2 + G6P.2 + R5P.2 → Ala.a3 + Gly.a3 + Val.a3 + Leu.a3 + Ile.a3 + Pro.a3 + Met.a3 + Ser.a3 + Thr.a3 + Phe.a3 + Asp.a3 + Glu.a3 + Lys.a3 + His.a3 + Tyr.a3 + G6P.a3 + R5P.a3 + Ala.2 + Gly.2 + Val.2 + Leu.2 + Ile.2 + Pro.2 + Met.2 + Ser.2 + Thr.2 + Phe.2 + Asp.2 + Glu.2 + Lys.2 + His.2 + Tyr.2 + G6P.2 + R5P.2	98.6	88.8	100.0
PEP.1 + 2 Gluc.Ext + PEP.2 -> G6P.1 + Pyr.1 + G6P.2 + Pyr.2 + X-glc1 + X-gluc2	100.0	100.0	100.0
CO2.M0 + CO2.1 -> CO2.1 + CO2.snk	1169.6	201.5	11482.4
CO2.M0 + CO2.2 -> CO2.2 + CO2.snk	62.1	27.8	105.3
Pyr.M0 + Pyr.1 -> Pyr.1 + Pyr.snk	137.9	12.7	378.9
Pyr.M0 + Pyr.2 -> Pyr.2 + Pyr.snk	0.0	0.0	4.4
OAC.M0 + OAC.1 -> OAC.1 + OAC.snk	0.8	0.0	27.8

AKG.M0 + AKG.1 -> AKG.1 + AKG.snk	0.0	0.0	1.4
AKG.M0 + AKG.2 -> AKG.2 + AKG.snk	1.4	0.0	3.2
Ser.M0 + Ser.1 -> Ser.1 + Ser.snk	0.0	0.0	0.3
R5P.M0 + R5P.1 -> R5P.1 + R5P.snk	1.6	0.0	4.7
R5P.M0 + R5P.2 -> R5P.2 + R5P.snk	2.1	0.7	2.7
Uptake rate of CO2.M0	1231.7	265.5	8944.5
Uptake rate of Gluc.Ext	200.0	200.0	200.0
Uptake rate of OAC.M0	0.8	0.0	27.8
Uptake rate of AKG.M0	1.4	0.0	3.2
Uptake rate of Pyr.M0	137.9	13.5	379.2
Uptake rate of R5P.M0	3.7	1.0	6.8
Uptake rate of Ser.M0	0.0	0.0	0.3
Uptake rate of O2.Ext	392.3	368.9	418.9
Uptake rate of NH3.Ext	49.5	43.1	57.2
Uptake rate of SO4.Ext	1.7	1.5	2.0
Output rate of Ac.Ext	251.2	236.3	265.1
Output rate of CO2.Ext	409.7	388.4	435.0
Output rate of CO2.snk	1231.7	265.5	8944.5
Output rate of OAC.snk	0.8	0.0	27.8
Output rate of AKG.snk	1.4	0.0	3.2
Output rate of Pyr.snk	137.9	13.5	379.2
Output rate of R5P.snk	3.7	1.0	6.8
Output rate of Ser.snk	0.0	0.0	0.3
Output rate of ATP.Ext	1834.7	1680.6	1964.6
Output rate of Biomass.1	11.0	0.0	40.3
Output rate of Biomass.2	279.9	248.4	310.9
Output rate of X-glc1	100.0	100.0	100.0
Output rate of X-glc2	100.0	100.0	100.0
Output rate of X-ac1	190.1	180.0	194.8
Output rate of X-ac2	61.1	49.8	72.2
Output rate of X-a1	100.0	100.0	100.0
Output rate of X-a2	100.0	100.0	100.0
Output rate of X-a3	100.0	100.0	100.0
Output rate of X-Norm	100.0	100.0	100.0
Net production rate of ADP.1	-1203.1	-1247	-1118.7
Net production rate of ADP.2	-631.7	-747.5	-506.5

Net production rate of Pi.1	-1203.6	-1246	-1120.6
Net production rate of Pi.2	-644.6	-759.5	-520.6
Fractional labeling of Ala.a1 (data set #1)	0.7	0.5	0.8
Fractional labeling of Gly.a1 (data set #1)	0.5	0.4	0.6
Fractional labeling of Val.a1 (data set #1)	0.0	0.0	0.0
Fractional labeling of Leu.a1 (data set #1)	0.0	0.0	0.0
Fractional labeling of Ile.a1 (data set #1)	0.0	0.0	0.0
Fractional labeling of Met.a1 (data set #1)	0.0	0.0	0.0
Fractional labeling of Ser.a1 (data set #1)	0.8	0.8	1.0
Fractional labeling of Thr.a1 (data set #1)	0.3	0.2	0.3
Fractional labeling of Phe.a1 (data set #1)	0.0	0.0	0.0
Fractional labeling of Asp.a1 (data set #1)	0.5	0.4	0.6
Fractional labeling of Glu.a1 (data set #1)	0.4	0.4	0.5
Fractional labeling of Lys.a1 (data set #1)	0.0	0.0	0.0
Fractional labeling of His.a1 (data set #1)	0.0	0.0	0.0
Fractional labeling of Tyr.a1 (data set #1)	0.3	0.3	0.3
Fractional labeling of R5P.a1 (data set #1)	1.0	0.9	1.0
Fractional labeling of G6P.a1 (data set #1)	0.9	0.9	0.9
Fractional labeling of Ala.a2 (data set #2)	0.7	0.6	0.7
Fractional labeling of Gly.a2 (data set #2)	0.6	0.6	0.7
Fractional labeling of Val.a2 (data set #2)	0.1	0.1	0.1
Fractional labeling of Leu.a2 (data set #2)	0.0	0.0	0.0
Fractional labeling of Ile.a2 (data set #2)	0.0	0.0	0.0
Fractional labeling of Met.a2 (data set #2)	0.5	0.5	0.5
Fractional labeling of Ser.a2 (data set #2)	0.9	0.9	0.9
Fractional labeling of Thr.a2 (data set #2)	0.6	0.6	0.7
Fractional labeling of Phe.a2 (data set #2)	0.0	0.0	0.0
Fractional labeling of Asp.a2 (data set #2)	0.7	0.6	0.7
Fractional labeling of Glu.a2 (data set #2)	0.7	0.7	0.8
Fractional labeling of Lys.a2 (data set #2)	0.2	0.2	0.2
Fractional labeling of His.a2 (data set #2)	0.4	0.4	0.4
Fractional labeling of Tyr.a2 (data set #2)	0.7	0.6	0.7
Fractional labeling of R5P.a2 (data set #2)	1.0	1.0	1.0
Fractional labeling of G6P.a2 (data set #2)	0.9	0.9	0.9
Fractional labeling of Ala.a3 (data set #3)	0.8	0.8	0.8
Fractional labeling of Gly.a3 (data set #3)	0.8	0.8	0.8

Fractional labeling of Val.a3 (data set #3)	0.5	0.5	0.5
Fractional labeling of Leu.a3 (data set #3)	0.5	0.5	0.5
Fractional labeling of Ile.a3 (data set #3)	0.5	0.5	0.5
Fractional labeling of Met.a3 (data set #3)	0.7	0.7	0.7
Fractional labeling of Ser.a3 (data set #3)	0.9	0.9	1.0
Fractional labeling of Thr.a3 (data set #3)	0.8	0.8	0.8
Fractional labeling of Phe.a3 (data set #3)	0.4	0.4	0.4
Fractional labeling of Asp.a3 (data set #3)	0.8	0.8	0.8
Fractional labeling of Glu.a3 (data set #3)	0.9	0.8	0.9
Fractional labeling of Lys.a3 (data set #3)	0.6	0.5	0.6
Fractional labeling of His.a3 (data set #3)	0.6	0.6	0.6
Fractional labeling of Tyr.a3 (data set #3)	0.8	0.8	0.8
Fractional labeling of R5P.a3 (data set #3)	1.0	1.0	1.0
Fractional labeling of G6P.a3 (data set #3)	1.0	1.0	1.0

Table D.5 Results of ^{13}C-MFA for *E. coli* grown on 1.7 g/L [1,2-^{13}C]glucose + 1 g/L yeast extract. The fluxes are normalized to a substrate uptake rate of 100. 95% confidence intervals of fluxes were determined by evaluating the sensitivity of the minimized SSR to flux variations.

Fit for *E. coli* 2 g/L [12]Gluc + 1 g/L YE			
Number of fitted data sets :			3
Number of fitted measurements :			498
SSR :			223
Flux	best fit	LB95	UB95
G6P.1 <=> F6P.1 (net)	81.8	78.2	85.6
G6P.1 <=> F6P.1 (exch)	139.9	85.8	289.7
G6P.2 <=> F6P.2 (net)	66.7	61.4	71.1
G6P.2 <=> F6P.2 (exch)	818.4	269.2	10964.9
F6P.1 + ATP.1 -> FBP.1 + ADP.1	93.4	90.6	95.1
F6P.2 + ATP.2 -> FBP.2 + ADP.2	83.1	81.0	85.2
FBP.1 <=> DHAP.1 + GAP.1 (net)	93.4	90.6	95.1
FBP.1 <=> DHAP.1 + GAP.1 (exch)	417.8	0.0	100418.0
FBP.2 <=> DHAP.2 + GAP.2 (net)	83.1	81.0	85.2
FBP.2 <=> DHAP.2 + GAP.2 (exch)	148.5	0.0	100149.0
DHAP.1 <=> GAP.1 (net)	93.4	90.6	95.1

DHAP.1 <=> GAP.1 (exch)	254.7	0.0	100255.0
DHAP.2 <=> GAP.2 (net)	83.1	81.0	85.2
DHAP.2 <=> GAP.2 (exch)	0.2	0.0	100000.0
GAP.1 + NAD.1 + ADP.1 + Pi.1 <=> 3PG.1 + ATP.1 + NADH.1 (net)	193.0	189.7	195.0
GAP.1 + NAD.1 + ADP.1 + Pi.1 <=> 3PG.1 + ATP.1 + NADH.1 (exch)	598.4	0.0	100598.0
GAP.2 + NAD.2 + ADP.2 + Pi.2 <=> 3PG.2 + ATP.2 + NADH.2 (net)	173.0	169.9	176.3
GAP.2 + NAD.2 + ADP.2 + Pi.2 <=> 3PG.2 + ATP.2 + NADH.2 (exch)	22657.0	1122.8	33402.2
3PG.1 <=> PEP.1 (net)	192.6	188.3	194.7
3PG.1 <=> PEP.1 (exch)	576.7	0.0	100577.0
3PG.2 <=> PEP.2 (net)	161.9	157.5	166.6
3PG.2 <=> PEP.2 (exch)	23707.5	910.9	34086.5
PEP.1 + ADP.1 -> Pyr.1 + ATP.1	91.6	63.4	94.5
PEP.2 + ADP.2 -> Pyr.2 + ATP.2	38.2	30.7	46.6
G6P.1 + NADP.1 -> 6PG.1 + NADPH.1	18.2	14.4	21.7
G6P.2 + NADP.2 -> 6PG.2 + NADPH.2	32.0	27.7	37.2
6PG.1 + NADP.1 -> Ru5P.1 + CO2.1 + NADPH.1	17.7	14.1	21.1
6PG.2 + NADP.2 -> Ru5P.2 + CO2.2 + NADPH.2	32.0	27.7	37.2
Ru5P.1 <=> X5P.1 (net)	11.6	9.2	13.9
Ru5P.1 <=> X5P.1 (exch)	61.5	22.1	10079.8
Ru5P.2 <=> X5P.2 (net)	16.9	14.3	20.3
Ru5P.2 <=> X5P.2 (exch)	52.4	42.3	63.9
Ru5P.1 <=> R5P.1 (net)	6.1	4.8	7.3
Ru5P.1 <=> R5P.1 (exch)	519.8	7.2	11295.7
Ru5P.2 <=> R5P.2 (net)	15.1	13.2	17.0
Ru5P.2 <=> R5P.2 (exch)	1966.2	20.0	12688.8
X5P.1 <=> GAP.1 + E-C2.1 (net)	11.6	9.2	13.9
X5P.1 <=> GAP.1 + E-C2.1 (exch)	57.6	22.1	10120.8
X5P.2 <=> GAP.2 + E-C2.2 (net)	16.9	14.3	20.3
X5P.2 <=> GAP.2 + E-C2.2 (exch)	18589.9	45.3	28780.8
F6P.1 <=> E4P.1 + E-C2.1 (net)	-5.8	-6.9	-4.5
F6P.1 <=> E4P.1 + E-C2.1 (exch)	10.7	7.7	14.5
F6P.2 <=> E4P.2 + E-C2.2 (net)	-7.3	-8.9	-6.0
F6P.2 <=> E4P.2 + E-C2.2 (exch)	11.1	8.9	14.7

S7P.1 <=> R5P.1 + E-C2.1 (net)	-5.9	-7.0	-4.7
S7P.1 <=> R5P.1 + E-C2.1 (exch)	93.4	0.0	10384.9
S7P.2 <=> R5P.2 + E-C2.2 (net)	-9.6	-11.3	-8.3
S7P.2 <=> R5P.2 + E-C2.2 (exch)	0.0	0.0	4.0
F6P.1 <=> GAP.1 + E-C3.1 (net)	-5.9	-7.0	-4.7
F6P.1 <=> GAP.1 + E-C3.1 (exch)	28.8	17.9	49.1
F6P.2 <=> GAP.2 + E-C3.2 (net)	-9.6	-11.3	-8.3
F6P.2 <=> GAP.2 + E-C3.2 (exch)	47.8	37.8	69.6
S7P.1 <=> E4P.1 + E-C3.1 (net)	5.9	4.7	7.0
S7P.1 <=> E4P.1 + E-C3.1 (exch)	0.0	0.0	11064.3
S7P.2 <=> E4P.2 + E-C3.2 (net)	9.6	8.3	11.3
S7P.2 <=> E4P.2 + E-C3.2 (exch)	494.6	0.0	100495.0
6PG.1 -> KDPG.1	0.5	0.0	3.5
6PG.2 -> KDPG.2	0.0	0.0	1.0
KDPG.1 -> GAP.1 + Pyr.1	0.5	0.0	3.5
KDPG.2 -> GAP.2 + Pyr.2	0.0	0.0	1.0
Pyr.1 + NAD.1 -> AcCoA.1 + CO2.1 + NADH.1	191.5	183.7	194.5
Pyr.2 + NAD.2 -> AcCoA.2 + CO2.2 + NADH.2	120.9	111.3	131.4
AcCoA.1 + OAC.1 -> Cit.1	0.5	0.0	10.4
AcCoA.2 + OAC.2 -> Cit.2	40.4	31.1	50.0
Cit.1 <=> ICit.1 (net)	0.5	0.0	10.4
Cit.1 <=> ICit.1 (exch)	268.0	0.0	100268.0
Cit.2 <=> ICit.2 (net)	40.4	31.1	50.0
Cit.2 <=> ICit.2 (exch)	206.3	0.0	100206.0
ICit.1 + NADP.1 <=> AKG.1 + CO2.1 + NADPH.1 (net)	0.5	0.0	10.4
ICit.1 + NADP.1 <=> AKG.1 + CO2.1 + NADPH.1 (exch)	325.3	0.0	17404.8
ICit.2 + NADP.2 <=> AKG.2 + CO2.2 + NADPH.2 (net)	40.1	28.6	50.0
ICit.2 + NADP.2 <=> AKG.2 + CO2.2 + NADPH.2 (exch)	32.7	0.0	15263.8
AKG.1 + NAD.1 -> SucCoA.1 + CO2.1 + NADH.1	0.2	0.0	10.1
AKG.2 + NAD.2 -> SucCoA.2 + CO2.2 + NADH.2	33.1	21.0	43.5
SucCoA.1 + ADP.1 + Pi.1 <=> Suc.1 + ATP.1 (net)	0.1	-0.4	10.0
SucCoA.1 + ADP.1 + Pi.1 <=> Suc.1 + ATP.1 (exch)	255.0	0.0	100255.0
SucCoA.2 + ADP.2 + Pi.2 <=> Suc.2 + ATP.2 (net)	30.0	17.7	40.7

SucCoA.2 + ADP.2 + Pi.2 <=> Suc.2 + ATP.2 (exch)	239.2	0.0	100239.0
Suc.1 + FAD.1 <=> Fum.1 + FADH2.1 (net)	0.2	0.0	10.2
Suc.1 + FAD.1 <=> Fum.1 + FADH2.1 (exch)	329.9	0.0	100330.0
Suc.2 + FAD.2 <=> Fum.2 + FADH2.2 (net)	33.3	23.6	43.5
Suc.2 + FAD.2 <=> Fum.2 + FADH2.2 (exch)	62.3	0.0	100062.0
Fum.1 <=> Mal.1 (net)	0.3	0.0	10.2
Fum.1 <=> Mal.1 (exch)	740.5	0.0	16845.2
Fum.2 <=> Mal.2 (net)	35.3	25.7	45.3
Fum.2 <=> Mal.2 (exch)	111.2	45.3	498.4
Mal.1 + NAD.1 <=> OAC.1 + NADH.1 (net)	0.3	-0.1	10.3
Mal.1 + NAD.1 <=> OAC.1 + NADH.1 (exch)	60.9	0.0	12689.2
Mal.2 + NAD.2 <=> OAC.2 + NADH.2 (net)	35.6	26.7	45.3
Mal.2 + NAD.2 <=> OAC.2 + NADH.2 (exch)	1986.4	52.2	12923.3
ICit.1 <=> Glyox.1 + Suc.1 (net)	0.0	0.0	3.9
ICit.1 <=> Glyox.1 + Suc.1 (exch)	0.0	0.0	1.1
ICit.2 <=> Glyox.2 + Suc.2 (net)	0.3	0.0	5.1
ICit.2 <=> Glyox.2 + Suc.2 (exch)	0.0	0.0	3.5
AcCoA.1 + Glyox.1 -> Mal.1	0.0	0.0	3.9
AcCoA.2 + Glyox.2 -> Mal.2	0.3	0.0	5.1
Mal.1 + NADP.1 -> Pyr.1 + CO2.1 + NADPH.1	0.0	0.0	33.0
Mal.2 + NADP.2 -> Pyr.2 + CO2.2 + NADPH.2	0.0	0.0	3.2
PEP.1 + CO2.1 -> OAC.1 + Pi.1	0.7	0.0	49.2
PEP.2 + CO2.2 -> OAC.2 + Pi.2	37.8	28.1	47.4
OAC.1 + ATP.1 -> PEP.1 + CO2.1 + ADP.1	0.0	0.0	47.5
OAC.2 + ATP.2 -> PEP.2 + CO2.2 + ADP.2	19.2	7.8	29.9
AcCoA.1 + ADP.1 + Pi.1 <=> Ac.1 + ATP.1 (net)	190.1	178.4	194.4
AcCoA.1 + ADP.1 + Pi.1 <=> Ac.1 + ATP.1 (exch)	231.4	0.0	100231.0
AcCoA.2 + ADP.2 + Pi.2 <=> Ac.2 + ATP.2 (net)	57.7	46.4	69.5
AcCoA.2 + ADP.2 + Pi.2 <=> Ac.2 + ATP.2 (exch)	339.2	0.0	100339.0
AKG.1 + NADPH.1 + NH3.1 -> Glu.1 + NADP.1	1.6	0.0	6.3
AKG.2 + NADPH.2 + NH3.2 -> Glu.2 + NADP.2	41.8	35.7	47.5
Glu.1 + ATP.1 + NH3.1 -> Gln.1 + ADP.1 + Pi.1	0.2	0.0	0.6
Glu.2 + ATP.2 + NH3.2 -> Gln.2 + ADP.2 + Pi.2	4.0	3.4	4.5
Glu.1 + 2 NADPH.1 + ATP.1 -> Pro.1 + 2 NADP.1 + ADP.1 + Pi.1	0.1	0.0	0.2
Glu.2 + 2 NADPH.2 + ATP.2 -> Pro.2 + 2 NADP.2	1.4	1.2	1.6

+ Pi.2 + ADP.2			
Glu.1 + CO2.1 + Gln.1 + NADPH.1 + Asp.1 + AcCoA.1 + 5 ATP.1 -> Arg.1 + AKG.1 + Fum.1 + Ac.1	0.1	0.0	0.3
Glu.2 + CO2.2 + Gln.2 + NADPH.2 + Asp.2 + AcCoA.2 + 5 ATP.2 -> Arg.2 + AKG.2 + Fum.2 + Ac.2	1.8	1.6	2.1
OAC.1 + Glu.1 -> Asp.1 + AKG.1	0.4	0.0	1.7
OAC.2 + Glu.2 -> Asp.2 + AKG.2	11.6	9.8	13.3
Asp.1 + NH3.1 + 2 ATP.1 -> Asn.1 + 2 ADP.1 + 2 Pi.1	0.1	0.0	0.2
Asp.2 + NH3.2 + 2 ATP.2 -> Asn.2 + 2 ADP.2 + 2 Pi.2	1.5	1.3	1.7
Pyr.1 + Glu.1 -> Ala.1 + AKG.1	0.1	0.0	0.5
Pyr.2 + Glu.2 -> Ala.2 + AKG.2	3.2	2.7	3.6
3PG.1 + Glu.1 + NAD.1 -> Ser.1 + NADH.1 + AKG.1 + Pi.1	0.3	0.0	1.1
3PG.2 + Glu.2 + NAD.2 -> Ser.2 + NADH.2 + AKG.2 + Pi.2	7.1	6.1	8.0
Ser.1 + THF.1 <=> Gly.1 + MEETHF.1 (net)	0.2	0.0	0.6
Ser.1 + THF.1 <=> Gly.1 + MEETHF.1 (exch)	0.0	0.0	0.1
Ser.2 + THF.2 <=> Gly.2 + MEETHF.2 (net)	3.8	3.3	4.4
Ser.2 + THF.2 <=> Gly.2 + MEETHF.2 (exch)	2.0	1.6	2.5
Gly.1 + THF.1 + NAD.1 <=> CO2.1 + MEETHF.1 + NH3.1 + NADH.1 (net)	0.0	0.0	0.4
Gly.1 + THF.1 + NAD.1 <=> CO2.1 + MEETHF.1 + NH3.1 + NADH.1 (exch)	562.6	562.6	19454.3
Gly.2 + THF.2 + NAD.2 <=> CO2.2 + MEETHF.2 + NH3.2 + NADH.2 (net)	0.2	0.1	0.4
Gly.2 + THF.2 + NAD.2 <=> CO2.2 + MEETHF.2 + NH3.2 + NADH.2 (exch)	0.0	0.0	1.1
Thr.1 + NAD.1 -> Gly.1 + AcCoA.1 + NADH.1	0.0	0.0	0.6
Thr.2 + NAD.2 -> Gly.2 + AcCoA.2 + NADH.2	0.1	0.0	0.6
Ser.1 + AcCoA.1 + SO4.1 + 3 ATP.1 + 4 NADPH.1 -> Cys.1 + Ac.1 + 4 NADP.1 + 3ADP.1	0.1	0.0	0.2
Ser.2 + AcCoA.2 + SO4.2 + 3 ATP.2 + 4 NADPH.2 -> Cys.2 + Ac.2 + 4 NADP.2 + 3ADP.2	1.5	1.3	1.7
Asp.1 + Pyr.1 + Glu.1 + 2 NADPH.1 + ATP.1 + SucCoA.1 -> LL-DAP.1 + AKG.1 + Suc.1 + 2NADP.1 + ADP.1	0.1	0.0	0.3

Asp.2 + Pyr.2 + Glu.2 + 2 NADPH.2 + ATP.2 + SucCoA.2 -> LL-DAP.2 + AKG.2 + Suc.2 + 2NADP.2 + ADP.2	2.1	1.8	2.4
LL-DAP.1 -> Lys.1 + CO2.1	0.1	0.0	0.3
LL-DAP.2 -> Lys.2 + CO2.2	2.1	1.8	2.4
Asp.1 + 2 NADPH.1 + 2 ATP.1 -> Thr.1 + 2 NADP.1 + 2 ADP.1 + 2 Pi.1	0.1	0.0	1.1
Asp.2 + 2 NADPH.2 + 2 ATP.2 -> Thr.2 + 2 NADP.2 + 2 ADP.2 + 2 Pi.2	3.5	2.9	4.3
Asp.1 + METHF.1 + Cys.1 + 2 NADPH.1 + ATP.1 + SucCoA.1 -> Met.1 + Pyr.1 + Suc.1 + NH3.1 + 2NADP.1 + ADP.1	0.0	0.0	0.1
Asp.2 + METHF.2 + Cys.2 + 2 NADPH.2 + ATP.2 + SucCoA.2 -> Met.2 + Pyr.2 + Suc.2 + NH3.2 + 2NADP.2 + ADP.2	1.0	0.8	1.1
2 Pyr.1 + NADPH.1 + Glu.1 -> Val.1 + CO2.1 + NADP.1 + AKG.1	0.1	0.0	0.4
2 Pyr.2 + NADPH.2 + Glu.2 -> Val.2 + CO2.2 + NADP.2 + AKG.2	2.6	2.3	3.0
2 Pyr.1 + AcCoA.1 + Glu.1 + NADPH.1 + NAD.1 -> Leu.1 + 2 CO2.1 + AKG.1 + NA	0.1	0.0	0.4
2 Pyr.2 + AcCoA.2 + Glu.2 + NADPH.2 + NAD.2 -> Leu.2 + 2 CO2.2 + AKG.2 + NA	2.8	2.4	3.2
Thr.1 + Pyr.1 + Glu.1 + NADPH.1 -> Ile.1 + CO2.1 + AKG.1 + NADP.1 + NH3.1	0.1	0.0	0.3
Thr.2 + Pyr.2 + Glu.2 + NADPH.2 -> Ile.2 + CO2.2 + AKG.2 + NADP.2 + NH3.2	1.8	1.6	2.1
E4P.1 + 2 PEP.1 + Glu.1 + NADPH.1 + ATP.1 -> Phe.1 + CO2.1 + AKG.1 + NADP.1	0.0	0.0	0.2
E4P.2 + 2 PEP.2 + Glu.2 + NADPH.2 + ATP.2 -> Phe.2 + CO2.2 + AKG.2 + NADP.2	1.2	1.0	1.3
E4P.1 + 2 PEP.1 + Glu.1 + NADPH.1 + NAD.1 + ATP.1 -> Tyr.1 + CO2.1 + AKG.1 + NADH.1	0.0	0.0	0.1
E4P.2 + 2 PEP.2 + Glu.2 + NADPH.2 + NAD.2 + ATP.2 -> Tyr.2 + CO2.2 + AKG.2 + NADH.2	0.9	0.7	1.0
E4P.1 + 2 PEP.1 + R5P.1 + Ser.1 + Gln.1 + NADPH.1 + 3 ATP.1 -> Trp.1 + CO2.1 + GAP.1 + Pyr.1 + Glu.1	0.0	0.0	0.1
E4P.2 + 2 PEP.2 + R5P.2 + Ser.2 + Gln.2 + NADPH.2 + 3 ATP.2 -> Trp.2 + CO2.2 + GAP.2 + Pyr.2 + Glu.2	0.4	0.3	0.4
R5P.1 + FTHF.1 + Gln.1 + Asp.1 + 5 ATP.1 + 2	0.0	0.0	0.0

NAD.1 -> His.1 + 2 NADH.1 + AKG.1 + Fum.1 + 2NADH.1			
R5P.2 + FTHF.2 + Gln.2 + Asp.2 + 5 ATP.2 + 2 NAD.2 -> His.2 + 2 NADH.2 + AKG.2 + Fum.2 + 2NADH.2	0.1	0.1	0.1
MEETHF.1 + NADH.1 -> METHF.1 + NAD.1	0.0	0.0	0.1
MEETHF.2 + NADH.2 -> METHF.2 + NAD.2	1.0	0.8	1.1
MEETHF.1 + NADP.1 -> FTHF.1 + NADPH.1	0.0	0.0	0.0
MEETHF.2 + NADP.2 -> FTHF.2 + NADPH.2	0.1	0.1	0.1
NADH.1 + NADP.1 <=> NADPH.1 + NAD.1 (net)	-32.1	-50.9	-19.6
NADH.1 + NADP.1 <=> NADPH.1 + NAD.1 (exch)	17.0	0.0	535.6
NADH.2 + NADP.2 <=> NADPH.2 + NAD.2 (net)	6.3	-13.6	28.7
NADH.2 + NADP.2 <=> NADPH.2 + NAD.2 (exch)	37.1	0.0	100037.0
0.488Ala.1+0.281Arg.1+0.229Asn.1+0.229Asp.1+ 0.087Cys.1+0.250Glu.1+0.250Gln.1+0.582Gly.1+ 0.09His.1+0.276Ile.1+0.428Leu.1+0.326Lys.1+0.146 Met.1 + 0.176Phe.1+0.210Pro.1 + 0.205Ser.1 + 0.241 Thr.1 + 0.054 Trp.1 +0.131Tyr.1+0.402Val.1 + 0.205 G6P.1 +0.071F6P.1+0.754R5P.1 + 0.129 GAP.1 + 0.619 3PG.1 +0.051PEP.1 + 0.083 Pyr.1 +2.510AcCoA.1+ 0.087AKG.1 + 0.340 OAC.1 + 0.443MEETHF.1+33.247ATP.1+5.363NADPH.1 → 39.68Biomass.1 + 1.455NADH.1	0.3	0.0	1.0
0.488Ala.2+0.281Arg.2+0.229Asn.2+0.229Asp.2+ 0.087Cys.2+0.250Glu.2+0.250Gln.2+0.582Gly.2+ 0.09His.2+0.276Ile.2+0.428Leu.2+0.326Lys.2+0.146 Met.2 + 0.176Phe.2+0.210Pro.2 + 0.205Ser.2 + 0.241 Thr.2 + 0.054 Trp.2 +0.131Tyr.2+0.402Val.2 + 0.205 G6P.2 +0.071F6P.2+0.754R5P.2 + 0.129 GAP.2 + 0.619 3PG.2 +0.051PEP.2 + 0.083 Pyr.2 +2.510AcCoA.2+ 0.087AKG.2 + 0.340 OAC.2 + 0.443MEETHF.2+33.247ATP.2+5.363NADPH.2 → 39.68Biomass.2 + 1.455NADH.2	6.6	5.6	7.5
ATP.1 -> ATP.Ext	1207.5	1126.1	1240.8
ATP.2 -> ATP.Ext	728.1	586.2	875.7
Ac.1 -> Ac.Ext + X-ac1	190.2	178.9	194.4
Ac.2 -> Ac.Ext + X-ac2	61.1	50.1	72.6
CO2.1 -> CO2.Ext	209.6	202.3	226.2
CO2.2 -> CO2.Ext	220.3	195.9	245.9
O2.Ext -> O2.1	209.0	200.1	224.5

O2.Ext -> O2.2	204.8	178.7	232.2
NH3.Ext -> NH3.1	1.7	0.0	6.7
NH3.Ext -> NH3.2	44.3	38.0	50.4
SO4.Ext -> SO4.1	0.1	0.0	0.2
SO4.Ext -> SO4.2	1.5	1.3	1.7
NADH.1 + 0.5 O2.1 + 2 ADP.1 + 2 Pi.1 -> NAD.1 + 2 ATP.1	417.8	399.8	439.1
NADH.2 + 0.5 O2.2 + 2 ADP.2 + 2 Pi.2 -> NAD.2 + 2 ATP.2	376.2	332.8	421.6
FADH2.1 + 0.5 O2.1 + ADP.1 + Pi.1 -> FAD.1 + ATP.1	0.2	0.0	10.2
FADH2.2 + 0.5 O2.2 + ADP.2 + Pi.2 -> FAD.2 + ATP.2	33.3	23.6	43.5
Ala.a1 + Gly.a1 + Val.a1 + Leu.a1 + Ile.a1 + Pro.a1 + Met.a1 + Ser.a1 + Thr.a1 + Phe.a1 + Asp.a1 + Glu.a1 + Lys.a1 + His.a1 + Tyr.a1 + G6P.a1 + R5P.a1 → X-a1	100.0	100.0	100.0
Ala.a2 + Gly.a2 + Val.a2 + Leu.a2 + Ile.a2 + Pro.a2 + Met.a2 + Ser.a2 + Thr.a2 + Phe.a2 + Asp.a2 + Glu.a2 + Lys.a2 + His.a2 + Tyr.a2 + G6P.a2 + R5P.a2 → X-a2	100.0	100.0	100.0
Ala.a3 + Gly.a3 + Val.a3 + Leu.a3 + Ile.a3 + Pro.a3 + Met.a3 + Ser.a3 + Thr.a3 + Phe.a3 + Asp.a3 + Glu.a3 + Lys.a3 + His.a3 + Tyr.a3 + G6P.a3 + R5P.a3 → X-a3	100.0	100.0	100.0
Ala.1 + Gly.1 + Val.1 + Leu.1 + Ile.1 + Pro.1 + Met.1 + Ser.1 + Thr.1 + Phe.1 + Asp.1 + Glu.1 + Lys.1 + His.1 + Tyr.1 + G6P.1 + R5P.1 → Ala.a1 + Gly.a1 + Val.a1 + Leu.a1 + Ile.a1 + Pro.a1 + Met.a1 + Ser.a1 + Thr.a1 + Phe.a1 + Asp.a1 + Glu.a1 + Lys.a1 + His.a1 + Tyr.a1 + G6P.a1 + R5P.a1 + Ala.1 + Gly.1 + Val.1 + Leu.1 + Ile.1 + Pro.1 + Met.1 + Ser.1 + Thr.1 + Phe.1 + Asp.1 + Glu.1 + Lys.1 + His.1 + Tyr.1 + G6P.1 + R5P.1	90.5	79.9	100.0
Ala.1 + Gly.1 + Val.1 + Leu.1 + Ile.1 + Pro.1 + Met.1 + Ser.1 + Thr.1 + Phe.1 + Asp.1 + Glu.1 + Lys.1 + His.1 + Tyr.1 + G6P.1 + R5P.1 → Ala.a2 + Gly.a2 + Val.a2 + Leu.a2 + Ile.a2 + Pro.a2 + Met.a2 + Ser.a2 + Thr.a2 + Phe.a2 + Asp.a2 + Glu.a2 + Lys.a2 + His.a2 + Tyr.a2 + G6P.a2 + R5P.a2 + Ala.1 + Gly.1 + Val.1 + Leu.1 + Ile.1 + Pro.1 + Met.1 + Ser.1 + Thr.1 + Phe.1 + Asp.1 + Glu.1 + Lys.1 +	51.6	41.8	62.5

His.1 + Tyr.1 + G6P.1 + R5P.1			
Ala.1 + Gly.1 + Val.1 + Leu.1 + Ile.1 + Pro.1 +Met.1 + Ser.1 + Thr.1 + Phe.1 + Asp.1 + Glu.1 + Lys.1 + His.1 + Tyr.1 + G6P.1 + R5P.1 → Ala.a3 + Gly.a3 + Val.a3 + Leu.a3 + Ile.a3 + Pro.a3 + Met.a3 + Ser.a3 + Thr.a3 + Phe.a3 + Asp.a3 + Glu.a3 + Lys.a3 + His.a3 + Tyr.a3 + G6P.a3 + R5P.a3 + Ala.1 + Gly.1 + Val.1 + Leu.1 + Ile.1 + Pro.1 + Met.1 + Ser.1 + Thr.1 + Phe.1 + Asp.1 + Glu.1 + Lys.1 + His.1 + Tyr.1 + G6P.1 + R5P.1	6.8	0.0	23.6
Ala.2 + Gly.2 + Val.2 + Leu.2 + Ile.2 + Pro.2 + Met.2 + Ser.2 + Thr.2 + Phe.2 + Asp.2 + Glu.2 + Lys.2 + His.2 + Tyr.2 + G6P.2 + R5P.2 → Ala.a1 + Gly.a1 + Val.a1 + Leu.a1 + Ile.a1 + Pro.a1 + Met.a1 + Ser.a1 + Thr.a1 + Phe.a1 + Asp.a1 + Glu.a1 + Lys.a1 + His.a1 + Tyr.a1 + G6P.a1 + R5P.a1 + Ala.2 + Gly.2 + Val.2 + Leu.2 + Ile.2 + Pro.2 + Met.2 + Ser.2 + Thr.2 + Phe.2 + Asp.2 + Glu.2 + Lys.2 + His.2 + Tyr.2 + G6P.2 + R5P.2	9.5	0.0	20.1
Ala.2 + Gly.2 + Val.2 + Leu.2 + Ile.2 + Pro.2 + Met.2 + Ser.2 + Thr.2 + Phe.2 + Asp.2 + Glu.2 + Lys.2 + His.2 + Tyr.2 + G6P.2 + R5P.2 → Ala.a2 + Gly.a2 + Val.a2 + Leu.a2 + Ile.a2 + Pro.a2 + Met.a2 + Ser.a2 + Thr.a2 + Phe.a2 + Asp.a2 + Glu.a2 + Lys.a2 + His.a2 + Tyr.a2 + G6P.a2 + R5P.a2 + Ala.2 + Gly.2 + Val.2 + Leu.2 + Ile.2 + Pro.2 + Met.2 + Ser.2 + Thr.2 + Phe.2 + Asp.2 + Glu.2 + Lys.2 + His.2 + Tyr.2 + G6P.2 + R5P.2	48.4	37.5	58.2
Ala.2 + Gly.2 + Val.2 + Leu.2 + Ile.2 + Pro.2 + Met.2 + Ser.2 + Thr.2 + Phe.2 + Asp.2 + Glu.2 + Lys.2 + His.2 + Tyr.2 + G6P.2 + R5P.2 → Ala.a3 + Gly.a3 + Val.a3 + Leu.a3 + Ile.a3 + Pro.a3 + Met.a3 + Ser.a3 + Thr.a3 + Phe.a3 + Asp.a3 + Glu.a3 + Lys.a3 + His.a3 + Tyr.a3 + G6P.a3 + R5P.a3 + Ala.2 + Gly.2 + Val.2 + Leu.2 + Ile.2 + Pro.2 + Met.2 + Ser.2 + Thr.2 + Phe.2 + Asp.2 + Glu.2 + Lys.2 + His.2 + Tyr.2 + G6P.2 + R5P.2	93.2	76.4	100.0
PEP.1 + 2 Gluc.Ext + PEP.2 -> G6P.1 + Pyr.1 + G6P.2 + Pyr.2 + X-glc1 + X-gluc2	100.0	100.0	100.0
CO2.M0 + CO2.1 -> CO2.1 + CO2.snk	1417.1	326.1	11433.2
CO2.M0 + CO2.2 -> CO2.2 + CO2.snk	81.7	27.9	184.5
Pyr.M0 + Pyr.1 -> Pyr.1 + Pyr.snk	0.0	0.0	241.5

Pyr.M0 + Pyr.2 -> Pyr.2 + Pyr.snk	13.0	1.5	22.2
OAC.M0 + OAC.1 -> OAC.1 + OAC.snk	1.2	0.0	67.5
AKG.M0 + AKG.1 -> AKG.1 + AKG.snk	0.4	0.0	14.0
AKG.M0 + AKG.2 -> AKG.2 + AKG.snk	3.6	0.0	10.6
Ser.M0 + Ser.1 -> Ser.1 + Ser.snk	0.1	0.0	0.5
R5P.M0 + R5P.1 -> R5P.1 + R5P.snk	2.8	1.0	5.8
R5P.M0 + R5P.2 -> R5P.2 + R5P.snk	1.7	0.0	3.6
Uptake rate of CO2.M0	1498.8	396.1	9166.8
Uptake rate of Gluc.Ext	200.0	200.0	200.0
Uptake rate of OAC.M0	1.2	0.0	67.5
Uptake rate of AKG.M0	4.0	0.0	20.1
Uptake rate of Pyr.M0	13.0	1.7	253.6
Uptake rate of R5P.M0	4.4	2.1	7.8
Uptake rate of Ser.M0	0.1	0.0	0.5
Uptake rate of O2.Ext	413.8	385.8	444.8
Uptake rate of NH3.Ext	46.0	38.8	53.8
Uptake rate of SO4.Ext	1.6	1.3	1.9
Output rate of Ac.Ext	251.3	235.7	265.7
Output rate of CO2.Ext	429.9	404.3	459.4
Output rate of CO2.snk	1498.8	396.1	9166.8
Output rate of OAC.snk	1.2	0.0	67.5
Output rate of AKG.snk	4.0	0.0	20.1
Output rate of Pyr.snk	13.0	1.7	253.6
Output rate of R5P.snk	4.4	2.1	7.8
Output rate of Ser.snk	0.1	0.0	0.5
Output rate of ATP.Ext	1935.6	1771.5	2092.9
Output rate of Biomass.1	10.1	0.0	39.1
Output rate of Biomass.2	260.3	223.0	296.1
Output rate of X-glc1	100.0	100.0	100.0
Output rate of X-glc2	100.0	100.0	100.0
Output rate of X-ac1	190.2	178.9	194.4
Output rate of X-ac2	61.1	50.1	72.6
Output rate of X-a1	100.0	100.0	100.0
Output rate of X-a2	100.0	100.0	100.0
Output rate of X-a3	100.0	100.0	100.0
Output rate of X-Norm	100.0	100.0	100.0

Net production rate of ADP.1	-1207.5	-1241	-1126.1
Net production rate of ADP.2	-728.1	-875.7	-586.2
Net production rate of Pi.1	-1208.0	-1241	-1128.0
Net production rate of Pi.2	-740.1	-886.4	-599.9
Fractional labeling of Ala.a1 (data set #1)	0.5	0.5	1.0
Fractional labeling of Gly.a1 (data set #1)	0.4	0.3	0.5
Fractional labeling of Val.a1 (data set #1)	0.0	0.0	0.0
Fractional labeling of Leu.a1 (data set #1)	0.0	0.0	0.0
Fractional labeling of Ile.a1 (data set #1)	0.0	0.0	0.0
Fractional labeling of Met.a1 (data set #1)	0.0	0.0	0.0
Fractional labeling of Ser.a1 (data set #1)	1.0	0.9	1.0
Fractional labeling of Thr.a1 (data set #1)	0.0	0.0	0.0
Fractional labeling of Phe.a1 (data set #1)	0.0	0.0	0.0
Fractional labeling of Asp.a1 (data set #1)	0.5	0.4	0.7
Fractional labeling of Glu.a1 (data set #1)	0.3	0.2	0.5
Fractional labeling of Lys.a1 (data set #1)	0.0	0.0	0.0
Fractional labeling of His.a1 (data set #1)	0.0	0.0	0.0
Fractional labeling of Tyr.a1 (data set #1)	0.0	0.0	0.0
Fractional labeling of R5P.a1 (data set #1)	0.9	0.9	1.0
Fractional labeling of G6P.a1 (data set #1)	0.9	0.9	0.9
Fractional labeling of Ala.a2 (data set #2)	0.4	0.4	0.6
Fractional labeling of Gly.a2 (data set #2)	0.5	0.4	0.5
Fractional labeling of Val.a2 (data set #2)	0.0	0.0	0.0
Fractional labeling of Leu.a2 (data set #2)	0.0	0.0	0.0
Fractional labeling of Ile.a2 (data set #2)	0.0	0.0	0.0
Fractional labeling of Met.a2 (data set #2)	0.1	0.1	0.1
Fractional labeling of Ser.a2 (data set #2)	0.9	0.9	1.0
Fractional labeling of Thr.a2 (data set #2)	0.5	0.4	0.5
Fractional labeling of Phe.a2 (data set #2)	0.0	0.0	0.0
Fractional labeling of Asp.a2 (data set #2)	0.6	0.5	0.7
Fractional labeling of Glu.a2 (data set #2)	0.6	0.5	0.8
Fractional labeling of Lys.a2 (data set #2)	0.1	0.0	0.1
Fractional labeling of His.a2 (data set #2)	0.0	0.0	0.0
Fractional labeling of Tyr.a2 (data set #2)	0.4	0.4	0.4
Fractional labeling of R5P.a2 (data set #2)	1.0	0.9	1.0
Fractional labeling of G6P.a2 (data set #2)	0.9	0.9	0.9

Fractional labeling of Ala.a3 (data set #3)	0.7	0.6	0.7
Fractional labeling of Gly.a3 (data set #3)	0.6	0.6	0.6
Fractional labeling of Val.a3 (data set #3)	0.1	0.1	0.1
Fractional labeling of Leu.a3 (data set #3)	0.0	0.0	0.0
Fractional labeling of Ile.a3 (data set #3)	0.0	0.0	0.0
Fractional labeling of Met.a3 (data set #3)	0.5	0.4	0.5
Fractional labeling of Ser.a3 (data set #3)	0.9	0.9	0.9
Fractional labeling of Thr.a3 (data set #3)	0.6	0.6	0.7
Fractional labeling of Phe.a3 (data set #3)	0.0	0.0	0.0
Fractional labeling of Asp.a3 (data set #3)	0.6	0.6	0.7
Fractional labeling of Glu.a3 (data set #3)	0.8	0.7	0.9
Fractional labeling of Lys.a3 (data set #3)	0.2	0.2	0.2
Fractional labeling of His.a3 (data set #3)	0.3	0.3	0.3
Fractional labeling of Tyr.a3 (data set #3)	0.6	0.6	0.7
Fractional labeling of R5P.a3 (data set #3)	1.0	0.9	1.0
Fractional labeling of G6P.a3 (data set #3)	1.0	1.0	1.0

Table D.6 Results of ^{13}C-MFA for *E. coli* grown on 1.7 g/L [1,2-^{13}C]glucose + 2 g/L yeast extract. The fluxes are normalized to a substrate uptake rate of 100. 95% confidence intervals of fluxes were determined by evaluating the sensitivity of the minimized SSR to flux variations.

Fit for *E. coli* 2 g/L [12]Gluc + 2 g/L YE			
Number of fitted data sets :			3
Number of fitted measurements :			498
SSR :			308
Flux	best fit	LB95	UB95
G6P.1 <=> F6P.1 (net)	79.0	76.3	82.7
G6P.1 <=> F6P.1 (exch)	94.4	59.3	151.7
G6P.2 <=> F6P.2 (net)	69.1	65.0	72.8
G6P.2 <=> F6P.2 (exch)	157.6	107.4	294.0
F6P.1 + ATP.1 -> FBP.1 + ADP.1	92.8	90.8	94.2
F6P.2 + ATP.2 -> FBP.2 + ADP.2	83.0	80.8	84.9
FBP.1 <=> DHAP.1 + GAP.1 (net)	92.8	90.8	94.2
FBP.1 <=> DHAP.1 + GAP.1 (exch)	473.2	0.0	100473.0
FBP.2 <=> DHAP.2 + GAP.2 (net)	83.0	80.8	84.9

FBP.2 <=> DHAP.2 + GAP.2 (exch)	168.2	0.0	100168.0
DHAP.1 <=> GAP.1 (net)	92.8	90.8	94.2
DHAP.1 <=> GAP.1 (exch)	288.5	0.0	100289.0
DHAP.2 <=> GAP.2 (net)	83.0	80.8	84.9
DHAP.2 <=> GAP.2 (exch)	0.2	0.0	100000.0
GAP.1 + NAD.1 + ADP.1 + Pi.1 <=> 3PG.1 + ATP.1 + NADH.1 (net)	192.6	189.9	193.8
GAP.1 + NAD.1 + ADP.1 + Pi.1 <=> 3PG.1 + ATP.1 + NADH.1 (exch)	677.8	0.0	100678.0
GAP.2 + NAD.2 + ADP.2 + Pi.2 <=> 3PG.2 + ATP.2 + NADH.2 (net)	171.2	168.3	174.3
GAP.2 + NAD.2 + ADP.2 + Pi.2 <=> 3PG.2 + ATP.2 + NADH.2 (exch)	2593.1	0.0	102593.0
3PG.1 <=> PEP.1 (net)	192.3	188.8	193.5
3PG.1 <=> PEP.1 (exch)	653.3	0.0	100653.0
3PG.2 <=> PEP.2 (net)	158.3	152.9	162.6
3PG.2 <=> PEP.2 (exch)	3935.0	0.0	103935.0
PEP.1 + ADP.1 -> Pyr.1 + ATP.1	91.6	0.0	93.3
PEP.2 + ADP.2 -> Pyr.2 + ATP.2	30.5	21.6	36.6
G6P.1 + NADP.1 -> 6PG.1 + NADPH.1	21.0	17.2	23.6
G6P.2 + NADP.2 -> 6PG.2 + NADPH.2	29.3	25.9	32.2
6PG.1 + NADP.1 -> Ru5P.1 + CO2.1 + NADPH.1	21.0	17.2	23.6
6PG.2 + NADP.2 -> Ru5P.2 + CO2.2 + NADPH.2	29.3	25.8	33.3
Ru5P.1 <=> X5P.1 (net)	13.9	11.3	15.6
Ru5P.1 <=> X5P.1 (exch)	69.0	25.0	10144.1
Ru5P.2 <=> X5P.2 (net)	14.4	12.5	16.2
Ru5P.2 <=> X5P.2 (exch)	47.4	40.8	60.2
Ru5P.1 <=> R5P.1 (net)	7.1	5.8	8.2
Ru5P.1 <=> R5P.1 (exch)	167.9	26.7	10542.9
Ru5P.2 <=> R5P.2 (net)	14.9	13.2	16.0
Ru5P.2 <=> R5P.2 (exch)	2227.9	15.8	13437.9
X5P.1 <=> GAP.1 + E-C2.1 (net)	13.9	11.3	15.6
X5P.1 <=> GAP.1 + E-C2.1 (exch)	65.0	25.0	10092.0
X5P.2 <=> GAP.2 + E-C2.2 (net)	14.4	12.5	16.2
X5P.2 <=> GAP.2 + E-C2.2 (exch)	21058.3	44.8	31633.9
F6P.1 <=> E4P.1 + E-C2.1 (net)	-6.9	-7.8	-5.6
F6P.1 <=> E4P.1 + E-C2.1 (exch)	13.3	8.9	17.2

F6P.2 <=> E4P.2 + E-C2.2 (net)	-5.8	-6.7	-5.0
F6P.2 <=> E4P.2 + E-C2.2 (exch)	14.9	11.2	18.2
S7P.1 <=> R5P.1 + E-C2.1 (net)	-7.0	-7.8	-5.7
S7P.1 <=> R5P.1 + E-C2.1 (exch)	105.4	0.0	10220.6
S7P.2 <=> R5P.2 + E-C2.2 (net)	-8.6	-9.5	-7.5
S7P.2 <=> R5P.2 + E-C2.2 (exch)	0.0	0.0	2.1
F6P.1 <=> GAP.1 + E-C3.1 (net)	-7.0	-7.8	-5.7
F6P.1 <=> GAP.1 + E-C3.1 (exch)	51.4	31.8	93.4
F6P.2 <=> GAP.2 + E-C3.2 (net)	-8.6	-9.5	-7.5
F6P.2 <=> GAP.2 + E-C3.2 (exch)	48.5	33.0	74.1
S7P.1 <=> E4P.1 + E-C3.1 (net)	7.0	5.7	7.8
S7P.1 <=> E4P.1 + E-C3.1 (exch)	0.0	0.0	2.5
S7P.2 <=> E4P.2 + E-C3.2 (net)	8.6	7.5	9.5
S7P.2 <=> E4P.2 + E-C3.2 (exch)	560.3	0.0	100560.0
6PG.1 -> KDPG.1	0.0	0.0	2.2
6PG.2 -> KDPG.2	0.0	0.0	2.2
KDPG.1 -> GAP.1 + Pyr.1	0.0	0.0	2.2
KDPG.2 -> GAP.2 + Pyr.2	0.0	0.0	2.2
Pyr.1 + NAD.1 -> AcCoA.1 + CO2.1 + NADH.1	191.1	182.8	193.3
Pyr.2 + NAD.2 -> AcCoA.2 + CO2.2 + NADH.2	110.4	100.5	123.4
AcCoA.1 + OAC.1 -> Cit.1	0.2	0.0	5.3
AcCoA.2 + OAC.2 -> Cit.2	27.7	21.0	33.2
Cit.1 <=> ICit.1 (net)	0.2	0.0	5.3
Cit.1 <=> ICit.1 (exch)	303.5	0.0	100304.0
Cit.2 <=> ICit.2 (net)	27.7	21.0	33.2
Cit.2 <=> ICit.2 (exch)	233.7	0.0	100234.0
ICit.1 + NADP.1 <=> AKG.1 + CO2.1 + NADPH.1 (net)	0.2	0.0	2.3
ICit.1 + NADP.1 <=> AKG.1 + CO2.1 + NADPH.1 (exch)	370.8	0.0	100371.0
ICit.2 + NADP.2 <=> AKG.2 + CO2.2 + NADPH.2 (net)	27.7	20.9	33.2
ICit.2 + NADP.2 <=> AKG.2 + CO2.2 + NADPH.2 (exch)	0.0	0.0	11189.4
AKG.1 + NAD.1 -> SucCoA.1 + CO2.1 + NADH.1	0.0	0.0	0.4
AKG.2 + NAD.2 -> SucCoA.2 + CO2.2 + NADH.2	19.5	8.9	25.0
SucCoA.1 + ADP.1 + Pi.1 <=> Suc.1 + ATP.1 (net)	-0.1	-0.5	0.0

SucCoA.1 + ADP.1 + Pi.1 <=> Suc.1 + ATP.1 (exch)	288.8	0.0	11913.0
SucCoA.2 + ADP.2 + Pi.2 <=> Suc.2 + ATP.2 (net)	15.9	6.7	21.4
SucCoA.2 + ADP.2 + Pi.2 <=> Suc.2 + ATP.2 (exch)	271.0	0.0	100271.0
Suc.1 + FAD.1 <=> Fum.1 + FADH2.1 (net)	0.0	0.0	4.9
Suc.1 + FAD.1 <=> Fum.1 + FADH2.1 (exch)	375.0	0.0	100375.0
Suc.2 + FAD.2 <=> Fum.2 + FADH2.2 (net)	19.5	10.9	25.0
Suc.2 + FAD.2 <=> Fum.2 + FADH2.2 (exch)	11080.5	0.0	40941.7
Fum.1 <=> Mal.1 (net)	0.1	0.0	5.1
Fum.1 <=> Mal.1 (exch)	839.2	0.0	11448.8
Fum.2 <=> Mal.2 (net)	21.8	14.9	27.3
Fum.2 <=> Mal.2 (exch)	110.1	17.5	10271.7
Mal.1 + NAD.1 <=> OAC.1 + NADH.1 (net)	0.1	-93.6	4.3
Mal.1 + NAD.1 <=> OAC.1 + NADH.1 (exch)	95.3	0.0	12286.1
Mal.2 + NAD.2 <=> OAC.2 + NADH.2 (net)	21.8	11.7	31.5
Mal.2 + NAD.2 <=> OAC.2 + NADH.2 (exch)	2248.2	2248.2	13777.5
ICit.1 <=> Glyox.1 + Suc.1 (net)	0.0	0.0	1.7
ICit.1 <=> Glyox.1 + Suc.1 (exch)	0.0	0.0	0.2
ICit.2 <=> Glyox.2 + Suc.2 (net)	0.0	0.0	2.5
ICit.2 <=> Glyox.2 + Suc.2 (exch)	2.0	0.0	4.4
AcCoA.1 + Glyox.1 -> Mal.1	0.0	0.0	1.7
AcCoA.2 + Glyox.2 -> Mal.2	0.0	0.0	2.5
Mal.1 + NADP.1 -> Pyr.1 + CO2.1 + NADPH.1	0.0	0.0	94.5
Mal.2 + NADP.2 -> Pyr.2 + CO2.2 + NADPH.2	0.0	0.0	8.5
PEP.1 + CO2.1 -> OAC.1 + Pi.1	0.5	0.0	126.3
PEP.2 + CO2.2 -> OAC.2 + Pi.2	21.9	19.2	26.2
OAC.1 + ATP.1 -> PEP.1 + CO2.1 + ADP.1	0.0	0.0	34.0
OAC.2 + ATP.2 -> PEP.2 + CO2.2 + ADP.2	0.0	0.0	19.1
AcCoA.1 + ADP.1 + Pi.1 <=> Ac.1 + ATP.1 (net)	190.3	178.4	193.2
AcCoA.1 + ADP.1 + Pi.1 <=> Ac.1 + ATP.1 (exch)	262.2	0.0	100262.0
AcCoA.2 + ADP.2 + Pi.2 <=> Ac.2 + ATP.2 (net)	56.4	44.9	68.1
AcCoA.2 + ADP.2 + Pi.2 <=> Ac.2 + ATP.2 (exch)	384.3	0.0	100384.0
AKG.1 + NADPH.1 + NH3.1 -> Glu.1 + NADP.1	1.1	0.0	6.2
AKG.2 + NADPH.2 + NH3.2 -> Glu.2 + NADP.2	48.5	42.9	54.7
Glu.1 + ATP.1 + NH3.1 -> Gln.1 + ADP.1 + Pi.1	0.1	0.0	0.6
Glu.2 + ATP.2 + NH3.2 -> Gln.2 + ADP.2 + Pi.2	4.6	4.1	5.2

Glu.1 + 2 NADPH.1 + ATP.1 -> Pro.1 + 2 NADP.1 + ADP.1 + Pi.1	0.0	0.0	0.2
Glu.2 + 2 NADPH.2 + ATP.2 -> Pro.2 + 2 NADP.2 + Pi.2 + ADP.2	1.6	1.4	1.8
Glu.1 + CO2.1 + Gln.1 + NADPH.1 + Asp.1 + AcCoA.1 + 5 ATP.1 -> Arg.1 + AKG.1 + Fum.1 + Ac.1	0.1	0.0	0.3
Glu.2 + CO2.2 + Gln.2 + NADPH.2 + Asp.2 + AcCoA.2 + 5 ATP.2 -> Arg.2 + AKG.2 + Fum.2 + Ac.2	2.1	1.9	2.4
OAC.1 + Glu.1 -> Asp.1 + AKG.1	0.3	0.0	2.5
OAC.2 + Glu.2 -> Asp.2 + AKG.2	13.4	11.8	15.3
Asp.1 + NH3.1 + 2 ATP.1 -> Asn.1 + 2 ADP.1 + 2 Pi.1	0.0	0.0	0.2
Asp.2 + NH3.2 + 2 ATP.2 -> Asn.2 + 2 ADP.2 + 2 Pi.2	1.7	1.6	2.0
Pyr.1 + Glu.1 -> Ala.1 + AKG.1	0.1	0.0	0.5
Pyr.2 + Glu.2 -> Ala.2 + AKG.2	3.7	3.3	4.2
3PG.1 + Glu.1 + NAD.1 -> Ser.1 + NADH.1 + AKG.1 + Pi.1	0.2	0.0	1.1
3PG.2 + Glu.2 + NAD.2 -> Ser.2 + NADH.2 + AKG.2 + Pi.2	8.3	7.3	9.2
Ser.1 + THF.1 <=> Gly.1 + MEETHF.1 (net)	0.1	0.0	0.6
Ser.1 + THF.1 <=> Gly.1 + MEETHF.1 (exch)	0.0	0.0	0.0
Ser.2 + THF.2 <=> Gly.2 + MEETHF.2 (net)	4.5	3.8	5.0
Ser.2 + THF.2 <=> Gly.2 + MEETHF.2 (exch)	1.8	1.5	3.1
Gly.1 + THF.1 + NAD.1 <=> CO2.1 + MEETHF.1 + NH3.1 + NADH.1 (net)	0.0	0.0	0.5
Gly.1 + THF.1 + NAD.1 <=> CO2.1 + MEETHF.1 + NH3.1 + NADH.1 (exch)	637.4	0.0	82073.6
Gly.2 + THF.2 + NAD.2 <=> CO2.2 + MEETHF.2 + NH3.2 + NADH.2 (net)	0.1	0.1	0.7
Gly.2 + THF.2 + NAD.2 <=> CO2.2 + MEETHF.2 + NH3.2 + NADH.2 (exch)	0.0	0.0	5.4
Thr.1 + NAD.1 -> Gly.1 + AcCoA.1 + NADH.1	0.0	0.0	1.0
Thr.2 + NAD.2 -> Gly.2 + AcCoA.2 + NADH.2	0.0	0.0	1.2
Ser.1 + AcCoA.1 + SO4.1 + 3 ATP.1 + 4 NADPH.1 -> Cys.1 + Ac.1 + 4 NADP.1 + 3ADP.1	0.0	0.0	0.2
Ser.2 + AcCoA.2 + SO4.2 + 3 ATP.2 + 4 NADPH.2 -> Cys.2 + Ac.2 + 4 NADP.2 + 3ADP.2	1.8	1.6	2.0

Asp.1 + Pyr.1 + Glu.1 + 2 NADPH.1 + ATP.1 + SucCoA.1 -> LL-DAP.1 + AKG.1 + Suc.1 + 2NADP.1 + ADP.1	0.1	0.0	0.3
Asp.2 + Pyr.2 + Glu.2 + 2 NADPH.2 + ATP.2 + SucCoA.2 -> LL-DAP.2 + AKG.2 + Suc.2 + 2NADP.2 + ADP.2	2.5	2.2	2.8
LL-DAP.1 -> Lys.1 + CO2.1	0.1	0.0	0.3
LL-DAP.2 -> Lys.2 + CO2.2	2.5	2.2	2.8
Asp.1 + 2 NADPH.1 + 2 ATP.1 -> Thr.1 + 2 NADP.1 + 2 ADP.1 + 2 Pi.1	0.1	0.0	1.5
Asp.2 + 2 NADPH.2 + 2 ATP.2 -> Thr.2 + 2 NADP.2 + 2 ADP.2 + 2 Pi.2	4.0	3.5	5.1
Asp.1 + METHF.1 + Cys.1 + 2 NADPH.1 + ATP.1 + SucCoA.1 -> Met.1 + Pyr.1 + Suc.1 + NH3.1 + 2NADP.1 + ADP.1	0.0	0.0	0.1
Asp.2 + METHF.2 + Cys.2 + 2 NADPH.2 + ATP.2 + SucCoA.2 -> Met.2 + Pyr.2 + Suc.2 + NH3.2 + 2NADP.2 + ADP.2	1.1	1.0	1.2
2 Pyr.1 + NADPH.1 + Glu.1 -> Val.1 + CO2.1 + NADP.1 + AKG.1	0.1	0.0	0.4
2 Pyr.2 + NADPH.2 + Glu.2 -> Val.2 + CO2.2 + NADP.2 + AKG.2	3.1	2.7	3.4
2 Pyr.1 + AcCoA.1 + Glu.1 + NADPH.1 + NAD.1 -> Leu.1 + 2 CO2.1 + AKG.1 + NA	0.1	0.0	0.4
2 Pyr.2 + AcCoA.2 + Glu.2 + NADPH.2 + NAD.2 -> Leu.2 + 2 CO2.2 + AKG.2 + NA	3.3	2.9	3.7
Thr.1 + Pyr.1 + Glu.1 + NADPH.1 -> Ile.1 + CO2.1 + AKG.1 + NADP.1 + NH3.1	0.0	0.0	0.3
Thr.2 + Pyr.2 + Glu.2 + NADPH.2 -> Ile.2 + CO2.2 + AKG.2 + NADP.2 + NH3.2	2.1	1.9	2.4
E4P.1 + 2 PEP.1 + Glu.1 + NADPH.1 + ATP.1 -> Phe.1 + CO2.1 + AKG.1 + NADP.1	0.0	0.0	0.2
E4P.2 + 2 PEP.2 + Glu.2 + NADPH.2 + ATP.2 -> Phe.2 + CO2.2 + AKG.2 + NADP.2	1.3	1.2	1.5
E4P.1 + 2 PEP.1 + Glu.1 + NADPH.1 + NAD.1 + ATP.1 -> Tyr.1 + CO2.1 + AKG.1 + NADH.1	0.0	0.0	0.1
E4P.2 + 2 PEP.2 + Glu.2 + NADPH.2 + NAD.2 + ATP.2 -> Tyr.2 + CO2.2 + AKG.2 + NADH.2	1.0	0.9	1.1
E4P.1 + 2 PEP.1 + R5P.1 + Ser.1 + Gln.1 + NADPH.1 + 3 ATP.1 -> Trp.1 + CO2.1 + GAP.1 + Pyr.1 + Glu.1	0.0	0.0	0.1
E4P.2 + 2 PEP.2 + R5P.2 + Ser.2 + Gln.2 +	0.4	0.4	0.5

NADPH.2 + 3 ATP.2 -> Trp.2 + CO2.2 + GAP.2 + Pyr.2 + Glu.2			
R5P.1 + FTHF.1 + Gln.1 + Asp.1 + 5 ATP.1 + 2 NAD.1 -> His.1 + 2 NADH.1 + AKG.1 + Fum.1 + 2NADH.1	0.0	0.0	0.0
R5P.2 + FTHF.2 + Gln.2 + Asp.2 + 5 ATP.2 + 2 NAD.2 -> His.2 + 2 NADH.2 + AKG.2 + Fum.2 + 2NADH.2	0.2	0.1	0.2
MEETHF.1 + NADH.1 -> METHF.1 + NAD.1	0.0	0.0	0.1
MEETHF.2 + NADH.2 -> METHF.2 + NAD.2	1.1	1.0	1.2
MEETHF.1 + NADP.1 -> FTHF.1 + NADPH.1	0.0	0.0	0.0
MEETHF.2 + NADP.2 -> FTHF.2 + NADPH.2	0.2	0.1	0.2
NADH.1 + NADP.1 <=> NADPH.1 + NAD.1 (net)	-39.1	-72.2	-24.1
NADH.1 + NADP.1 <=> NADPH.1 + NAD.1 (exch)	14.8	0.0	526.8
NADH.2 + NADP.2 <=> NADPH.2 + NAD.2 (net)	41.8	27.7	57.6
NADH.2 + NADP.2 <=> NADPH.2 + NAD.2 (exch)	42.0	0.0	100042.0
0.488Ala.1+0.281Arg.1+0.229Asn.1+0.229Asp.1+ 0.087Cys.1+0.250Glu.1+0.250Gln.1+0.582Gly.1+ 0.09His.1+0.276Ile.1+0.428Leu.1+0.326Lys.1+0.146 Met.1 + 0.176Phe.1+0.210Pro.1 + 0.205Ser.1 + 0.241 Thr.1 + 0.054 Trp.1 +0.131Tyr.1+0.402Val.1 + 0.205 G6P.1 +0.071F6P.1+0.754R5P.1 + 0.129 GAP.1 + 0.619 3PG.1 +0.051PEP.1 + 0.083 Pyr.1 +2.510AcCoA.1+ 0.087AKG.1 + 0.340 OAC.1 + 0.443MEETHF.1+33.247ATP.1+5.363NADPH.1 → 39.68Biomass.1 + 1.455NADH.1	0.2	0.0	1.0
0.488Ala.2+0.281Arg.2+0.229Asn.2+0.229Asp.2+ 0.087Cys.2+0.250Glu.2+0.250Gln.2+0.582Gly.2+ 0.09His.2+0.276Ile.2+0.428Leu.2+0.326Lys.2+0.146 Met.2 + 0.176Phe.2+0.210Pro.2 + 0.205Ser.2 + 0.241 Thr.2 + 0.054 Trp.2 +0.131Tyr.2+0.402Val.2 + 0.205 G6P.2 +0.071F6P.2+0.754R5P.2 + 0.129 GAP.2 + 0.619 3PG.2 +0.051PEP.2 + 0.083 Pyr.2 +2.510AcCoA.2+ 0.087AKG.2 + 0.340 OAC.2 + 0.443MEETHF.2+33.247ATP.2+5.363NADPH.2 → 39.68Biomass.2 + 1.455NADH.2	7.6	6.8	8.4
ATP.1 -> ATP.Ext	1221.6	1102.3	1242.5
ATP.2 -> ATP.Ext	523.3	402.4	621.1
Ac.1 -> Ac.Ext + X-ac1	190.4	178.8	193.2
Ac.2 -> Ac.Ext + X-ac2	60.3	49.2	71.7

CO2.1 -> CO2.Ext	212.2	203.5	215.6
CO2.2 -> CO2.Ext	179.9	153.1	193.8
O2.Ext -> O2.1	211.8	201.3	215.4
O2.Ext -> O2.2	161.8	133.3	176.8
NH3.Ext -> NH3.1	1.2	0.0	6.5
NH3.Ext -> NH3.2	51.5	45.8	57.6
SO4.Ext -> SO4.1	0.0	0.0	0.2
SO4.Ext -> SO4.2	1.8	1.6	2.0
NADH.1 + 0.5 O2.1 + 2 ADP.1 + 2 Pi.1 -> NAD.1 + 2 ATP.1	423.5	402.7	429.8
NADH.2 + 0.5 O2.2 + 2 ADP.2 + 2 Pi.2 -> NAD.2 + 2 ATP.2	304.1	256.4	330.2
FADH2.1 + 0.5 O2.1 + ADP.1 + Pi.1 -> FAD.1 + ATP.1	0.0	0.0	4.9
FADH2.2 + 0.5 O2.2 + ADP.2 + Pi.2 -> FAD.2 + ATP.2	19.5	10.9	25.0
Ala.a1 + Gly.a1 + Val.a1 + Leu.a1 + Ile.a1 + Pro.a1 + Met.a1 + Ser.a1 + Thr.a1 + Phe.a1 + Asp.a1 + Glu.a1 + Lys.a1 + His.a1 + Tyr.a1 + G6P.a1 + R5P.a1 → X-a1	100.0	100.0	100.0
Ala.a2 + Gly.a2 + Val.a2 + Leu.a2 + Ile.a2 + Pro.a2 + Met.a2 + Ser.a2 + Thr.a2 + Phe.a2 + Asp.a2 + Glu.a2 + Lys.a2 + His.a2 + Tyr.a2 + G6P.a2 + R5P.a2 → X-a2	100.0	100.0	100.0
Ala.a3 + Gly.a3 + Val.a3 + Leu.a3 + Ile.a3 + Pro.a3 + Met.a3 + Ser.a3 + Thr.a3 + Phe.a3 + Asp.a3 + Glu.a3 + Lys.a3 + His.a3 + Tyr.a3 + G6P.a3 + R5P.a3 → X-a3	100.0	100.0	100.0
Ala.1 + Gly.1 + Val.1 + Leu.1 + Ile.1 + Pro.1 + Met.1 + Ser.1 + Thr.1 + Phe.1 + Asp.1 + Glu.1 + Lys.1 + His.1 + Tyr.1 + G6P.1 + R5P.1 → Ala.a1 + Gly.a1 + Val.a1 + Leu.a1 + Ile.a1 + Pro.a1 + Met.a1 + Ser.a1 + Thr.a1 + Phe.a1 + Asp.a1 + Glu.a1 + Lys.a1 + His.a1 + Tyr.a1 + G6P.a1 + R5P.a1 + Ala.1 + Gly.1 + Val.1 + Leu.1 + Ile.1 + Pro.1 + Met.1 + Ser.1 + Thr.1 + Phe.1 + Asp.1 + Glu.1 + Lys.1 + His.1 + Tyr.1 + G6P.1 + R5P.1	96.5	79.6	100.0
Ala.1 + Gly.1 + Val.1 + Leu.1 + Ile.1 + Pro.1 + Met.1 + Ser.1 + Thr.1 + Phe.1 + Asp.1 + Glu.1 + Lys.1 + His.1 + Tyr.1 + G6P.1 + R5P.1 → Ala.a2 + Gly.a2 + Val.a2 + Leu.a2 + Ile.a2 + Pro.a2 + Met.a2	56.0	43.2	79.7

+ Ser.a2 + Thr.a2 + Phe.a2 + Asp.a2 + Glu.a2 + Lys.a2 + His.a2 + Tyr.a2 + G6P.a2 + R5P.a2 + Ala.1 + Gly.1 + Val.1 + Leu.1 + Ile.1 + Pro.1 + Met.1 + Ser.1 + Thr.1 + Phe.1 + Asp.1 + Glu.1 + Lys.1 + His.1 + Tyr.1 + G6P.1 + R5P.1			
Ala.1 + Gly.1 + Val.1 + Leu.1 + Ile.1 + Pro.1 +Met.1 + Ser.1 + Thr.1 + Phe.1 + Asp.1 + Glu.1 + Lys.1 + His.1 + Tyr.1 + G6P.1 + R5P.1 → Ala.a3 + Gly.a3 + Val.a3 + Leu.a3 + Ile.a3 + Pro.a3 + Met.a3 + Ser.a3 + Thr.a3 + Phe.a3 + Asp.a3 + Glu.a3 + Lys.a3 + His.a3 + Tyr.a3 + G6P.a3 + R5P.a3 + Ala.1 + Gly.1 + Val.1 + Leu.1 + Ile.1 + Pro.1 + Met.1 + Ser.1 + Thr.1 + Phe.1 + Asp.1 + Glu.1 + Lys.1 + His.1 + Tyr.1 + G6P.1 + R5P.1	0.0	0.0	47.5
Ala.2 + Gly.2 + Val.2 + Leu.2 + Ile.2 + Pro.2 + Met.2 + Ser.2 + Thr.2 + Phe.2 + Asp.2 + Glu.2 + Lys.2 + His.2 + Tyr.2 + G6P.2 + R5P.2 → Ala.a1 + Gly.a1 + Val.a1 + Leu.a1 + Ile.a1 + Pro.a1 + Met.a1 + Ser.a1 + Thr.a1 + Phe.a1 + Asp.a1 + Glu.a1 + Lys.a1 + His.a1 + Tyr.a1 + G6P.a1 + R5P.a1 + Ala.2 + Gly.2 + Val.2 + Leu.2 + Ile.2 + Pro.2 + Met.2 + Ser.2 + Thr.2 + Phe.2 + Asp.2 + Glu.2 + Lys.2 + His.2 + Tyr.2 + G6P.2 + R5P.2	3.5	0.0	20.4
Ala.2 + Gly.2 + Val.2 + Leu.2 + Ile.2 + Pro.2 + Met.2 + Ser.2 + Thr.2 + Phe.2 + Asp.2 + Glu.2 + Lys.2 + His.2 + Tyr.2 + G6P.2 + R5P.2 → Ala.a2 + Gly.a2 + Val.a2 + Leu.a2 + Ile.a2 + Pro.a2 + Met.a2 + Ser.a2 + Thr.a2 + Phe.a2 + Asp.a2 + Glu.a2 + Lys.a2 + His.a2 + Tyr.a2 + G6P.a2 + R5P.a2 + Ala.2 + Gly.2 + Val.2 + Leu.2 + Ile.2 + Pro.2 + Met.2 + Ser.2 + Thr.2 + Phe.2 + Asp.2 + Glu.2 + Lys.2 + His.2 + Tyr.2 + G6P.2 + R5P.2	44.0	19.9	56.8
Ala.2 + Gly.2 + Val.2 + Leu.2 + Ile.2 + Pro.2 + Met.2 + Ser.2 + Thr.2 + Phe.2 + Asp.2 + Glu.2 + Lys.2 + His.2 + Tyr.2 + G6P.2 + R5P.2 → Ala.a3 + Gly.a3 + Val.a3 + Leu.a3 + Ile.a3 + Pro.a3 + Met.a3 + Ser.a3 + Thr.a3 + Phe.a3 + Asp.a3 + Glu.a3 + Lys.a3 + His.a3 + Tyr.a3 + G6P.a3 + R5P.a3 + Ala.2 + Gly.2 + Val.2 + Leu.2 + Ile.2 + Pro.2 + Met.2 + Ser.2 + Thr.2 + Phe.2 + Asp.2 + Glu.2 + Lys.2 + His.2 + Tyr.2 + G6P.2 + R5P.2	100.0	52.4	100.0
PEP.1 + 2 Gluc.Ext + PEP.2 -> G6P.1 + Pyr.1 + G6P.2 + Pyr.2 + X-glc1 + X-gluc2	100.0	100.0	100.0

CO2.M0 + CO2.1 -> CO2.1 + CO2.snk	11883.4	222.1	23148.2
CO2.M0 + CO2.2 -> CO2.2 + CO2.snk	125.0	53.9	677.9
Pyr.M0 + Pyr.1 -> Pyr.1 + Pyr.snk	0.0	0.0	486.4
Pyr.M0 + Pyr.2 -> Pyr.2 + Pyr.snk	6.7	0.0	46.8
OAC.M0 + OAC.1 -> OAC.1 + OAC.snk	1.4	0.0	382.4
AKG.M0 + AKG.1 -> AKG.1 + AKG.snk	0.0	0.0	9.3
AKG.M0 + AKG.2 -> AKG.2 + AKG.snk	32.3	0.0	46.0
Ser.M0 + Ser.1 -> Ser.1 + Ser.snk	0.0	0.0	0.7
R5P.M0 + R5P.1 -> R5P.1 + R5P.snk	7.0	3.3	11.9
R5P.M0 + R5P.2 -> R5P.2 + R5P.snk	4.2	1.1	6.0
Uptake rate of CO2.M0	12008.4	7954.4	15478.6
Uptake rate of Gluc.Ext	200.0	200.0	200.0
Uptake rate of OAC.M0	1.4	0.0	382.4
Uptake rate of AKG.M0	32.3	0.0	46.0
Uptake rate of Pyr.M0	6.7	0.0	489.8
Uptake rate of R5P.M0	11.2	7.0	13.7
Uptake rate of Ser.M0	0.0	0.0	0.7
Uptake rate of O2.Ext	373.5	350.7	390.1
Uptake rate of NH3.Ext	52.7	46.6	60.3
Uptake rate of SO4.Ext	1.8	1.6	2.1
Output rate of Ac.Ext	250.7	234.6	263.9
Output rate of CO2.Ext	392.0	363.1	407.1
Output rate of CO2.snk	12008.4	7954.4	15478.6
Output rate of OAC.snk	1.4	0.0	382.4
Output rate of AKG.snk	32.3	0.0	46.0
Output rate of Pyr.snk	6.7	0.0	489.8
Output rate of R5P.snk	11.2	7.0	13.7
Output rate of Ser.snk	0.0	0.0	0.7
Output rate of ATP.Ext	1744.9	1591.8	1859.2
Output rate of Biomass.1	7.1	0.0	38.4
Output rate of Biomass.2	302.7	269.1	341.9
Output rate of X-glc1	100.0	100.0	100.0
Output rate of X-glc2	100.0	100.0	100.0
Output rate of X-ac1	190.4	178.8	193.2
Output rate of X-ac2	60.3	49.2	71.7
Output rate of X-a1	100.0	100.0	100.0

Output rate of X-a2	100.0	100.0	100.0
Output rate of X-a3	100.0	100.0	100.0
Output rate of X-Norm	100.0	100.0	100.0
Net production rate of ADP.1	-1221.6	-1243	-1102.3
Net production rate of ADP.2	-523.3	-621.1	-355.1
Net production rate of Pi.1	-1221.9	-1243	-1103.6
Net production rate of Pi.2	-537.2	-633.8	-390.7
Fractional labeling of Ala.a1 (data set #1)	0.4	0.4	1.0
Fractional labeling of Gly.a1 (data set #1)	0.1	0.0	0.3
Fractional labeling of Val.a1 (data set #1)	0.0	0.0	0.0
Fractional labeling of Leu.a1 (data set #1)	0.0	0.0	0.0
Fractional labeling of Ile.a1 (data set #1)	0.0	0.0	0.0
Fractional labeling of Met.a1 (data set #1)	0.0	0.0	0.0
Fractional labeling of Ser.a1 (data set #1)	0.6	0.5	0.9
Fractional labeling of Thr.a1 (data set #1)	0.0	0.0	0.0
Fractional labeling of Phe.a1 (data set #1)	0.0	0.0	0.0
Fractional labeling of Asp.a1 (data set #1)	0.3	0.2	0.6
Fractional labeling of Glu.a1 (data set #1)	0.1	0.1	0.4
Fractional labeling of Lys.a1 (data set #1)	0.0	0.0	0.0
Fractional labeling of His.a1 (data set #1)	0.0	0.0	0.0
Fractional labeling of Tyr.a1 (data set #1)	0.0	0.0	0.0
Fractional labeling of R5P.a1 (data set #1)	0.9	0.9	1.0
Fractional labeling of G6P.a1 (data set #1)	0.8	0.8	0.8
Fractional labeling of Ala.a2 (data set #2)	0.5	0.4	0.9
Fractional labeling of Gly.a2 (data set #2)	0.3	0.3	0.7
Fractional labeling of Val.a2 (data set #2)	0.0	0.0	0.0
Fractional labeling of Leu.a2 (data set #2)	0.0	0.0	0.0
Fractional labeling of Ile.a2 (data set #2)	0.0	0.0	0.0
Fractional labeling of Met.a2 (data set #2)	0.0	0.0	0.0
Fractional labeling of Ser.a2 (data set #2)	0.9	0.7	1.0
Fractional labeling of Thr.a2 (data set #2)	0.0	0.0	0.1
Fractional labeling of Phe.a2 (data set #2)	0.0	0.0	0.0
Fractional labeling of Asp.a2 (data set #2)	0.6	0.5	0.8
Fractional labeling of Glu.a2 (data set #2)	0.3	0.2	0.5
Fractional labeling of Lys.a2 (data set #2)	0.0	0.0	0.0
Fractional labeling of His.a2 (data set #2)	0.0	0.0	0.0

Fractional labeling of Tyr.a2 (data set #2)	0.0	0.0	0.0
Fractional labeling of R5P.a2 (data set #2)	1.0	1.0	1.0
Fractional labeling of G6P.a2 (data set #2)	0.9	0.9	0.9
Fractional labeling of Ala.a3 (data set #3)	0.4	0.4	0.5
Fractional labeling of Gly.a3 (data set #3)	0.4	0.4	0.4
Fractional labeling of Val.a3 (data set #3)	0.0	0.0	0.0
Fractional labeling of Leu.a3 (data set #3)	0.0	0.0	0.0
Fractional labeling of Ile.a3 (data set #3)	0.0	0.0	0.0
Fractional labeling of Met.a3 (data set #3)	0.0	0.0	0.0
Fractional labeling of Ser.a3 (data set #3)	0.8	0.8	0.9
Fractional labeling of Thr.a3 (data set #3)	0.4	0.3	0.4
Fractional labeling of Phe.a3 (data set #3)	0.0	0.0	0.0
Fractional labeling of Asp.a3 (data set #3)	0.5	0.4	0.6
Fractional labeling of Glu.a3 (data set #3)	1.0	0.4	1.0
Fractional labeling of Lys.a3 (data set #3)	0.0	0.0	0.0
Fractional labeling of His.a3 (data set #3)	0.0	0.0	0.0
Fractional labeling of Tyr.a3 (data set #3)	0.4	0.3	0.4
Fractional labeling of R5P.a3 (data set #3)	1.0	0.9	1.0
Fractional labeling of G6P.a3 (data set #3)	0.9	0.9	1.0

Appendix E

REPRINT PERMISSION LETTERS

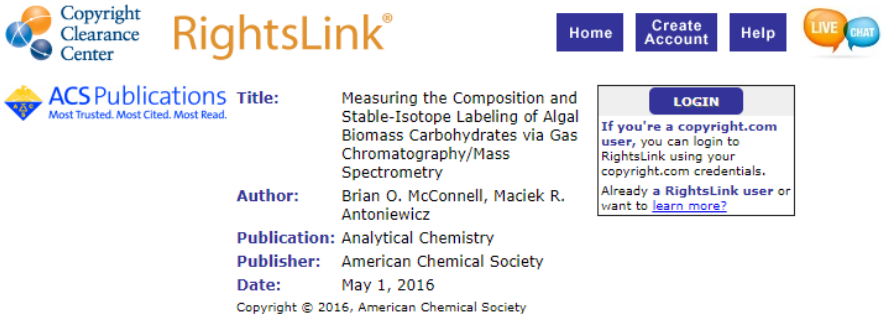

Copyright Clearance Center RightsLink®

Home | Create Account | Help | LIVE CHAT

ACS Publications
Most Trusted. Most Cited. Most Read.

Title: Measuring the Composition and Stable-Isotope Labeling of Algal Biomass Carbohydrates via Gas Chromatography/Mass Spectrometry

Author: Brian O. McConnell, Maciek R. Antoniewicz

Publication: Analytical Chemistry

Publisher: American Chemical Society

Date: May 1, 2016

Copyright © 2016, American Chemical Society

LOGIN

If you're a copyright.com user, you can login to RightsLink using your copyright.com credentials.

Already a RightsLink user or want to learn more?

PERMISSION/LICENSE IS GRANTED FOR YOUR ORDER AT NO CHARGE

This type of permission/license, instead of the standard Terms & Conditions, is sent to you because no fee is being charged for your order. Please note the following:

- Permission is granted for your request in both print and electronic formats, and translations.
- If figures and/or tables were requested, they may be adapted or used in part.
- Please print this page for your records and send a copy of it to your publisher/graduate school.
- Appropriate credit for the requested material should be given as follows: "Reprinted (adapted) with permission from (COMPLETE REFERENCE CITATION). Copyright (YEAR) American Chemical Society." Insert appropriate information in place of the capitalized words.
- One-time permission is granted only for the use specified in your request. No additional uses are granted (such as derivative works or other editions). For any other uses, please submit a new request.

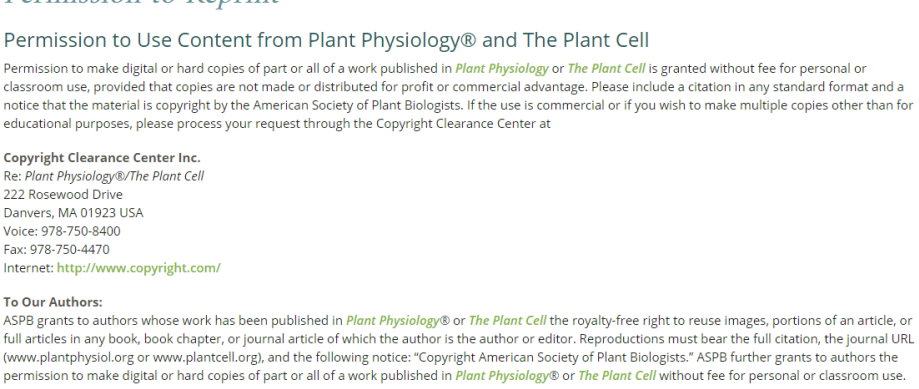

Permission to Reprint

Permission to Use Content from Plant Physiology® and The Plant Cell

Permission to make digital or hard copies of part or all of a work published in *Plant Physiology* or *The Plant Cell* is granted without fee for personal or classroom use, provided that copies are not made or distributed for profit or commercial advantage. Please include a citation in any standard format and a notice that the material is copyright by the American Society of Plant Biologists. If the use is commercial or if you wish to make multiple copies other than for educational purposes, please process your request through the Copyright Clearance Center at

Copyright Clearance Center Inc.
Re: *Plant Physiology®/The Plant Cell*
222 Rosewood Drive
Danvers, MA 01923 USA
Voice: 978-750-8400
Fax: 978-750-4470
Internet: http://www.copyright.com/

To Our Authors:
ASPB grants to authors whose work has been published in *Plant Physiology®* or *The Plant Cell* the royalty-free right to reuse images, portions of an article, or full articles in any book, book chapter, or journal article of which the author is the author or editor. Reproductions must bear the full citation, the journal URL (www.plantphysiol.org or www.plantcell.org), and the following notice: "Copyright American Society of Plant Biologists." ASPB further grants to authors the permission to make digital or hard copies of part or all of a work published in *Plant Physiology®* or *The Plant Cell* without fee for personal or classroom use.